Energy Research and Development Division

FINAL PROJECT REPORT

IMPROVED MODELING TOOLS DEVELOPMENT FOR HIGH PENETRATION SOLAR

PIER and Department of Energy ARRA Grant EE0002055 (PHASE I)

Prepared for: California Energy Commission

Prepared by: University of California, San Diego

JUNE 2016

CEC-500-2016-044

PREPARED BY:

Primary Author(s):
Byron Washom

University of California, San Diego
9500 Gilman Drive, #0057
La Jolla, CA 92093
Phone: 858-822-0585| Fax: 858-534-9836
http://www.ucsd.edu

Contract Number: PIR-10-003

Prepared for:

California Energy Commission

Hassan Mohammed
Contract Manager

Aleecia Gutierrez
Office Manager
Energy Generation Research Office

Laurie ten Hope
Deputy Director
ENERGY RESEARCH AND DEVELOPMENT DIVISION

Robert P. Oglesby
Executive Director

DISCLAIMER

This report was prepared as the result of work sponsored by the California Energy Commission. It does not necessarily represent the views of the Energy Commission, its employees or the State of California. The Energy Commission, the State of California, its employees, contractors and subcontractors make no warranty, express or implied, and assume no legal liability for the information in this report; nor does any party represent that the uses of this information will not infringe upon privately owned rights. This report has not been approved or disapproved by the California Energy Commission nor has the California Energy Commission passed upon the accuracy or adequacy of the information in this report.

PREFACE

The California Energy Commission Energy Research and Development Division supports public interest energy research and development that will help improve the quality of life in California by bringing environmentally safe, affordable, and reliable energy services and products to the marketplace.

The Energy Research and Development Division conducts public interest research, development, and demonstration (RD&D) projects to benefit California.

The Energy Research and Development Division strives to conduct the most promising public interest energy research by partnering with RD&D entities, including individuals, businesses, utilities, and public or private research institutions.

Energy Research and Development Division funding efforts are focused on the following RD&D program areas:

- Buildings End-Use Energy Efficiency
- Energy Innovations Small Grants
- Energy-Related Environmental Research
- Energy Systems Integration
- Environmentally Preferred Advanced Generation
- Industrial/Agricultural/Water End-Use Energy Efficiency
- Renewable Energy Technologies
- Transportation

Improved Modeling Tools Development of High Penetration Solar is the final report for the PIER and Department of Energy ARRA Grant (EE0002055 Phase I) project, grant number PIR-10-003 conducted by University of California, San Diego. The information from this project contributes to Energy Research and Development Division's Renewable Energy Technologies Program.

For more information about the Energy Research and Development Division, please visit the Energy Commission's website at www.energy.ca.gov/research/ or contact the Energy Commission at 916-327-1551.

ABSTRACT

DOE ARRA EE0002055

The scope of this project was to develop the preliminary, publicly available modeling tools for high penetration scenarios of photovoltaics (PV) on a distribution feeder system. A high density network of ground stations with a hemispherical sky imager were used to develop intra-hour PV output forecasts. Probabilistic models characterize the frequency and magnitude of the extreme solar generation ramp rates for individual solar panels and model the geographic dispersion effects on variability through a fleet of PV systems or a large PV plant. The tool can simulate and help mitigate the impact of the solar resource's variability. These tools are open source and available for utilities and planners at the DOE High Solar Penetration Portal.

Steady-state and dynamic models of PV systems were incorporated into advanced power flow modeling software. Open-source inverter simulation files were made available to power system designers and planners to assess maximum loading of solar PV on a distribution feeder based upon power flow, short circuit and transient stability analyses. To validate the transient modeling work, the research team examined the performance of a PV system interconnected to the grid. Different levels of PV penetration and a number of scenarios (peak system load, light load conditions, etc.) were examined. Based on these results, the research team developed planning guidelines for PV integration and the maximum safe penetration level.

Benefits to California: The solar forecast algorithms developed in this project were applied at the Copper Mountain Solar power plant, the largest solar power plant powering California at the time. In addition, the team consolidated the PV system modeling tools into an open simulation application for power system designers and planners throughout the state. The generic model is a readily available non-proprietary subset of variables based on published and name plate data for PV power inverters. These tools benefit analyses of feeder hosting capacity that are now starting to be adapted by utilities throughout California.

Keywords: High penetration solar, solar forecasting, photovoltaic systems

Please use the following citation for this report:

Washom, Byron. (University of California, San Diego). 2016. ***Improved Modeling Tools Development for High Penetration Solar.*** California Energy Commission. Publication number: CEC-500-2016-044.

TABLE OF CONTENTS

PREFACE ..... **i**

ABSTRACT ..... **ii**

TABLE OF CONTENTS ..... **iii**

EXECUTIVE SUMMARY **1**

CHAPTER 1: Introduction **5**

CHAPTER 2: High-Frequency Irradiance Fluctuations and Geographic Smoothing **7**

2.1 Problem Statement and Literature Review 7

2.2 Data Collection 9

2.3 Methods for Variability Analysis 10

2.3.1 Ramp Rate Analysis at One Site Over One Year 11

2.3.2 Geographic smoothing at six sites over one month 11

2.4 Results of the Variability Analysis 13

2.4.1 Ramp Rate Analysis at One Site 13

2.4.2 Coherence Spectra 19

2.4.3 Wavelet Decomposition 19

2.4.4 Fluctuation Power Index 20

2.5 A Wavelet Variability Model (WVM) 21

2.5.1 Wavelet Decomposition 22

2.5.2 Distances 23

2.5.3 Correlations 23

2.5.4 Variability Reduction 23

2.5.5 Simulate Wavelet Modes of Powerplant 24

2.5.6 Convert to Power Output 24

2.6 Application to Ota City and Copper Mountain Powerplants 25

2.6.1 Inputs and Running the Model 26

2.6.2 Validation of Plant Power Output 28

2.6.3 Simulate Adding More Residential PV 32

2.7 Summary of PV Variability 33
2.8 Ramp rates for Power Analytics Software 35
2.8.1 Clear Sky Index 35
2.8.2 Data Normalization 37
2.8.3 Integration with Power Analytics Software 39
2.8.4 Application to Large PV Arrays 39
2.8.5 User-Supplied Lookup Table Option 40
2.8.6 Example 1. Medium Size PV System 40
2.8.7 Example 2. Medium Size PV System, Modeling Ramp Up 41
2.8.8 Load Following Capacity 42
CHAPTER 3: Modeling of a Photovoltaic System for Power Engineering Applications 45
3.1 Photovoltaic cells and Modules 45
3.2 Stability Related to Distributed Photovoltaic Generation 47
3.3 Power Flow, Short Circuit and Photovoltaic Penetration Levels 47
3.4 Dynamic Simulation - Transient Stability (time domain) Model of PV System 49
3.5 Development of Open Source Application Programming Interface (API) 50
3.6 Benchmarking 52
CHAPTER 4: Integration Study and Interconnection Guideline 53
4.1 Integration Study 53
4.1.1 Data requirements 53
4.1.2 Modeling Scenarios 53
4.1.3 Results and Conclusions 54
4.2 General Mitigation Options for PV Variability 56
4.2.1 Voltage Control (Automatic Voltage Regulator) 56
4.2.2 Frequency Control (Governor) 57
4.2.3 Low Voltage Rid-Through (LVRT) 57
4.2.4 Reactive Power Capability and Power Factor 57
4.2.5 Power System Stabilizers 58

4.3 Considerations for PV Power Plant Modeling and Mitigation Options Depending on Plant Size 58

4.4 Mitigation Measures for Large PV Plants (>10 MVA) 59

4.4.1 Active Power Generation 59

4.4.2 Zero/Low Voltage Ride Through 59

4.4.3 Voltage/Frequency Operating Limits 60

4.4.4 Power Quality 62

4.4.5 Control Interactions 62

4.4.6 Reactive Power Requirements 62

4.4.7 Protection Requirements 63

4.5 Interconnection Recommendations for Large PV Plants 63

4.5.1 Automatic Voltage Regulators 63

4.5.2 Disturbance Monitoring System 63

4.5.3 Telemetry 63

4.6 Summary of Interconnection Guideline 64

CHAPTER 5: Accomplishments and Future Work 66

5.1 Three-dimensional Cloud Tracking and Insolation Forecast Model 66

5.2 Command, Control and Communications for Power Flow Management 67

5.3 Field Testing and Validation of the Suite of Models 67

5.4 Raise Situational Awareness of Virtual Power Plants and Microgrids by Distribution Utilities and RTO/ISOs 67

5.5 Acknowledgments and Disclaimer 68

CHAPTER 6: Publications under this Award and References 69

6.1 Publications under this Award 69

REFERENCES 70

GLOSSARY 78

APPENDIX A: Detailed Results of PV Integration Study in Typical Power Systems A-1

APPENDIX B: Modeling of PV system in the Power Analytics' Power System Analysis Software B-1

LIST OF FIGURES

Figure 2.1: A map of the UCSD solar resource sites, showing proximity to the Pacific Ocean (left), and Interstate 5 (center) 10

Figure 2.2: Top hat wavelet ψt (solid line) and the scaled and translated wavelet ψj, τt (dashed line) (right) 10

Figure 2.3: Cumulative distribution function of SSs for block averages over 1-sec to 1-h at EBU2 for 2009 14

Figure 2.4: Moving averages of the clear-sky index, Kc, over various averaging intervals for EBU2 on August 22, 2009 15

Figure 2.5: Cumulative distribution function of 1-sec RRs and RRs of moving averages over various timescales 16

Figure 2.6: Means of all ramps at EBU2 in 2009 that were greater than 25% 18

Figure 2.7: Coherence spectra for EBU2 and each of the other 5 sites for July 31 through August 25, 2009 18

Figure 2.8: Clear-Sky Index (blue and green thin lines) and Wavelet Periodogram 20

Figure 2.9: Fluctuation Power Index 21

Figure 2.10: Polygons showing the footprints of the Ota City (left) and Copper Mountain (right) powerplants 25

Maps © Google Maps 25

Figure 2.11. GHI at 1-sec resolution at Ota City on October 12th, 2007, and at Copper Mountain on September 23, 2011 26

Figure 2.12: Correlations of wavelet modes for pairs of point sensors at Ota City (a) and Copper Mountain (b) on the test days 27

Figure 2.13. [top most plots] Clear-sky index timeseries, and [bottom 12 plots] wavelet modes for Ota City on the test day 28

Figure 2.14. Fluctuation power index (fpi) for the GHI point sensor (black), actual power output of Ota City (red), and simulated power output (blue line) 29

Figure 2.15. Point sensor GHI (black), powerplant area-averaged GHI (red), and simulated area-averaged GHI (red) for Ota City on the test day 30

Figure 2.16: Original Ota City neighborhood (labeled 1) 31

Figure 2.17: Extreme ramp rate distributions 32

Figure 2.18 33

Figure 2.19. Clear sky index values for the 60 seconds period with the highest change in irradiance 36

Figure 2.20. The normalized 30-second sequence of the clear sky index implemented in the Power Analytics software 38

Figure 2.21. Clear sky index extreme ramp values for a single cell and for a 1 MW PV array 41

Figure 2.22: Clear sky index ramp up rates for a single cell and for a 1 MW PV array 42

Figure 2.23: Sizing the storage unit to mitigate the effects of extreme irradiance ramp rates 43

Figure 3.1: Schematic Diagram of a photovoltaic inverter for Grid Connected Operation 46

Figure 3.2: Diagram of Basic Grid connected Photovoltaic System Operation 46

Figure 3.3 Generic Model of New Forms of Generation 47

Figure 3.4 The steady-state photovoltaic model 48

Figure 3.5: The developed photovoltaic cell 51

Figure 3.6: Building Photovoltaic Models in a Graphical User Interface 51

Figure 4.1: Transient Voltage Performance Parameters 61

LIST OF TABLES

Table 2.1: Probabilities of SSs larger than 10%, 25% or 50% at each timescale of block averages along with approximate number of occurrences per day 14

Table 2.2: Probabilities of RRs exceeding 0.1%, 1%, or 5% s^{-1} at moving average timescales along with approximate number of occurrences per day 17

Table 2.3: Nomenclature for GHI, simulated power output, and actual power output 26

Table 2.4. The clear sky index values shown in Figure 2.19 37

Table 2.5. The clear sky index values shown in Figure 2 39

Table 4.1.: Scenarios simulated for PV unit connected close to Power Substation (S); the PV unit power output is a function of irradiance/time provided by the user 54

Table 4.2: Typical Off-Nominal Frequency Operating Requirements 57

Table 4.3: Example of off-Nominal Voltage Performance, [24, 25, 26, 27, 23] 60

Table 4.4: WECC/NERC Disturbance-Performance Table of Allowable Effects on other Systems 61

Table 4.5: Suggested Voltage Fluctuations Limits, [23] 62

EXECUTIVE SUMMARY

The scope of this 18-month project was to develop the preliminary, publicly available modeling tools for high penetration scenarios of photovoltaics on a distribution feeder system. The University of California, San Diego partnered with Power Analytics (PA) to apply Power Analytics' modeling software using data from a network of sixteen densely spaced microclimate monitoring systems (>1 per 100 acres), a hemispherical sky imager, and a ceilometer modeled by the University of California, San Diego's. The goal was to develop a one-hour-ahead PV output forecasts and develop a scheduler/optimizer model that makes possible demand/load adjustments based on dynamic price signals.

The approach was for Power Analytics to develop and validate steady-state and dynamic models of PV systems based upon the most advanced information publicly available through a literature search. Both the steady-state power flow and short circuit models of a PV system were incorporated into Power Analytics' advanced modeling software. Both the models were then benchmarked against any available published work.

The steady-state models were supplemented with a PV system transient stability (time domain) model using Power Analytics' advanced transient stability program. The transient model is a dynamic model of a PV system which includes its protection and control using PA's Universal Control Logic Modeling and Simulation features. The inverter models are located on the Department of Energy High Penetration Solar Portal along with an explanation with the structure provided. The files can be accessed and downloaded at https://solarhighpen.energy.gov/open_source_inverter_models. Power Analytics will continue to present, promote and enhance the use of these and more PV inverter models in public forums and future High Penetration Solar industry events.

To validate the transient modeling work, the research team examined the performance of a PV system interconnected to the grid using a network model that corresponds to the Western Electricity Coordinating Council system. Different levels of PV penetration and a number of scenarios (peak system load, light load conditions, etc.) were examined. Based on these results, the research team developed planning guidelines for PV integration and the maximum safe penetration level. The impact of PV system integration on the power system reliability indices was examined for a typical distribution system using a composite (generation and transmission facility loss) system reliability analysis program.

In addition, UCSD derived a historical probabilistic ramp rate model from 1sec GHI data. This report summarizes how often an event with a given extreme ramp rate occurs. This information is incorporated into a modeling tool to allow the estimation how much load-following capacity or energy storage would be required to mitigate the effects of the extreme ramp rates. The modeling tool is provided at https://solarhighpen.energy.gov/wavelet_based_variability_model_wvm. The time series was mapped to a spatial field assuming a constant cloud advection velocity. In this way the analysis was interpreted for the averaged solar irradiance across a solar array of variable size.

Finally, the team consolidated this review and analysis into an open simulation application for power system designers and planners with a website and other relevant information provided. The Open Source Application Programming Interface (API) includes a Control Logic Model Library. This package provides any user the ability to assess maximum loading of solar PV on a distribution feeder (10 percent to 50 percent of the feeder's peak load demand) based upon power flow, short circuit and transient stability analyses and adherence to power system reliability indices.

The approach taken by the Power Analytics team in providing both a generic PV inverter model and specific PV models reflects the results of industry experience and reviewing existing open source and proprietary power modeling software. The existing power modeling software is diverse and extensive. Investment in existing models and modeling environments represents thousands and thousands of man hours invested in learning the modeling software and the creation of models. The legacy of the software and models presents a significant hurdle to the adoption of universal approaches to the challenges of modeling PV inverters. Within this baseline knowledge, Power Analytics focused on contributing open data that represents the greatest opportunity for integration with existing proprietary as well as open source power modeling software. The Power Analytics generic model is a non-proprietary subset of variables that should be readily available to any user or researcher based on published and name plate data for PV power inverters. Armed with this information, Power Analytics is also providing an example of how to integrate this into any power modeling environment familiar to the user. Power Analytics used Simulink® software as a generally accepted and broadly known example to integrate this data in modeling environments. This ability is for dynamic and static power modeling software. In addition, Power Analytics continues to work with research organizations and universities to advance and publish how to use this inverter data in a broad population of existing modeling environments to advance the goals of the Department of Energy High Penetration Solar initiative.

The Control Logic Model library provides a structure for loading, saving, and editing enhancements for new PV inverter models that can interact with each other. The modeling, simulation and reporting enhancements allow power system designers and planners to accurately assess the impact in the time domain of PV sources with respect to physical characteristics such as:

- rated power,
- total number of cells
- connection method,
- cell dimensions and area,
- cell technology (a vendor library),
- incident angle based on sun's azimuth and zenith angles,
- system efficiency rating in % with I-V plot support.

The critical accomplishments of Phase 1 are the following:

- An open-source inverter simulation file to be used by power system designers and planners to assess maximum loading of solar PV on a distribution feeder based upon power flow, short circuit and transient stability analyses and adherence to power system reliability indices.
- Models that incorporate statistical characterization of the frequency and magnitude of the extreme ramp rates on individual solar panels to model the geographic dispersion effects on variability through a fleet of PV systems or a large PV plant.
- Simulated measures demonstrating how to mitigate the impact of the solar resource's variability.
- These tools are open source and available for utilities and planners at the DOE High Solar Penetration Portal.

For American Recovery and Reinvestment Act reporting purposes, 3.64 FTEs were supported through this award.

CHAPTER 1: Introduction

As photovoltaic systems continue to gain a more significant share of the U.S. electricity generation mix, it becomes increasingly important to better understand the effects of integrating higher penetrations of PV on the reliability and stability of the electric power system. Evaluating the steady state and dynamic performance of PV generation technologies on the power system is very important since many utilities in the US are receiving an increasing number of requests for interconnection of PV plants. As pointed out in DOE's Funding Opportunity Announcement number DE-FOA-0000085 "High Penetration Solar Deployment" to accurately model the effects of high-penetration levels of PV on the system, analysis tools for distribution system planning must be upgraded with appropriate PV performance models, and the fidelity of modeling results must be validated using simulations and field data. A requirement of the new and improved distribution system tools is that they be capable of dynamically analyzing the interactions of all distributed generators on a feeder to satisfy anti-islanding needs, as well as their interactions with protection equipment, loads, demand response, and/or different types of energy storage under varying operating conditions. The goal of this 18-month project was to develop the needed modeling tools for high penetration scenarios of PV on distribution feeder systems. This work was supported through the American Recovery and Reinvestment Act.

A few important characteristics of PV generation that are notable as compared to other conventional generation technologies include:

- PV plants are composed of large numbers of panels spread out across a relatively large geographical area, as opposed to conventional generation plants where a single turbine is capable of generating the same order of magnitude of power.
- Variable nature of the power generated as a function primarily of cloud cover and time of day.
- The different PV generator technologies rely on power electronics causing a lack of inertia and active power spinning reserve (assuming no battery storage system).

These characteristics give rise to the need for modeling the variability of the fuel or solar resource as well as the power electronics that control the delivery of the power to the grid. Consequently, the project objectives are to

- Develop simulation tools for distribution feeder design by power system designers.
- Characterize PV output variability over space and time and how it relates to aggregate variability for many PV systems on a distribution feeder.
- Reduce integration costs and remove barriers to high PV penetration.

The research team consists of prime contractor UC San Diego and subcontractor Power Analytics. UC San Diego is responsible for the overall project management and the modeling and forecasting of the solar resource. Power Analytics is responsible for developing power engineering models for advanced modeling of PV system impacts on the electric distribution system.

This report will describe in detail the goals of the work, the approach, significant accomplishments and future plans. The work is divided into two tasks, each the responsibility of one of the partners in the research team. The objective of Task 1 was for Power Analytics to apply advanced "mission critical" power analytics for development and validation of steady state and dynamic models of PV systems, and this work is presented in Chapter 3. Specific subtasks included the development of a power flow (steady-state), a short circuit (steady-state), and a transient stability (time domain) model of the PV System. Finally the PV system models are applied in a PV integration study which is described in Section 4. The objective of the integration study is to analyze the impact of different PV penetration levels and configurations onto bus voltages, energy losses, short circuit, security, and reliability. Planning guidelines and interconnection criteria for integrating PV generation into the power systems (transmission and distribution) are presented. Detailed system impact studies on several typical power systems related to PV plant interconnections are presented in Appendix B.

As part of the effort to establish a valid and accurate PV variability model (Task 2), in Section 2 spatial and temporal characteristics of irradiance fluctuations at a point are examined by the UC San Diego team. Based on the data analysis a model is developed to predict aggregate PV variability for any configuration of distributed or central PV systems. In addition, characteristic irradiance time series are developed for input to the power flow analysis. The enhanced irradiance models and their integration into existing distribution system planning and engineering analysis tools should improve analysis capabilities for high PV penetration.

Since the two tasks are distinct, the major conclusions and significance of the findings are provided separately in each section. Section 5 discusses the proposed follow-on work.

CHAPTER 2: High-Frequency Irradiance Fluctuations and Geographic Smoothing

After summarizing the existing literature (Section 2.1.), spatial and temporal characteristics of irradiance fluctuations are reviewed in Sections 2.2 to 2.4. Based on the data analysis a wavelet variability model is developed to predict aggregate PV variability for any configuration of distributed or central PV systems (Section 2.5). The model is applied to two real cases in Section 2.6 and conclusions are presented in Section 2.7. In addition, characteristic irradiance time series are developed for input to the transient power flow analysis as described in Section 2.8. The enhanced irradiance models and their integration into existing distribution system planning and engineering analysis tools should improve analysis capabilities for high PV penetration.

2.1 Problem Statement and Literature Review

As PV gains higher and higher penetration, it is important to understand the fluctuations or ramp rates in PV output on various timescales, as well as the potential for geographic dispersion to dampen these fluctuations. For example, when the marine layer clouds cover coastal California with all its distributed PV systems there is little solar output but also little variability. In completely clear skies the solar output is high, and the variability is also small. Sunny days with scattered clouds have been a concern for utilities, because then the output of individual solar systems fluctuates dramatically. Our modeling tools will make it easier for utilities managers to consider the reduced variability effects on feeders and avoid unnecessary investments in infrastructure.

The variable nature of solar radiation is a concern in realizing high penetrations of solar photovoltaics (PV) into an electric grid. High frequency fluctuations of irradiance caused by fast moving clouds can lead to unpredictable variations in power output on short timescales. Short-term irradiance fluctuations can cause voltage flicker and voltage fluctuations that can trigger automated line equipment (e.g. tap changers) on distribution feeders leading to larger maintenance costs for utilities. Given constant load, counteracting such fluctuations would require dynamic inverter reactive power control or a secondary power source (e.g. energy storage) that could ramp up or down at high frequencies to provide load-following services. Such ancillary services are costly to operate, so reducing short-term variation is essential. Longer scale variations caused by cloud groups or weather fronts are also problematic as they have been shown to lead to a large reduction in power generation over a large area. These long-term fluctuations are easier to forecast and can be mitigated by slower ramping (but larger) supplementary power sources, but the ramping and scheduling of power plants also adds costs to the operation of the electric grid. Grid operators are often concerned with worst-case scenarios, and it is important to understand the behavior of PV power output fluctuations over various timescales.

Previous studies have shown the benefit of high-frequency irradiance data. For example 1-min averaged irradiance data were shown to have a more bi-modal (one mode for cloudy times and

one for clear times) distribution than 1-hour or 1-day data [1],[2]. Further studies have characterized high frequency fluctuations, often by comparing fluctuations at one site to fluctuations at the average of multiple sites. For example in the study by Otani et al. (1997), a fluctuation factor defined as the root mean squared (RMS) value of a high-pass filtered 1-min time series of solar irradiance was used to demonstrate a 2-5 times reduction in variability when considering 9 sites located within a 4 km by 4 km grid [3]. 1-min timeseries showed reductions in the mean, maximum, and standard deviation of ramp rates (RRs) when considering the average of three or four sites versus only one site[4],[5]. Power spectral densities (PSDs) also showed strong reductions in power content of fluctuations of the average of multiple sites versus the power content of fluctuations at one site[3],[4],[5]. Coherence spectra showed that sites in Colorado which were 60 km or more apart were uncorrelated on timescales shorter than 12-hours. Two sites that were only 19 km apart were uncorrelated on timescales shorter than 3-hours [5].

1-min power data from 52 PV systems spread across Japan was analyzed to determine the "smoothing effect" of aggregating multiple systems [6]. The authors introduce a fluctuation index, which is the maximum difference in aggregated power output over a given time interval. They found that over 1-min, sites more than about 50-100 km apart were uncorrelated and thus that there was a limit reached whereby adding more PV sites had no effect on reducing variability, since the variability introduced by the diurnal cycle eventually becomes larger than the cloud-induced variability. For times greater than 10-min, however, they reject the hypothesis that sites within 1000 km are independent, though some of the dependence may be due to diurnal solar cycles and could be eliminated by using a normalized solar radiation.

All these studies have indicated that mathematical modeling can assist in the analysis of the impacts of solar variability. For example, Hoff and Perez (2010) derived that reduction in standard deviation is a function of the number of PV sites and a dispersion factor, D, defined as the number of time intervals it takes for a cloud to pass over all PV sites across the region being considered [7]. The dispersion factor is useful in determining when the transition from PV sites being uncorrelated to correlated occurs. For example, standard deviation of power output of the average of N sites decreases by a factor of $\sqrt{N}$ compared to the standard deviation of one site for the "spacious region," where the number of sites is much less than the dispersion factor, $N < D$. If the number of sites is larger than the dispersion factor, $N > D$, the standard deviation will be reduced by a factor of D, since the sites are at least partially dependent. A limited model validation was performed by simulating a fleet of PV systems based on measured irradiance at only one site using frozen cloud advection. In another study, Woyte et al. (2007) used very high frequency data (1-sec, 5-sec, or 1-min depending on the site) collected for up to 2-years, an instantaneous clearness index, and a wavelet transform to analyze fluctuations of all scales in time. Woyte et al. (2007) introduce a fluctuation power index, which is the sum of the square of the wavelet mode at each timescale, and is used to quantify the amplitude and frequency of occurrence of fluctuations on a specific timescale.

The research team will apply the approach of Woyte et al. (2007) to characterize variability and further expand it to obtain a variability model. The variability results will be compared against the framework of Hoff and Perez (2010). Since the analysis in this report is based on real data

the assumption of Hoff and Perez (2010) can be avoided. In this work 1-sec clear-sky index (K_c) data from 6 sites on a microgrid similar to urban distribution feeders (Section 2.2) is analyzed to quantify extreme ramp rates (RRs). Methods are described in Section 2.3. RRs were analyzed by computing statistics at different time steps and by using varying moving average intervals to represent large PV plants or storage (Section 2.4.1). Coherence spectra are employed in Section 2.4.2 to analyze the correlation between six sites at different time scales. A wavelet is applied to detect variability over various timescales relevant to the operation of a power grid (Section 2.4.3). Wavelet analysis allowed for a localized study of the power content of variations over various timescales. The power content of variations at one site was compared to the power content of variations at the average of six sites in close proximity to study the reduction in variability over various timescales achieved by using multiple site locations (Section 2.4.4).

2.2 Data Collection

Global Horizontal Irradiance (GHI) was recorded once per second at six sites throughout the University of California, San Diego (UCSD) campus ([9], Fig. 2.1). The sites are abbreviated in the following using four-letter acronyms as EBU2, MOCC, HUBB, RIMC, TIOG, and BMSB. All sites employ a LICOR Li-200SZ silicon pyranometer sampling at 1Hz. The collection of 1-sec data proved to be a challenge of both data storage on the data logger and sensor reliability, and so data availability is inconsistent. While there are 8 sites maintained, at any given time a maximum of 6 sites recorded 1-sec data. The main site was the Engineering Building Unit II (EBU2, 32.8813^{0}N, 117.2329^{0}W), for which data was available for all of 2009 (1-year dataset). Five other sites also recorded data from July 31 to August 25, 2009 (1 month dataset), and are used to study the benefits of aggregating sites (Fig. 2.1).

After applying the pyranometer factory calibration, clear days were used (assuming identical atmospheric composition) to create linear fits against RIMC, and each site was cross-calibrated by this linear fit. In addition, careful quality control was carried out by visually examining each site for shading and other errors. To eliminate the deterministic effect of diurnal cycles, a dimensionless clear-sky index was computed by dividing the measured GHI by the clear-sky irradiance from the sunny days model ([10]) based on Long and Ackerman (2000). The sunny days model uses input GHI and diffuse horizontal irradiance (DHI, measured by a Dynamax SPN1 pyranometer) to calculate clear-sky irradiance. Times when the solar altitude angle was less than 10° were removed to eliminate both night time and early morning and late evening periods when the pyranometer is subject to errors in cosine response.

The clear sky index provides the best measure to compared cloud induced solar variability analyses between different sites. It should be noted that if the occurrence of clouds is independent of TOD, the clear sky index also provides the most relevant measure to characterize solar energy variability at a site, especially for 2D tracking power plants (whose output fluctuates less over a clear day). However, if clouds occur preferentially over certain TODs and a fixed-tilt plant is considered, then clear sky index variability does not translate directly to power output variability of a PV plant and analysis of variability should be conducted also as a function of TOD.

Figure 2.1: A map of the UCSD solar resource sites, showing proximity to the Pacific Ocean (left), and Interstate 5 (center)

From EBU2, distances and headings are: BMSB(0.69km, 205^0), HUBB (2.47km, 230^0), MOCC (0.95km, 105^0), RIMC (0.80km, 300^0), and TIOG (1.00km, 255^0).

Map © 2010 Google – Image © 2010 TerraMetrics

Figure 2.2: Top hat wavelet $\psi(t)$ (solid line) and the scaled and translated wavelet $\psi_{j,\tau}(t)$ (dashed line) (right)

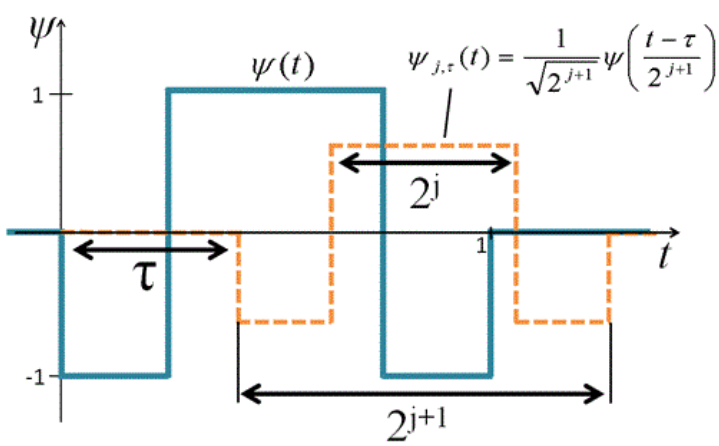

This scaled wavelet would capture a clear period of duration 2^j bordered by cloudy periods.

2.3 Methods for Variability Analysis

Several methods to quantify variability were studied. First the variability as a function of time and averaging period was studied for a single site. Then geographic smoothing or the reduction of variability from one site to six sites was quantified using coherence spectrum and wavelet approaches. The coherence spectrum is instructive to quantify correlations at different time

scales, but the wavelet approach is more mathematically correct and lends itself to modeling variability. The different approaches are described in the sections below.

2.3.1 Ramp Rate Analysis at One Site Over One Year

The frequency of occurrence and magnitude of RRs of solar PV are of critical interest to power system operators. From the 1-sec clear-sky indices one can extract two different averages which have different practical relevance.

First, *block* averages were taken on time intervals varying from 1-sec to 1-hour, which shows the difference in statistics over various data averaging intervals. Typically irradiance or power output data are averaged over longer periods and the analysis allows comparison to such data. The block average method produces fewer data points as the block size increases.

Second, *moving* averages over intervals of $T = 2^j$ sec ($j = 1,2, \ldots 12$ corresponding to $T = 2,4, \ldots 4096$ sec) were computed at time steps of 1-sec such that the average at any given time, t, is the average of values $(2^j - 1)$ seconds before and 2^j seconds after t. Intervals of 2^j seconds were chosen to be consistent with wavelet analysis presented later. Moving averages at different T are representative of power sampled every second, but averaged spatially over the dimensions of a solar power plant or by using energy storage.

From either the block average or the moving average, RRs were computed as the difference between successive clear-sky indices. Cumulative distribution functions (cdf) of RRs show the statistical distributions and extreme values. RRs of clear sky indices give the percent change (as a fraction of clear-sky irradiance) over one timestep, regardless of the time-of-day (TOD) when that change occurred.

2.3.2 Geographic smoothing at six sites over one month

Several factors are included in geographic smoothing and are described below.

A) Coherence spectrum: As a measure of spatial correlation of the clear-sky index over various time scales, the coherence spectrum between EBU2 and the other 5 sites was calculated. The coherence spectrum provides normalized covariance at each frequency, allowing for visualization of correlation over various timescales. The coherence is expected to be large at long timescales as large weather systems will lead to similar clear-sky indices for all the sites. Note, however, that solar cycles have been removed by using the clear-sky index and thus the coherence will not be as large as if irradiances had been used. The timescale at which sites become weakly correlated is an indication of the longest timescale on which the sites are nearly independent and will dampen aggregate variability. Although negative correlation would reduce variability more than zero correlation, negative correlation is not expected physically.

B) Wavelet analysis: The stationary or dyadic wavelet transform, W, of a signal $x(t)$ is

C) $$W_{2^j}^{\tau} = \int_{-\infty}^{\infty} x(t) \frac{1}{\sqrt{2^{j+1}}} \psi\left(\frac{t-\tau}{2^{j+1}}\right) dt \qquad (1)$$

where t is time, τ is the time offset from the beginning of the day, ψ is the wave used to produced the wavelet transform, and s is the scaling factor. Although typically in wavelet analysis $s = 2^j$ is used in Eq. 1, $s \equiv 2^{j+1}$ was defined instead. This altered definition allows for the timescale, 2^j seconds, to describe the duration of the clear or cloudy period of interest rather than the duration of the entire wavelet.

Using a real wavelet and a discrete transform requires that j be a positive integer. The Haar wavelet [11] was found to be lacking in that large wavelet coefficients exist only at sharp signal transitions. This means that changes from one state to another (e.g. a step from cloudy to clear) are detected by the Haar wavelet rather than the duration of an up or down fluctuation (a top hat). Instead the top hat wavelet was employed as the basis function (Figure 2.2). Substituting the clear-sky index, $x(t) = K_c(t)$, into Eq. 1 will result in a separate timeseries $w_j(\tau)$ for each j value (mode), where $w_j(\tau)$ is defined such that

$$W_{2^j}^{\tau} = \sum_{j=1}^{12} w_j(\tau) \quad . \tag{2}$$

Just as for the moving averages, the analysis was limited to $j \leq 12$ (corresponding to 1.1 hours or less), and only τ values for which data were available over the entire interval of size 2^{j+1} around τ were retained. As such, early morning and late evening periods are not resolved at the longer modes.

The power content of each timeseries $w_j(\tau)$, which is the variance at each timescale, can be found by calculating the wavelet periodogram I. Following the definition of the Fourier periodogram, the wavelet periodogram is the square of the coefficients of the wavelet transform, normalized by the length over which the wavelet was applied, which in this case is 2^{j+1}:

$$I_{2^j}^{\tau} = \frac{1}{2^{j+1}} \left| W_{2^j}^{\tau} \right|^2. \tag{3}$$

Application of wavelet analysis to determine reduction in variability from averaging 6 sites: The wavelet periodograms are still timeseries, and are difficult to examine visually for periods longer than one day. Therefore, the 'fluctuation power index,' [11] was used to quantify the power contained in fluctuations at each timescale. The fluctuation power index, fpi, is:

$$\text{fpi}(j) = \frac{1}{T_j} \int_0^{T_j} I_{2^j}^{\tau} d\tau, \tag{4}$$

where T_j is the length of the timeseries $I_{2^j}^{\tau}$, which decreases as j increases due to unresolved periods of the higher modes. Using T_j instead of a constant value based on the length of the original $K_c(t)$ timeseries means that fpi(j) is an average value, which allows for comparison of fpi at different j values.

Since fpi represent variance at each timescale, fpi was used to evaluate the reduction in variability achieved by averaging six sites versus the variability at EBU2 alone. The results were compared to the model by Hoff and Perez (2010, hereinafter HP10) who define a dispersion factor $D = \frac{L}{V\,T}$, where L is the length of the region with the PV sites, V is the cloud velocity, and T is the relevant timescale. Although L and V remain constant for a given area and time, varying

the timescale over which the fpi is computed changes D allowing testing of the HP10 model over various dispersion factors for the 1-month data.

2.4 Results of the Variability Analysis

The results of the modeling analysis are presented in this section for the ramp rates at a single site (Section 2.4.1) as well as the geographic smoothing effect of several sites (Section 2.4.2).

2.4.1 Ramp Rate Analysis at One Site

The cumulative distribution function (cdf) of the absolute value of step sizes (SS) for K_c averaged over blocks of 1-sec, 10-sec, 1-min, 10-min, and 1-hr simulating data averaged over, and sampled at those intervals, are shown in Figure 2.3. The probability of occurrence of SSs greater than 5%, 10%, and 25% are shown in Table 2.1. Both Fig. 2.3 and Table 2.1 show SS statistics vary significantly over all timescales, which is consistent with previous findings that 1-min and 1-hr data have different statistics (i.e., [1] and [2]). These variations in statistics of SSs down to 1-sec show the importance of sampling data as frequently as possible when studying irradiance fluctuations. Large step sizes have a much greater probability of occurring when using 1-hr averages than when using 1-sec averages. However, due to the nature of block averaging, at longer time intervals, the sample size is small and events with high probabilities of occurrence do not happen very often in a day (Table 2.1). Still, the cdf of SSs shows a trend toward SS magnitude decreasing as the averaging time decreases. Bottom line, as the data analysis verified and common sense would indicate, short-time steps will not be as extreme as long-time steps.

Figure 2.3: Cumulative distribution function of SSs for block averages over 1-sec to 1-h at EBU2 for 2009

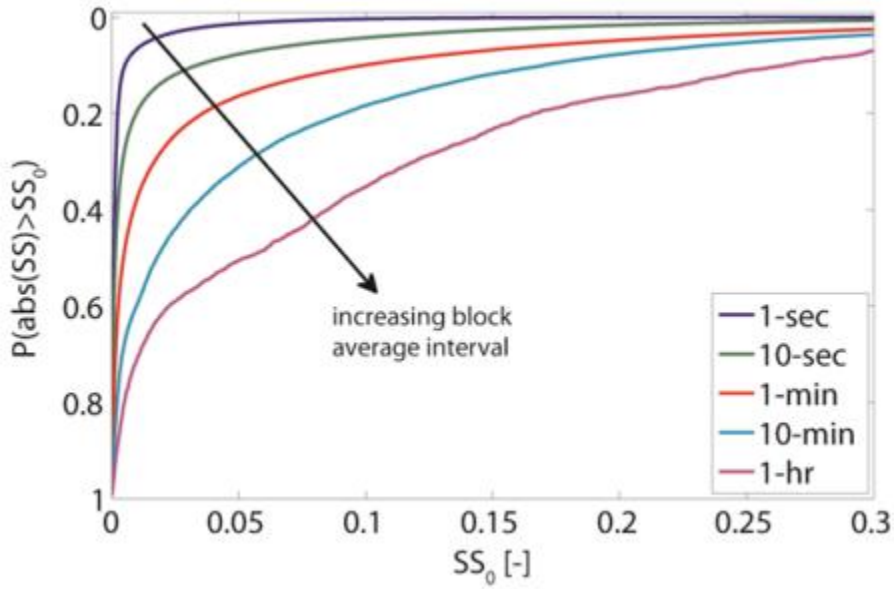

Instructions for how to read this figure: The probability of occurrence of a certain SS (or larger SSs) can be determined by locating the SS on the *x*-axis and going up to intercept the line of the desired block averages. The *y*-value at that point provides the probability. For example, a 25% SS for 1-h block averages occurs 11% of the time or about once per day, on average. The 1-hr curve appears less statistically converged than the other curves. This is due to the fewer 1-hr intervals contained in 1-year of data versus other, shorter timescales (i.e., there are 6x more 10-min data points over 1-hr data points).

Table 2.1: Probabilities of SSs larger than 10%, 25% or 50% at each timescale of block averages along with approximate number of occurrences per day

Block average interval	abs(SS)>0.10		abs(SS)>0.25		abs(SS)>0.50	
	P(abs(SS)>0.10)	#/day	P(abs(SS)>0.25)	#/day	P(abs(SS)>0.50)	#/day
1-sec	0.37%	132	0.02%	6.3	0.0002%	0.1
10-sec	4.29%	155	1.07%	38.4	0.10%	3.5
1-min	9.96%	59.8	3.48%	20.9	0.63%	3.8
10-min	18.39%	11.0	5.26%	3.2	0.85%	0.5
1-hr	35.22%	3.5	11.23%	1.1	0.91%	0.1

Occurrences per day were found using an estimated annual average of 10-hours per day when solar altitude angle is greater than 10^0

While block averages represent sampling data at certain periods where the actual variability is unaffected, moving averages can be used to simulate the effects of fast-ramping energy storage (e.g. flywheels or capacitors). Moving averages are also relevant to simulating power output of

a large PV array or a fleet of PV sites that all sit along the cloud motion vector and are spaced such that there is perfect correlation (with a time shift equal to the moving average time interval) between successive PV panels (or inverters). In this case, a longer moving average interval will simulate the output of a larger PV plant, since large systems will ideally average over a timescale of $A^{1/2} / V$, where $A^{1/2}$ is the square root of the area of the array and V is the cloud velocity. Moving averages at various timescales are shown in Figure 2.4 for August 22, 2009.

Figure 2.4: Moving averages of the clear-sky index, K_c, over various averaging intervals for EBU2 on August 22, 2009

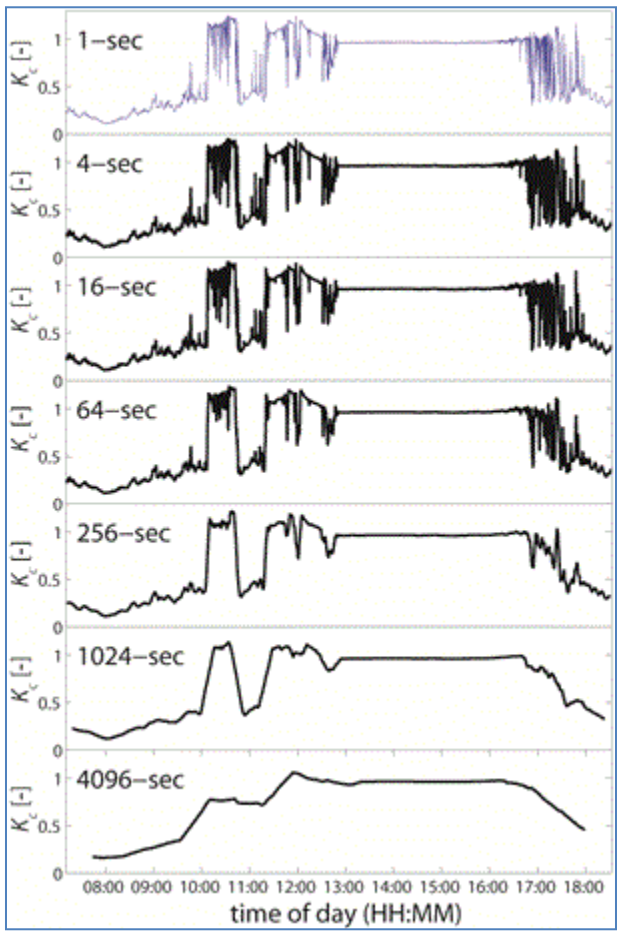

The cdf of RRs for various moving averages is shown in Figure 2.5, and specific values are shown in Table 2.2. For the moving averages, increasing the averaging time decreases the probability of a large ramp. For example, for a 4096-sec (about 1-hour) moving average, the probability of a ramp larger than 0.1% s^{-1} is zero. This is intuitive, since the change in the moving average is the change in the step size divided by the averaging interval. Since a 1-sec average under both the block and moving averages simply represents the original timeseries, the 1-sec cdf which appears in both Figures 2.3 and 2.5 and Tables 2.1 and 2.2 serves as a reference for comparison between the two averaging methods. To create the power plant size

column Table 2.2, it was assumed that the 1-sec data was representative of the fluctuations of a typical household PV installation of 2.5kW. Then, using the $A^{1/2}$ / V relation mentioned earlier, the relationship between moving average intervals and PV plant sizes was determined. This assumed a frozen cloud field traveling at a constant speed, V, over the entire PV plant. While this is unlikely physically, it givens an indication of the best-case scenario and allows for a comparison of fluctuations over various PV plant sizes. This is a useful and simple starting tool, illustrating what ramp rates that can be expected for different power plant sizes based on measurements from a point sensor. The analysis in Section 2.4.3 will consider six point sensors illustrating how ramp rates behave over space and time.

Figure 2.5: Cumulative distribution function of 1-sec RRs and RRs of moving averages over various timescales

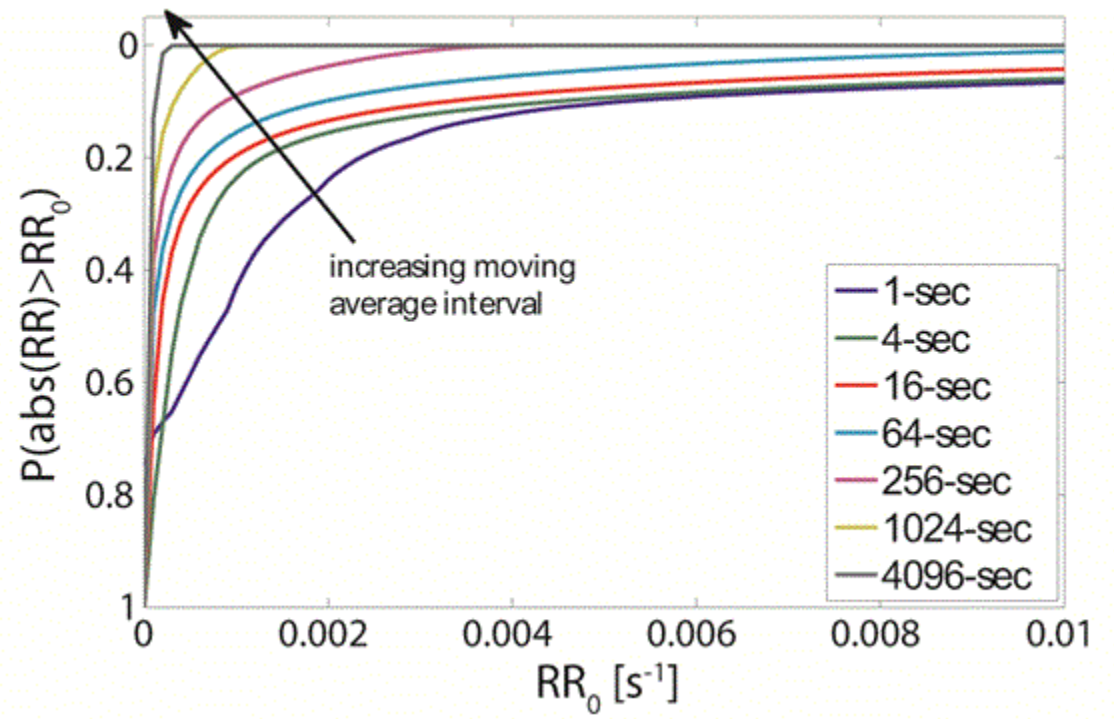

Cumulative distribution function of 1-sec RRs and RRs of moving averages over various timescales (representing large PV plants or plants with energy storage) at EBU2 for 2009. The 1-sec value at $RR_0 = 0$ is 0.75 and not 1.0 due to the very small changes that can occur over 1-sec resulting in $RR < 0.0001$. For all other timescales, $RRs < 0.0001$ never occur.

Table 2.2: Probabilities of RRs exceeding 0.1%, 1%, or 5% s^{-1} at moving average timescales along with approximate number of occurrences per day

Moving average interval	Power plant size	RR>0.001 s^{-1}		RR>0.01s^{-1}		RR>0.05 s^{-1}	
		P(RR>0.001)	#/day	P(RR>0.01)	#/day	P(RR>0.05)	#/day
1-sec	2.5 kW	42.98%	15,472	6.55%	2,359	1.35%	486
4-sec	40 kW	23.57%	8,486	5.90%	2,125	0.81%	292
16-sec	640 kW	19.53%	7,031	42.98%	1,511	0.04%	15
64-sec	10.2 MW	15.46%	5,564	1.03%	370	0%	0
256-sec	164 MW	8.84%	3,181	0%	0	0%	0

Occurrences per day are based on a 10 sunlight-hour day.

In order to examine the typical behavior leading up to and after the largest 1-sec ramps, Figure 2.6 displays the mean (or conditional average) of all 1-sec ramp events greater than 25%, separated into positive and negative ramps. An 'ideal' ramp would simply be a step function from a small K_c to a large K_c or vice versa. However, in practice K_c is variable before or after large ramps. This is because the clear or cloudy period before or after the ramp is often shorter than one minute. For the negative (or clear to cloudy) ramp, there is successive enhancement in clear-sky index in the 1-min before the ramp. This is a manifestation of short clear periods but also of cloud edge enhancement; as a cloud nears the path between the sun and the sensor, some sunlight is reflected off the near edge of the cloud and down to the sensor, while the sun-sensor path is mostly unobstructed. Cloud enhancement leads to irradiances larger than the clear-sky model due to additional diffuse irradiance, resulting in a clear-sky index greater than 1 (Fig. 2.6). A similar but opposite behavior is observed for the up-ramp. The change in mean clear-sky index from one minute before a large negative ramp to one minute after is about 10%. This indicates a change of state from clear to cloudy. For large positive ramps, this change is only about 3%, and so represents a much smaller change in average state of the sky.

Figure 2.6: Means of all ramps at EBU2 in 2009 that were greater than 25%

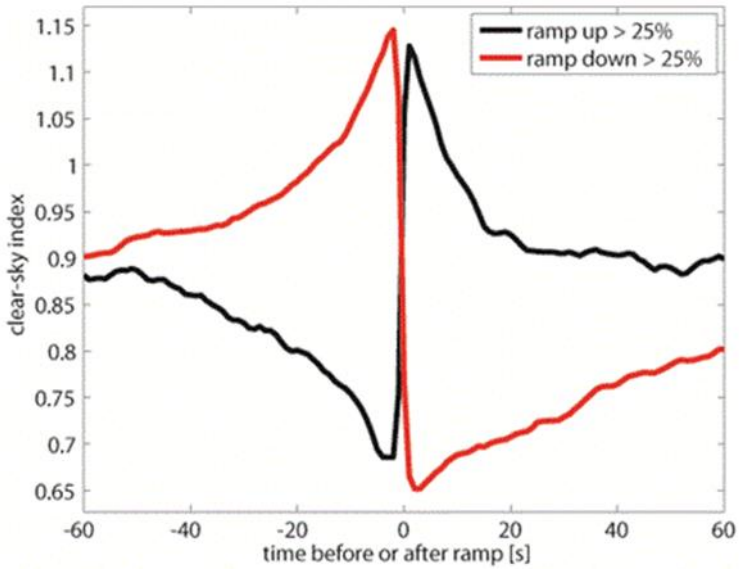

Means of all ramps at EBU2 in 2009 that were greater than 25%, separated into positive and negative ramps. The red line shows the mean of 1006 timeseries starting 1-min before and ending 1-min after a ramp that was more than a 25% s-1 decrease in clear-sky index. The black line shows the mean of 511 such timeseries that were centered around a greater than 25% s-1 increase in clear-sky index.

Figure 2.7: Coherence spectra for EBU2 and each of the other 5 sites for July 31 through August 25, 2009

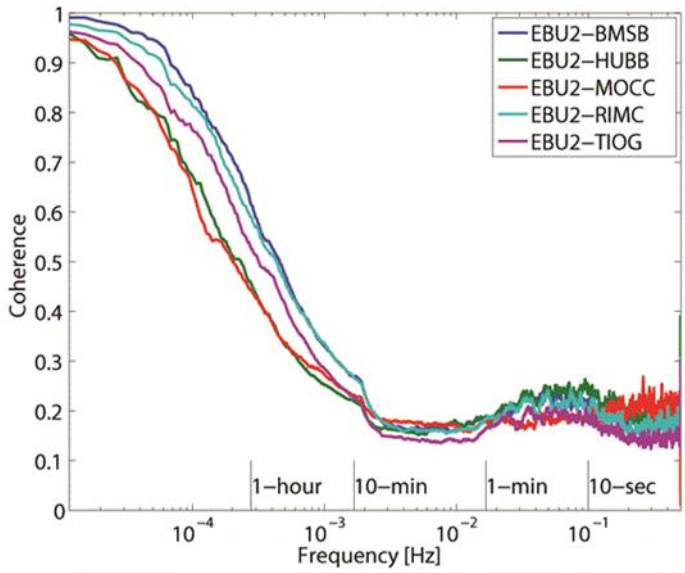

Coherence spectra for EBU2 and each of the other 5 sites for July 31 through August 25, 2009. Each spectrum is smoothed by a moving average smoothing filter for clarity. Different time scales are marked through vertical lines.

Over the entire year at UC San Diego (Jan – Dec 2009) there were five 1-sec ramps up (probability of 2.1×10^{-7} s^{-1}) and 17 1-sec ramps down (probability of 7.3×10^{-7} s^{-1}) with magnitudes greater than 50%. The maximum up ramp was 58% s^{-1} and maximum down ramp was 59% s^{-1}. Thus, as an absolute worst case scenario for this data set, a maximum change of 60% over 1-sec can be assumed. The worst irradiance fluctuations were 432 W m^{-2} for an up ramp (June 5, 14:01:42) and 516 W m^{-2} for a down ramp (April 15, 13:33:42), which corresponded to 45% and 54% clear-sky index ramps, respectively. It has to be emphasized, however, that this applies only for one point sensor, and when sites are averaged or PV arrays are considered, these maximum ramps are strongly reduced.

2.4.2 Coherence Spectra

The coherence spectra over 1-month between EBU2 and the other 5 sites are shown in Fig. 2.7. At long timescales (several hours), the coherence spectra all approach 1. This is expected since hourly and longer weather phenomena such as changes in synoptic cloudiness and atmospheric composition changes affect all sites. Since the coherence spectra were calculated using clear-sky indices, the spectra do not approach 1 as quickly as would be expected with irradiances since the daily cycle of the sun rising and setting is (mostly) removed. The sites are uncorrelated (coherence near zero) for time scales shorter than 10 min. BMSB, RIMC, and TIOG have the highest coherence values against EBU2 at long timescales. HUBB has lower coherence due to it being at the coast and more than twice as far away from EBU2 than the other sites. MOCC (~1km east-south-east) and TIOG (~1km west-south-west) are almost the same distance away from EBU2, albeit in nearly opposite directions, and yet the coherence spectra for each is markedly different. This indicates different weather patterns to the west of EBU2 as to the east. Anecdotal sky observations have confirmed that clouds often evaporate as they move eastward which would result in a smaller coherence.

2.4.3 Wavelet Decomposition

Wavelet periodograms were computed from the clear-sky index for EBU2 as well as from the clear-sky index for the average of 6 sites for each timescale, $j = 1$ to 12 for the month when 6 sites were simultaneously available. The periodograms from August 22, 2009 over modes $j = 6$ (about 1-min) to $j = 12$ (about 1-hr) are shown in Fig. 2.8. August 22 was chosen because it has both cloudy and clear periods and because it has a distinct clear period followed by a distinct overcast period both lasting about 30-min. This serves as a validation of the application of top-hat wavelets, as this period would be expected to produce two peaks at the $j = 11$ mode (34-min). Indeed, the most distinct peaks in the wavelet periodogram shown in Fig. 2.8 are on the $j = 11$ mode, and occur at about 10:30 and 11:00. The periodogram also shows that the dominant timescale of fluctuations between 16:30 and 18:00 was 256-sec ($j = 8$). This was not obvious by inspecting the original timeseries, but rather is a useful result found through wavelet decomposition.

Inspection of the wavelet periodogram shows that the amplitude is only slightly reduced for the average versus EBU2 at high modes ($j \geq 10$), but the average amplitude is much smaller at modes corresponding to shorter timescales. Since the amplitude of the periodogram at each

scale is the variance at that scale, this allows quantifying how averaging multiple sites will lead to a stronger reduction in variability at shorter timescales.

Figure 2.8: Clear-Sky Index (blue and green thin lines) and Wavelet Periodogram

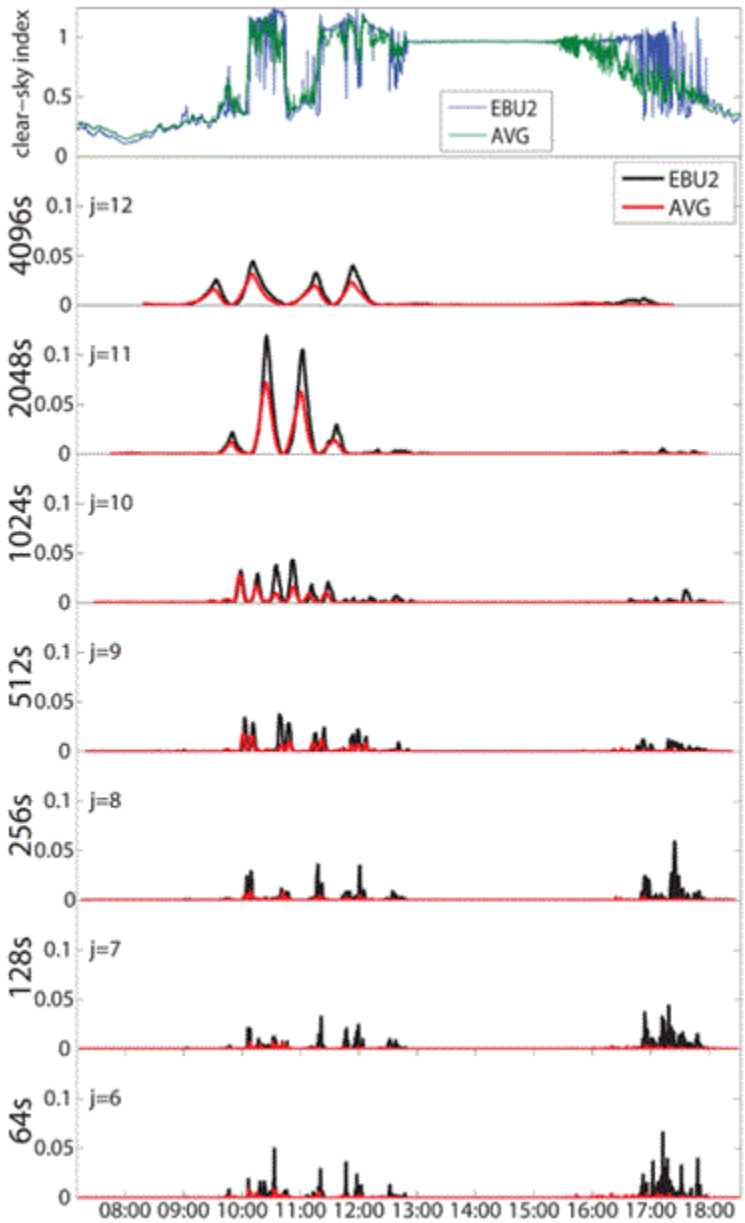

Clear-sky index (blue and green thin lines) and wavelet periodogram (black and red thick lines) of modes j=6 through j=11 for EBU2 and the average of all 6 sites on August 22, 2009.

2.4.4 Fluctuation Power Index

The reduction in variability as a function of timescale due to averaging sites for the 1-month period is shown in Figure 2.9, by plotting the fpi for each timescale. Figure 2.9 also shows the

ratio fpi_{EBU2}/fpi_{AVG}, which will be called the variability ratio (VR), for each timescale. The VR is a measure of the reduction in the power (or variance) of fluctuations. A higher VR means a larger reduction in fluctuations, while a variability ratio of 1 means no reduction in variability compared to a single site. For timescales shorter than 256s (about 4-min), VR was close to 6 for the average of the 6 sites. This is consistent with the factor of 6 reduction in variance that one would expect for 6 sites spread far enough apart such that their clear-sky indices can be considered independent of one another (or uncorrelated). At timescales longer than 128s, the fpi ratio decreased in an exponential fashion as the sites become more and more correlated. Eventually, at 4096-sec, the VR was nearly one, indicating that on timescales longer than 1-hour, the clear-sky indices at these 6 sites are too correlated to cause significant reductions in variability.

Figure 2.9: Fluctuation Power Index

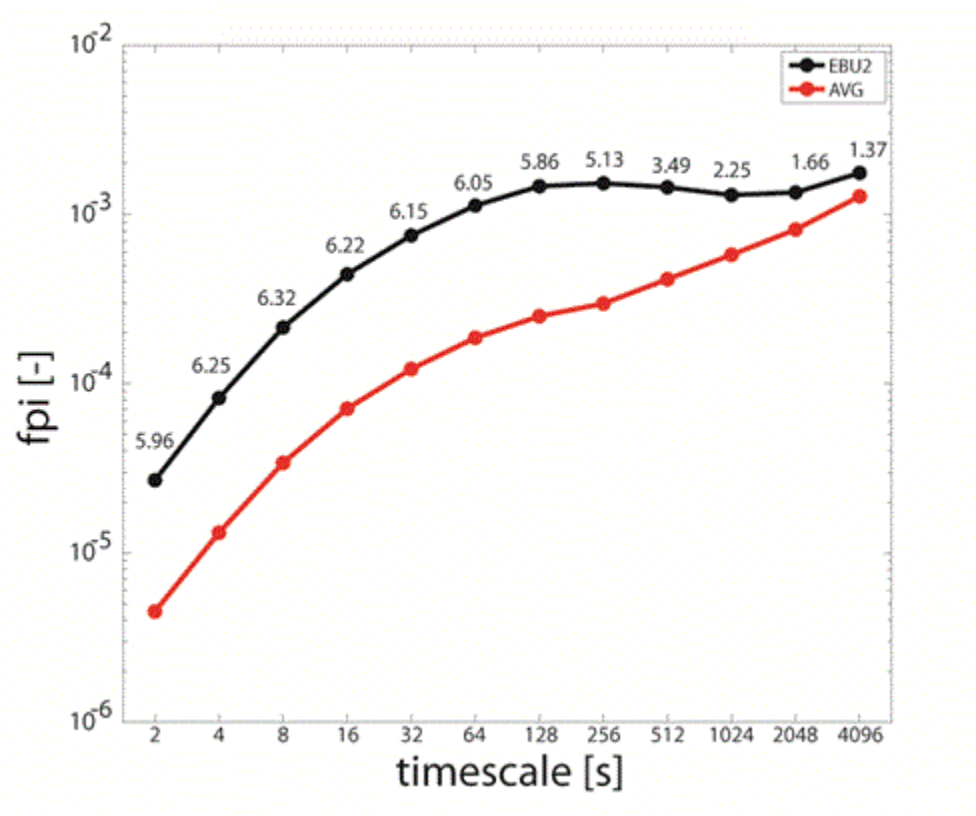

Fluctuation power index for EBU2 and the average of 6 (AVG) sites over 1-month. The numbers above the EBU2 black line are the ratio of fpiEBU2/fpiAVG for each timescale.

2.5 A Wavelet Variability Model (WVM)

In this section based on the results of Sections 2.4.2 and 2.4.3, a wavelet variability model (WVM) will be defined and discussed. Each step of the model will be discussed in the following sections and the derivation and significance of each described. These include wavelet decomposition, distances, correlations, variability reduction, simulation of wavelet modes of

power plant, and convert to power output. Finally, the model will be applied to irradiance and power output measurements in Section 2.6.

A wavelet variability model (WVM) is proposed for simulating power plant output given measurements from only a single irradiance point sensor by determining the geographic smoothing that will occur over the area of the plant. The simulated powerplant may be made up of either distributed generation (i.e., a neighborhood with rooftop PV), centrally located PV as in a utility-scale powerplant, or a combination of both. In the WVM, a statistically invariant irradiance field both spatially and in time over the day is assumed. Furthermore the correlations between sites are assumed to be isotropic – that is, they depend only on distance, not direction. The main steps to this procedure are:

1) Apply a wavelet transform to the clear-sky index of the original irradiance timeseries, creating wavelet modes $w_{\bar{t}}(t)$ at various timescales, $\bar{t}$.
2) Determine the distances, $d_{m,n}$, between all pairs of sites in the PV powerplant; $m = 1, \dots, N$, $n = 1, \dots, N$.
3) Determine the correlations, $\rho(d_{m,n}, \bar{t})$, between the irradiances all sites in the plant at timescales corresponding to wavelet modes.
4) Use the correlations to find the variability reduction, $\mathrm{VR}(\bar{t})$, at each timescale.
5) Divide each mode of the wavelet transform by the VR corresponding to that timescale to create simulated wavelet modes of the entire power plant. Apply an inverse wavelet transform to create a simulated clear sky index of area-averaged irradiance over the whole powerplant, $< GHI_{norm}^{sim} >_{pp} (t)$.
6) Convert this area-averaged irradiance into power output, $P(t)^{sim}$.

2.5.1 Wavelet Decomposition

The input point sensor timeseries is decomposed into its components at various timescales by using a wavelet transform. To obtain a stationary signal, the irradiance timeseries from the point sensor is normalized such that output during clear conditions is

$$GHI_{norm}(t) = GHI(t)/GHI_{clr}(t), \tag{5}$$

where $GHI_{norm}(t)$ is the normalized signal, and $GHI_{clr}(t)$ is the clear-sky model (here the Ineichen model [13]). For simplicity of notation, it is assumed that the point sensor is a global horizontal irradiance (GHI) sensor. If instead a plane of array (POA) sensor were used, a POA clear-sky model would be required.

The wavelet transform of the clear-sky index, $GHI_{norm}(t)$, is:

$$w_{\bar{t}}(t) = \int_{t_{start}}^{t_{end}} GHI_{norm}(t') \frac{1}{\sqrt{\bar{t}}} \psi\left(\frac{t'-t}{\bar{t}}\right) dt', \tag{6}$$

where the wavelet timescale (duration of fluctuations) is $\bar{t}$, t_{start} and t_{end} designate the start and end of the GHI timeseries, and t' is a variable of integration. For the discrete wavelet

transform, $\bar{t}$ is increased by factors of 2, such that values of $\bar{t}$ are defined by $\bar{t} = 2^j$. The top hat wavelet was applied, defined by:

$$\psi(T) = \begin{cases} 1, & \frac{1}{4} < T < 3/4 \\ -1, & 0 < T < \frac{1}{4} \quad || \quad \frac{3}{4} < T < 1, \\ 0, & else \end{cases} \tag{7}$$

because of its simplicity and similarity to the shape of solar power fluctuations. Wavelet modes (timeseries) were computed for $\bar{t}$ values ranging from 2-sec ($j = 1$) to 4096-sec ($j = 12$), thus decomposing the $GHI_{norm}(t)$ timeseries into 12 modes $w_{\bar{t}}(t)$ showing fluctuations at these various timescales. Symmetric signal extension is used to ensure resolution at endpoints. A special definition is adopted for the highest wavelet mode, defining $w_{\bar{t}=2^{12}}(t)$ to be the moving average with window 4096-sec. This achieve the property that the sum of all wavelet modes equals the original input signal:

$$\sum_{j=1}^{12} w_{\bar{t}=2^j}(t) = GHI_{norm}(t). \tag{8}$$

2.5.2 Distances

Next, the powerplant is discretized into individual 'sites'. A single site is chosen to be an area over which $\rho(d_{m,n}, \bar{t}) \approx 1$ for the timescales of interest. For distributed plants, a single site is usually one house rooftop PV system. For utility-scale plants, a single site is a small container of PV panels as dictated by computational limitations. When using larger containers, a correction is applied for the in-container smoothing. Once discrete sites have been defined, the distance between each pair of sites is computed.

2.5.3 Correlations

To determine correlations between sites correlation is assumed to be a function of distance divided by timescale [12]

$$\rho(d_{m,n}, \bar{t}) = \exp(-\frac{1}{A}\frac{d_{m,n}}{\bar{t}}), \tag{9}$$

where ρ is the correlation between sites, $d_{m,n}$ is the distance between sites m and n, $\bar{t}$ is the timescale, and A is a correlation scaling factor that is calibrated using local measurements, e.g. from a network of irradiance sensors.

2.5.4 Variability Reduction

The variability reduction as a function of timescale, $\mathrm{VR}(\bar{t})$ is defined as the variance of the point sensor divided by the variance of the entire PV powerplant at each timescale:

$$\mathrm{VR}(\bar{t}) = \frac{\sigma^2{}_{point\ sensor}(\bar{t})}{\sigma^2{}_{PV\ powerplant}(\bar{t})}. \tag{10}$$

A large VR indicates a large reduction in relative variability for the powerplant compared to the point sensor, while a VR value of one indicates no reduction in variability, i.e. no benefit from geographic smoothing. VR can be expressed through the average of all correlations modeled in Eq. 9:

$$\mathrm{VR}(\bar{t}) = \frac{\mathrm{N}^2}{\sum_{\mathrm{m}=1}^{\mathrm{N}} \sum_{\mathrm{n}=1}^{\mathrm{N}} \rho(d_{m,n}, \bar{t})}, \qquad 11)$$

where N is the total number of sites. Defined this way, $VR = N$ for entirely independent sites ($\rho = 0, \mathrm{m} \neq \mathrm{n}$), and $VR = 1$ for entirely dependent sites.

2.5.5 Simulate Wavelet Modes of Powerplant

By combining the wavelet modes $\mathrm{w}_{\bar{t}}(\mathrm{t})$ found in section 2.5.1 with the variability reductions $\mathrm{VR}(\bar{t})$ from section 2.5.4, the wavelet modes of the powerplant were simulated. The simulated wavelet modes of normalized power are reduced in magnitude by the square root of VR:

$$w_{\bar{t}}^{sim}(t) = \frac{w_{\bar{t}}(t)}{\sqrt{VR(\bar{t})}}, \qquad 12)$$

where $w_{\bar{t}}^{sim}(t)$ are the simulated powerplant wavelet modes. One can sum the simulated wavelet modes to create a simulated clear-sky index of area-averaged GHI over the powerplant:

$$< GHI_{norm}^{sim} >_{pp} (t) = \sum_{j=1}^{12} w_{\bar{t}=2^j}^{sim}(t). \qquad 13)$$

2.5.6 Convert to Power Output

Power output is obtained by multiplying the spatially averaged irradiance by a clear-sky power output model, $P(t)_{clr}$.

$$P(t)^{sim} =< GHI_{norm}^{sim} >_{pp} (t) * P(t)_{clr} \qquad 14)$$

$P(t)_{clr}$ is created by combining a plane of array irradiance clear-sky model and a constant conversion factor.

$$P(t)_{clr} = C \times POI_{clr}(t) \qquad 15)$$

To obtain $POI_{clr}(t)$, the Page Model [14] was applied to $GHI_{clr}(t)$. The Page Model requires GHI and diffuse irradiance as inputs, so diffuse fraction was estimated as in [15]. The constant conversion factor, C, is determined based on the powerplant's conversion efficiency.

Since AC power output is nearly linearly proportional to spatially averaged irradiance [16], using only a constant multiplier (C) has been shown to be a reasonable approximation. In practice, though, more sophisticated performance models [17] should be used that depend on ambient temperature, wind speed, and panel specifications. The improvement in accuracy of power output achieved by using such a non-linear model is usually less than 10%, but depends on how far variables such as temperature deviate from standard test conditions (STC). Errors in estimating the variability at short timescales will be even smaller, since most of the non-linear irradiance to power effects occur over long timescales.

2.6 Application to Ota City and Copper Mountain Powerplants

To demonstrate the use of this WVM model, the 2.13MW$_P$ distributed generation (rooftop) plant in Ota City, Japan, and the Copper Mountain 48MW$_P$ utility scale PV powerplant in Boulder City, NV are used in a case study. Footprints of each plant are shown in Fig. 2.10. For both, the results of the WVM simulation were compared to the actual measured power output for the whole plant.

Fig. 2.10: Polygons showing the footprints of the Ota City (left) and Copper Mountain (right) powerplants

The red shading shows the polygon footprints, while the blue dots show the simulation containers representing either houses (Ota City), or small groups of PV panels (Copper Mountain). The large yellow dots indicate the location of the GHI point sensors used as input. The Ota City map shows approximately 1 × 1 km, while the Copper Mountain map is approximately 3 × 2 km.

Maps © Google Maps

The Ota City (OC) plant consists of 550 houses, most with polycrystalline silicon PV systems ranging from 3-5kW, at varying tilts and azimuths. The average orientation of all PV panels producing power at OC on the test day was found to be 15° tilted from horizontal and 10° azimuth east of south.

GHI recorded once per second using an EKO instruments ML-020VM silicon pyranometer for a typically variable day (October 12th, 2007) was used as an input to the WVM, and power output of the entire neighborhood also at 1-sec resolution was used for validation. The total power output is simply the sum of the output of each house, so ignores transmission losses.

The Sempra Generation Copper Mountain (CM) plant contains ground-mounted cadmium telluride (CdTe) thin-film PV modules at a fixed tilt of 25°. The GHI at 1-sec resolution from a Kipp&Zonen CMP11 was input to the WVM model, and the output was compared to power output of the entire plant also measured at 1-sec. Total power output was the sum of all inverter power outputs, so ignores AC transmission losses. September 24th, 2011 was chosen as a typically variable test day at CM.

For purposes of validating the WVM, irradiances at a point, area-averaged irradiances, and power output are employed (for nomenclature see Table 2.3).

Table 2.3: Nomenclature for GHI, simulated power output, and actual power output

	GHI units [W m^{-2}]	Clear-sky index [-]	Power units [MW]
measured point sensor	GHI	GHI_{norm}	P^{GHI}
simulated powerplant output	$< GHI^{sim} >_{pp}$	$< GHI^{sim}_{norm} >_{pp}$	P^{sim}
actual powerplant output	$< GHI >_{pp}$	$< GHI_{norm} >_{pp}$	P^{sim}

Angle brackets denote averaging. GHI_{norm} is the clear-sky index, while $< GHI_{norm} >_{pp}$ is the ratio of actual to clear-sky output power. Since the later does not align with the definition of the clear-sky index, the GHI_{norm} notation was chosen.

2.6.1 Inputs and Running the Model

Polygons were drawn around the outlines of OC and CM, and the WVM picked discrete points inside these polygons to use as sites in the simulation, as shown in Fig. 2.10. The spacing of these points was chosen based on the input PV capacity and hence density of the plant. For OC discrete sites were spaced roughly 20m apart such that each site represented a single house with rooftop PV. For CM sites were closer together (a few meters), with each site representing a sufficiently small group of PV panels that can be assumed to have a correlation coefficient of 1.

Fig. 2.11. GHI at 1-sec resolution at Ota City on October 12th, 2007, and at Copper Mountain on September 23, 2011

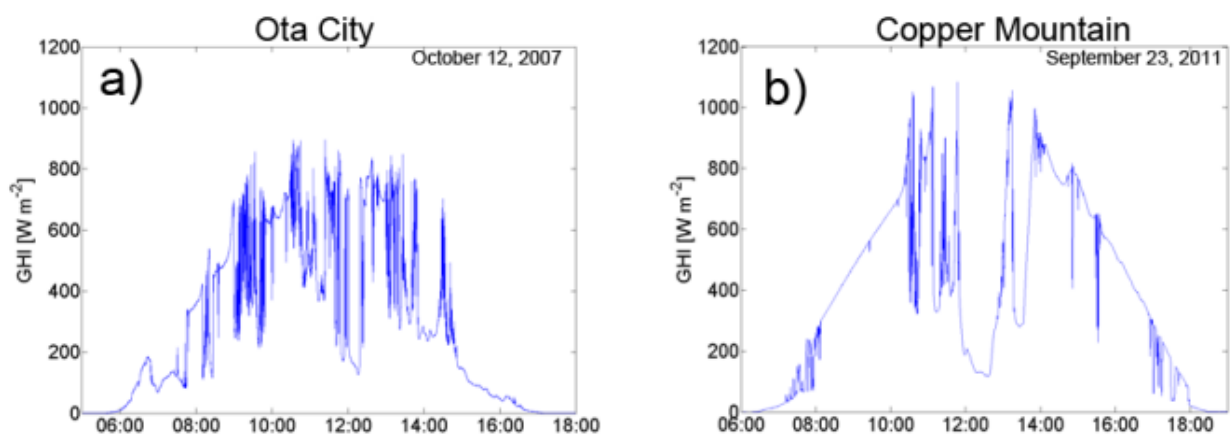

X-axis is time in [HH:MM].

The input to the WVM should consist of time and GHI measurement vectors, as well latitude, longitude, and UTC offset. GHI at OC and CM at the locations in Fig. 2.10 are shown in Figure 2.11. The test day at OC contains large cloud-induced irradiance fluctuations throughout the day. The test day at Copper Mountain was mostly clear in the early morning and late afternoon periods, with a large amount of variability in the middle of the day. Thus, the WVM model is

validated at two different sites and different types of daily cloud conditions (highly variable and partly variable).

Fig. 2.12: Correlations of wavelet modes for pairs of point sensors at Ota City (a) and Copper Mountain (b) on the test days

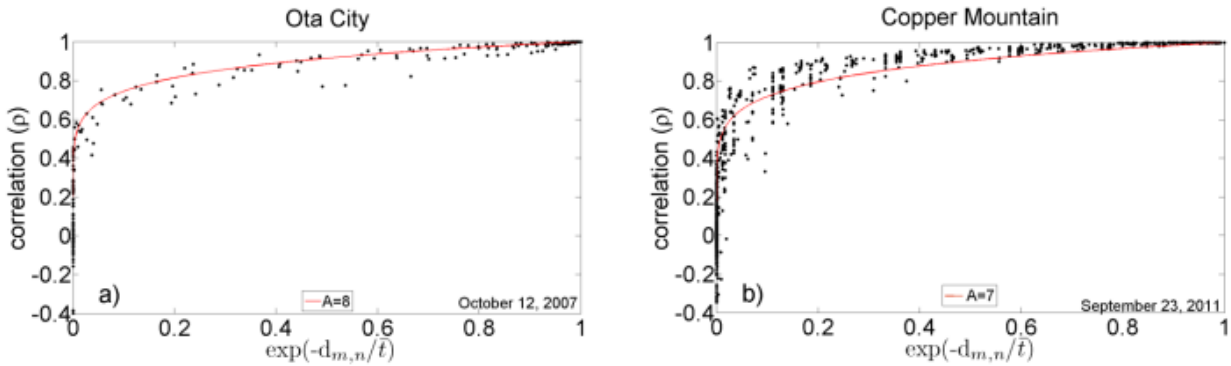

The x-axis is $\mathbf{exp}(-\frac{\mathbf{d_{m,n}}}{\bar{\mathbf{t}}})$ to show the exponential relationship between correlation and the distance divided by timescale.. Six GHI points sensors were used at Ota City, and 15 plane-of-array reference cells were used at Copper Mountain. Time scales range from 2-sec to 2048-sec. Dots to the far left have either very short timescales or very long distances, while dots to the far right have very long timescales or very short distances. The red line is the line of best fit and corresponds to using $\mathbf{A} = \mathbf{8}$ (Ota City) or $\mathbf{A} = \mathbf{7}$ (Copper Mountain) in Eq. 9).

Currently, the A value in Eq. 9) must be derived manually using the correlations between the wavelet modes of spatially dispersed measurements at the site at different time scales. Through further research a closed form solution for A will be determined.

For OC on the test day, $A = 8$ for the six GHI point sensors. Similarly, 15 plane-of-array reference cells at CM were used to determine $A = 7$ on September 23 (Fig. 2.12) The small scatter of correlation points (black dots) around the best-fit curve is likely due to small anisotropic effects (i.e., pairs of sensors arranged in a certain direction may have higher correlation for all timescales).

Following steps 2.5.1 to 2.5.5, a simulated normalized irradiance (similar to a clear-sky index, see Table 2.3) timeseries for the entire Ota City and Copper Mountain powerplants was created, $< GHI_{norm}^{sim} >_{pp} (t)$.

2.13a shows the effect of spatial averaging on the (simulated) reduction in variability for timescales of 64s and shorter. At longer time scales, though, the wavelet modes between the GHI point sensor and the simulation are essentially identical. The powerplant output 'clear-sky index' agrees with the simulation results across all timescales (2.13b). Fluctuations on timescales less than 8-sec are essentially zero and the fluctuations are reduced for timescales of 64-sec and shorter.

Fig. 2.13. [top most plots] Clear-sky index timeseries, and [bottom 12 plots] wavelet modes for Ota City on the test day

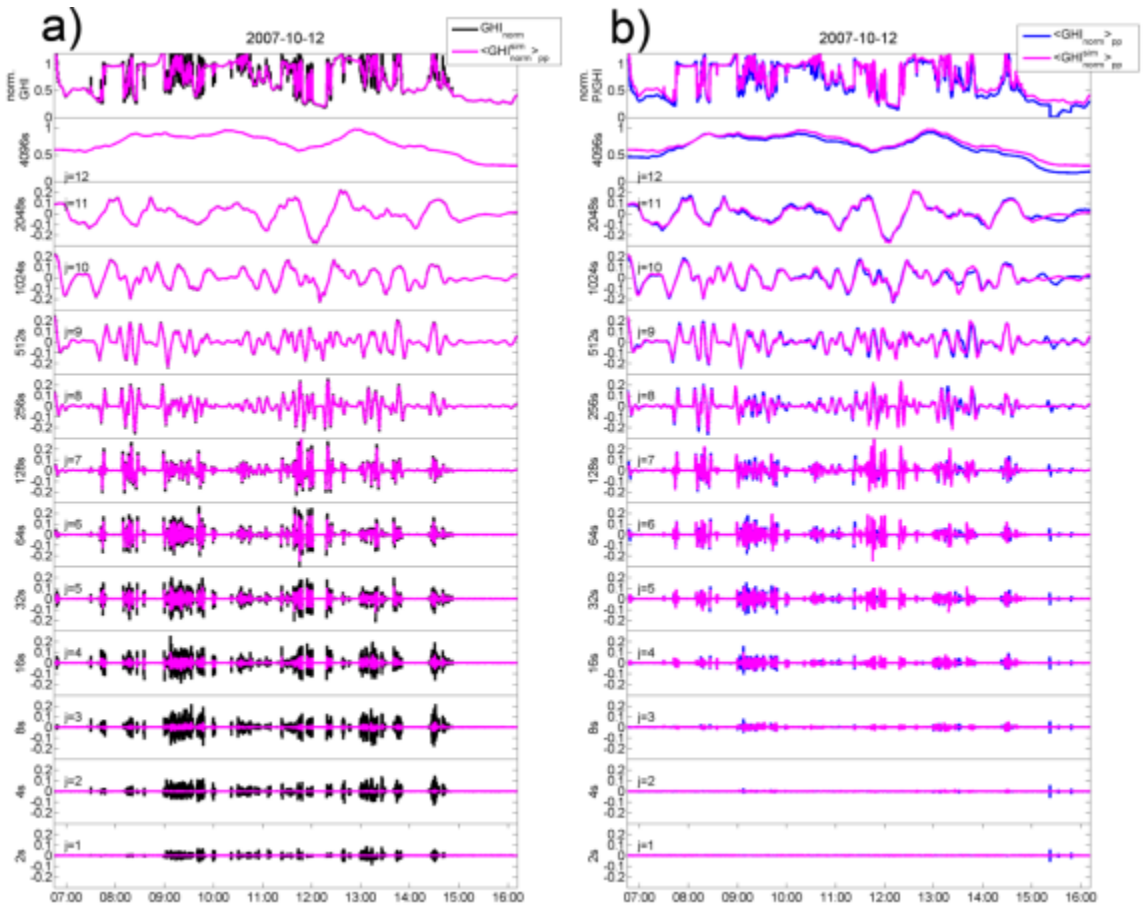

[Left] Clear-sky index measured (GHI_{norm} , black) and simulated spatially averaged across the powerplant ($< GHI_{norm}^{sim} >_{pp}$, magenta). [Right] Powerplant output 'clear-sky index' measured ($< GHI_{norm} >_{pp}$, blue) and simulated ($< GHI_{norm}^{sim} >_{pp}$, magenta).

2.6.2 Validation of Plant Power Output

Here comparisons of the simulated and actual power output, the fluctuation power index (fpi), and ramp rate (RR) distributions are presented. The simulated normalized power plant variability $< GHI_{norm}^{sim} >_{pp}$ (t) is derived from measurements at a single irradiance sensor GHI_{norm} (an input to the WVM model), combined with correlations from Eq. 9 based on relationships established from the spatial analysis (the A value). For validation, as a variability metric the fpi is used, which is the power content of fluctuations in the wavelet modes at each timescale. The goal of the WVM is to create simulated power output that statistically has the same variability distribution across timescales as the actual power output. Note that the main output of the WVM is the VR as a function of timescale based on irradiance measurements at a single site. Small errors in VR are irrelevant if the fpi is small (such as on clear days or at very short timescales), as errors will also be very small. However, when the fpi is large (such as on

cloudy days or at long timescales), errors in VR can lead to large errors in fpi. Additionally, GHI and total power output can be slightly offset in time based on the direction of cloud movement and the location of the GHI sensor versus the centroid of the power plant. Since the fpi describes the variability content (and total variance) rather than the time of occurrence it allows measuring the accuracy of the WVM independent of these limitations.

Fig. 2.14. Fluctuation power index (fpi) for the GHI point sensor (black), actual power output of Ota City (red), and simulated power output (blue line)

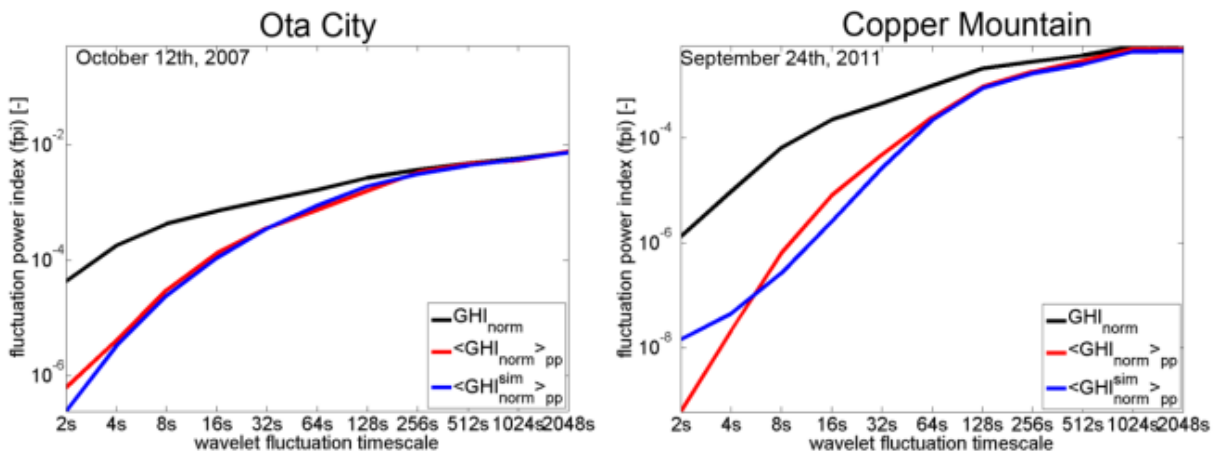

The point sensor is included to show how the WVM output differs from the simple assumption of linear variability increasing with power plant size.

Figure 2.14 shows the $fpis$ of GHI_{norm}, $< GHI_{norm} >_{pp}$, and $< GHI_{norm}^{sim} >_{pp}$ for both OC and CM. As expected based on Figure 2.13, the fpi of the irradiance at a point sensor, GHI_{norm}, deviates from the fpi of the spatial average, $< GHI_{norm} >_{pp}$, at short timescales due to geographic smoothing. There is good agreement between simulated and actual fpis of the power output 'clear-sky index' at all timescales. The match between $< GHI_{norm} >_{pp}$ and $< GHI_{norm}^{sim} >_{pp}$ is better at OC than at CM, but this is to be expected since the CM simulation is using a single point sensor to simulate 48MW of PV, and so more error due to inhomogeneity of irradiance statistics results than when simulating the 2MW of PV at OC. The variability at CM is overestimated at timescales of 2 to 4-sec, and underestimated at timescales of 8 to 32-sec. Overall, at both sites, $< GHI_{norm}^{sim} >_{pp}$ better quantified the fluctuation power content of the actual power output than GHI_{norm}. Therefore, the WVM simulation was accurate for the test days at both OC and CM.

Another validation of the model is to compare the irradiance profile of the input GHI point sensor, WVM output areal averaged irradiance, and the 'actual' area-averaged irradiance derived from the power output. To obtain the actual area-averaged irradiance, the power output clear-sky index was multiplied by the GHI clear-sky model:

$$< GHI(t) >_{pp} = < GHI(t)_{norm} >_{pp} * GHI(t)_{clr}. \quad 16)$$

The simulated area-averaged irradiance clear-sky index must also be multiplied by the GHI clear-sky model to obtain simulated areal averaged irradiance:

$$< GHI^{sim}(t) >_{pp} = < GHI(t)^{sim}_{norm} >_{pp} * GHI(t)_{clr}. \quad 17)$$

Figure 2.15 shows that $< GHI^{sim}(t) >_{pp}$ is essentially a filtered version of $GHI(t)$; during long clear or cloudy periods the areally-averaged GHI approaches the point sensor while short fluctuations e.g., at 09:09, are more strongly reduced. The timeseries of fluctuations, $< GHI(t) >_{pp}$ and $< GHI^{sim}(t) >_{pp}$ are not expected to match perfectly, since only a single point sensor is used as input, but the statistics of the fluctuations are expected to agree. For the eight minute segment shown in Figure 2.15, the 'upper envelope' of a really-averaged irradiance is accurately simulated. However, especially during long cloud events (large timescales), the lower envelope of the powerplant is as small as or even smaller than the envelope of the point sensor. Physically this could mean that the optical depth of the cloud at the point sensor was less than the average of the cloud system over the powerplant (spatial heterogeneity); it could also mean that the panel tilt and azimuth (versus the horizontal GHI) resulted in a smaller diffuse irradiance at the powerplant during these morning hours.

Fig. 2.15. Point sensor GHI (black), powerplant area-averaged GHI (red), and simulated area-averaged GHI (red) for Ota City on the test day

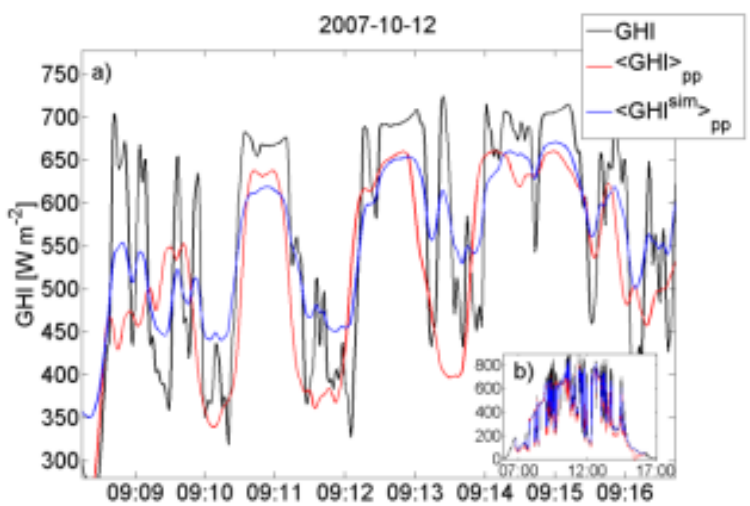

(a) Zoomed in to eight minutes in the morning, and (b) the entire day

Fig. 2.16: Original Ota City neighborhood (labeled 1)

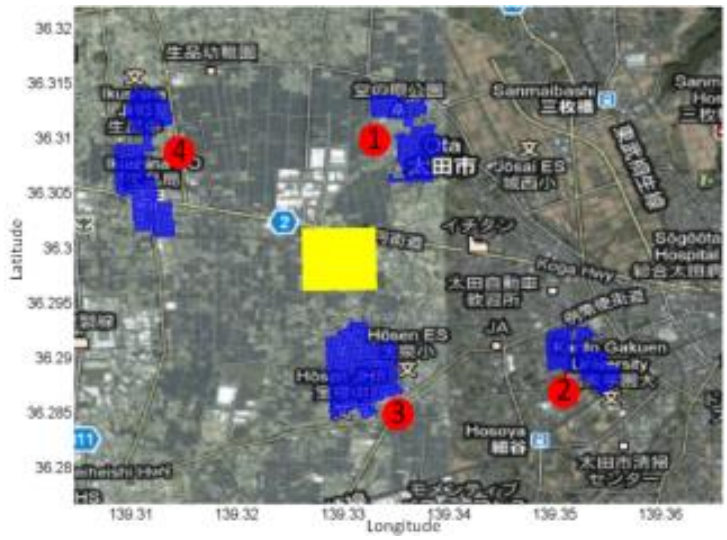

The other neighborhoods (other blue areas labeled 2 through 4) used to realistically simulate various capacities of PV on a single feeder. PV capacity scenarios were 1.88MW (1 only), 3.44MW (1 and 2), 6.33 MW (1, 2, and 3), and 9.41MW (1, 2, 3, and 4). The yellow square in the center shows a central PV plant of 9.41MW.

Ramp rate statistics are often of greater interest to powerplant and grid operators. Fig. 2.17 shows the cdf of ramp rates at 1s, 10s, 30s, and 1-min, for both Ota City and Copper Mountain. For comparison between the RRs of GHI(t) and P(t), and since RRs are more relevant in units of power rather than irradiance, GHI was converted to power units as:

$$P(t)^{GHI} = GHI(t)_{norm} * P(t)_{clr}. \qquad 18)$$

For 1-sec, 10-sec, and 30-sec, and even for 60-sec at Copper Mountain, the same trend exists as in the short-timescale fpis: the RRs are much reduced in P versus P^{GHI}, and P and P^{sim} show similar RR distributions. At Ota City, the same observation holds up to 30-sec, but at 60-sec, the RRs are similar between P^{GHI} and P, since there is relatively little geographic smoothing over the 2MW plant footprint at this timescale. As shown in Figure 2.17 for timescales longer than 4-min, it is expected that the RRs of P^{GHI} and P will be identical meaning that P^{GHI} can be used as a good approximation of P. At timescales shorter than 4-min, though, P^{GHI} would dramatically overestimate the RRs. While for Ota City the "cut-off time" for when it is appropriate to use P^{GHI} is around 4-min, this time varies with plant size, layout, and location.

Fig. 2.17: Extreme ramp rate distributions

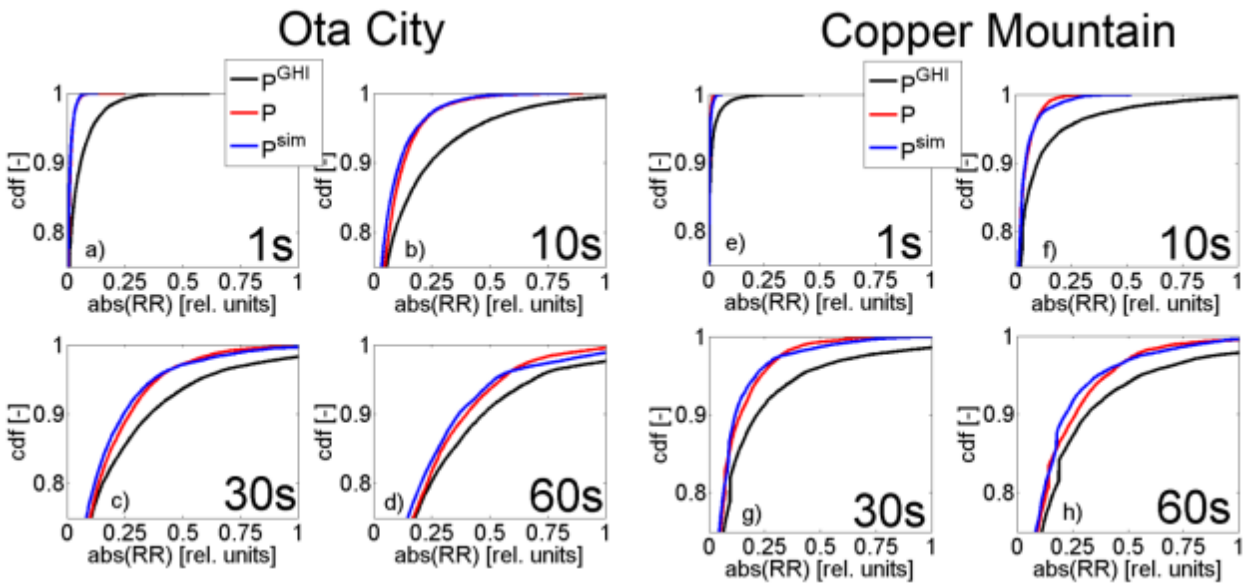

At 1-sec (a, e), 10-sec (b, f), 30-sec (c, g), and 1-min (d, h) for P^{GHI}, P, and P^{sim} for Ota City (a-d) and Copper Mountain (e-h). X-axis units are multiplied by an arbitrary scaling factor to protect the confidentiality of the power data.

2.6.3 Simulate Adding More Residential PV

Since the WVM has performed well on the test days for Ota City and Copper Mountain, it was applied to simulate the power output for a hypothetical addition of more residential PV to the Ota City area. Areas of similar density of houses as Ota City were selected and assumed to accommodate the same density of rooftop PV. Four distinct neighborhoods were selected (shown in Figure 2.16) and added sequentially, to create PV scenarios of 1.88MW (original Ota City), 3.44MW, 6.33MW, and 9.41MW. For each scenario, both the distributed plant (blue dots in Figure 2.16), and a central plant of the same power capacity (yellow square in Figure 2.16) were simulated. The central plants were assumed to have a PV density of 25 W m^{-2}, roughly 3.5 times the PV density of Ota City. The distributed simulations and central plant simulations will be referred to P^{sim} and $P^{sim}_{central}$, respectively.

Fig. 2.18a shows the fpis of the distributed plants for each of the four scenarios. The GHI_{norm} and 1.88MW $< GHI^{sim}_{norm} >_{pp}$ fpi curves are the same as shown in Figure 2.18b. There is always less power content in the wavelet modes for the larger distributed plants, but the reduction in power content depends on timescale. The variability reductions for the four scenarios, and for central plants, are shown in Fig. 2.18b. The VR at the distributed plants is much larger than the VR at the central plants at nearly all timescales, indicating a large amount of geographic smoothing. Increasing plant capacity always increases the VR, but the incremental benefit is not directly proportional to plant size. For the 3.44MW, 6.33MW, and 9.41MW distributed plants, the VR does not reach 1 even at 2048s (>30-min) because the distance between PV panels in

different neighborhoods is large and so there is some geographic smoothing even at 2048-sec timescales.

Fig. 2.18

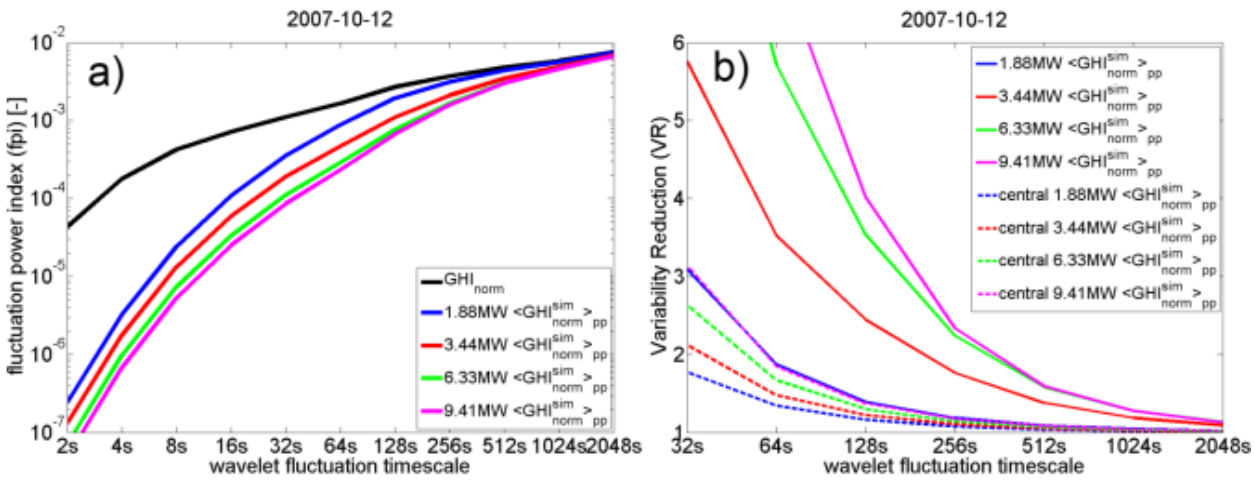

a) fpi of four different neighborhood distributed PV scenarios (1.88, 3.44MW, 6.33MW, and 9.41MW). b) Variability reduction (VR) for the various scenarios. Shown are both the VR for the residential rooftop distributed plants (solid lines), and the VR for the dense central plants (dashed lines). While short timescale fpi is always reduced with increased MW capacity, the longer timescale fpi is also reduced slightly (high VRs still exist at long timescales) due to the relatively long distances (2-5 km) between added neighborhoods.

2.7 Summary of PV Variability

Clear-sky indices at 1-sec resolution from a solar resource station at UC San Diego were used to compute statistics over an entire year, showing the benefits of high-frequency data to obtain accurate irradiance statistics. Two types of averages were applied to the 1-year data: a block average representing different temporal resolutions of averaged solar radiation data, and a moving average. For the block averages, the probability of a large SS increases with increasing averaging time, but the number of occurrences per day decreases. This was consistent with Fig. 3 in [12] where 10-min and 1-hour block averages had increasingly higher probabilities at any given ramp than the 1-min block average. This same trend was also seen down to 1-sec resolution for one day in Fig. 4 in Mills et. al (2009).

With moving averages, the probability and number of occurrences per day of large RRs both decrease with increasing averaging interval. If the length of the moving average is equal to the time over which energy storage has the capacity to eliminate fluctuations through charging or discharging, then a moving average timeseries will be representative of the PV + storage output timeseries. PV power output similar to the moving average over an interval equivalent to the storage-time capacity, and will therefore lead to a reduction in both magnitude and occurrence of extreme RRs. Likewise large solar systems will ideally average irradiance over a time scale of $A^{1/2} / V$, where $A^{1/2}$ is the square root of the area of the array (which is a proxy for array length

in the direction of the cloud velocity V) and a frozen cloud field with infinite lateral dimension is assumed (similar as in HP10). This leads to RR reductions at short time scales.

A new framework for quantifying geographic smoothing was presented through coherence spectra and wavelet analysis of 1-sec K_c data over one month at six sites within three km distance. The distances allowed observing how power generation changed over time and distance. Strong correlations between solar irradiances at different sites would indicate weak geographic smoothing of power and would be a concern to utilities and independent system operators needing to adjust for power variability. Comparisons of clear-sky indices showed the reduction in variability when averaging 6 sites. Coherence spectra indicated strong correlations between sites up to timescales as short as 10-min and the correlation at longer timescales decreased with distance but not isotropically. A top hat wavelet transform was applied to both EBU2 and the average of the 6 sites. At timescales of 256-sec and shorter, there was approximately a factor of 6 reduction in variance for the average versus just the one site. This indicates that even at the small 1200 acre UC San Diego microgrid, ramps over timescales of up to 5 minutes were uncorrelated. Consequently, the short-term variance of aggregated power output from dispersed locations decreases dramatically compared to that of a centralized PV plant. At longer timescales, however, the reduction in variance becomes smaller, and there was almost no reduction in variance at 4096-sec.

As PV gains higher and higher penetration, it is important to understand the typical fluctuations on various timescales, as well as the potential for storage, PV array size, and geographic dispersion to dampen these fluctuations. The top hat wavelet transform is a novel approach to deconstruct clear-sky indices into separate timescale components, and was very useful in determining the benefits of storage and geographic averaging. The PV system power drop caused by incoming cloud cover was shown to be smooth over time, when output from several dispersed systems is considered. Since scattered clouds rarely if ever cover all the dispersed solar arrays at the same time, the aggregated power production drops more slowly than for a single panel, over the course of minutes to an hour.

A wavelet-based variability model (WVM) for simulating the power output of a solar photovoltaic (PV) plant was presented and tested. The WVM uses the plant footprint, density of PV panels in the footprint, and the timeseries measurements from a single point sensor to create a simulated power output timeseries. First, correlations between sites (i.e., houses or small groups of PV panels) within the powerplant are determined using an equation based on the distance between sites, timescales, and a correlation scaling coefficient (A value). From these correlations, variability reductions (VRs), or the ratio of variability of a single point sensor to the variability of the entire PV plant, at each fluctuation timescale were determined. Wavelet decomposition was then used to separate the normalized input point sensor timeseries by fluctuation timescale. By combining the wavelet modes at each timescale with the VRs at each timescale, the normalized plant power output was simulated. Actual power output (in MW) could then be obtained by using a clear-sky model for power output.

The WVM was validated at the 2MW distributed residential rooftop plant in Ota City, Japan, and the Copper Mountain, NV 48MW central powerplant. For both test cases, the WVM

simulation matched the statistics of the actual power output well. Fluctuation power index (fpi) comparisons showed that the WVM accurately represented variability by timescale at both Ota City and Copper Mountain. Ramp rates (RRs) were also compared between simulated and actual power, and again, the WVM fared well at both test sites.

The WVM was then used to evaluate the variability impacts of a hypothetical addition of PV to the Ota City area. Residential rooftop PV was added progressively to three other neighborhoods besides the original Ota City PV plant creating four different distributed PV plants ranging in size from 1.88MW to 9.41MW. Adding additional PV always lead to a decrease in relative variability, although absolute variability increased since the capacity was increased. Additionally, dense central PV plants of the same MW capacities were simulated. Relative variability was strongly reduced at the distributed over the central PV plants. The 9.41MW central PV plant was found to have roughly the same variability reduction (VR) as the 1.88MW distributed PV plant, meaning roughly the same relative variability and making a strong case for distributed generation.

To facilitate the use of the WVM, a computer program was developed in MATLAB (the MathWorks, Inc., available for download at https://solarhighpen.energy.gov/wavelet_based_variability_model_wvm.) that allows drawing polygons on a satellite map of the world to easily input the PV plant footprint. The program is setup to be as generally applicable as possible: multiple polygons of any shape may be drawn to simulate any possible central or distributed plant footprint; the user may input a point sensor time series, or use a highly variable day from a library of timeseries provided by the authors; and the powerplant capacity may be specified to allow for appropriate sizing of site containers, or, if unknown, the PV density in W of PV per m^{-2} of land area may be estimated or a default value can be used.

2.8 Ramp rates for Power Analytics Software

Extreme irradiance ramp rates were implemented as input into PV system models in the Power Analytics' advanced network simulation software. The PV output current is one of the inputs to the PV inverter block implemented in the Power Analytics software. Thus, by multiplying the PV output current by the appropriate normalized ramp rate, the resulting change in the overall PV system power output can be modeled. Since the relative ramp rates decrease as the size of the PV system increases, an averaging algorithm is utilized to reduce the ramp rates based on the area covered by the PV system. Finally, in addition to the prescribed 30-second ramp rate obtained by the UC San Diego, an option for user-supplied lookup table is implemented.

2.8.1 Clear Sky Index

The clearness index is the ratio of global horizontal irradiance at the ground level and the extra-terrestrial irradiance. The clear sky index (k_t) is the ratio of global horizontal irradiance at the ground level and the clear sky global horizontal irradiance. The clear sky irradiance assumes typical clear sky atmospheric transmissivity based on the atmospheric air mass. For this reason, in this research task the clear sky index was used to quantify the reduction in irradiance that reaches the surface due to the presence of clouds. UC San Diego calculated the values of clear

sky index based on the measured data of global horizontal irradiance (GHI), and calculated values for the corresponding clear sky GHI. The measurement period spanned a period of one year with the sampling rate of one second. Figure 2.1 shows the 60-second period in which largest fluctuations in the clear sky index were observed.

It is important to note that these extreme ramp rate values may have not occurred at the time when the actual irradiance was at the maximum. However, since the clear sky index is effectively decoupled from the actual amount of irradiance at the time, the user can apply these values at any irradiance level. By applying these clear sky index values at the time of the peak irradiance, the user will obtain the largest fluctuations in irradiance, and consequently in the PV system power output. This scenario can be used in the modeling stage as the absolute worst-case scenario – the onset of o a cloud cover that produces the extreme irradiance ramp rates at the time when irradiance was at its peak.

Figure 2.19. Clear sky index values for the 60 seconds period with the highest change in irradiance

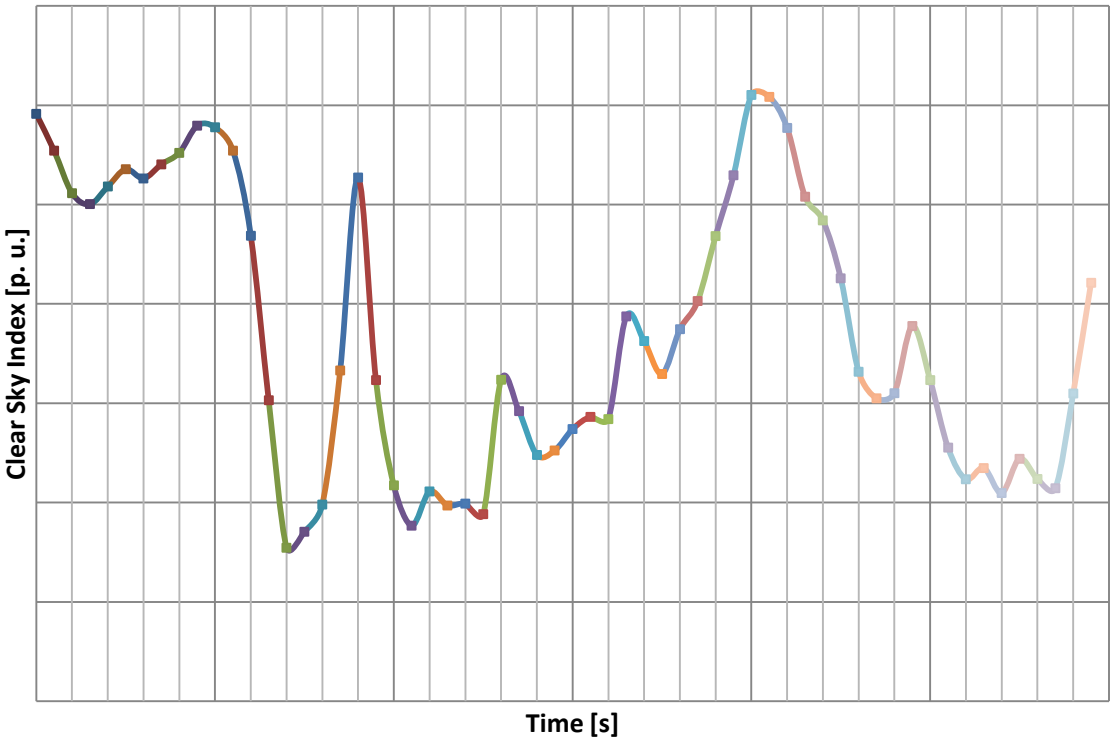

Table 2.4. The clear sky index values shown in Figure 2.19

Time [s]	0	1	2	3	4	5	6	7	8	9
k_t	1.1825	1.1084	1.0230	1.0008	1.0362	1.0712	1.0528	1.0812	1.1043	1.1587
Time [s]	10	11	12	13	14	15	16	17	18	19
k_t	1.1554	1.1087	0.9373	0.6062	0.3092	0.3413	0.3961	0.6658	1.0545	0.6465
Time [s]	20	21	22	23	24	25	26	27	28	29
k_t	0.4344	0.3536	0.4221	0.3943	0.3976	0.3763	0.6471	0.5838	0.4959	0.5049
Time [s]	30	31	32	33	34	35	36	37	38	39
k_t	0.5479	0.5725	0.5682	0.7747	0.7251	0.6590	0.7488	0.8060	0.9369	1.0589
Time [s]	40	41	42	43	44	45	46	47	48	49
k_t	1.2205	1.2172	1.1544	1.0160	0.9683	0.8515	0.6634	0.6096	0.6205	0.7552
Time [s]	50	51	52	53	54	55	56	57	58	59
k_t	0.6465	0.5104	0.4470	0.4697	0.4192	0.4882	0.4475	0.4286	0.6197	0.8428

2.8.2 Data Normalization

The change in irradiance leads to the almost instant change in power output of the solar cells. For the purpose of modeling, it is assumed that this change occurs instantaneously, i.e. the reduction in irradiance leads to the immediate change in the current provided by the PV module. As the PV current is already a variable used in the control block of the PV inverter, its value is simply adjusted accordingly at appropriate times during the simulation run. This will be accomplished via a predefined lookup table which will vary the value of the PV current during the simulation run.

The values shown in Figure 2.19 were modified slightly to allow better integration with the Power Analytics simulation software. Specifically, the power output of a PV system at the time t=0 (prior to irradiance change) is determined by the user and can be set to any value between zero and nominal PV power output. For modeling purposes, the data values presented in Figure 2.19 were scaled to the [0, 1] range, to avoid instances where PV power output would exceed the rated value. In addition, a thirty second interval was chosen to reduce the simulation time; the interval between 10s and 40s was chosen as the most representative. Finally, the value at t=0 was set to unity to assure the initial conditions are correct (the original scaled value was 0.9467).

The resulting 30-second interval is shown in Figure 2.20. This sequence was implemented in the Power Analytics modeling software, as discussed in detail further in the text. As discussed previously, it is recommended that the power output of the PV system is set to the nominal

power output prior to applying this sequence, in order to produce the maximum variance in its output power.

Figure 2.20. The normalized 30-second sequence of the clear sky index implemented in the Power Analytics software

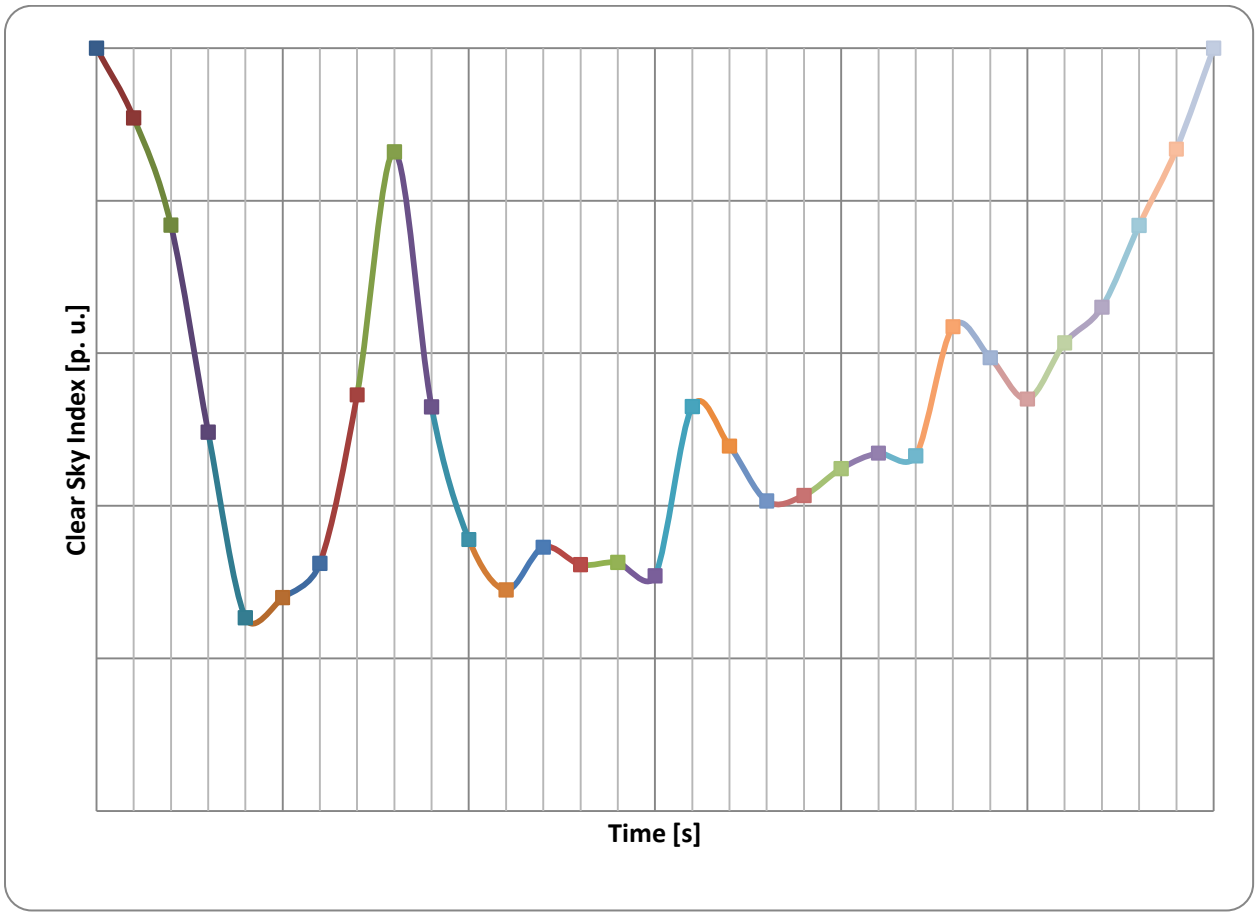

Table 2.5. The clear sky index values shown in Figure 2.

Time [s]	0	1	2	3	4	5	6	7	8	9
k_t	1.0000	0.9084	0.7680	0.4967	0.2533	0.2796	0.3245	0.5455	0.8640	0.5297
Time [s]	10	11	12	13	14	15	16	17	18	19
k_t	0.3559	0.2897	0.3458	0.3231	0.3258	0.3083	0.5302	0.4783	0.4063	0.4137
Time [s]	20	21	22	23	24	25	26	27	28	29
k_t	0.4489	0.4691	0.4655	0.6347	0.5941	0.5399	0.6135	0.6604	0.7676	0.8676
Time [s]	30									
k_t	1.0000									

2.8.3 Integration with Power Analytics Software

This section discusses the integration of the extreme irradiance ramp rates in the Power Analytics simulation package. One of the internal parameters in Power Analytics' model of the PV inverter is the PV system current. A lookup table is used to modify the PV output current throughout the simulation run. The lookup table is a two-dimensional table of (t, k_t) values, where t represents the time instant, and k_t is the value of clear sky index (and PV power output) at time t. Power Analytics software assumes that the k_t changes monotonically between two successive time steps and interpolates the k_t values accordingly.

2.8.4 Application to Large PV Arrays

The extreme ramp rates calculated by UCSD were obtained using measured irradiance data from a single point. For a PV system spanning a significant area, the corresponding change in the PV output current will be less extreme, as it will take some time for the cloud to cover the whole array. The following calculation has been incorporated in the Power Analytics package.

The (t, kt) sequence obtained from a single irradiance sensor can be modified by applying a running average filter with a window size of Δ. The window size Δ is a function of the area covered by the PV system and the cloud speed, and can be calculated using the following formula.

$$\Delta = round\left(\frac{\sqrt{A}}{U}\right) \tag{21}$$

where A is area covered by PV [m^2], and U is the cloud speed [m/s]. Both the area A and cloud speed C can be specified by the user; if the values are not supplied the following assumptions are used. If U is not supplied by the user, the program assumes U = 10 m/s. If A is not supplied by the user, the program estimates it by using the following formula.

$$A = \frac{P_{DC}}{\eta G} \tag{22}$$

where P_{DC} is the nominal power output of the PV system [W], $\eta = 0.15$ is the typical cell efficiency, and $G = 1000$ W/m² is the typical irradiance.

The running average filter with a window size of Δ can be calculated by using the following formula for the modified clear sky coefficient k_t' at time t.

$$k_t'(t) = \frac{\sum_{i=0}^{\Delta-1} k_t(t-i)}{\Delta} \tag{23}$$

with the assumption that the k_t was constant prior to the disturbance, i.e. all k_t values prior to t<0 are equal to $k_t(t=0)$.

2.8.5 User-Supplied Lookup Table Option

In addition to the procedure described in sections 2.8.2 to 2.8.4 for modeling the impact of extreme irradiance ramp rates, the Power Analytics software package allows the user to supply her/his own (t, k_t) lookup table. While the significant data sample has been utilized to determine the ramp rates presented in the previous sections, there may be situations where other ramp rates should be utilized. This approach also provides additional flexibility to model a variety of other transient scenarios (ramp up, ramp down, etc.). In addition, this approach allows the user to use other techniques to estimate the reduction in ramp rates due to the size of the system.

2.8.6 Example 1. Medium Size PV System

Given: $P_{DC} = 1$ MW, No data on area covered by the system or cloud speed.

Using equations (21) and (22), the filter size is calculated to be $\Delta = 8$s. Both the original and filtered k_t values are shown in Figure 2.21 below.

Figure 2.21. Clear sky index extreme ramp values for a single cell and for a 1 MW PV array

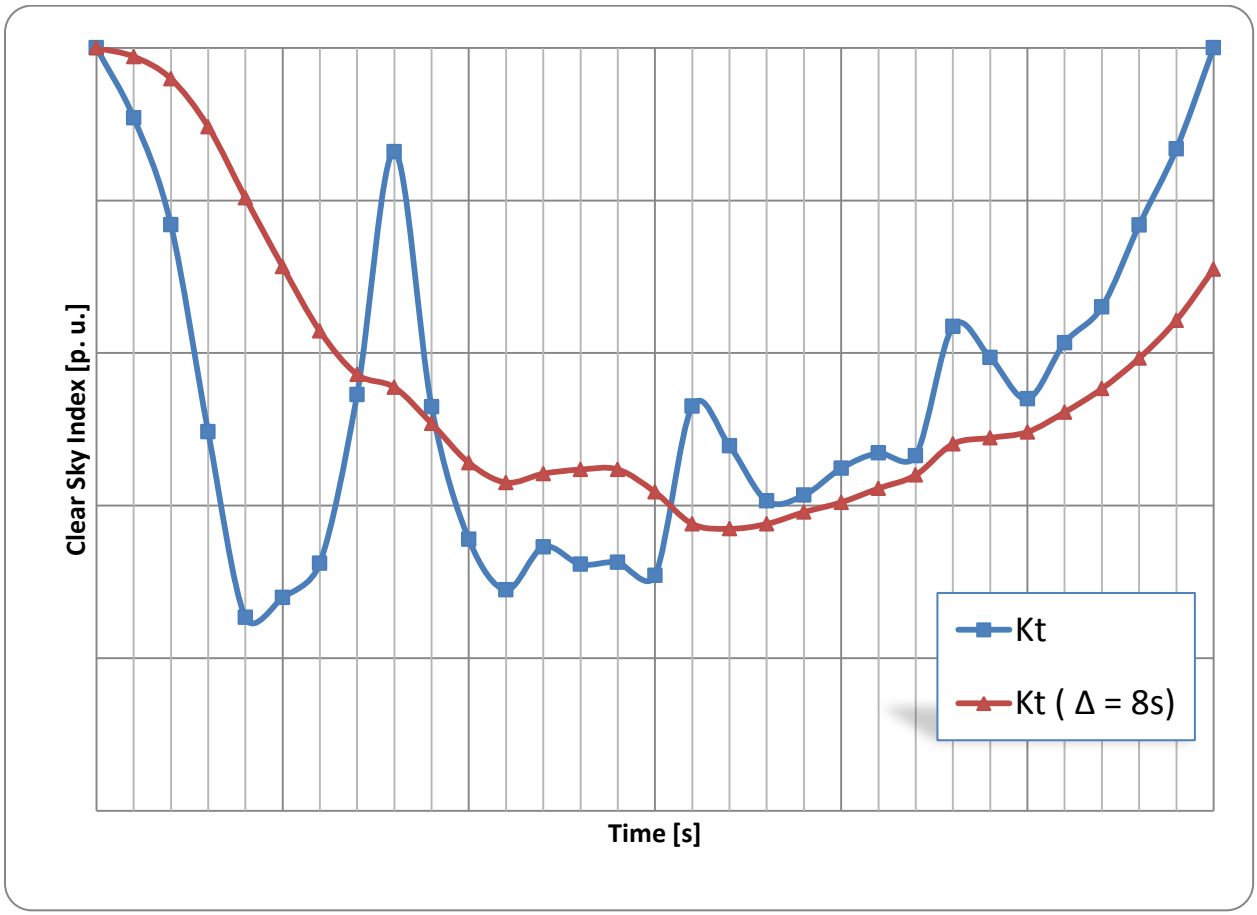

2.8.7 Example 2. Medium Size PV System, Modeling Ramp Up

Given: P_{DC} = 1 MW. Design parameter to test is reduction in irradiance from full sun to zero in 4 seconds, based on a single point irradiance measurement. The cloud speed is estimated at U=15 m/s.

Since no information on the PV system area is given, using Eqns. 21 and 22, the filter size is calculated to be Δ=5s. Both the original and filtered k_t values are shown in Figure 2.22 below.

Figure 2.22: Clear sky index ramp up rates for a single cell and for a 1 MW PV array

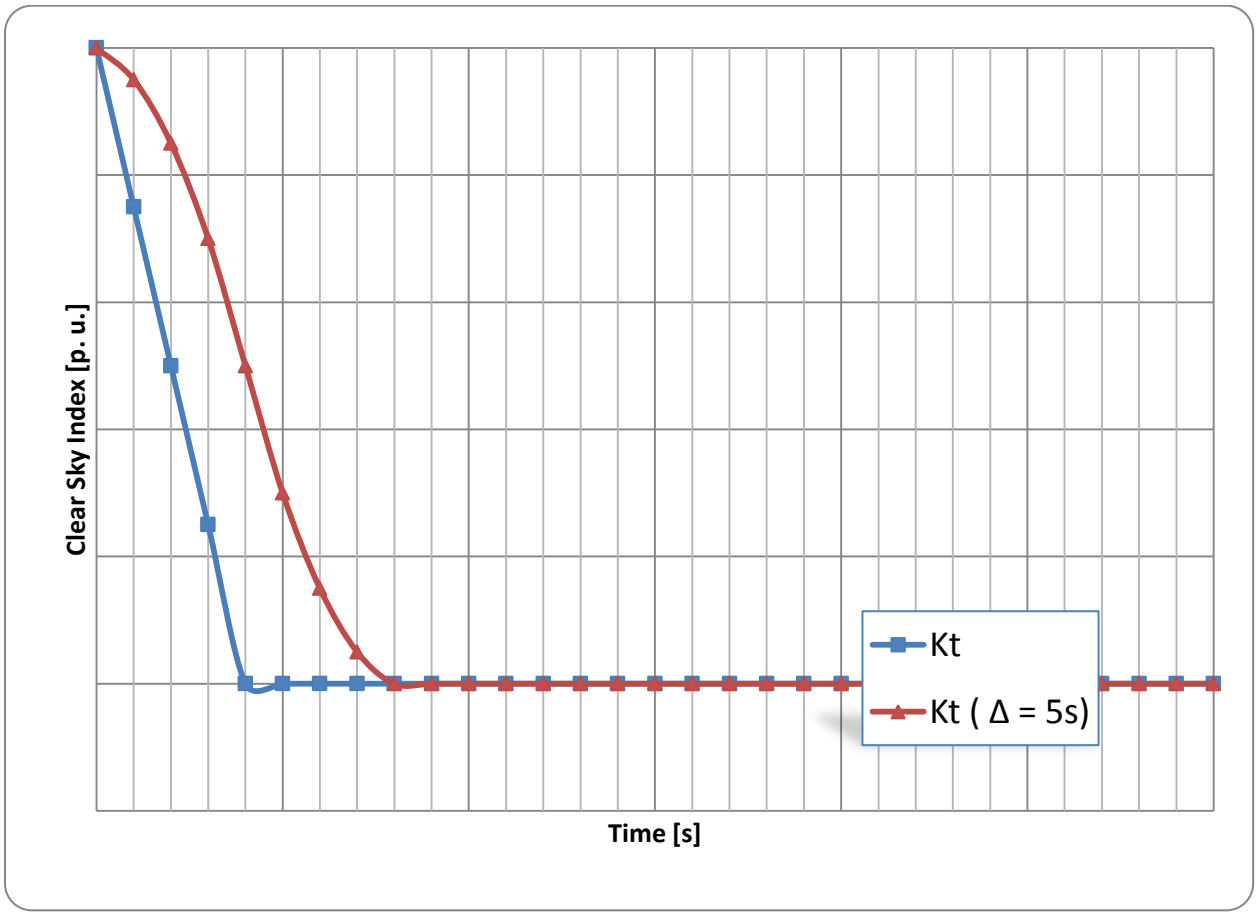

2.8.8 Load Following Capacity

Once the impact of the extreme irradiance ramp rates is known, the next task is to determine the ways to reduce these undesirable effects. This can be done by either adding fast-acting storage component to the PV system, or incorporating the real-time information of the position of the clouds in the PV system control algorithm.

2.8.8.1 Storage Option

The extreme irradiance ramp rate can be used to determine the size of the storage unit. The basic idea is shown in Figure 2.23, which shows the output of the PV system subjected to the UCSD ramp rate, and the output of the storage system needed to keep the combined output constant, i.e. completely eliminate the effect of the ramp rate. The size of the storage unit can be easily obtained by integrating the storage unit's output during the ramp rate event. The size can be further reduced if the requirement is relaxed to hold the PV power output ramp rate to some predetermined level, which can be either given as a design parameter, or estimated using network simulations for a particular PV installation.

Figure 2.23: Sizing the storage unit to mitigate the effects of extreme irradiance ramp rates

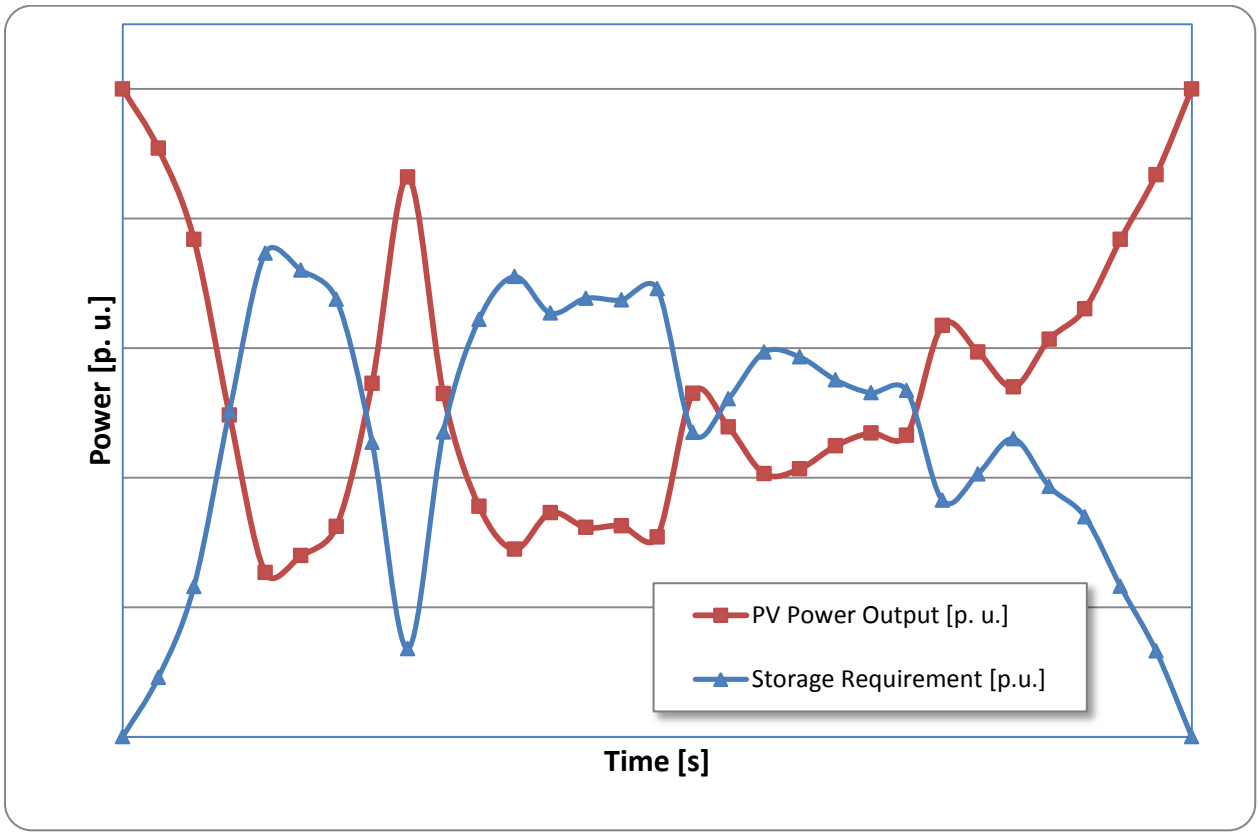

Several fast-acting storage technologies have been proposed for this task, such as fuel cells, super-conducting magnetic storage, batteries, electric double-layer capacitors (EDLC), flywheels, etc. While many authors assume that the storage unit can compensate for all PV-induced transients, few experimental results have been presented.

Kakimoto[1], et al. in 2009 presented a method for controlling the ramp rate of a PV generator by utilizing an over-sized EDLC. In addition to the storage unit's sizing algorithm, he presented the modifications to the inverter control strategy, as well as experimental results.

2.8.8.2 Non-Storage Option

If accurate information is known about the position and movement of the clouds, it can be incorporated in the PV system control algorithm and used to smooth out the PV output fluctuations. The majority of PV systems incorporate the algorithm for maximum power point tracking, assuring that they operate at the maximum possible power output. However, they can operate at any point between zero and the maximum power point. If the information about the

[1] Kakimoto, N., et al., Ramp-Rate Control of Photovoltaic Generator with Electric-Double Layer Capacitor, IEEE Transactions on Energy Conversion, Vol. 24, No. 2, pp. 465-472, June 2009.

approaching cloud is known, PV system control algorithm can proactively decrease the PV power output in a controlled fashion, keep it low throughout the duration of the cloud, and then ramp it back up once the cloud passes.

CHAPTER 3:
Modeling of a Photovoltaic System for Power Engineering Applications

The scope of this portion of work is based on advancing modeling for high penetration solar on a distribution feeder. The Power Analytics team used the Power Analytics DesignBase power modeling software as underlying modeling software. The project included development of steady state models for power flow (1) and short circuit (2), dynamic modeling for transient stability (3) and user designed models for inverter design and comparison (4). The inverter models and structures are based on existing inverters from Schneider Electric (Xantrex grid tie inverter model 250 and 500), OptiSolar GT Series, and SunPower SPRm series). The inverter work is also the basis for the open software contribution and structure.

Included in the appendices are a detailed survey of the available literature, the results of the various integration studies and the specific inverter designs as well as their associated performance scripts generated by Power Analytics Universal Control Logic Modeling and Simulation (UCLMS). While the target area of work is UCSD's power network several other power networks were analyzed to validate the approach. The networks used are representative examples of a broad range of distribution circuits.

3.1 Photovoltaic cells and Modules

The photovoltaic (PV) panel uses semiconductor cells (wafers), each of which is basically a large area p-n diode with the junction positioned close to the top surface. The photovoltaic effects results in the generation of direct voltage and current from the sunlight (solar irradiance) falling on the cell. To achieve higher voltage and current multiple cells are used as needed. The output current is a function of *solar radiation, cell temperature* and *coefficients* that are particular to the cell technology.

The PV array is an unregulated DC power source, which has to be conditioned appropriately in order to interconnect to power systems. Figure 3.1 shows the schematic diagram of an inverter for a small photovoltaic grid connected system. The inverter typically consists of the following parts:

- Maximum power point tracking (MPPT) circuit
- Optional energy storage element, usually a capacitor (and/or batteries)
- Optional DC/DC converter for higher voltage
- An AC inverter (DC to AC)
- An Isolation transformer to prevent DC from being injected into the power system

The block diagram of a typical grid-connected photovoltaic power station is shown in Figure 3.2. It comprises the photovoltaic array, a DC/DC converter and the DC/AC inverter at the grid side. Multiple arrays may use the same DC/AC converter, or multiple converters may also be

used. A battery storage system may be present at the DC bus (optional storage for independent and small installations). The role of the DC/DC converter (chopper) is to regulate the array output voltage (or current) so that the maximum available power is extracted (MPPT, i.e. for extracting the maximum available power for a given insolation level, i.e. maintaining the voltage as close as possible to the MPPT). The output stage (inverter) is functionally identical to the units used in other renewable energy converters, such as variable speed wind turbines. In earlier plants line-commutated units were used due to their low cost, simplicity and reliability. In modern installations self commutated PWM inverters are utilized, basically of the *voltage-source* type, for their key advantages of output power factor control and low harmonics

Figure 3.1: Schematic Diagram of a photovoltaic inverter for Grid Connected Operation

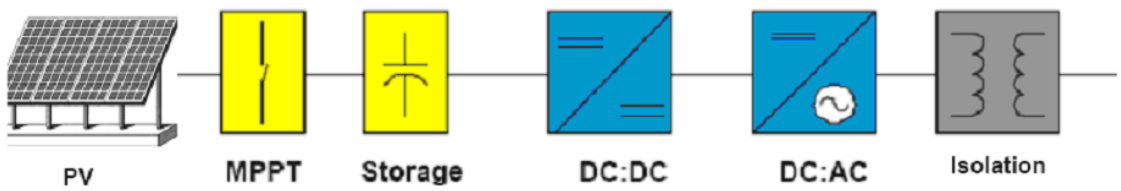

Figure 3.2: Diagram of Basic Grid connected Photovoltaic System Operation

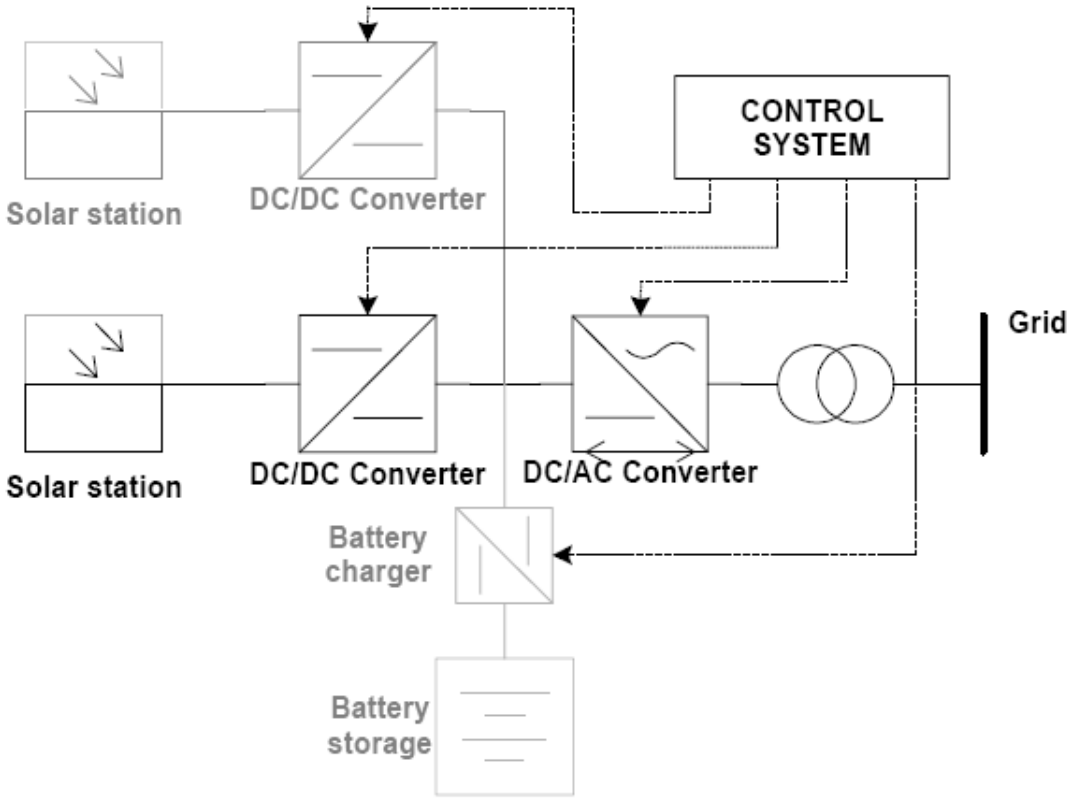

3.2 Stability Related to Distributed Photovoltaic Generation

The integration of new forms of generation and storage systems can significantly affect all types of power system stability, i.e. angle stability, frequency stability, and voltage stability. The majority of these power sources are connected at the distribution level.

Distribution systems are designed to accept bulk power from the transmission network and to distribute it to load centers. Thus the flow of both real power and reactive power was normally from the higher to the lower voltage levels. However, with significant penetration of embedded generation the power flows may become reversed and the distribution network is no longer a passive circuit supplying loads but an active system with power flows and voltages determined by the generation as well as the loads. The change in real and reactive power flows caused by embedded generation has important technical and economic implications for the power system.

Traditionally, distribution system analysis did not include issues of stability since network was passive and remained stable under most circumstances (provided the transmission network was stable).

3.3 Power Flow, Short Circuit and Photovoltaic Penetration Levels

Figure 3.3 shows the generic model of new forms of generation. Electrical Generator Models for Geothermal, Biomass, Hydro Power, Wave, Tidal, Micro Turbine and most Wind Energy Conversion, Fuel Cell (optional) and Flywheel (optional) systems employ synchronous or asynchronous generators. Their modeling characteristics depend on the generator type (induction, synchronous, etc.), the governor controls and VAR compensation devices (if any).

Figure 3.3 Generic Model of New Forms of Generation

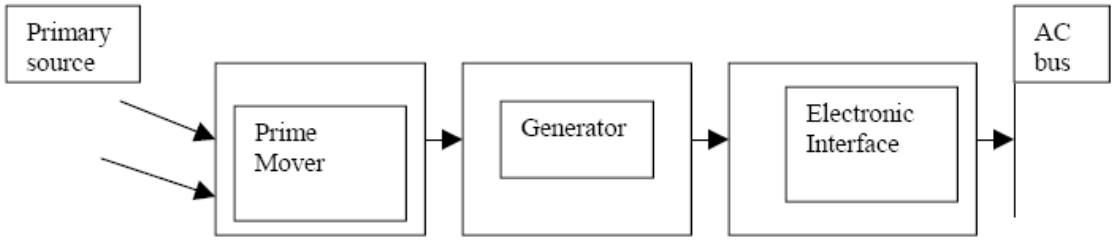

An equivalent **PV Power Plant** is modeled for Power Flow purposes as a Generator connected to a system bus, with the bus voltage 208 or 480 V.

The photovoltaic steady state model developed has the following attributes (Figure 3.4):

- Manufacturer, PV rating and actual voltage, (manufacturer information);
- Power Flow attributes, like operation mode: PV control mode or P, Q mode, controlled bus ID, reactive power limits, PV rated and actual voltage;
- Short Circuit attributes, like PV equivalent impedance;

- Dynamic model, an open architecture of the photovoltaic dynamic model, including panel dynamic model, inverter dynamic model and its controls and protection functions.

Figure 3.4 The steady-state photovoltaic model

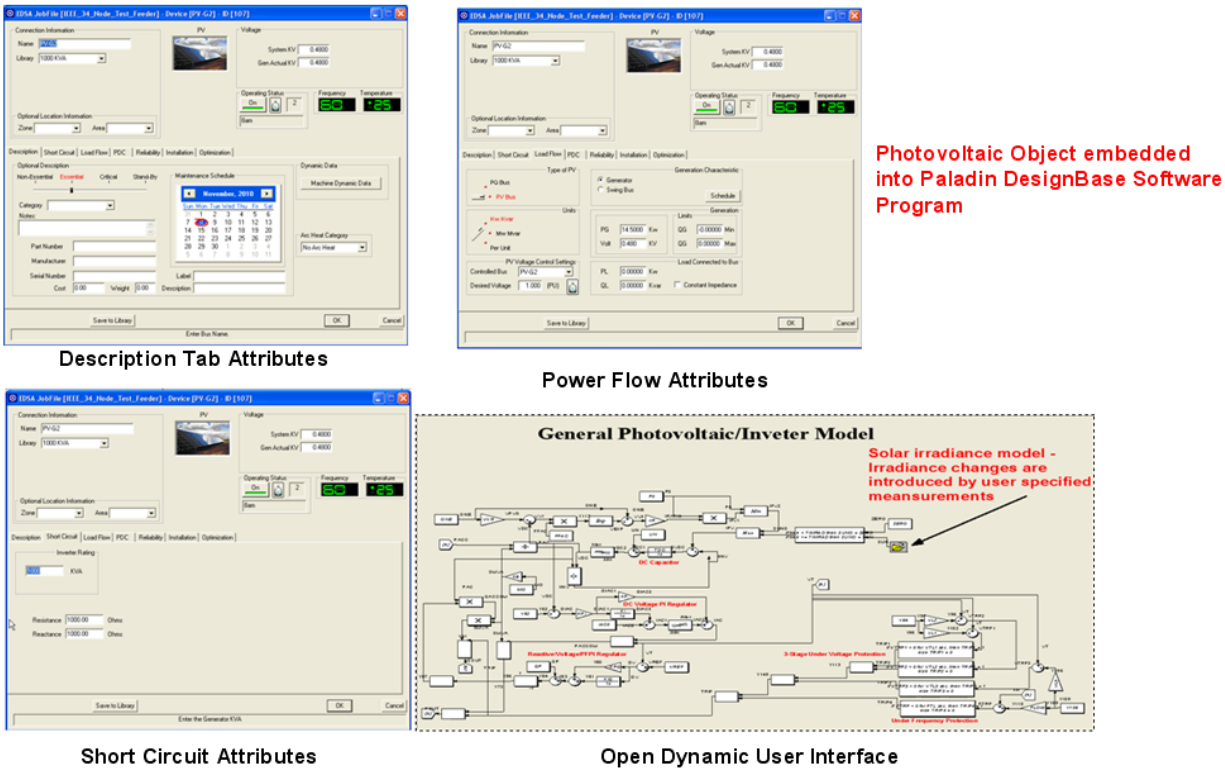

For Power Flow Analysis the following is required:

- Only inverters of the same type can be connected in parallel
- The active power dispatch for power flow simulation can be from 0 up to the MVA plant ratings.
- The default operating mode of the inverter is with fixed unity power factor. The generator reactive power will be Qmax = Qmin = 0.

  Some inverters operate with +/- 0.95-power factor. In this case only 95% of the equivalent inverter current is available for active power dispatch. The difference remains for reactive power control. If the inverter operates at non unity power factor / desired power factor, then Qg, Qmax and Qmin should be provided by the user and Q should be in the remain limits;
- If the inverter will control the voltage of a given system bus, then the control bus should be defined and the photovoltaic reactive power output should be set to +/- 0.344 P;

Three manufacturers (Xantrex, OptiSolar, SunPower) inverters were modeled for power flow, short circuit and dynamically for transient stability. The details of that analysis are provided in Appendix B. In addition, a fourth generic inverter is included in the study of PV power generation. These inverter models were then used to investigate penetration levels of distribution circuits.

The understand the impact of PV penetration on distribution systems, two types of power system layouts were investigated:

- PV units connected to loop power systems; the network secondary distribution system, service is redundantly provided through multiple transformers;
- PV units connected to a radial distribution feeder; there is only one path for power to flow from the distribution substation to a particular load. For the PV units connected to radial distribution system, two cases were investigated:
    - PV unit connected to the radial distribution feeder close to the Utilization Power Substation.
    - PV unit connected at the end of the distribution feeder.

The IEEE 39 Bus system was employed for investigating the PV penetration into the distribution feeder. The IEEE 39 Bus system was altered by connecting the PV units close to power substation and at the end of the distribution circuit.

3.4 Dynamic Simulation - Transient Stability (time domain) Model of PV System

The dynamic modeling aspect of this research is of particular importance because of the ability to incorporate time domain series data associated with solar irradiation timeseries described in Section 2.8. In addition, Power Analytics DesignBase's transient stability program supports a large number of dynamic elements for exciters, governors and power system stabilizers (PSS) offered by a variety of manufactures.

For most transient stability studies, the response of the PV to grid disturbances (short circuits) is of primary interest. For these studies, the approach should calculate the initial solar irradiation based on the plant's active power output in the power flow solution. This irradiation should be kept constant throughout the transient simulation time. The output power of the inverter and radiation result in a DC voltage that is a predictable function of the PV characteristics with virtually no dynamics. The DC voltage error is processed through a proportional-integral regulator whose output is the inverter direct axis current Ip that results in active power production.

The algorithm used to maximum power generated from the PV (MPPT) and determines a reference DC voltage. At steady state operating point the MPPT reference voltage remains almost constant since the MPPT voltage is not a strong function of irradiation. For applications that require the optional reactive power control capability, an additional source of excitation is the power factor angle command that produces a quadrature axis current Iq that results in

reactive power absorption or delivery. The approach also supports under/over voltage protection in addition to under/over frequency protection.

A literature survey was conducted to identify and summarize available PV models. The survey showed that even though a large number of papers, thesis, and journals exist on the subject solar power and renewable energy resources, very few papers provide details of PV and inverter modelling. Three commercially available products were found to have more details on their modeling, namely, Xantrex, SunPower and OptiSolar. Based on the above models, Power Analytics also developed a general model which included best features of the aforementioned models. The selected four models were built in the Power Analytics transient stability program using the user-defined capability (see Appendix C for details). These models were then tested on a functional level.

3.5 Development of Open Source Application Programming Interface (API)

Options were considered for the framework where the developed PV cell, inverter controllers and protection models can be compared and rated with ease of use, integration complexity, communication issues, etc. In addition to the development of complete PV plant models, the project requirements called for testing developed PV models in realistic power systems of different sizes and types (i.e. distribution as well as transmission systems) in the steady-state and dynamic operations. This required access to powerflow, fault analysis, and transient stability computational engines.

A number of commercial power system software packages were reviewed including Siemens/PTI, GE, Power Analytics (DesignBase), and others. The DesignBase was selected mainly due to the fact that is well suited for integrating PV models into the package, and most importantly the DesignBase offered advanced user-defined modeling feature which allowed the developed PV models become available in an open source approach to the end-users. This analogy of the approach adopted by the research team is similar to SIMULINK relationship to MATLAB platform. The use of DesignBase facilitated the creation mathematical models of PV plants in an advanced graphical user interface by assembling algebraic and differential equations governing PV plant models by elementary functions such as adder (+), division (/), multiplication (X), integral, lead-lag, etc. The models built are then written in two different formats one in a binary form (to be used by the DesignBase analysis engine for efficient operation) and one in plain readable text form that is extremely easy to follow (similar to scripting languages such as Python, pearl script, etc.). An example is shown in Fig. 3.5 and the models for three inverters are also posted on the DOE High Solar Penetration Portal along with an explanation with the structure provided. The files can be accessed and downloaded at https://solarhighpen.energy.gov/open_source_inverter_models. The files can be converted to binary for direct use in the Power Analytics Designbase software, MATLAB Simulink, or other power engineering software packages.

Figure 3.5: The developed photovoltaic cell

```
…

…

…

Parameters,Ti,Integration time constant. Ti = 0.3 * T'do generator,0.000100,3.368000,99999.000000

Parameters,VRMAX,Positive ceiling voltage of the thyristor converter in pu,0.000000,4.840000,20.000000

Parameters,VRMIN,Negative ceiling voltage of the thyristor converter in pu,-20.000000,-3.300000,999.000000

Constant,VS,0

Constant,VREF2,VT0*1.05

Sum 2,+Y22,-VTT,VERR

Limit,DV2,DV3,VIMAX,VIMIN

Lead-Lag,VF2,VF1,Td,0,Tf,1

Lead-Lag,DV,DV1,HT4N,1,T4HP,1

Sum 1,+VS,+VERR,-VF,DV

Gain,DV1,DV2,Kp

Integrator,DV3,DV4,1,Ti,KE*EFD0/Ka

Sum 2,+DV3,+DVV,DV5

Limit,DV6,DV7,VRMAX,VRMIN

Gain,DV5,DV6,Ka
```

The developed photovoltaic cell, inverter controllers and protection models developed under the DOE award are made available on the DOE High PV Penetration Portal. Three models are provided for an OptiSolar inverter, a Xantrex inverter, and a SunPower inverter. The files posted here can be opened with a text editor and edited / extended as necessary. They can be converted to binary for direct use in the Power Analytics software or other power engineering software packages. A sample is show in this figure.

Figure 3.6: Building Photovoltaic Models in a Graphical User Interface

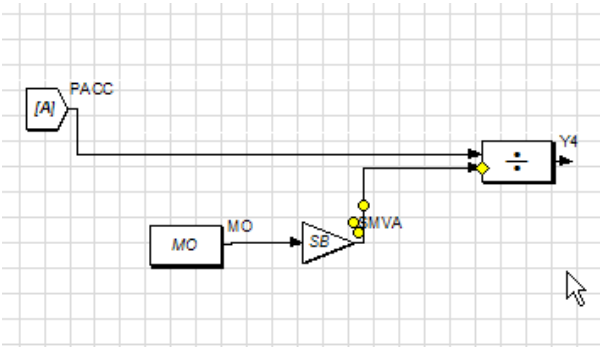

There is no need for the user to even to master the scripting language shown above since as discussed earlier the user can build the PV models in a graphical user interface (Fig. 3.6). The three inverter models created in the research and the generic model are all provided as input into other modeling applications as source files.

All of the developed PV plant models in this research project have been created in the approach described above. Every detail of the developed PV models is fully open to the user for modification or simply inspection. The open source PV models are then to interact with the DesignBase analysis packages in a totally transparent fashion. Thereby, these models are linked to powerflow, fault, and transient stability simulations for testing and assessment of performance in realistic power systems.

3.6 Benchmarking

The work includes validation of the approach based on a variety of distribution networks and IEEE standard networks. An essential element of this work was the selection of power networks that become the basis for the simulation. The selection criteria requires target networks be well documented, available for peer review and representative of real world distribution circuits. Two such networks that were selected for this work include the IEEE 34 Bus network and the WECC 9 Bus network for dynamic simulation. These standards were used for the primary benchmarking and results included in the detailed Appendix B. Both standards are readily available and used globally by respective power engineering communities for proofing and verification of the two primary benchmark standards.

CHAPTER 4:
Integration Study and Interconnection Guideline

In this section the steady state models described in Section 3 are applied in an integration study. The effect of various PV penetration levels and configurations for a typical daily irradiance profile are quantified. Mitigation options are outlined in Section 4.2. Based on general power plant modeling considerations, recommendations for application of mitigation measures (Section 4.4) and Interconnection guidelines are provide (Section 4.5). These recommendations are primarily based on a survey of the literature and national and international experience of the Power Analytics team in power engineering and renewable generator interconnection.

4.1 Integration Study

4.1.1 Data requirements

The integration study is intended to provide a systematic approach for the engineering review process of a typical system study and to determine PV impacts on the system. It includes the steps that must be taken to properly account for site-specific concerns and address the technical and procedural requirements of the PV integration. The intention is to give to the PV users a clear understanding of how the integration analysis will be conducted.

4.1.2 Modeling Scenarios

The IEEE 39 Bus system was employed for investigating the PV penetration into the distribution feeder. The IEEE 39 Bus system was altered by connecting the PV units close to power substation and at the end of the distribution circuit.

In order to investigate the penetration of PV system and understand the impact of PV penetration, PV units connected to a radial distribution feeder were examined; there is only one path for power to flow from the distribution substation to a particular load. For the PV units connected to radial distribution system, two cases were investigated (Table 4.1):

- PV unit connected close to the Power Substation;
- PV unit connected at the end of the distribution feeder.

The common typical approach of investigating the penetration of PV system is by considering the PV name plate data. This approach is conservative, but does not consider the irradiance impact to PV system and however does not consider the PV capacity factor. For power flow modeling several scenarios should be generated to account for irradiance magnitude and time variation. To account for the irradiance, the irradiance measured data were considered and however the PV unit output power is considered as a function of time. For system studies purposes, the PV unit output power was considered at 6 am, 8 am, 10 am, 12 pm, 2 pm, 4 pm, 6 pm and 8 pm., based on field measurements on a typical day.

PV penetration levels should be scaled up on % of total system load – 10%, 20%, 30% up to the thermal limits of the connection circuit;

Table 4.1.: Scenarios simulated for PV unit connected close to Power Substation (S); the PV unit power output is a function of irradiance/time provided by the user

PV Unit Connection Type	Scenarios:	System Studies:	PV Penetration Level
PV Unit Connected near **Power Substation** or **at the end of distribution feeder**	PV Unit is disconnected; PV Power Output at 6am, 8 am, 10 am, 12 pm, 2 pm, 4 pm, 6 pm, 8 pm.	Total system load is constant and equal to the system peak load. The following studies were performed: • Power Flow studies (Appendix B.1) • Short Circuit studies (Appendix B.2) • Security analysis (Appendix B.3) • Reliability analysis (Appendix B.4)	For each scenario the following penetration level were considered: 10%; 20%; 30%; 40%; 50%.

4.1.3 Results and Conclusions

Detailed results are provided in appendix A for each scenario. Appendix A.1 shows the power flow results, A.2 shows the short circuit analysis, appendix A.3 shows the security analysis, and A.4 shows the reliability analysis.

General considerations:

- For radial distribution feeder the absolute maximum PV penetration is dictated by the feeder maximum allowed ampacity (feeder thermal limits);
- While PV level is increased attentions should be paid to bus voltage profiles, branch loadings (circuit maximum loadings) and power flow direction;
- When PV size is larger than the total aggregated load at the PV terminals, PV power may be injected into the feeder system and consequently the flow directions are changed. In this situation islanding operations may occur.

Detailed results for a PV unit connected close to the power substation. In summary, there are no major impacts onto the feeder distribution system performances downstream of the PV location:

- The photovoltaic penetration level changes the amount of active power injected by the Utility into the distribution feeder at the PCC point;
- The system total losses are reduced proportional with the PV penetration level;
- The PV penetration level is limited by the ampacity of the feeder which connects the PV unit to the distribution feeder;
- During the peak loads (10 am to 12 pm) the increase of the PV penetration level helps the power utility by increasing the power utility total active output power;

- A key question for each PV installation is whether the PV applicant intends to export generation across the point of common coupling (PCC). If power is to be exported across the PCC point then:
    - PV unit that exports can cause reverse voltage drops (from the PV towards the substation). Thus, the power utility may need to study the local distribution system and determine if adjustments to local voltage regulation schemes are necessary.

Detailed results for a PV unit connected at the end of the distribution feeder. There are significant impacts onto the feeder distribution system performances, as follows:

- PV penetration level improves system bus voltage profile, by reducing both the bus voltage drops and the branch loadings;
- PV penetration level reduces the system losses proportional with the penetration level; when transmitting electric energy through the distribution systems, typically system-wide on the order of 4 to 7% of the total energy generated is lost in transit from generation sources to loads. However, PV can reduce line losses by providing more of the power supply locally rather than through transmission and distribution lines. This benefit is more likely to be quantified on radial distribution lines than on networked distribution or transmission lines. The reduction in line loading due to a distributed generator can be directly seen on a distribution feeder, whereas the impact on a system network is spread over the multiple lines. The system losses reduction also has implications for capacity requirements. A 5% reduction in energy losses from PV use at the point of customer load translates into that much less generation, distribution capacity that would otherwise have to be built to generate and transport that energy;
- PV penetration level increases the distribution feeder reliability; PV generation can have a positive impact on system and local distribution reliability. For the power utility the primary economic impact of poor reliability is the increased expenditures for emergency maintenance. However, an analysis of the applicant loads and local reliability data would allow a Power Utility to identify locations where PV could have the best impact on reliability improvement.
- The improvement of the feeder reliability is due to the reduced branch loading;
- Attentions should be paid to the penetration level. If the PV unit output power is higher than the total load connected at the PV terminal, then
    - the PV injection power changes the direction of power flow in the distribution feeder towards power substation. This will have a negative impact on system protection selectivity;

- there is a danger of having system islanding operation. In this situation, the PV inverter should be equipped with anti-island operation protection: voltage protection and frequency protection to disconnect the PV unit;
- during faults at points situated towards the power substation, the PV inverters should be equipped with "faults ride through" protections;
- and the feeder segments are relatively long, flicker may occur at buses situated towards power substation due to irradiance fluctuations over time;

Power Quality issues:

- Minimum harmonics and flicker standards are defined for PV. These limits are established in IEEE 519. In summary, this standard, in Chapter 10 for individual consumers, requires current total demand distortion (TDD) of 5% or less of the fundamental. The standard, in Chapter 11 requires voltage total harmonic distortion (THD) of 5% or less and 3% for any single harmonic, measured at the point of common coupling. Described in Chapter 10 of the standard, flicker, typically associated with induction generator start-up, may not cause a voltage dip of more than 3% as indicated on the border lines of irritation curve of the standard.
- One should notice that power quality is related to reliability in some ways, and the potential solutions can be similar to those for reliability. However, in general, power quality problems tend to be short in duration and small in magnitude, but frequent or constant in occurrence. They may include voltage sags or spikes, switching transients, harmonics (frequencies other than 60 Hz), noise, and momentary outages (less than 5 minutes, according to the definition in the EEE Reliability Standard 1366; there is no similar standard for power quality).

The proliferation of solid-state electronics in customerequipment is frequently the source of many PQ anomalies. Resolving the power quality issues can be difficult since the problems may have their origin in the power utility system, the customer's own equipment, the equipment of other customers on the feeder, or an interaction between any combination of these parties systems;

Single-phase systems will primarily be used on residential or small commercial applications. For three-phase connected PV units the requirements are further broken down by PV capacity, with larger systems having more requirements than smaller systems.

4.2 General Mitigation Options for PV Variability

4.2.1 Voltage Control (Automatic Voltage Regulator)

There is a need for automatic voltage regulation for PV plants. PV plant technologies with voltage source inverters can apply automatic regulators to regulate the reactive output to maintain a certain voltage e.g. at the point of interconnection between the PV plant and power system. In other cases voltage regulation can come from a supervisory control system regulating the reactive resources throughout the PV plant. For larger PV installations, SVC

(static VAR compensator) or STATCOM (static synchronous compensator) coordinated together with a number of mechanically switched capacitors can provide the required voltage regulation. For smaller PV plants in distribution systems, DVAR (dynamic VAR compensator) or DSTATCOM (distribution static compensator) can be utilized.

4.2.2 Frequency Control (Governor)

Frequency control for PV is possible but not to the same degree as frequency control with a governor on a classical generator. PV plants should not actively participate in primary frequency control during under-frequency. Having a "governor like" control for a PV plant control scheme to assist the power system in the event of an over frequency condition is a technical possibility and even desirable. It is reasonable to recommend that a PV plant meet an off-nominal frequency operating condition similar to Table 4.2 that is used by many utilities for wind farms and classical generating plants.

Table 4.2: Typical Off-Nominal Frequency Operating Requirements

Frequency Range (Hz)	Time (seconds)
>61.7	0
61.6 to 61.7	30
60.6 to <61.6	180
>59.4 to <60.6	Continuous Operation
>58.4 to 59.4	180
>57.8 to 58.4	30

4.2.3 Low Voltage Rid-Through (LVRT)

Typically PV plants operate continuously between 90-110% of nominal voltage at the point of connection to power system. PV plants should be able to stay connected to the power system for voltage dips or voltage rises. Typically PV will be required to ride-through voltages for the duration required to achieve fault clearing times of a normally cleared fault. The cost of achieving ride-through down to zero voltage (using a combination of battery storage system and voltage source inverter) can be significant and may only be reasonable for larger PV plants installations (greater than 10 MW).

4.2.4 Reactive Power Capability and Power Factor

Reactive power capability requirements and power factor (PF) control for larger PV should be similar to those for wind generation. Reactive power compensation is desirable for PV. Reactive power capability is measured at the low voltage side of the PV substation. A PV plant at its full load should be capable of 0.90 pf lagging and 0.95 pf leading. Automatic voltage regulation that

is able to regulate the voltage at this point to a "desired"[2] set-point should be within +/-0.5%. The voltage regulation system should have adjustable gain, droop and a reference set-point. Voltage regulation should be provided to adequately control voltage at the point of interconnection throughout the range of power delivery of the PV plant and coordinated with other voltage regulating devices on the transmission system.

In cases where a good portion of reactive compensation is provided at the PV substation in the form of an SVC or STATCOM, such coordination is more easily achieved since it is done through a centralized control. Moreover, the device may be more easily used for voltage regulation even when the PV is disconnected since it is directly connected to the substation. Finally, based on general consensus it is believed that a power factor requirement of +/- 0.95 at the point of interconnection is a reasonable requirement.

4.2.5 Power System Stabilizers

Power System Stabilizers (PSS) in the traditional sense do not apply to PV generation since they are essentially used for synchronous units. PV units are essentially decoupled from the system and do not really participate in electromechanical modes of rotor oscillation. The fundamental concept behind PSS tuning is to introduce a component of damping torque on the shaft of a generator in the range of frequencies associated with electromechanical modes of rotor oscillation. However, based on the generalization of concept of power system stabilizer, it may be possible to design stabilizer for a PV plant controller to modulate the output power to improve the damping of inter-area modes. Similar stabilizers have been proposed for SVC, STATCOM and HVDC. This, however, would be contingent on the location of the PV plant and thus the controllability of the mode from the PV plant location. To be fully effective, a PV plant needs to be on-line to obtain the full benefit of all stabilizers (the PV output and status are difficult to predict). Therefore, at this time, PSS application on the PV plant controllers it is not generally recommended.

4.3 Considerations for PV Power Plant Modeling and Mitigation Options Depending on Plant Size

The cost of implementing some of the recommended control functionalities described below and mentioned earlier may exceed the benefits. Smaller PV systems (e.g. 5 to 10 MW), are less significant to the distribution system and have no net active power delivery into the transmission system. As such, these units may not significantly contribute to the overall system performance. Therefore, the operator should waive requirements where such requirements may not deliver any significant benefit to their system operation.

It is important to note that the distinction between distribution connected and transmission connected PV generation may be somewhat subjective when a number of smaller (<10 MVA) distribution connected PV systems make up a substantial power delivery to the transmission

---

[2] Determined through system analysis or specified by the control center operators based on the system conditions

systems. An easy way to make this distinction is to quantify the PV penetration level. If, for example, the megawatt output from small distribution-connected PV systems is being consumed locally at the distribution level such that a system disturbance that disconnects the PV plant from the system also disconnects the load (i.e. no net imbalance in system load generation) then low-voltage ride-through and power limitation/curtailment may be doubtful for such a PV plant.

However, if megawatts are being transported over the transmission system to remote loads then the loss of the generation following a disturbance would constitute load/generation imbalance and thus would not be acceptable in large amounts. In general the research team recommends adoption of the IEEE Std. 1547™ Standard for Interconnection Distributed Resources with Electric Power Systems, and its applicable guides, for PV plants with an aggregated combined power output of <10 MVA. This standard was recently developed for distributed generation facilities of <10 MVA.

Applied to large PV plants (>10 MVA) connected to a transmission system benefits of the PV mitigation options discussed in section 4.1. are substantial. In order to plan and operate a power system with embedded PV plants similar to conventional generators the active power output, voltage control, protection and monitoring schemes this research team recommends adherence to a set of agreed upon rules (standard/guideline). Below is a summary of recommendations for establishing requirements of a standard/guideline for PV plants integration into power systems. The IEEE Std. 1547.5 for facilities with a combined capacity of more than 10 MVA is under development.

4.4 Mitigation Measures for Large PV Plants (>10 MVA)

4.4.1 Active Power Generation

- The system control center (transmission system operator - TSO) should have a means to observe the megawatt output of a PV plant in real-time;
- The system control center must have a means of issuing a directive to curtail the megawatt output of the PV plant in an emergency condition where the PV plant output is to be reduced to respect thermal limits on nearby transmission corridors or when otherwise generation far exceeds demand. Alternatively, the PV plant operator may intentionally disconnect blocks of PV modules in the plant to effect a reduction in generation. In any case, this research team recommends this to be done in a controlled fashion and at the specified rate by the operator (e.g. certain number of MW/minute);
- All PV modules in a single PV plant must not start or stop simultaneously. This can be achieved through sequencing of the start-up and shutdown controls of the PV inverters in a plant.

4.4.2 Zero/Low Voltage Ride Through

This research team recommends for PV plants to be able to ride through faults taking place at the high side (transmission voltage level) of the substation transformer. This requirement does

not apply to a radial PV plant connection. In such cases, this research team recommends that the PV plant be able to ride through any normally cleared faults external to the radial line feeding the plant. This requirement would translate to the PV plant being required to ride-through a 3-phase fault (normally the most severe fault) close to the point of interconnection which means that the PV plant can "survive" a near zero voltage for duration of approximately 100 ms, [21, 22, 23].

In FERC (Federal Energy Regulatory Commission) discussions, it is suggested that zero/low voltage ride through may still be a relatively new development and still requires further development. What cannot be tolerated is to have a single disturbance that results in the loss of multiple generating plants. In the future as the technology progresses (and PV penetration increases) then a fault ride-through strategy may be adopted. The recommendation here is to slowly transition to requiring that the PV plant be able to ride-through fault external to the plant for the normal fault clearing durations. For system disturbances with longer durations, where the system voltage does not recover for an extended period of time, the PV plant must be tripped by under voltage protection. Also, any shunt capacitors that are used for power factor correction must disconnect from the system to prevent overvoltage conditions when the system recovers after fault is cleared.

4.4.3 Voltage/Frequency Operating Limits

For steady state, transient voltage conditions, and for off-nominal frequency operation, this research team recommends that PV plants meet the existing criteria of the respective utilities. The table below shows a typical example of the off-nominal voltage performance. Clearly, all PV plants must operate continuously at and between ± 10% of nominal system voltage and ± 0.5 HZ of nominal system frequency.

Table 4.3: Example of off-Nominal Voltage Performance, [24, 25, 26, 27, 23]

Overvoltage	Undervoltage	Minimum Delay
<1.10 pu	>0.90 pu	Continuous
-	≤0.90 pu	10.0 seconds
≥1.10 pu	-	5.0 seconds
≥1.20 pu	≤0.80 pu	2.0 seconds
≥1.25 pu	≤0.75 pu	0.8 seconds
≥1.30 pu	-	0 seconds

Any single or multiple contingencies as defined by NERC, (North American Electric Reliability Corporation, i.e. categories A, B, C, and D) with PV plant interconnections and operated at full output should not cause transient voltage and/or frequency violations as specified in table 4.4.

Table 4.4: WECC/NERC Disturbance-Performance Table of Allowable Effects on other Systems

NERC and WECC Categories	Outage Frequency Associated with the Performance Category (outage / year)	Transient Voltage Dip Standard	Minimum Transient Frequency Standard	Post-Transient Voltage Deviation Standard (see Note 2)
A	Not applicable	Nothing in addition to NERC		
B	>0.33	Not to exceed 25% at load buses or 30% at non-load buses. Not to exceed 20% for more than 20 cycles at load buses.	Note below 59.6 Hz for 6 cycles more at a load bus.	Not to exceed 5% at any bus
C	0.033 – 0.33	Not to exceed 30% at any bus. Not to exceed 20% for more than 40 cycles at load buses.	Note below 59.0 Hz for 6 cycles more at a load bus.	Not to exceed 10% at any bus
D	< 0.033	Nothing in addition to NERC		

Figure 4.1: Transient Voltage Performance Parameters

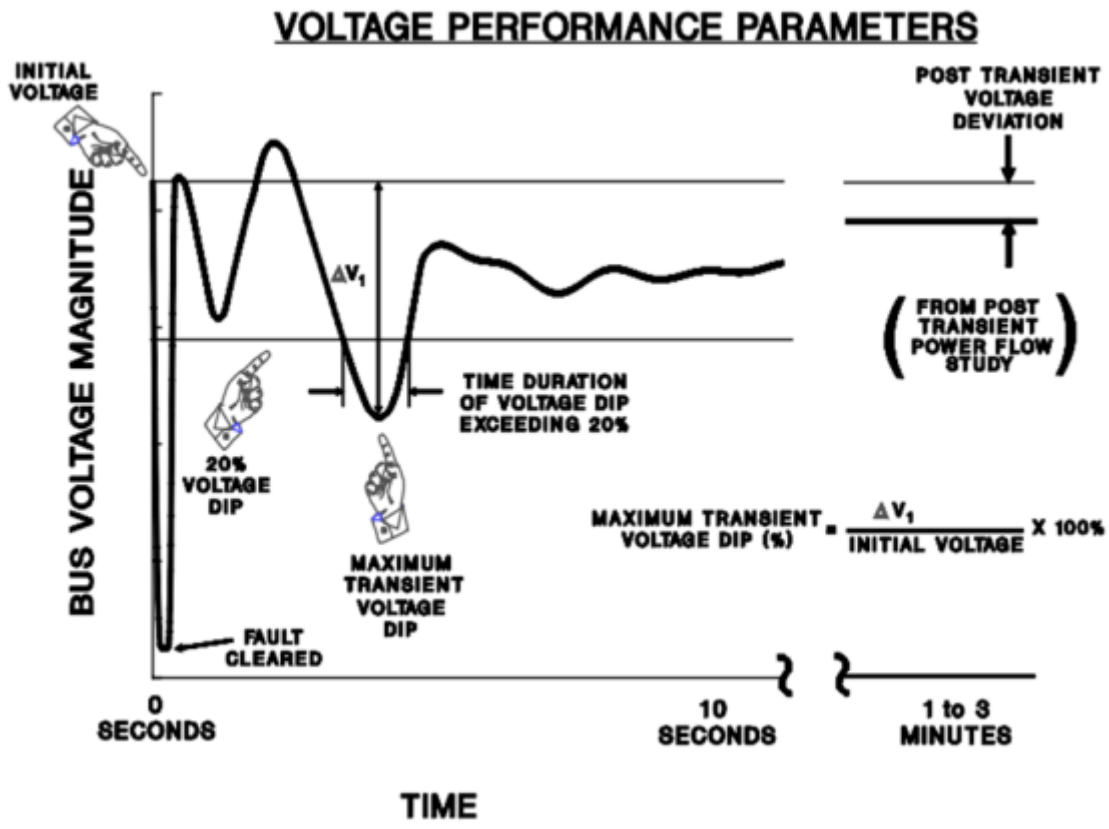

4.4.4 Power Quality

This research team recommends that PV plants meet the power quality requirements of their respective operator, in line with IEEE Std 519. This research team recommends that PV plant owners be responsible for performing studies where necessary to ensure that they avoid low-order harmonic resonance phenomenon on their system due to shunt capacitors (or cable charging) and power electronics. PV voltage/power variation due to variation in the solar irradiance may also cause voltage flicker. Although such large voltage changes are unlikely for most PV systems and feeder configurations, this research team recommends that PV owners comply with standards for voltage fluctuations at the point of connection of the PV plant facility to the power system as outlined in Table 4.5. Voltage dips more frequent than once per hour must be limited to the WECC "Border Line of Visibility Curve".

Table 4.5: Suggested Voltage Fluctuations Limits, [23]

Voltage Change	Maximum Rate of Occurrence
+/-3% of normal level	once per hour
+5/-6% of normal level	once per 8-hour
Exceeding +5/-6%	As agreed by utility

Voltage and current harmonics can cause telecommunication interference and thermal heating in transformers; that can disable solid-state equipment and create resonant over-voltages. In order to protect the distribution system infrastructure, this research team recommend that the PV plant power electronic interface not cause voltage and current harmonics on the power system and adhere to IEEE Standard 519.

4.4.5 Control Interactions

Where necessary, this research team recommends that the PV plant owner be responsible for performing studies to ensure that automatic controls on the PV plant do not adversely interact with other automatically control transmission devices such as nearby SVC, STATCOM, HVDC, etc.

4.4.6 Reactive Power Requirements

Based on standard industry practice it is recommended that PV plant facilities be able to operate with 0.90 pf lagging and 0.95 pf leading power factor (when generating its peak megawatt output) at the point of interconnection. This point is defined as the high voltage side of the substation transformer. This research team recommends that this reactive capability be in the appropriate ratio of discrete (mechanically switched shunt capacitors) and dynamic (SVC, STATCOM, etc.) to ensure both steady state and transient stability during and after a disturbance. Studies may of course determine that the actual reactive needs are higher or lower depending on the size and location of the PV plant.

4.4.7 Protection Requirements

The PV plant operator/developer:

- Is responsible to implement adequate protection to safeguard all PV generation equipment within the PV plant. Such protection, however, must properly be coordinated with other controls and the protection of the utility power system in its vicinity;
- To design and implement such protection. In special cases, the plant developer may be required to perform specialized analysis such as:
    - Electromagnetic transient/harmonic analysis such as switching including the energizing of transformer, capacitor banks, etc.;
    - Controls interaction studies, if the PV plant is being placed in-service in close vicinity to an existing power plant or HVDC system, etc.

4.5 Interconnection Recommendations for Large PV Plants

4.5.1 Automatic Voltage Regulators

This research team recommends that the PV plant developer be responsible to provide adequate steady state and dynamics models of the PV plant to utility where PV plant will be interconnected and that these models be updated when commissioning the PV plant if any model structures or parameters are substantially changed between the planning and commissioning phase of the plant. This research team recommends that field verification tests or studies be performed to demonstrate that the PV plant meets all of the requirements set forth by interconnection policy of the utility. In particular, this research team recommends that the low-voltage ride-through capability of the PV be demonstrated either through detailed modeling of the PV controls, or by field/ factory tests.

4.5.2 Disturbance Monitoring System

For the purpose of continued understanding of PV plant operation and control, utility may consider requiring that each PV plant be equipped with a disturbance monitor for voltage and current, active power transfer, reactive power transfer, and system frequency at the interconnection point.

4.5.3 Telemetry

This research team recommend that a large PV plant should make the following information available via telemetry:

- Active and reactive power output at the PV plant;
- Status of circuit breakers on substation transformer and all shunt compensation devices located at the PV plant substation;
- Tap position of the PV plant substation transformer if it is equipped with on-load tap-changers;

- Meteorological data including average solar irradiance at the site, as required to facilitate the use of forecasting models;

This research team recommends that the telemetry provide options for control such as curtailment and specification of voltage regulation set-points for the point of interconnection.

4.6 Summary of Interconnection Guideline

Interconnection standards adopted by utilities for integrating classical and alternative sources of power generation including PV into the power system have been surveyed to provide guidelines for PV plants. The outcome is a series of recommendations, all technically feasible and viable, for possible incorporation into broader standards for interconnecting PV plants to the utility system. The goal of any such standard will be to establish minimum technical requirements for connecting PV plants to the power systems at transmission and/or distribution levels. Such a standard will make no distinction as to the preferred technologies or types of PV generation equipment, but rather rely on the ingenuity of the PV plant developers, PV plant manufacturers and other power equipment manufacturers to come up with the most cost effective means of meeting and/or exceeding the technical established standards.

Salient issues of the PV plant interconnection are outlined below:

A. Reactive power capability;

B. Power Factor and voltage regulation;

C. Low voltage ride through capability;

D. Frequency control;

E. PV plant modelling for conducting power system studies to establish:

    1. Thermal limits;

    2. Voltage violations;

    3. Frequency stability;

    4. Transient response- dynamic response;

    5. Post disturbance steady state.

Based on background information obtained and the project team's experience with PV integration studies (see Appendix B), recommendations are given on the best practices and emerging standards for interconnecting large PV plants to the power system:

Potential technical PV integration problems can be addressed regardless of the type or manufacturer of the PV generation system, provided proper analysis and design is performed at early stages.

Most PV systems were designed to disconnect from the power system immediately following a system disturbance, especially a system fault in the vicinity of the PV plant. With large-scale PV

generation connected to the transmission systems, this is no longer an acceptable response. Low voltage ride through capability should be mandated for PV plants.

Power quality requirements including voltage flicker, harmonics, as well as coordination of controls and protection are an important part of the interconnection guideline. The power quality, control and protection requirements for PV should be adopted from the existing guidelines and standards such as IEEE Standard 1547, 1547.5, 519, and 929-2000, IEC 555, IEC 61000.

In general, the maximum size of PV plant that can be accommodated in a power system should be limited by the available short circuit capability at the point of common coupling (POI) of the PV plant to the power system. A ratio of available short circuit at POI to the PV plant size of less than five will likely introduce voltage control problems.

The maximum level of PV penetration into a power system beyond a certain minimum threshold (currently 15%), cannot be determined from a simple set of rules. Maximum level of PV penetration into a given power system should be determined via on-line or off-line analysis for a specific power system.

CHAPTER 5: Accomplishments and Future Work

Power flow and short circuit models of PV systems have been developed and implemented in Power Analytics Designbase. Also, transient stability (time domain) models of the PV System using three inverters have been completed using the Universal Control Logic Modeling and Simulation (UCLMS) feature available in the advanced transient stability program. Treatment of dynamic variations in solar irradiance has been implemented and is described in Chapter 2.8.

An Open Source Application Programming Interface (API) was developed and the open source files for the three inverter types were posted to the DOE High Solar Penetration Portal. Since most inverter manufacturers hold their data as proprietary, despite a request sent to all major manufacturers only two inverter models could be added to the vendor library.

Chapter 4.1 presented the summary of simulations conducted for different levels of PV penetration (10% to 50%) and scenarios (far away from vs. close to substation, morning vs. noon PV output) with detailed results in Appendix B.1. Contingencies and disturbances were simulated (Appendix B.3 and B.4). Detailed results allowing other engineers to recreate the models developed in this project are presented in Appendix B. Planning guidelines are presented in Chapters 4.2 to 4.6 and recommendations are summarized in the executive summary.

Given a 1-year dataset of 1-second Global Horizontal Irradiance (GHI) measurements, ramp rates for individual panels and aggregated sites were quantified. A ramp rate model was developed and validated.

The following work will be conducted in future years:

5.1 Three-dimensional Cloud Tracking and Insolation Forecast Model

Accurate solar forecasting and energy storage can dramatically reduce integration costs. A real time observation network of insolation measurements that operates continuously at high temporal (1 second) and spatial (16 stations over 1200 acres) resolution will be utilized. It is collocated with a sky imager, a ceilometer, and 1 MWp distributed solar PV array. Using this infrastructure, an energy storage controller function of the master controller will be developed to respond to the cloud detection and forecast system using a three-tiered mechanism.

Tier 1 is the real-time cloud detection, when on a clear day the detection of clouds by a sky imager or satellite will signal the controller to start diverting an appropriate amount of the PV output to charge the storage system. Conversely, the detection by the sky imager of a reduction in cloud cover will signal the controller to start discharging the storage system in anticipation of a rapid increase in solar power output. Tier 2 is the three-dimensional cloud position forecast that uses pattern recognition algorithms to derive cloud motion vector fields from sequential sky images and forecasts cloud positions for the hour ahead. Cloud height will be determined by a ceilometer. Given typical reductions in solar irradiance due to clouds, the controller will

compute the amount of storage required to smooth out the PV power production curve. Tier 3 is the power output forecast, which is recomputed as cloud-related solar radiation reductions are observed at the micro climate stations, the optical depth of each cloud will be computed and used by the cloud position algorithm to determine expected solar power output at each PV array for the following hour. This will result in a full three-dimensional model that tracks and forecasts the movement, optical depth, and shadow locations of individual clouds with respect to solar PV arrays on the ground.

5.2 Command, Control and Communications for Power Flow Management

A Utility Command/Control Interface (UCCI) will be developed to enable visibility into the status of distributed generation systems. The UCCI will establish a common interface for bi-directional communications between the system controller (SC) and the electrical power service provider, or Utility. The UCCI's operation will comply with the OSI seven layer model and utilize non-proprietary methods whenever possible. The UCCI application layer will define a structure and method to process price signals from the utility or RTO/ISO, energy dispatch signals from the utility or RTO/ISO, acknowledgements with the utility or RTO/ISO, system performance and status from the PV system to the utility or RTO/ISO, metered performance to the utility or RTO/ISO and/or third party certification, operating software upgrades from the utility or RTO/ISO to the PV system, and, possibly, the demand management gateway to the user premises.

The UCCI will also incorporate other modes of operation depending on local and external conditions, including: Net Metering (when the utility grid is viewed as an infinite source or sink for power); Utility Dispatch Source (where the utility is always sourcing some energy to the local load); Utility Dispatch Sink (where the PV system is always sourcing some energy to the utility grid, to the extent that local energy is available); Price Signal (which allows the PV system to determine when favorable economic conditions warrant a particular energy flow action); and Override (when the customer takes total control of operation regardless of utility dispatch of price signals).

5.3 Field Testing and Validation of the Suite of Models

The power flow models developed by the research team will be field-tested and validated using data at the UC San Diego solar energy testbed. In addition, distributed energy storage and PV to electric vehicle charging as mitigating measures at its existing 2 MW of PV will be implemented and evaluated. The resource forecasting models will be applied to predict PV output operationally and will be verified against actual PV system performance.

5.4 Raise Situational Awareness of Virtual Power Plants and Microgrids by Distribution Utilities and RTO/ISOs

The research team will perform real-world simulations, evaluating and verifying microgrid renewable integration operations in the controlled and well-instrumented environment and to raise the awareness and understanding of the RTO/ISO operators.

The anticipated proliferation of Distributed Energy Resources (DERs), including, but not limited to, distributed energy storage and electric vehicles, has the potential to significantly complicate or enhance the operation of local electricity distribution networks and transmission grids. These DER are often small and "behind the meter," where they will not even appear as supply, but as load reductions. Several issues need to be addressed to enable the distribution grid and Regional Transmission Operators/Independent System Operators (RTO/ISO) to maintain the appropriate level of situational awareness. With greater penetration of DERs observability, dispatchability, and permitted autonomous actions by DERs must be established. One approach to addressing these issues is to organize the DERs into structures that can be more easily characterized and understood. Three such structures are virtual power plants (VPPs), microgrids and aggregations.

This project will raise the distribution and RTO/ISO operators' understanding of VPPs and microgrids to a level that will permit these resources to become competitive operational assets for power generation, demand response and ancillary services responding to dynamic price signals. This will be accomplished by performing real-world simulations, evaluating and verifying microgrid renewable integration operations in the controlled and well-instrumented environment on UC San Diego's microgrid. The demonstration will incorporate renewable resources including solar PV coupled with advanced energy storage and demand response to test the ability of the microgrid to adjust its internal operations. Adjustments made will stabilize the variable renewable generation and allow the local utility to better balance their networks and the RTO/ISO to reliably schedule and dispatch the microgrid. A similar test will be performed for a VPP, including storage and load management capabilities with local thermal generation. This additional generation will simply appear to the system as supply and be modeled and dispatched within the RTO/ISO systems in exactly the same manner as any generation resource.

5.5 Acknowledgments and Disclaimer

This material is based upon work supported by the Department of Energy under Award Number 10DE-EE002055.

This report was prepared as an account of work sponsored by an agency of the United States Government. Neither the United States Government nor any agency thereof, nor any of their employees, makes any warranty, express or implied, or assumes any legal liability or responsibility for the accuracy, completeness, or usefulness of any information, apparatus, product, or process disclosed, or represents that its use would not infringe privately owned rights. Reference herein to any specific commercial product, process, or service by trade name, trademark, manufacturer, or otherwise does not necessarily constitute or imply its endorsement, recommendation, or favoring by the United States Government or any agency thereof. The views and opinions of authors expressed herein do not necessarily state or reflect those of the United States Government or any agency thereof.

CHAPTER 6:
Publications under this Award and References

6.1 Publications under this Award

1. Washom, B., Solar and the Smart Grid, Solar Power International, Los Angeles, October 2010.
2. Washom, B., Microgrid Optimization for Demand Response, 6th Annual Utility Integration Conference Integrating DER into the Smart Grid, November 2010.
3. Washom, B., UC San Diego Campus Microgrid, 4th International Conference on the Integration of Distributed Energy Resources, December 2010.
4. Lave M, Kleissl J, 'Solar Intermittency of Four Sites Across the State of Colorado', *Renewable Energy*, 35:2867-2873, 2010
5. Lave M, Kleissl J, Optimum fixed orientations and benefits of tracking for capturing solar radiation in the continental United States, Renewable Energy, 36:1145-1152, 2011
6. Lave, M., J. Kleissl, Arias-Castro, E., High-frequency fluctuations in clear-sky index, *Solar Energy*, doi:10.1016/j.solener.2011.06.031, August 2011
7. Kleissl, J., Solar Forecasting, Communities for Advanced Distributed Energy Resources, April 2010
8. Kleissl, J., PV Variability and Solar Forecasting, SEPA / DOE / NREL / Utility Workshop on PV Technology and Systems, November 2010

REFERENCES

A. Chouder, S. Silvestre, and A. Malek, "Simulation of photovoltaic grid connected inverter in case of grid-failure", Revue des Energies Renouvelables Vol. 9 N°4 (2006) 285 – 296

A. Chouder, S. Silvestre, and A. Malek, "Simulation of photovoltaic grid connected inverter in case of grid-failure", Revue des Energies Renouvelables Vol. 9 N°4 (2006) 285 – 296

A. D. Hansen, Paul Sorensen, Lars H. Hansen, and Henrik Bindner, "Models for Standalone PV system", Riso National Laboratory, (Roskilde 2000)

A. F. Farret and M. G. Simoes. Integration of Alternative Sources of Energy. JohnWiley & Sons, Ltd, New Jersey, 2006.

A. Lay-Ekuakille, G. Vendramin, A. Fedele, L.Vasanelli, A. Trotta, "PV maximum power point tracking through pyranometric Sensor: Modelling and characterization", International Journal On Smart Sensing And Intelligent Systems, VOL. 1, NO. 3, (Italy September 2008)

Addison, P., 2002. The illustrated wavelet transform handbook: introductory theory and applications in science, engineering, medicine, and finance. Institute of Physics Publishing, London.

Alberta Electric System Operator, Wind Power Facility Technical Requirements, 15 November 2004. www.aeso.ca

Alberta Electric System Operator, Wind Power Facility Technical Requirements, 15 November 2004. www.aeso.ca

American Wind Energy Association, "Standardizing Generator Interconnection Agreements and Procedures" No. RM02-1-001, submitted to FERC www.ferc.gov

ANSI C84.1 – Voltage Ratings for Electric Power Systems and Equipment (60 Hz) CSA C22.1, C22.2 and C22.3 – Canadian Electric Code Parts I, II & III.

Anton Driesse, Steve Harrison, and Praveen Jain, "A Finite State Machine Model to Represent

B. Lindgren. A Power Converter for Photovoltaic Applications. PhD thesis, Department of Electric Power Engineering, Chalmers University of Technology, Göteborg, Sweden, 2000.

B. Lindgren. A Power Converter for Photovoltaic Applications. PhD thesis, Department of Electric Power Engineering, Chalmers University of Technology, Göteborg, Sweden,2000.

BC Hydro, "69 kV to 500 kV Interconnection Requirements for Power Generators", January 2002.

Beyer, H. G., Luther, J. and Steinberger-Willms, R., 1991. Reduction of fluctuations in lumped power output from distantly spaced PV-arrays, in: 1991 Solar World Congress

Proceedings of the Biennial Congress of the ISES. Denver, Colorado, USA, 19–23 August 1991, pp. 321–326. Pergamon Press, Oxford, New York.

Bo Yang, Wuhua Li, Yi Zhao, and Xiangning He, "Design and Analysis of a Grid-Connected Photovoltaic Power System," IEEE, (China 2010)

C. Hansen, J. Stein, and A. Ellis, "Simulation of One-Minute Power Output from Utility-Scale Photovoltaic Generation System," 2011.

C. T. Chiang, T. S. Chiang, and H. S. Huang. Modeling a photovoltaic power system by CMAC-GBF. In Proc. of 3rd World Conference on Photovoltaic Energy Conversion, 2431– 2434, Osaka, Japan, 11-18 May 2003.

Chow, C.W., Urquhart, B., Lave, M., Kleissl, J., Shields, J., 2011. Intra-hour forecasting with a total sky imager at the UC San Diego solar energy testbed. submitted to *Solar Energy*.

Curtright, A.E., Apt, J., 2008. The character of power output from utility-scale photovoltaic systems. *Prog. Photovolt* 16, 241-247.

D. King, W. Boyson, and J. Kratochvil, "Photovoltaic Array Performance Model," 2004

D.L. King, W.E. Boyson, J.A. Kratochvil, "Photovoltaic Array performance model", Sandia National Laboratories, (Dec 2003)

Didier Thevenard, "Review And Recommendations For Improving The Modelling of Building Integrated Photovoltaic Systems," Building Simulations 2005, Montreal Canada, Pages 1221-1228

Didier Thevenard, Gregory Leng, Sylvain Martel, "The Retscreen model for assessing potential PV projects", PV Horizon: Workshop on Photovoltaic Hybrid systems, (Canada September 2001)

Dorin Petreuş, Ionuţ Ciocan, and Cristian Fărcaş, "An Improvement on Empirical Modelling of Photovoltaic Cells," IEEE, (Romania 2008)

Ebrahim M. Ali Alfegi, Kamaruzzaman Sopian, Mohd Yusof Hj Othman and Baharudin Bin Yatim, "Mathematical Model of Double Pass Photovoltaic Thermal Air Collector with Fins", American Journal of Environmental Sciences 5 (5), (Seattle 2009), Pages 592-598

Ebrahim M. Ali Alfegi, Kamaruzzaman Sopian, Mohd Yusof Hj Othman, Baharudin Bin Yatim "Transient mathematical model of both side single pass photovoltaic thermal air collector", ARPN Journal of Engineering and Applied Sciences, Vol. 2, No. 5, (Malaysia October 2007)

Eduardo I. Ortiz-Rivera, and F.Z. Peng, "Analytical Model for a Photovoltaic Module using the Electrical Characteristics provided by the Manufacturer Data Sheet", IEEE, (USA 2005)

ESB National Grid, WFPS1: Wind Farm Power Station Grid Code Provisions, July, 2004. www.eirgrid.com

F. Adamo, F. Attivissimo, A. Di Nisio, A. M. L. Lanzolla, and M. Spadavecchia, "Parameters Estimation For A Model Of Photovoltaic Panels", XIX IMEKO World Congress Fundamental and Applied Metrology (Portugal 2009) 964-967

F. Sarhaddi, S. Farahat, H. Ajam, A. Behzadmehr, "Exergetic performance evaluation of solar Photovoltaic Array", Australian Journal of Basic and Applied Sciences, 4(3): 502-519, (Iran 2010)

Faisal A. Mohamed, "Microgrid Modelling and Online Management", Ph.D. Thesis, Helsinki University of Technology Control Engineering, January 2008

Francisco M. González-Longatt, "Model of Photovoltaic Module in Matlab™", 2do Congreso Iberoamericano De Estudiantes De Ingeniería Eléctrica, Electrónica Y Computación (Ii Cibelec 2005)

G. Petrone, G.Spagnuolo, M. Vitelli, "A Model of mismatched photovoltaic fields for simulating hybrid solar vehicles" (Italy 2002)

Gansler, R.A., Klein, S.A., Beckman, W.A., 1995. Investigation of minute solar radiation data. *Solar Energy* 55 (1), 21-27.

Geoff Walker, "Evaluating MPPT converter topologies using a Matlab PV model", (Australia 2000)

Geoffrey T. Klise and Joshua S. Stein, "Models Used to Assess the Performance of Photovoltaic Systems", SANDIA Report, (New Mexico 2009)

Geoffrey T. Klise and Joshua S. Stein, "Models Used to Assess the Performance of Photovoltaic Systems", SANDIA Report, (New Mexico 2009)

Gonzales, C., Wilcox, S., 2004. Sunny Days. Developed by the National Renewable energy Laboratory. Algorithm based on methods developed in Long and Ackerman (2000).

H. Altas and A.M. Sharaf, "A Photovoltaic Array Simulation Model for Matlab-Simulink GUI Environment", IEEE (2007)

H. I. Cho, S. M. Yeo, C. H. Kim, V. Terzija, and Z. M. Radojevic, "A Steady-State Model of the photovoltaic System in EMTP", MKE, (Japan 2009)

H. I. Cho, S. M. Yeo, C. H. Kim, V. Terzija, and Z. M. Radojevic, "A Steady-State Model of the photovoltaic System in EMTP", MKE, (Japan 2009)

Hoff, T.E., Perez, R., 2010. Quantifying PV power output variability. *Solar Energy* 84 , 1782-1793.

IEC Standard 1000-3-7, Electromagnetic Compatibility: Part 3 – Limits – Section 7. Assessment of emission limits for fluctuating loads in MV and HV power systems, 1996.

IEEE Std 100 – The New IEEE Standard Dictionary of Electrical and Electronics Terms (ANSI).

IEEE Std 1109 – Guide for the Interconnection of User-Owned Substations of Electric Utilities

IEEE Std 519 – IEEE Recommended Practices and Requirements for Harmonic Control in Electrical Power Systems

IEEE Std. 122 –Recommended Practice for Functional and Performance Characteristics of Control Systems for Steam Turbine-Generator Units.

IEEE Std. 421-4 – Guide for the Preparation of Excitation System Specifications

IEEE Std. C37.1 – Standard Definition, Specification and Analysis of Systems Used for Supervisory Control, Data Acquisition and Automatic Control.

IEEE Std. C37.2 – Standard Electrical Power System Device Function Numbers

IEEE Std. C57.116 – Guide for Transformers Directly Connected to Generators

IEEE Std. C57.116 – Guide for Transformers Directly Connected to Generators

Ineichen, P. Perez, R., 2002. A new airmass independent formulation for the Linke turbidity coefficient. *Solar Energy* 73 (3), 151-157.

Inverters in Photovoltaic System Simulations", IEEE (Canada 2008)

J. Boland, B. Ridley, and B. Brown, "Models of diffuse solar radiation," Renewable Energy, vol. 33, pp. 575-584, Apr 2008.

J. Page, "The role of solar radiation climatology in the design of photovoltaic systems," in Practical handbook of photovoltaics: fundamentals and applications, T. Markvart and L. Castaner, Eds., ed Oxford: Elsevier, 2003, pp. 5-66.

J. Pedersen, P. B. Eriksen and P. Mortensen, "Present and Future Integration of Large-Scale Wind Power Into Eltra's Power System", Eltra, www.eltra.com

J.A. Gow and C.D Manning, "Development of a photovoltaic array model for use in power-electronics simulation studies," IEEE, (UK 1999)

Jurgen Schumacher, Ursula Eicker, Dirk Pietruschka, Alberto Catani, "Exact Analytical calculation of the one-diode model parameters from PV module data sheet information", (2006)

K. H. Hussein, I. Muta, T. Hoshino, and M. Osakada. Maximum photovoltaic power tracking: an algorithm for rapidly changing atmospheric conditions. In Generation, Transmission and Distribution, IEE Proceedings, volume 142, 59 – 64, Jan1995.

Kawasaki, N., Oozeki, T., Kurokawa, K., Otani, K., 2006. An evaluation method of the fluctuation characteristics of photovoltaic systems by using frequency analysis. *Solar Energy Materials and Solar Cells* 90. doi:10.1016/j.solmat.2006.02.034.

Kleissl, J., Harper, J., Dominguez, A., 2010. A solar resource measurement network at high spatio-temporal resolution, American Solar Energy Society 2010 Conference, Phoenix, AZ.

Kuei-Hsiang Chao, Ching-Ju Li, and Sheng-Han Ho, "Modeling and Fault Simulation of Photovoltaic Generation Systems Using Circuit-Based Model", ICSET 2008, (Taiwan 2008)

Lave, M., Kleissl, J,. 2010. Solar variability of four sites across the state of Colorado. *Renewable Energy* 35, 2867-2873.

Ljubisav Stamenic, Eric Smiley and Karim Karim, "Low light conditions modelling for building integrated photovoltaic (BIPV) systems", Solar Energy Volume 77, Issue 1 (2004), Pages 37-45

Long, C.N., Ackerman, T.P., 2000. Identification of clear skies from broadband pyranometer measurements and calculation of downwelling shortwave cloud effects. *J. Geophys. Res.* 105, 15609-15626.

M. Klein, G. J. Rogers and P. Kundur, "A Fundamental Study of Inter-Area Oscillations in Power Systems", IEEE Trans. PWRS, pg 914-921, August 1991.

M. Milligan and B. Parsons, "A Comparison and Case Study of Capacity Credit Algorithms for Intermittent Generators", Presented at Solar'97, Washington DC, April 27-30, 1997.

Marcelo Gradella Villalva, Jonas Rafael Gazoli, and Ernesto Ruppert Filho, "Modeling And Circuit-Based Simulation of Photovoltaic Arrays", IEEE, (Brazil 2009)

Maria Carmela Di Piazza and Gianpaolo Vitale, "Photovoltaic field emulation including dynamic and partial shadow conditions", National Research Council (CNR), Institute of Intelligent Systems for Automation (ISSIA), Section of Palermo Via Dante, 12, 90141 Palermo, (Italy 2009)

Maria Carmela Di Piazza, Antonella Ragusa, Gianpaolo Vitale, "Identification of Photovoltaic Array Model Parameters by Robust Linear Regression Methods", ICREPQ 2009

Mills, A., Ahlstrom, M., Brower, M. Ellis, A., George, R., Hoff, T., Kroposki, B., Lenox, C., Miller, N., Stein, J., Wan, Y., 2009. Understanding variability and uncertainty of photovoltaics for integration with the electric power system.Berkley National Laboratory. LBNL-2855E.

MISO, Generator Interconnection Procedures and Agreement, December 2002. www.midwestiso.org

Murata, A., Yamaguchi, H., Otani, K., 2009. A method of estimating the output fluctuation of many photovoltaic power generation systems dispersed in a wide area. *Electrical Engineering in Japan* 166 (4), 9-19.

N. Hamrouni* and A. Chérif, "Modelling and control of a grid connected photovoltaic system", Revue des Energies Renouvelables Vol. 10 N°3 (2007) 335 – 344

N. Hamrouni* and A. Chérif, "Modelling and control of a grid connected photovoltaic system", Revue des Energies Renouvelables Vol. 10 N°3 (2007) 335 – 344

N. Hamrouni* and A. Chérif, "Modelling and control of a grid connected photovoltaic system", Revue des Energies Renouvelables Vol. 10 N°3 (2007) 335 – 344

N. Jenkins, R. Allan, P. Crossley, D. Kirschen, and G. Strbac. Embedded Generation. The Institution of Electrical Engineers, UK, 2000.

N. Jenkins, R. Allan, P. Crossley, D. Kirschen, and G. Strbac. Embedded Generation. The Institution of Electrical Engineers, UK, 2000.

N.J. Ekins-Daukes, T.R. Betts, Y. Kemmoku, K. Araki, H.S. Lee, R.Gottschlag, M.B. Borelano, D.G. Infield "Syracuse a multi-junction concentrator system computer model" (2005)

Nathan Blair, Mark Mehos, Craig Christensen, Chris Cameron, "Modelling Photovoltaic and concentrating solar power Trough performance, cost, and financing with the solar advisor model", National Renewable Energy Laboratory, (USA May 2008)

NEG Micon (brochure), NEG Micon Power Quality , 2003 J. Niiranen, "Application of Power Electronics", presentation on Distributed Generation at University of Vaasa, May 23, 2003.

NERC/WECC Planning Standards, August 2002.

NERC/WECC Planning Standards, August 2002.

NERC/WECC Planning Standards, August 2002.

News briefs, "US renewables increase after five years of decline", Refocus, Nov/Dec 2003.

Otani, K. Minowa, J. Kurokawa, K., 1997. Study of areal solar irradiance for analyzing areally-totalized PV systems. *Solar Energy Materials and Solar Cells* 47, 281-288.

P. Kundur, Power System Stability and Control, McGraw-Hill, 1994.

Pan Lei, Gong Wei, and Wang Yinghong," Maximum Power Point Tricking Control of Solar Photovoltaic Power Generation System Based on Model Reference Adaptive", IEEE (China 2007)

Paul gilman, "A comparison of three free computer models for evaluating PV and Hybrid system designs: Homer, Hybrid2, and retscreen", (USA 2008)

Perpinan, O., Lorenzo, E., 2011. Analysis and synthesis of the variability of irradiance and PV power time series with the wavelet transform. *Solar Energy* 85 (1), 188-197.

R. Mukund. Wind and solar power systems. CRC Press, CRC Press LLC, 2000 N.W., Corporate Blvd., Boca Raton, Florida 33431, 1999.

R.K. Nema, Savita Nema, Gayatri Agnihotri, "Computer Simulation based on study of photovoltaic cells/modules and their experimental verification" International Journal of Recent Trends in Engineering, Vol. 1, No. 3, (India May 2009)

Ramos Hernanz, Campayo Martín, Zamora Belver, Larrañaga Lesaka, Zulueta Guerrero, Puelles Pérez, "Modelling of photovoltaic module", ICREPQ'10, (Spain 2010)

Robert S. Balog, Yingying Kuai, and Greg Uhrhan, "A Photovoltaic Module Thermal Model Using Observed Insolation and Meteorological Data to Support a Long Life, Highly Reliable Module-Integrated Inverter Design by Predicting Expected Operating Temperature", IEEE, (Illinois, USA 2009)

Robert Stala, "Testing of the Grid-connected Photovoltaic Systems Using FPGA-based Real-Time Model", IEEE, (Poland 2008)

Ryan C. Campbell, "Circuit based Photovoltaic array model for power system studies", PSCAL, (Seattle 2006)

S.I. Sulaiman, T.K. Abdul Rahman, I. Musirin, and S. Shaari, "Optimizing Three-layer Neural Network Model for Grid-connected Photovoltaic System Output Prediction", IEEE (Malaysia 2009)

Should be reference 58…but that does not seem to be found in the list of references

St. Kourtesi, L.Ekonomou, A. Nakulas, G.P. Fotis, E. Zoulias, "Modeling and simulation of a single phase photovoltaic inverter and investigation of switching strategies for harmonic minimization", (Greece 2004)

Stefania Conti, Salvatore Raiti, and Giuseppe Tina, "Simulink Modelling Of LV Photovoltaic Grid-Connected Distributed Generation",CIRED 2005, (Turin 2005)

Suehrcke, H., McCormick, P.G., 1989. Solar radiation utilizability. *Solar Energy* 43 (6), 339-345.

T.Chayavanich, C. Limsakul, N. Chayavanich, D. Chenvidhya, C. Jivacate, K. Kirtikara, " Voltage and frequency Dependent model for PV module dynamic impendance", (Thailand 2005)

The European Wind Energy Association, "Wind is Power", www.ewa.org

Ulrich Boke, "A simple model of photovoltaic module electric characteristics", (Germany 2008)

United State of America Federal Energy Regulatory Commission, "Interconnection for Wind Energy and Other Alternative Technologies", January 24, 2005, Docket No. RM05-4-000.

V. Di Dio, D. La Cascia, R. Miceli, C. Rando, "A Mathematical Model to Determine the Electrical Energy Production in Photovoltaic Fields Under Mismatch Effect", IEEE, (Italy 2009)

WECC Coordinated Off-Nominal Frequency Load Shedding and Restoration Plan

WECC Generator Test Guide

WECC Undervoltage Load Shedding Guidelines

WECC Undervoltage Load Shedding Guidelines

WECC, Generator Electrical Grid Fault Ride Through Capability, October 2004.

WECC, Generator Electrical Grid Fault Ride Through Capability, October 2004.

Widalys De Soto, "Improvement and Validation of a model for photovoltaic Array Performance", Solar Energy Laboratory University of Wisconsin-Madison 2004

Wiemken, E. Beyer, H.G., Heydenreich, W. Kiefer, K., 2001. Power characteristics of PV ensembles: experiences from the combined power production of 100 grid connected PV systems distributed over the area of Germany. *Solar Energy* 70 (6), 513-518.

Woyte, A., Belmans, R., Nijsb, J., 2007. Fluctuations in instantaneous clearness index: analysis and statistics. *Solar Energy* 81 (2), 195-206.WECC Reliability Criteria (WECC website)

Xcel Energy, Interconnection Guidelines for Transmission Interconnected Producer-Owned Generation, Version 1.0L, 1/27/03.

Z. Hamadi, J. Moncef, H. N´ejib, and A. Cherif, "Modelling And Simulation of Photovoltaic Pumping Systems Under Matlab Simulink", International Journal of Power and Energy Systems, Vol. 27, No. 1, 2007

GLOSSARY

API	Application Programming Interface
ATSP	Advanced Transient Stability Program
AVR	Automatic Voltage Regulators
BMSB	Biomedical Science Building (a solar resource site on the UC San Diego campus)
CDF	Cumulative Distribution Function
CM	Copper Mountain
DHI	Diffuse Horizontal Irradiance
DSTATCOM	Distribution Static Compensator
DVAR	Dynamic VAR Compensator.
EBU2	Engineering Building Unit 2
ESE	East-South-East
FERC	Federal Energy Regulatory Commission
FTE	Full Time Equivalent
fpi	fluctuation power index
GHI	Global Horizontal Irradiance
HP10	Hoff and Perez (2010)
HUBB	Hubbs Hall (a solar resource site on the UC San Diego campus)
HVDC	High Voltage Direct Current
IEEE	Institute of Electrical and Electronics Engineers
IGBT	Insulated Gate Bipolar Transistor
MPPT	Maximum Power Point Tracking.
MOCC	Moores Cancer Center (a solar resource site on the UC San Diego campus)
NERC	North American Electric Reliability Corporation.
OC	Ota City
PF	Power Factor
POI	Point of Interconnection
PSD	Power spectral densities
PSS	Power System Stabilizers

PWM	Pulse Width Modulation
PV	Photovoltaic
QG	Gate Charge for power transistors
RR	Ramp Rates
RIMC	Recreation, Intramural, and Athletics Complex (a solar resource site on the UC San Diego campus)
SOPO	Statement of Project Objectives
SS	Step Sizes
STC	Standard Test Conditions
TDD	Total Demand Distortion
THD	Total Harmonic Distortion
TIOG	Tioga Hall (a solar resource site on the UC San Diego campus)
TOD	Time of Day
TSO	transmission system operator.
UCLMS	Universal Control Logic Modeling and Simulation
UCSD	University of California, San Diego
WECC	Western Electricity Coordination Council
WVM	Wavelet Variability Model
VR	Variability Ratio

APPENDIX A:
Detailed Results of PV Integration Study in Typical Power Systems

A. Detailed Results of PV Integration Study in Typical Power Systems

A.1. IEEE 34 Bus system – Power Flow Analysis

Input Data: PV Output Power at Gilman Parking Structure on **September 1, 2010 (P in kW).**

PV Unit Name Plate Data:

Total Rated Power: 195 kW DC
Panel Model: Kyocera KD 205 GX-LP at 10° tilt and 180° azimuth

Inverter #1 Model: Xantrex GT100 with 490 modules

Inverter #2 Model: Xantrex GT100 with 462 modules

PV Measured Output Power

6 am	8 am	10 am	12 pm	2 pm	4 pm	6 pm	8 pm
P = 0	P = 14.5	P = 30.2	P = 152	P = 142	P = 96.3	P = 19.8	P = 0

PV Penetration Level and Output Power as Function of Time:

IEEE 34 - Total Load in KVA:	**832.713**	**KVA**						
195	6:00 AM	8:00 AM	10:00 AM	12:00 PM	2:00 PM	4:00 PM	6:00 PM	8:00 PM
KW Output Power	0	14.5	30.2	152	142	96.3	19.8	0
Output Power in pu	0	0.074359	0.154872	0.779487	0.728205	0.493846	0.101538	0
Penetration Level, in %	Actual Time							
10%:	6:00 AM	8:00 AM	10:00 AM	12:00 PM	2:00 PM	4:00 PM	6:00 PM	8:00 PM
83.271	0	6.191946	12.89633	64.90868	60.63837	41.12306	8.455209	0
20%:	6:00 AM	8:00 AM	10:00 AM	12:00 PM	2:00 PM	4:00 PM	6:00 PM	8:00 PM
166.542	0	12.38389	25.79266	129.8174	121.2767	82.24613	16.91042	0
30%:	6:00 AM	8:00 AM	10:00 AM	12:00 PM	2:00 PM	4:00 PM	6:00 PM	8:00 PM
249.813	0	18.57584	38.68899	194.726	181.9151	123.3692	25.36563	0
40%:	6:00 AM	8:00 AM	10:00 AM	12:00 PM	2:00 PM	4:00 PM	6:00 PM	8:00 PM
333.084	0	24.76778	51.58532	259.6347	242.5535	164.4923	33.82084	0
50%:	6:00 AM	8:00 AM	10:00 AM	12:00 PM	2:00 PM	4:00 PM	6:00 PM	8:00 PM
416.355	0	30.95973	64.48165	324.5434	303.1918	205.6153	42.27605	0

S10: Power Flow Results – 10% PV penetration level; PV Unit Near Substation:

PV Penetration Level - 10% **PV Near Subst:**

Power Flow Results

Actual Time	**System Power, PCC**		**PV Total Generation**		**System Total Load**		**System Total Losses**	
	Active Power, in KW	**Reactive Power, in KVAR**	**Active Power, in KW**	**Reactive Power, in KVAR**	**Active Power, in KW**	**Reactive Power, in KVAR**	**Active Power, in KW**	**Reactive Power, in KVAR**
Peak Load	771	421	0	0	744	374	27	47
8:00 AM	764	420	6	0	744	374	26	47
10:00 AM	757	420	13	0	744	374	26	46
12:00 PM	704	415	65	0	744	374	25	41
2:00 PM	708	416	61	0	744	374	25	42
4:00 PM	718	409	41	0	744	374	25	42
6:00 PM	762	420	8	0	744	374	26	46
`	771	421	0	0	744	374	27	47

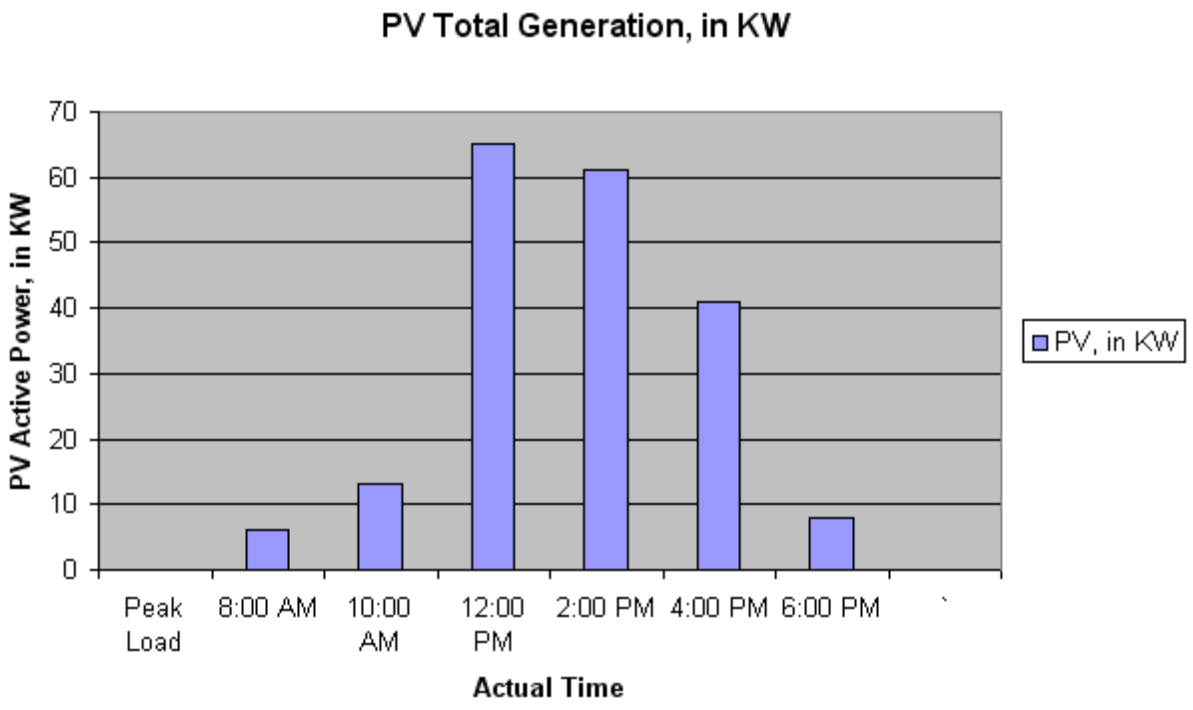
PV Total Generation, in KW
PV Active Power, in KW
70
60
50
40
30
20
10
0
Peak Load
8:00 AM
10:00 AM
12:00 PM
2:00 PM
4:00 PM
6:00 PM
Actual Time
PV, in KW

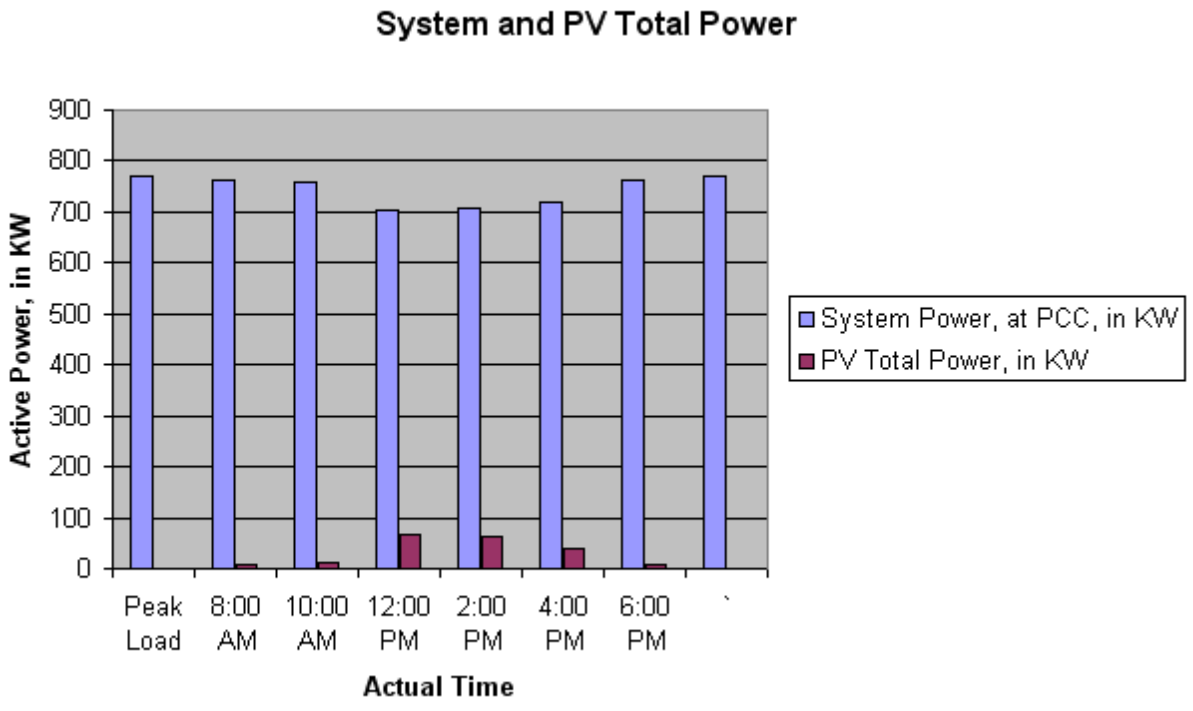
System and PV Total Power
Active Power, in KW
900
800
700
600
500
400
300
200
100
0
Peak Load
8:00 AM
10:00 AM
12:00 PM
2:00 PM
4:00 PM
6:00 PM
Actual Time
System Power, at PCC, in KW
PV Total Power, in KW

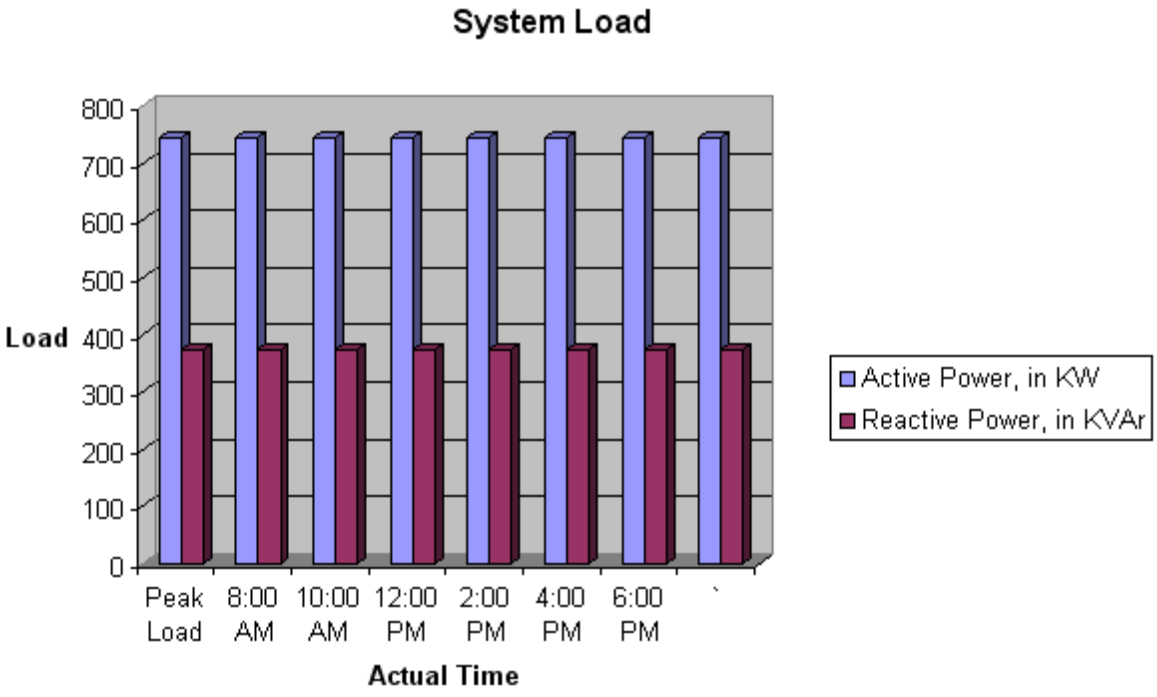
System Load
Load
800
700
600
500
400
300
200
100
0
Peak Load
8:00 AM
10:00 AM
12:00 PM
2:00 PM
4:00 PM
6:00 PM
Actual Time
Active Power, in KW
Reactive Power, in KVAr

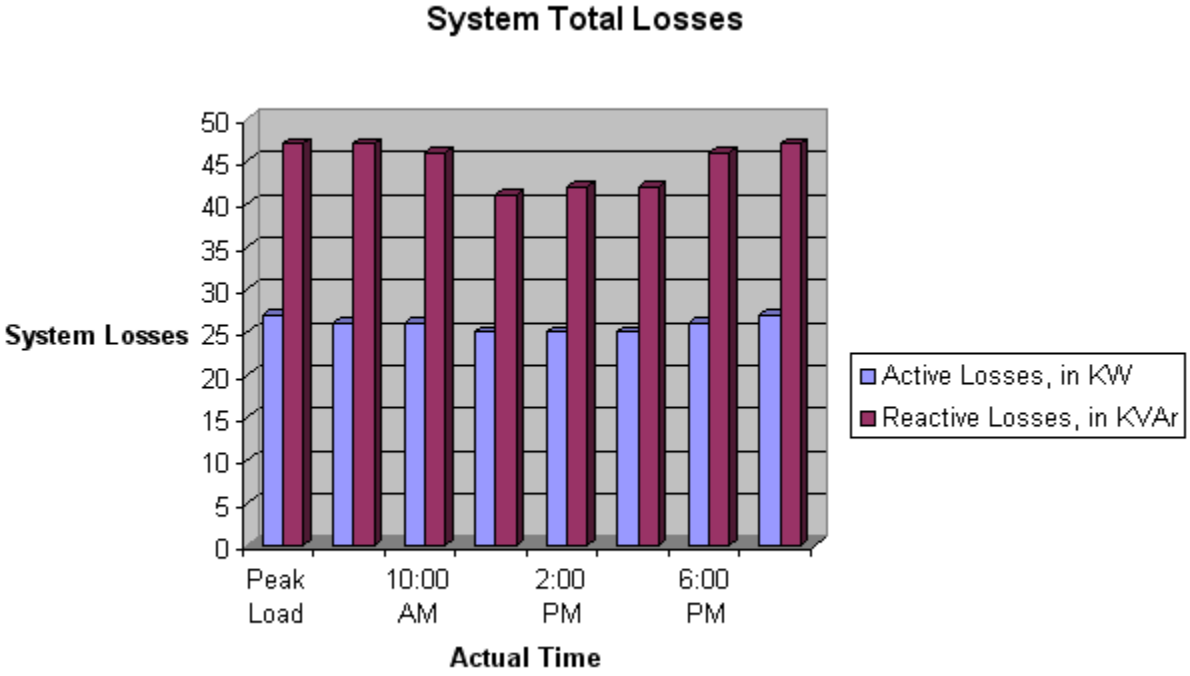
System Total Losses
System Losses
50
45
40
35
30
25
20
15
10
5
0
Peak Load
10:00 AM
2:00 PM
6:00 PM
Actual Time
Active Losses, in KW
Reactive Losses, in KVAr

Bus Voltage Results and Bus Voltage Profile; 10% PV Penetration; PV Near Substation:

Bus Voltages in pu - 10% PV Penetration - PV Near Substation

Bus Name	NoPV	8:00 AM	10:00 AM	12:00 PM	2:00 PM	4:00 PM	6:00 PM	8:00 PM
830-L	0.948	0.949	0.948	0.949	0.949	0.95	0.948	0.948
840-L	0.948	0.949	0.948	0.949	0.949	0.95	0.948	0.948
844-L	0.948	0.949	0.948	0.949	0.949	0.95	0.948	0.948
860-L	0.948	0.949	0.948	0.949	0.949	0.95	0.948	0.948
PV-BUS1	0.964	0.964	0.964	0.966	0.966	0.966	0.964	0.964
PV-BUS1-L	0.964	0.964	0.964	0.966	0.966	0.965	0.964	0.964
PV-BUS2	0.945	0.946	0.946	0.947	0.947	0.947	0.946	0.945
PV-BUS2-L	0.945	0.946	0.946	0.947	0.946	0.947	0.945	0.945
PV-G1	0	0.964	0.964	0.966	0.966	0.966	0.964	0

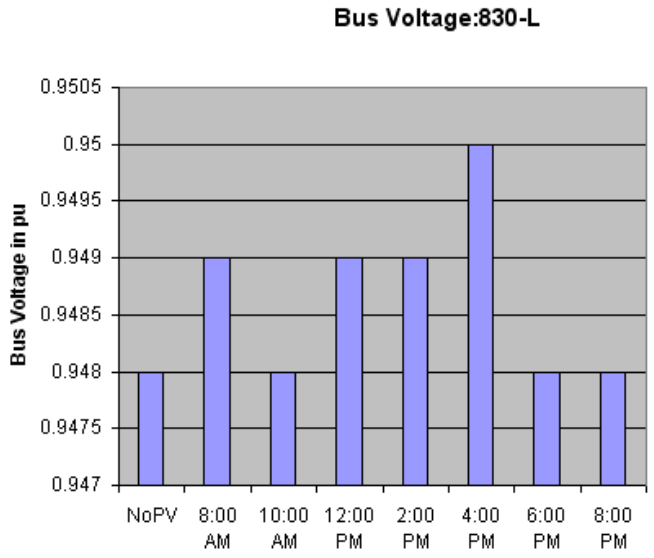

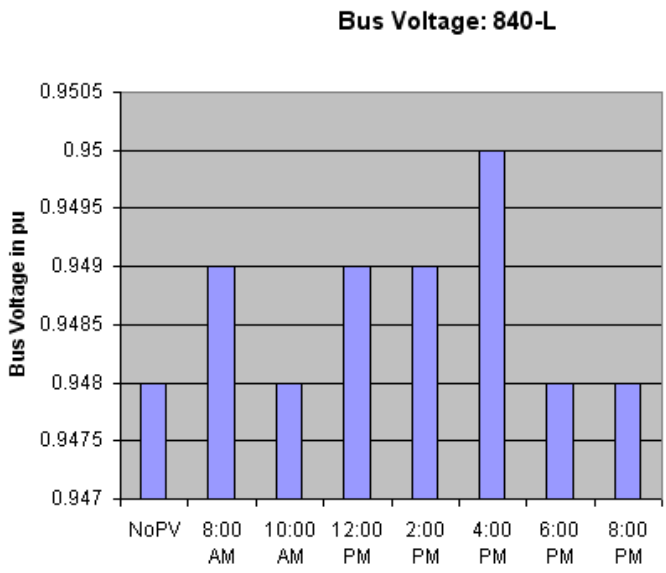
Bus Voltage: 840-L
Bus Voltage in pu
0.9505
0.95
0.9495
0.949
0.9485
0.948
0.9475
0.947
NoPV
8:00 AM
10:00 AM
12:00 PM
2:00 PM
4:00 PM
6:00 PM
8:00 PM

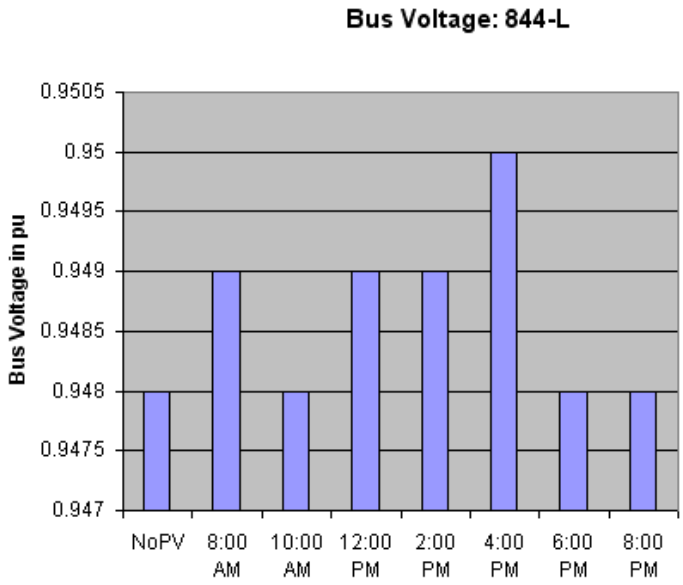
Bus Voltage: 844-L
Bus Voltage in pu
0.9505
0.95
0.9495
0.949
0.9485
0.948
0.9475
0.947
NoPV
8:00 AM
10:00 AM
12:00 PM
2:00 PM
4:00 PM
6:00 PM
8:00 PM

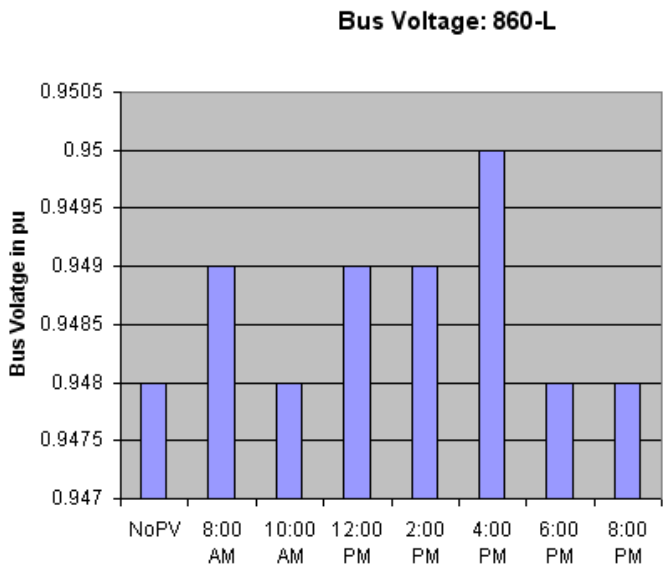
Bus Voltage: 860-L
Bus Volatge in pu
0.9505
0.95
0.9495
0.949
0.9485
0.948
0.9475
0.947
NoPV
8:00 AM
10:00 AM
12:00 PM
2:00 PM
4:00 PM
6:00 PM
8:00 PM

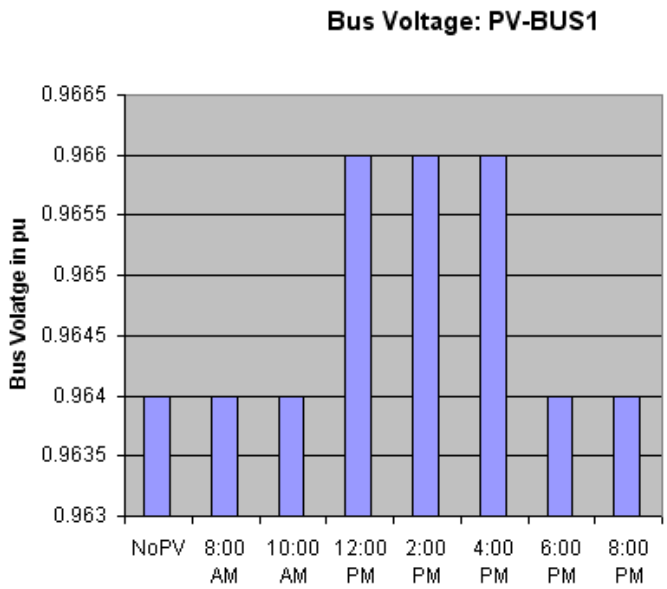
Bus Voltage: PV-BUS1
Bus Volatge in pu
0.9665
0.966
0.9655
0.965
0.9645
0.964
0.9635
0.963
NoPV
8:00 AM
10:00 AM
12:00 PM
2:00 PM
4:00 PM
6:00 PM
8:00 PM

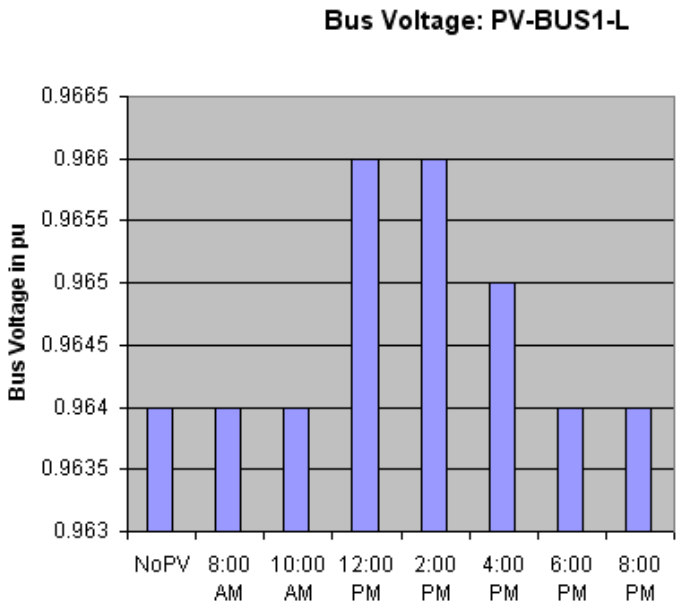
Bus Voltage: PV-BUS1-L
Bus Voltage in pu
0.9665
0.966
0.9655
0.965
0.9645
0.964
0.9635
0.963
NoPV
8:00 AM
10:00 AM
12:00 PM
2:00 PM
4:00 PM
6:00 PM
8:00 PM

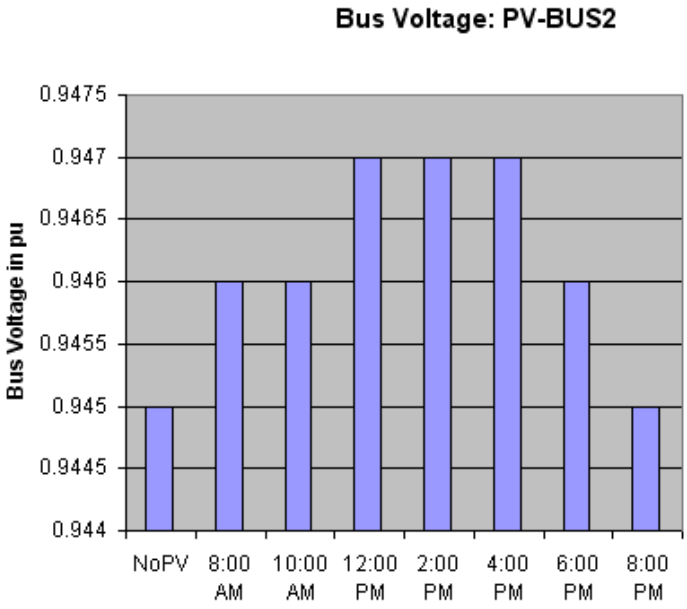
Bus Voltage: PV-BUS2
Bus Voltage in pu
0.9475
0.947
0.9465
0.946
0.9455
0.945
0.9445
0.944
NoPV
8:00 AM
10:00 AM
12:00 PM
2:00 PM
4:00 PM
6:00 PM
8:00 PM

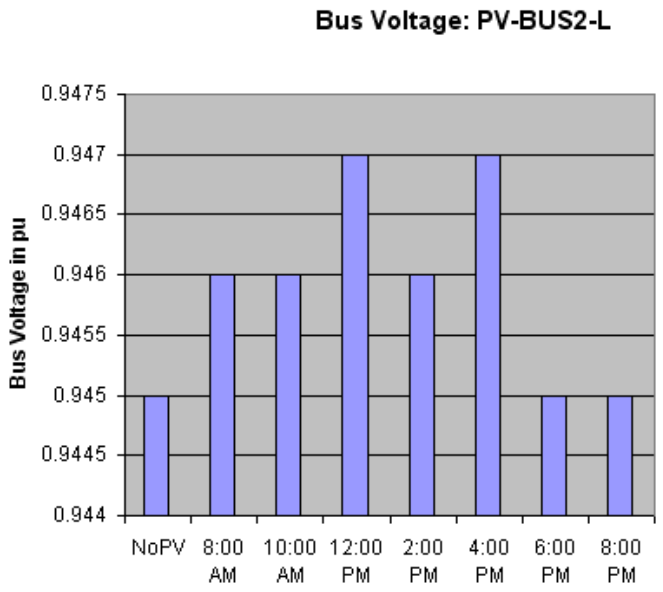
Bus Voltage: PV-BUS2-L
Bus Voltage in pu
0.9475
0.947
0.9465
0.946
0.9455
0.945
0.9445
0.944
NoPV
8:00 AM
10:00 AM
12:00 PM
2:00 PM
4:00 PM
6:00 PM
8:00 PM

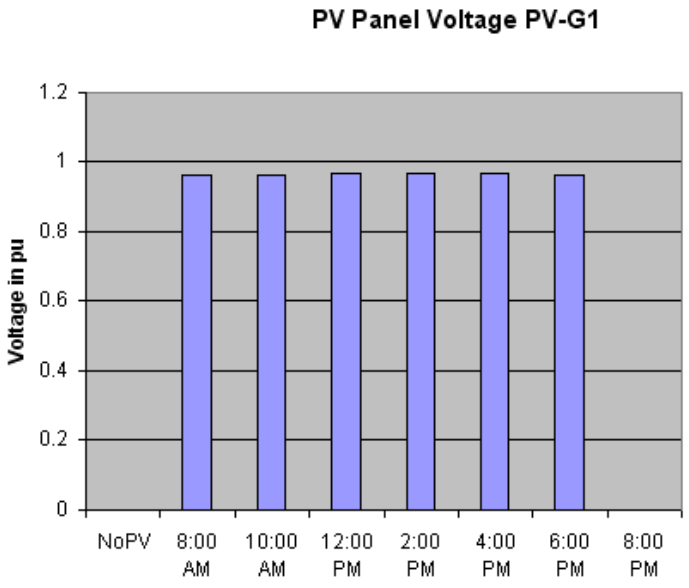
PV Panel Voltage PV-G1
Voltage in pu
1.2
1
0.8
0.6
0.4
0.2
0
NoPV
8:00 AM
10:00 AM
12:00 PM
2:00 PM
4:00 PM
6:00 PM
8:00 PM

E10: Power Flow Results – 10% PV Penetration Level; PV Unit at the End of Circuit:

PV Penetration Level: 10 % ; PV Unit at The End of Circuit

Bus Name	NoPV	8:00 AM	10:00 AM	12:00 PM	2:00 PM	4:00 PM	6:00 PM	8:00 PM
830-L	0.948	0.948	0.948	0.951	0.951	0.951	0.948	0.948
840-L	0.948	0.948	0.948	0.951	0.951	0.951	0.948	0.948
844-L	0.948	0.948	0.948	0.951	0.951	0.951	0.948	0.948
860-L	0.948	0.948	0.948	0.951	0.951	0.951	0.948	0.948
890-L	0.948	0.948	0.948	0.951	0.951	0.951	0.948	0.948
PV-BUS1	0.964	0.964	0.964	0.965	0.965	0.965	0.964	0.964
PV-BUS1-L	0.964	0.964	0.964	0.965	0.965	0.965	0.964	0.964
PV-BUS2	0.945	0.946	0.946	0.949	0.948	0.948	0.946	0.945
PV-BUS2-L	0.945	0.946	0.946	0.949	0.948	0.948	0.946	0.945
PV-G3	0	0.948	0.949	0.952	0.951	0.951	0.948	0

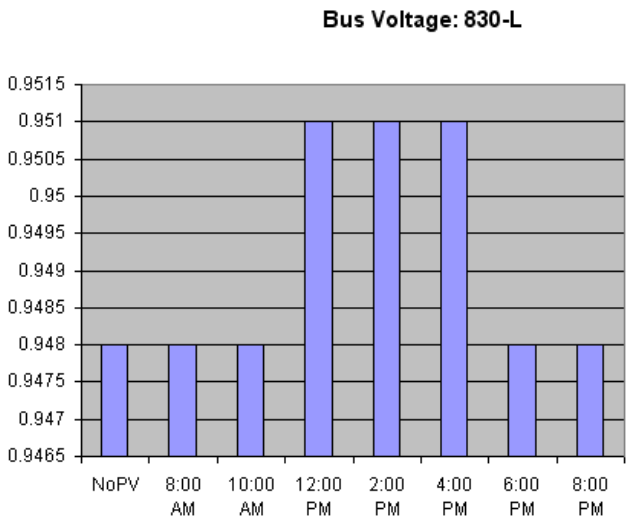
Bus Voltage: 830-L
0.9515
0.951
0.9505
0.95
0.9495
0.949
0.9485
0.948
0.9475
0.947
0.9465
NoPV
8:00 AM
10:00 AM
12:00 PM
2:00 PM
4:00 PM
6:00 PM
8:00 PM

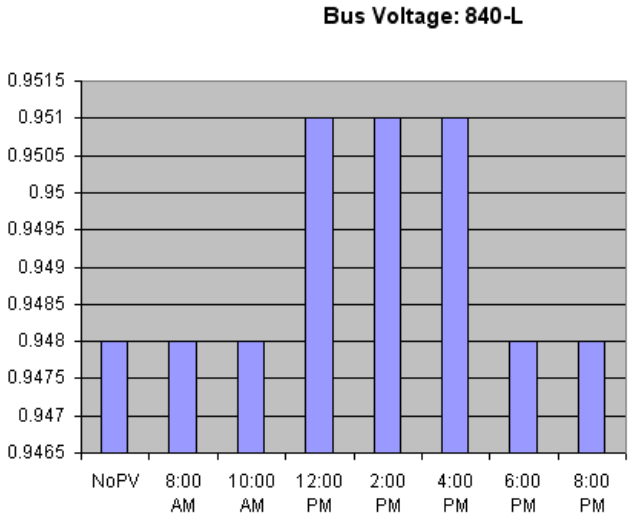
Bus Voltage: 840-L
0.9515
0.951
0.9505
0.95
0.9495
0.949
0.9485
0.948
0.9475
0.947
0.9465
NoPV
8:00 AM
10:00 AM
12:00 PM
2:00 PM
4:00 PM
6:00 PM
8:00 PM

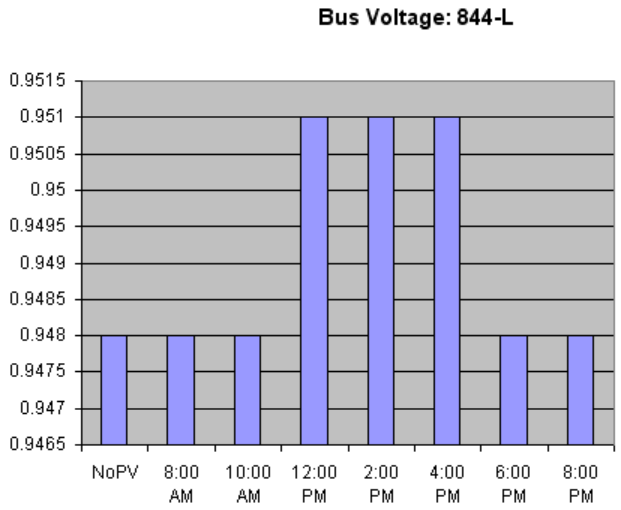
Bus Voltage: 844-L
0.9515
0.951
0.9505
0.95
0.9495
0.949
0.9485
0.948
0.9475
0.947
0.9465
NoPV
8:00 AM
10:00 AM
12:00 PM
2:00 PM
4:00 PM
6:00 PM
8:00 PM

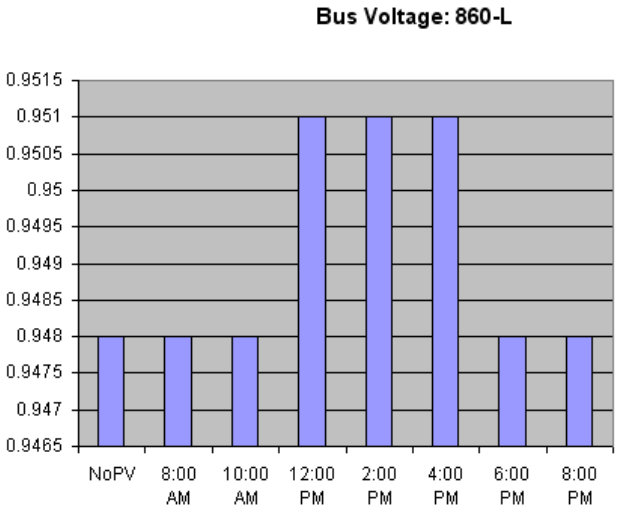
Bus Voltage: 860-L
0.9515
0.951
0.9505
0.95
0.9495
0.949
0.9485
0.948
0.9475
0.947
0.9465
NoPV
8:00 AM
10:00 AM
12:00 PM
2:00 PM
4:00 PM
6:00 PM
8:00 PM

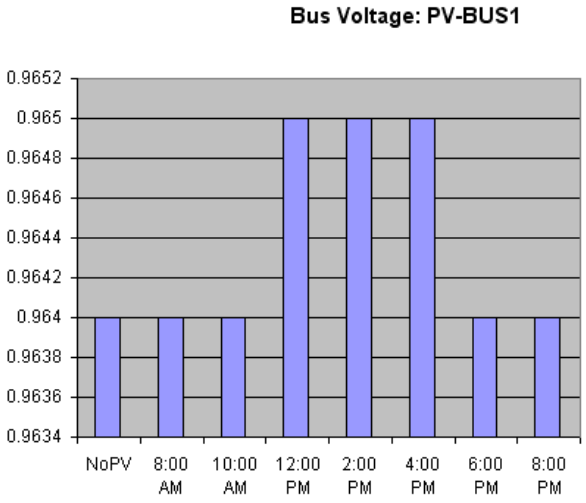
Bus Voltage: PV-BUS1
0.9652
0.965
0.9648
0.9646
0.9644
0.9642
0.964
0.9638
0.9636
0.9634
NoPV
8:00 AM
10:00 AM
12:00 PM
2:00 PM
4:00 PM
6:00 PM
8:00 PM

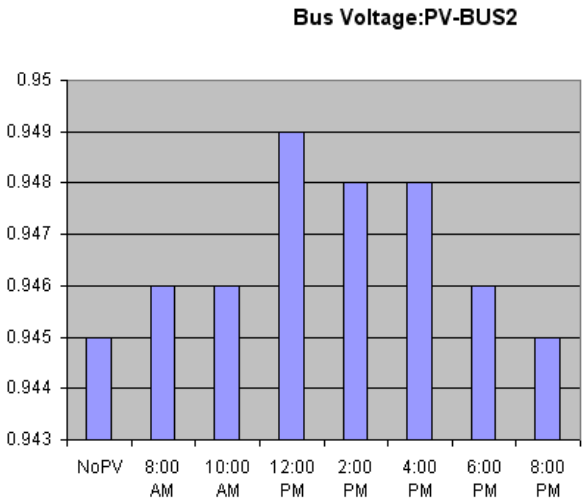
Bus Voltage:PV-BUS2
0.95
0.949
0.948
0.947
0.946
0.945
0.944
0.943
NoPV
8:00 AM
10:00 AM
12:00 PM
2:00 PM
4:00 PM
6:00 PM
8:00 PM

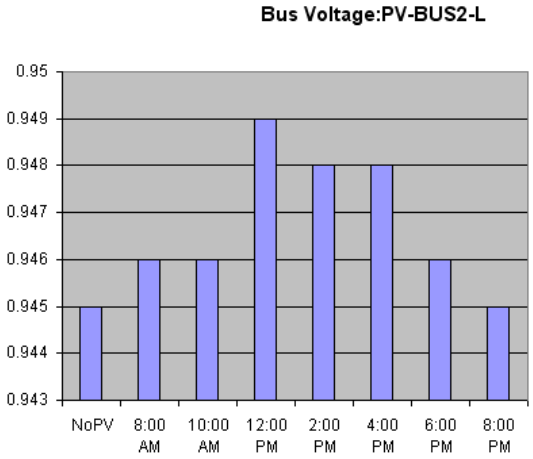
Bus Voltage:PV-BUS2-L
0.95
0.949
0.948
0.947
0.946
0.945
0.944
0.943
NoPV
8:00 AM
10:00 AM
12:00 PM
2:00 PM
4:00 PM
6:00 PM
8:00 PM

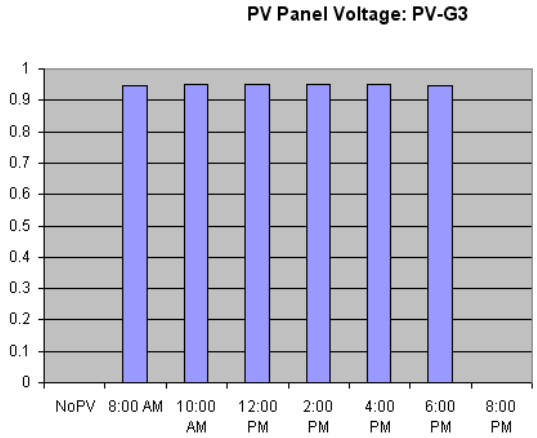
PV Panel Voltage: PV-G3
1
0.9
0.8
0.7
0.6
0.5
0.4
0.3
0.2
0.1
0
NoPV
8:00 AM
10:00 AM
12:00 PM
2:00 PM
4:00 PM
6:00 PM
8:00 PM

S20: Power Flow Results – 20% PV Penetration Level; PV Unit Near Substation:

Actual Time	System Power, PCC		PV Total Generation		System Total Load		System Total Losses	
	Active Power, in KW	Reactive Power, in KVAR	Active Power, in KW	Reactive Power, in KVAR	Active Power, in KW	Reactive Power, in KVAR	Active Power, in KW	Reactive Power, in KVAR
Peak Load	771	421	0	0	744	374	27	47
8:00 AM	758	420	12	0	744	374	26	46
10:00 AM	744	419	26	0	744	374	26	45
12:00 PM	637	411	130	0	744	374	23	37
2:00 PM	646	411	121	0	744	374	23	37
4:00 PM	676	406	82	0	744	374	23	39
6:00 PM	753	419	17	0	744	374	26	46
8:00 PM	771	421	0	0	744	374	27	47

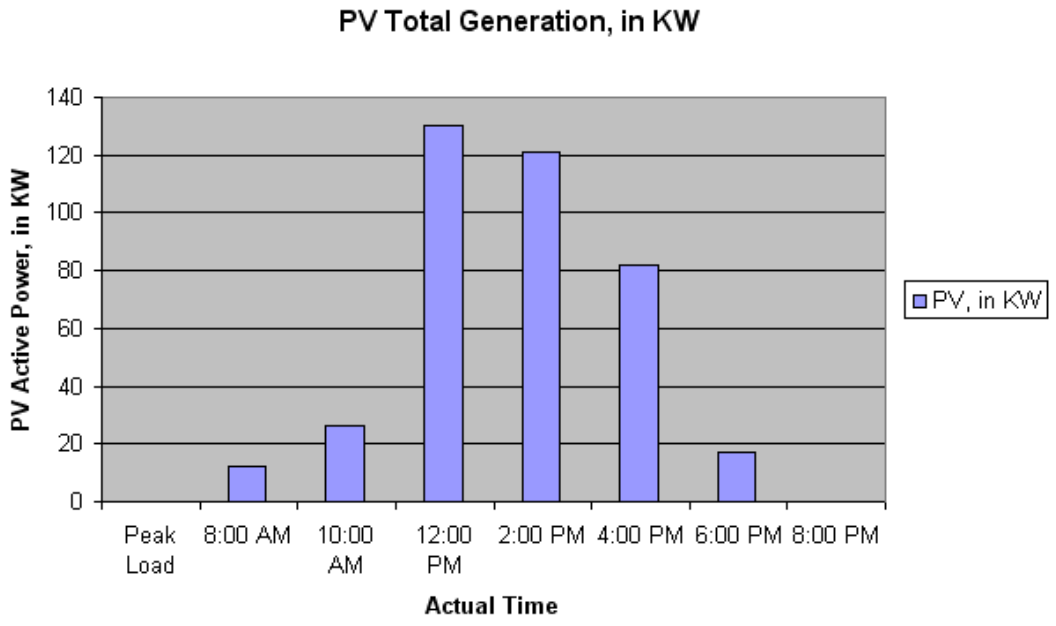
PV Total Generation, in KW
PV Active Power, in KW
140
120
100
80
60
40
20
0
Peak Load
8:00 AM
10:00 AM
12:00 PM
2:00 PM
4:00 PM
6:00 PM
8:00 PM
Actual Time
PV, in KW

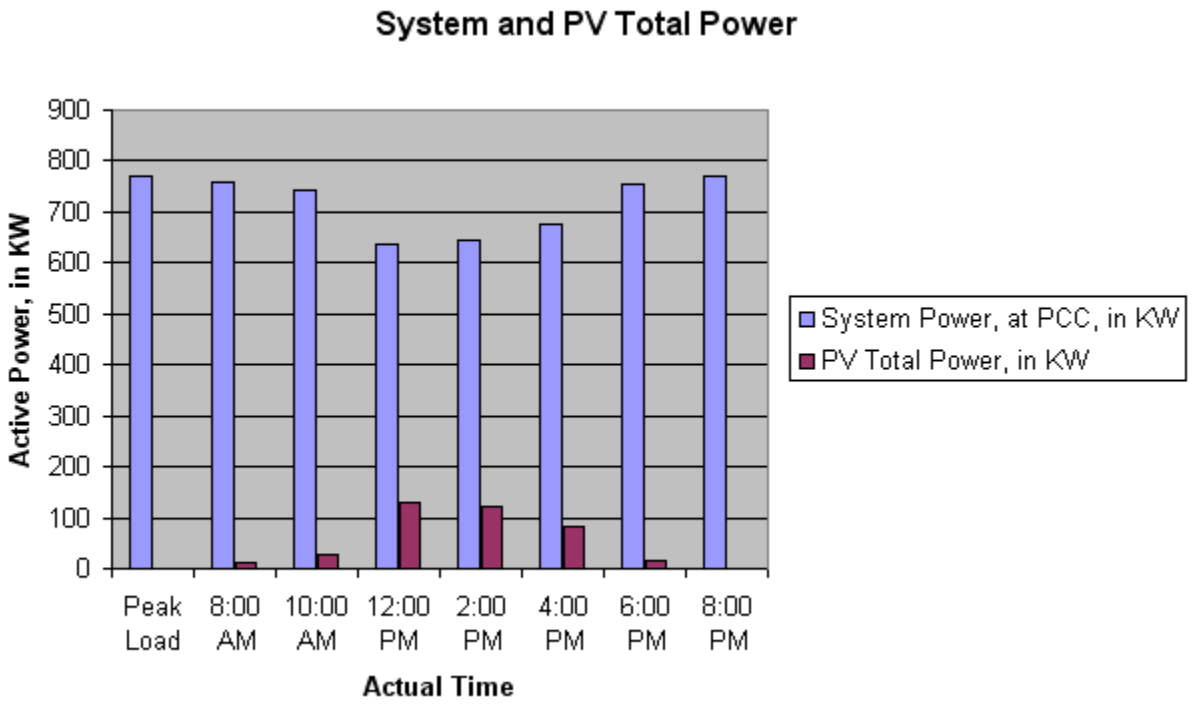
System and PV Total Power
Active Power, in KW
900
800
700
600
500
400
300
200
100
0
Peak Load
8:00 AM
10:00 AM
12:00 PM
2:00 PM
4:00 PM
6:00 PM
8:00 PM
Actual Time
System Power, at PCC, in KW
PV Total Power, in KW

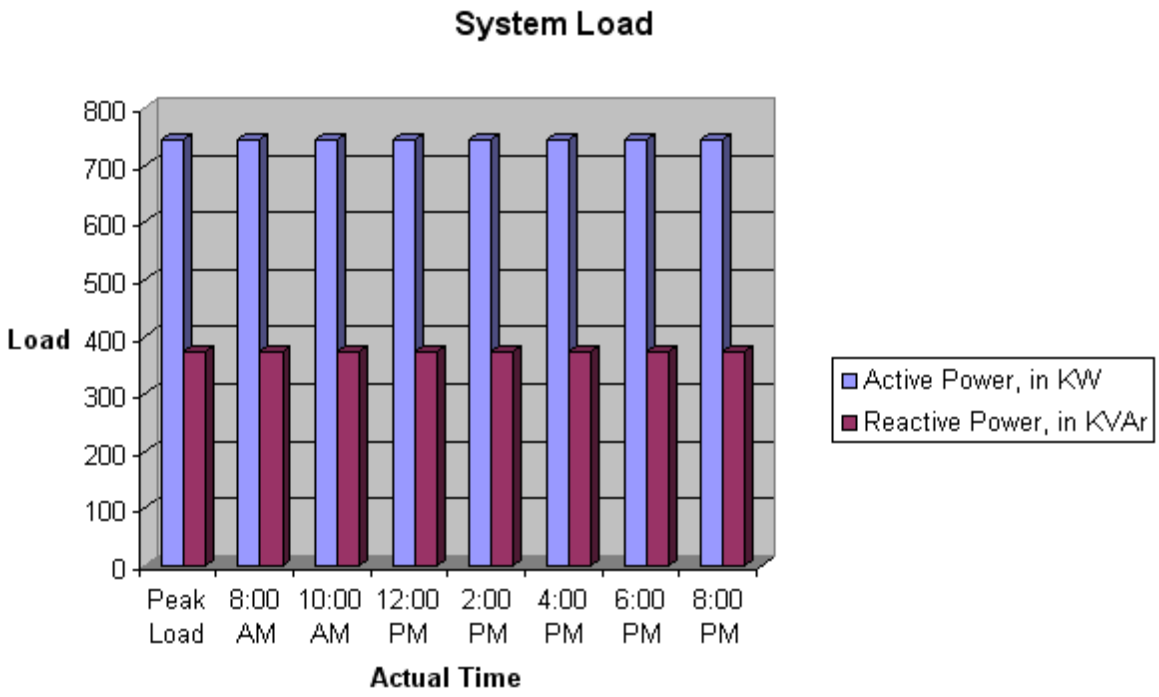
System Load
Load
800
700
600
500
400
300
200
100
0
Peak Load
8:00 AM
10:00 AM
12:00 PM
2:00 PM
4:00 PM
6:00 PM
8:00 PM
Actual Time
Active Power, in KW
Reactive Power, in KVAr

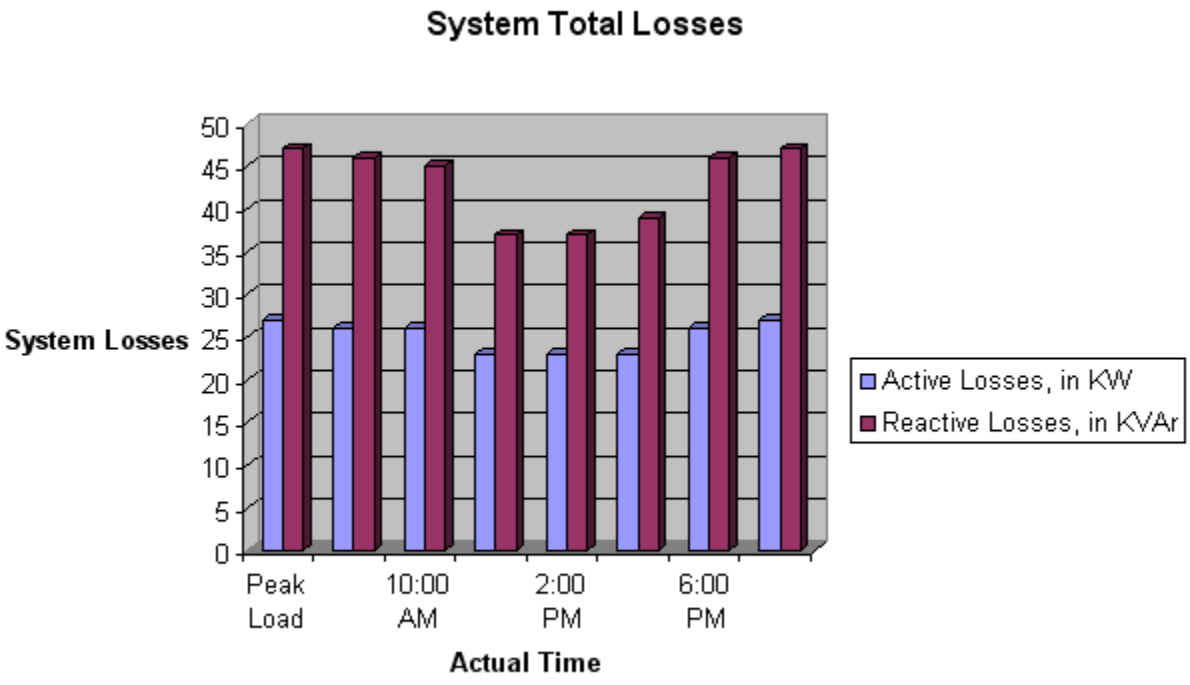
System Total Losses
System Losses
50
45
40
35
30
25
20
15
10
5
0
Peak Load
10:00 AM
2:00 PM
6:00 PM
Actual Time
Active Losses, in KW
Reactive Losses, in KVAr

E20: Power Flow Results – 20% PV Penetration Level; PV Unit at the End of Circuit:

Actual Time	System Power, PCC		PV Total Generation		System Total Load		System Total Losses	
	Active Power, in KW	Reactive Power, in KVAR	Active Power, in KW	Reactive Power, in KVAR	Active Power, in KW	Reactive Power, in KVAR	Active Power, in KW	Reactive Power, in KVAR
Peak Load	771	421	0	0	744	374	27	47
8:00 AM	757	420	12	0	744	374	26	46
10:00 AM	743	418	26	0	744	374	25	45
12:00 PM	634	411	130	0	744	374	20	37
2:00 PM	643	411	121	0	744	374	20	37
4:00 PM	674	406	82	0	744	374	21	39
6:00 PM	753	419	17	0	744	374	26	46
8:00 PM	771	421	0	0	744	374	27	47

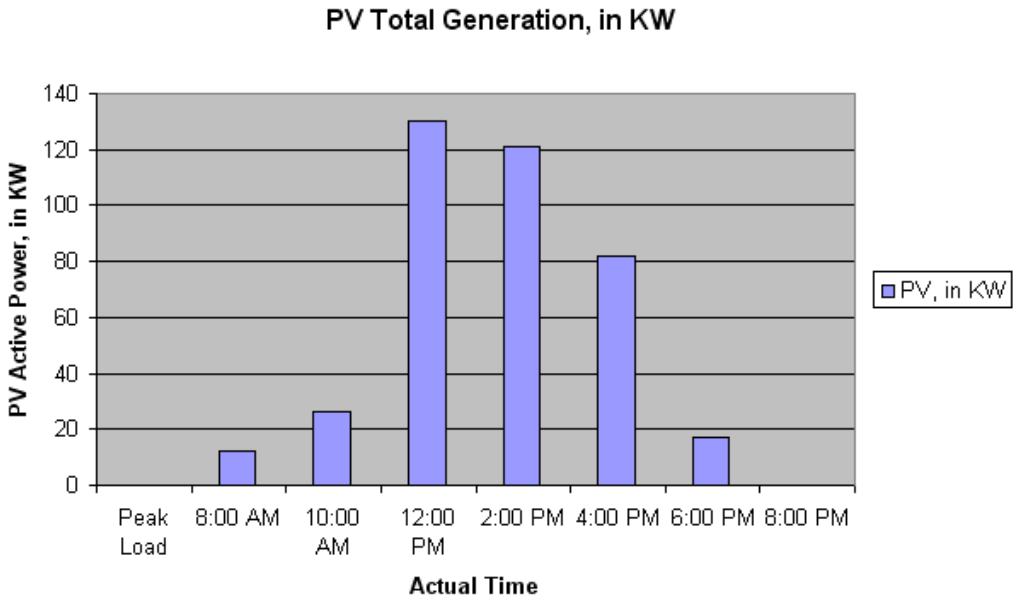
PV Total Generation, in KW
PV Active Power, in KW
140
120
100
80
60
40
20
0
Peak Load
8:00 AM
10:00 AM
12:00 PM
2:00 PM
4:00 PM
6:00 PM
8:00 PM
Actual Time
PV, in KW

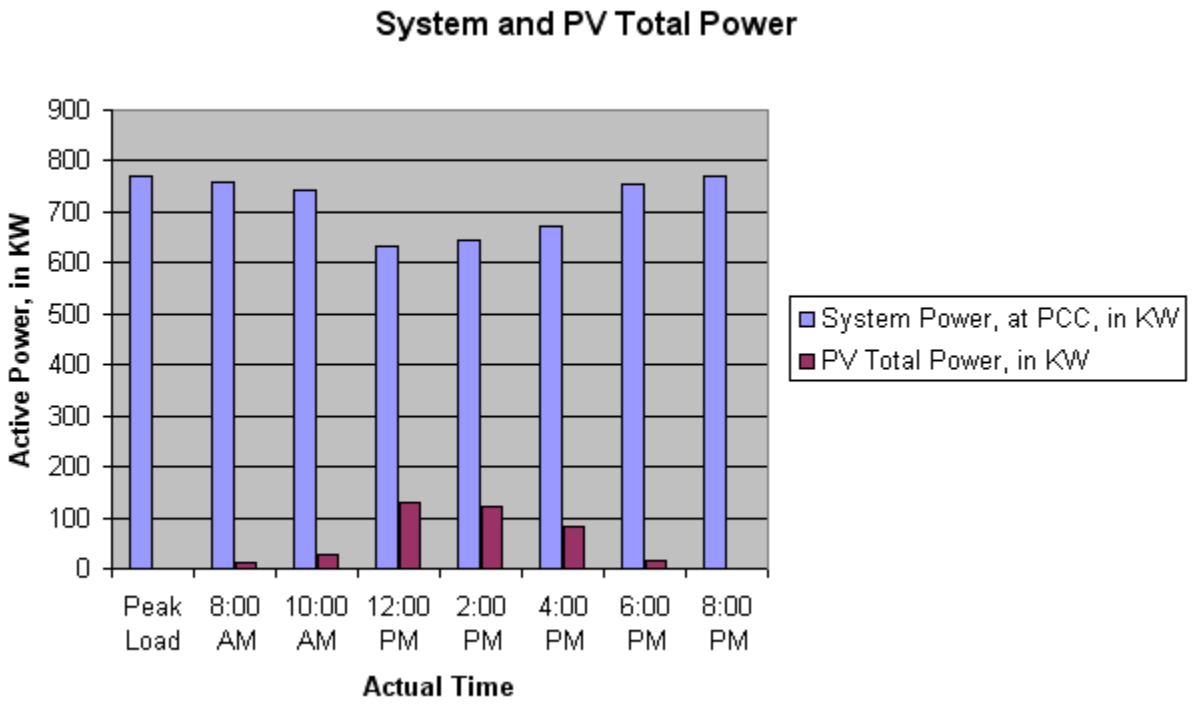
System and PV Total Power
Active Power, in KW
900
800
700
600
500
400
300
200
100
0
Peak Load
8:00 AM
10:00 AM
12:00 PM
2:00 PM
4:00 PM
6:00 PM
8:00 PM
Actual Time
System Power, at PCC, in KW
PV Total Power, in KW

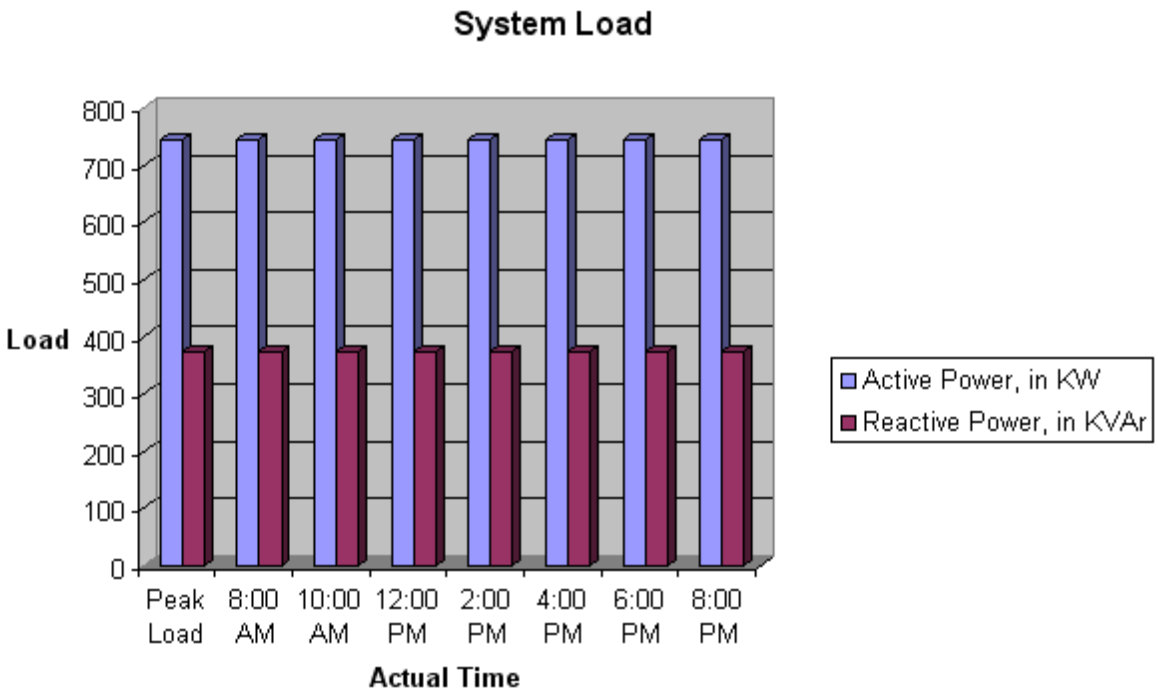
System Load
Load
800
700
600
500
400
300
200
100
0
Peak Load
8:00 AM
10:00 AM
12:00 PM
2:00 PM
4:00 PM
6:00 PM
8:00 PM
Actual Time
Active Power, in KW
Reactive Power, in KVAr

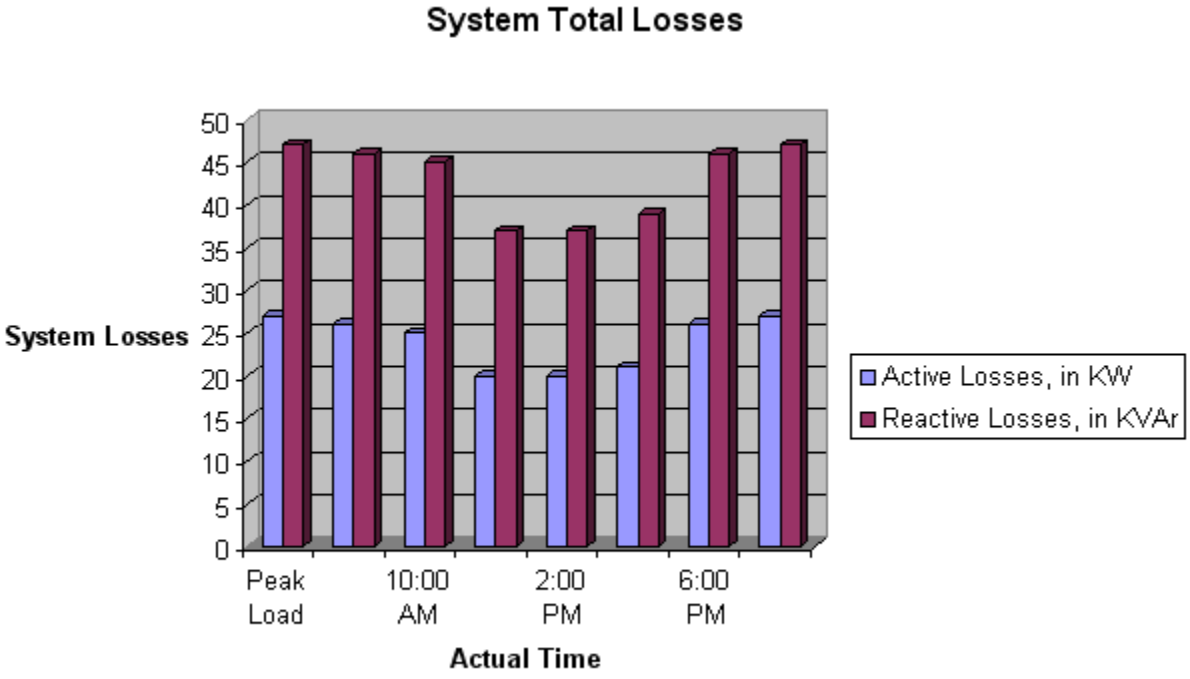
System Total Losses
System Losses
50
45
40
35
30
25
20
15
10
5
0
Peak Load
10:00 AM
2:00 PM
6:00 PM
Actual Time
Active Losses, in KW
Reactive Losses, in KVAr

S30: Power Flow Results – 30% PV Penetration Level; PV Unit Near to Substation:

Actual Time	System Power, PCC		PV Total Generation		System Total Load		System Total Losses	
	Active Power, in KW	Reactive Power, in KVAR	Active Power, in KW	Reactive Power, in KVAR	Active Power, in KW	Reactive Power, in KVAR	Active Power, in KW	Reactive Power, in KVAR
Peak Load	771	421	0	0	744	374	27	47
8:00 AM	751	419	19	0	744	374	26	45
10:00 AM	731	417	39	0	744	374	25	44
12:00 PM	571	407	195	0	744	374	22	33
2:00 PM	584	407	182	0	744	374	22	34
4:00 PM	634	403	123	0	744	374	22	36
6:00 PM	744	419	25	0	744	374	26	45
8:00 PM	771	421	0	0	744	374	27	47

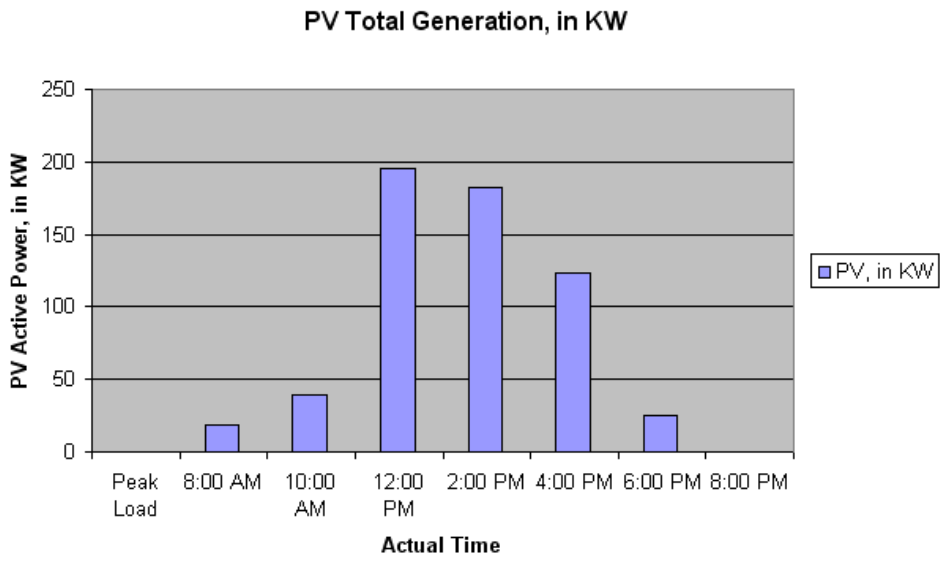
PV Total Generation, in KW
PV Active Power, in KW
250
200
150
100
50
0
Peak Load
8:00 AM
10:00 AM
12:00 PM
2:00 PM
4:00 PM
6:00 PM
8:00 PM
Actual Time
PV, in KW

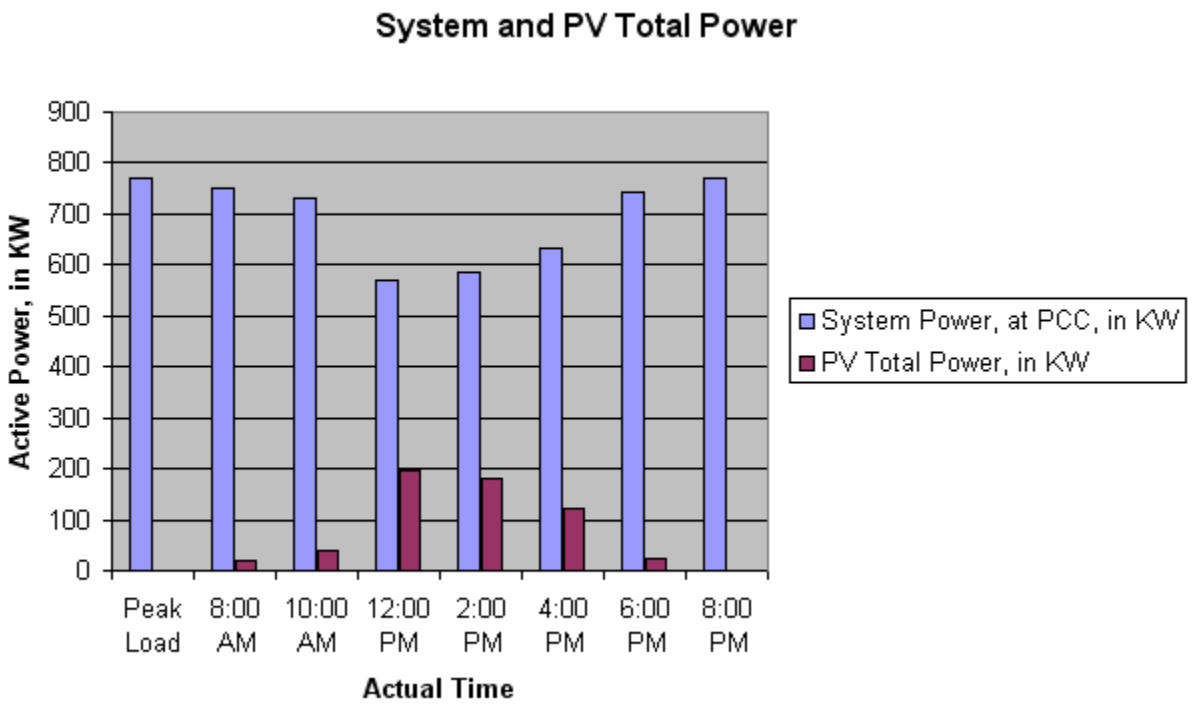
System and PV Total Power
Active Power, in KW
900
800
700
600
500
400
300
200
100
0
Peak Load
8:00 AM
10:00 AM
12:00 PM
2:00 PM
4:00 PM
6:00 PM
8:00 PM
Actual Time
System Power, at PCC, in KW
PV Total Power, in KW

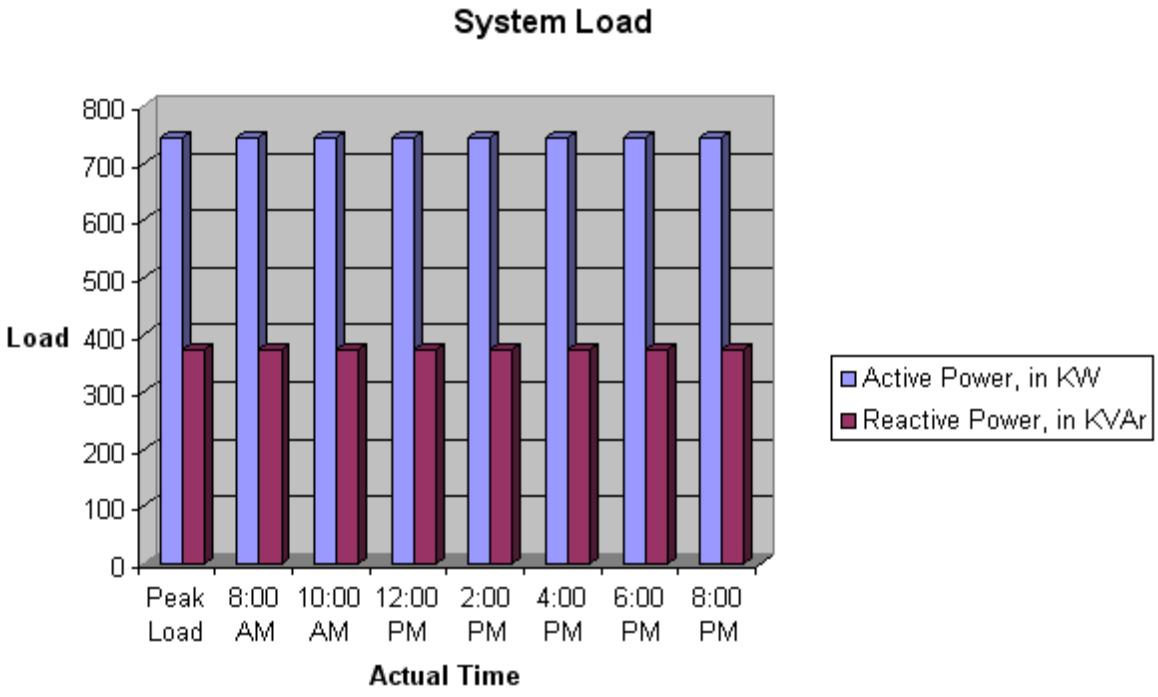
System Load
Load
800
700
600
500
400
300
200
100
0
Peak Load
8:00 AM
10:00 AM
12:00 PM
2:00 PM
4:00 PM
6:00 PM
8:00 PM
Actual Time
Active Power, in KW
Reactive Power, in KVAr

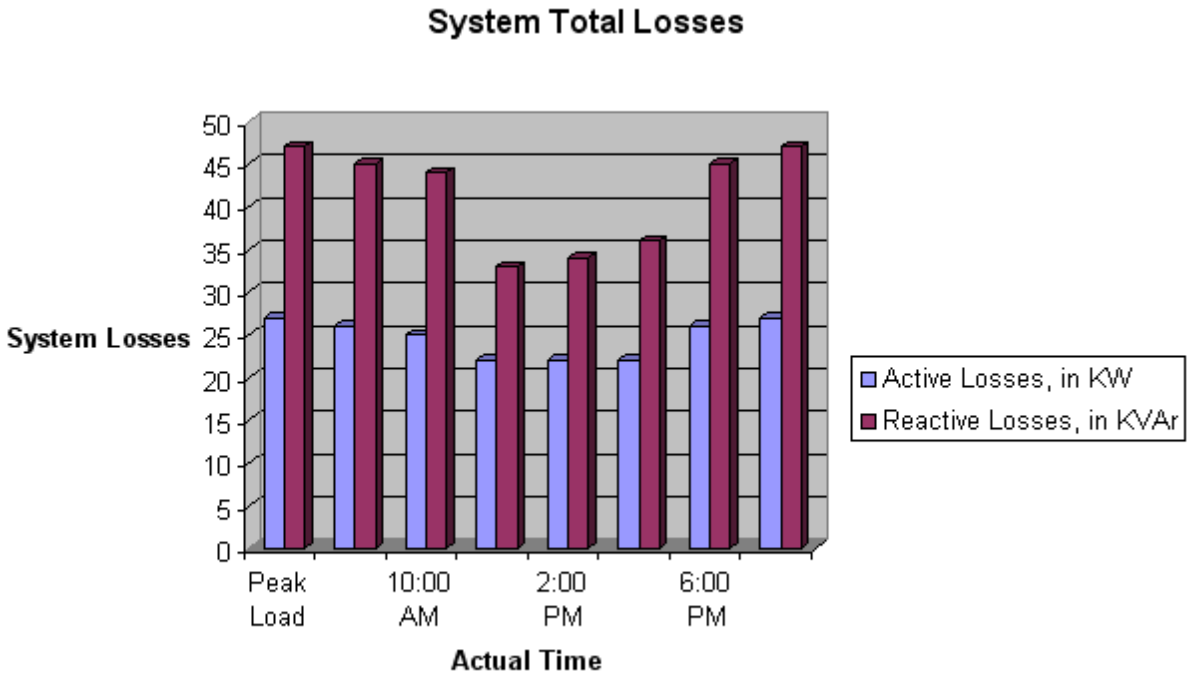
System Total Losses
System Losses
50
45
40
35
30
25
20
15
10
5
0
Peak Load
10:00 AM
2:00 PM
6:00 PM
Actual Time
Active Losses, in KW
Reactive Losses, in KVAr

E30: Power Flow Results – 30% PV Penetration Level; PV Unit at the End of Circuit:

Actual Time	System Power, PCC		PV Total Generation		System Total Load		System Total Losses	
	Active Power, in KW	Reactive Power, in KVAR	Active Power, in KW	Reactive Power, in KVAR	Active Power, in KW	Reactive Power, in KVAR	Active Power, in KW	Reactive Power, in KVAR
Peak Load	771	421	0	0	744	374	27	47
8:00 AM	751	419	19	0	744	374	26	45
10:00 AM	729	417	39	0	744	374	24	44
12:00 PM	566	407	195	0	744	374	17	34
2:00 PM	579	408	182	0	744	374	17	34
4:00 PM	631	403	123	0	744	374	19	36
6:00 PM	744	418	25	0	744	374	25	45
8:00 PM	771	421	0	0	744	374	27	47

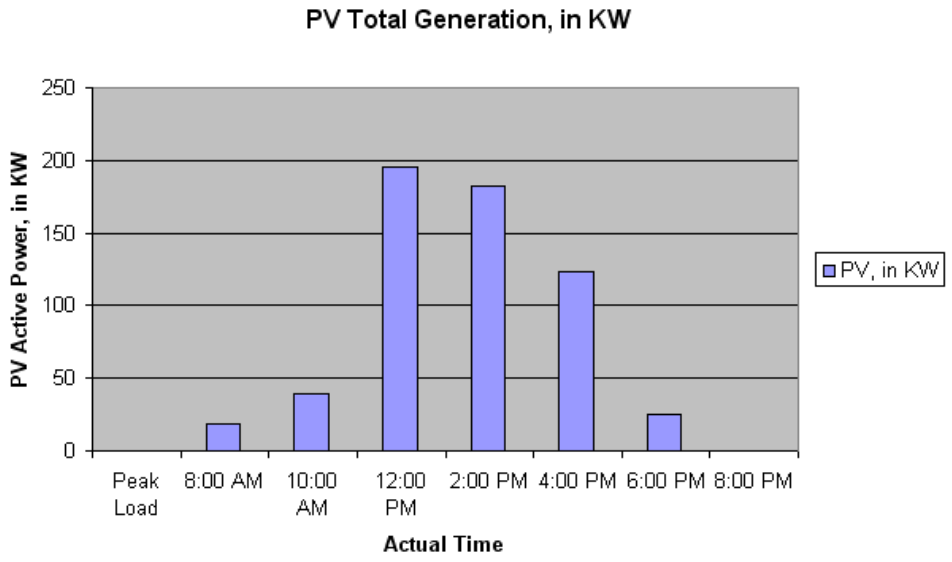
PV Total Generation, in KW
PV Active Power, in KW
250
200
150
100
50
0
Peak Load
8:00 AM
10:00 AM
12:00 PM
2:00 PM
4:00 PM
6:00 PM
8:00 PM
Actual Time
PV, in KW

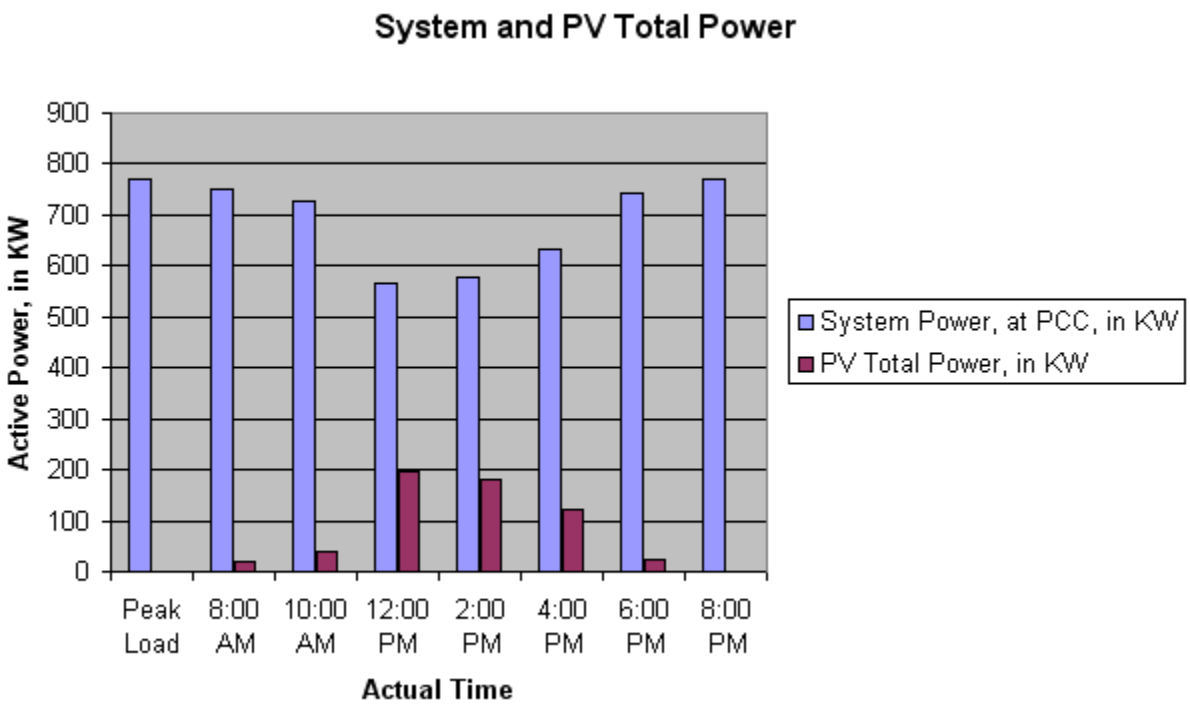
System and PV Total Power
Active Power, in KW
900
800
700
600
500
400
300
200
100
0
Peak Load
8:00 AM
10:00 AM
12:00 PM
2:00 PM
4:00 PM
6:00 PM
8:00 PM
Actual Time
System Power, at PCC, in KW
PV Total Power, in KW

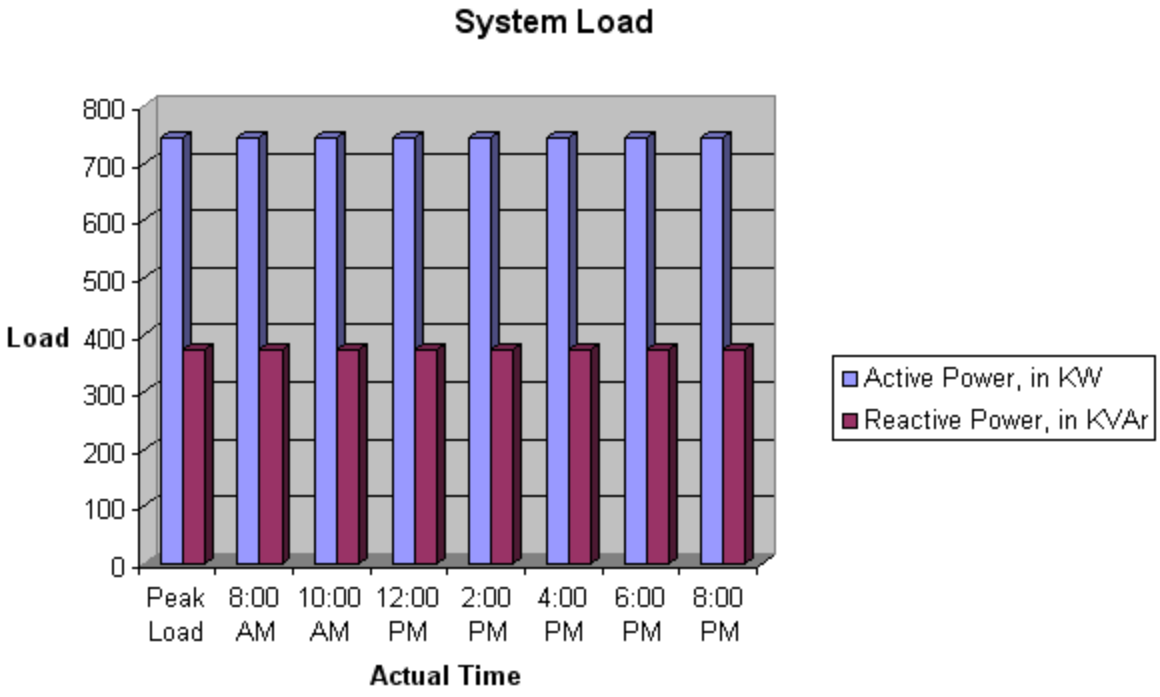
System Load
Load
800
700
600
500
400
300
200
100
0
Peak Load
8:00 AM
10:00 AM
12:00 PM
2:00 PM
4:00 PM
6:00 PM
8:00 PM
Actual Time
Active Power, in KW
Reactive Power, in KVAr

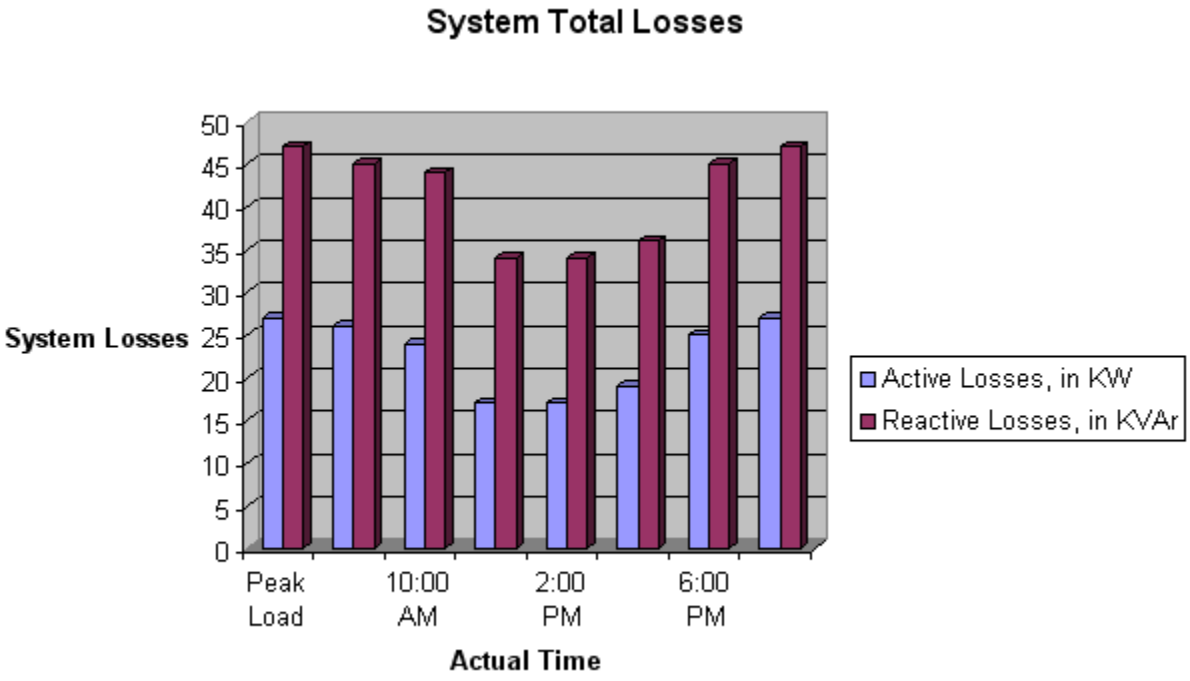
System Total Losses
System Losses
50
45
40
35
30
25
20
15
10
5
0
Peak Load
10:00 AM
2:00 PM
6:00 PM
Actual Time
Active Losses, in KW
Reactive Losses, in KVAr

S40: Power Flow Results – 40% PV Penetration Level; PV Unit Near to Substation:

Actual Time	System Power, PCC		PV Total Generation		System Total Load		System Total Losses	
	Active Power, in KW	Reactive Power, in KVAR	Active Power, in KW	Reactive Power, in KVAR	Active Power, in KW	Reactive Power, in KVAR	Active Power, in KW	Reactive Power, in KVAR
Peak Load	771	421	0	0	744	374	27	47
8:00 AM	745	419	25	0	744	374	26	45
10:00 AM	717	416	52	0	744	374	25	43
12:00 PM	505	404	260	0	744	374	20	30
2:00 PM	522	405	243	0	744	374	21	31
4:00 PM	592	400	164	0	744	374	21	34
6:00 PM	736	418	34	0	744	374	26	44
8:00 PM	771	421	0	0	744	374	27	47

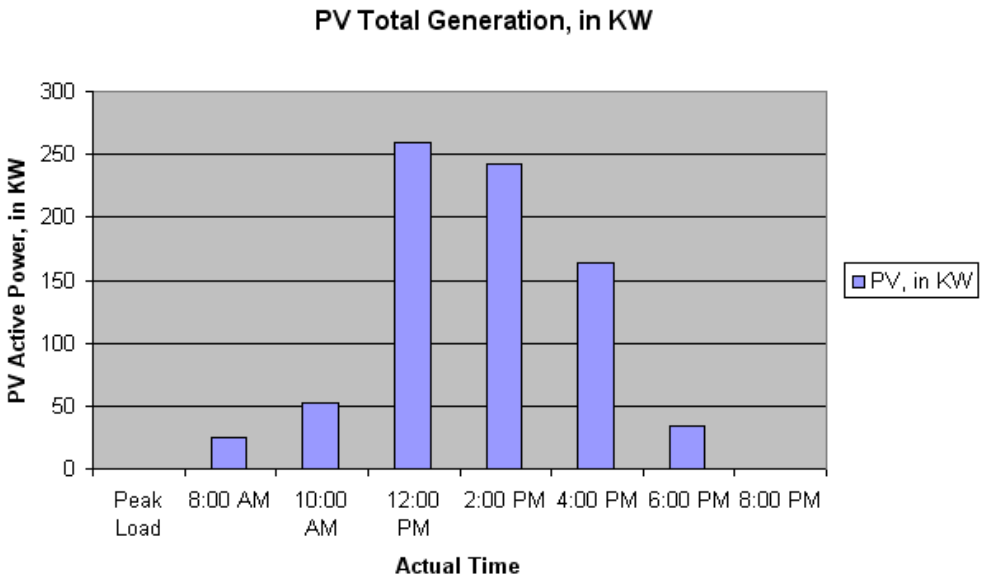
PV Total Generation, in KW
PV Active Power, in KW
300
250
200
150
100
50
0
Peak Load
8:00 AM
10:00 AM
12:00 PM
2:00 PM
4:00 PM
6:00 PM
8:00 PM
Actual Time
PV, in KW

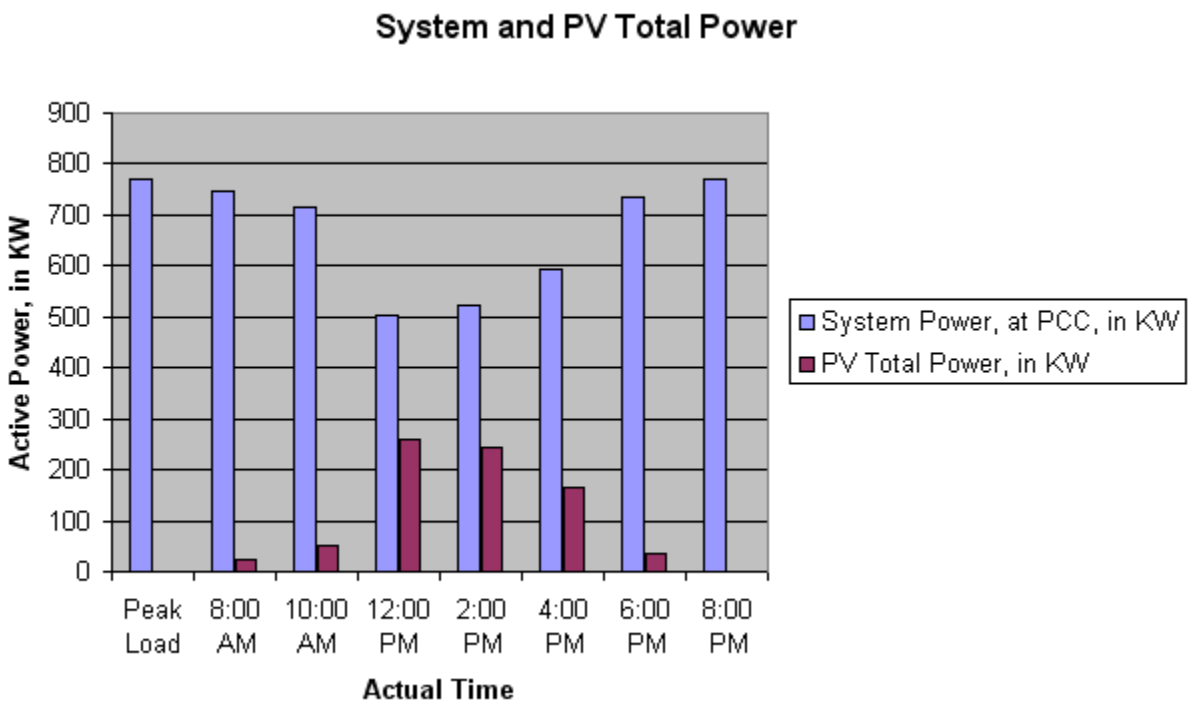
System and PV Total Power
Active Power, in KW
900
800
700
600
500
400
300
200
100
0
Peak Load
8:00 AM
10:00 AM
12:00 PM
2:00 PM
4:00 PM
6:00 PM
8:00 PM
Actual Time
System Power, at PCC, in KW
PV Total Power, in KW

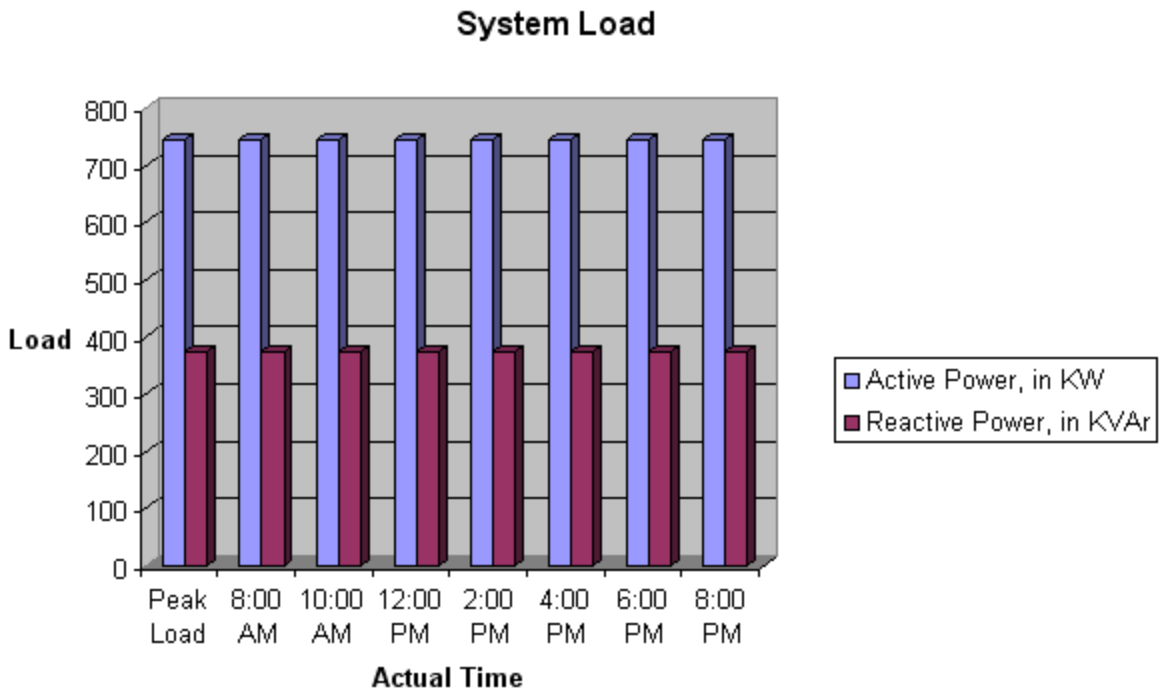
System Load
Load
800
700
600
500
400
300
200
100
0
Peak Load
8:00 AM
10:00 AM
12:00 PM
2:00 PM
4:00 PM
6:00 PM
8:00 PM
Actual Time
Active Power, in KW
Reactive Power, in KVAr

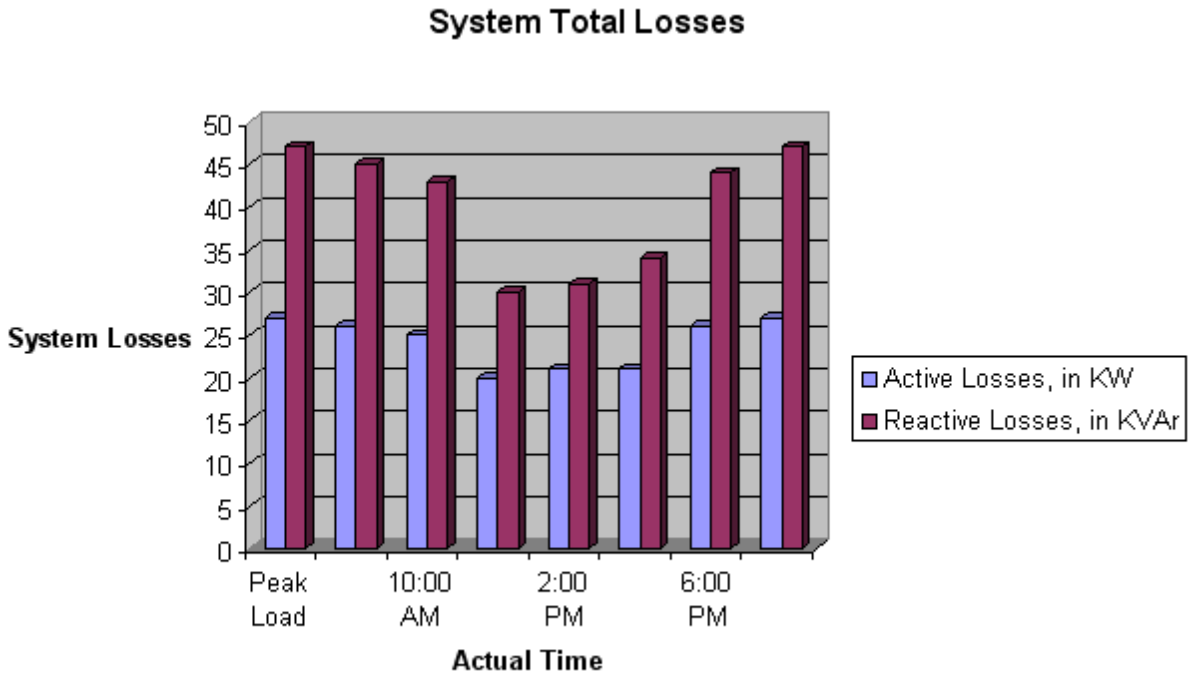
System Total Losses
System Losses
50
45
40
35
30
25
20
15
10
5
0
Peak Load
10:00 AM
2:00 PM
6:00 PM
Actual Time
Active Losses, in KW
Reactive Losses, in KVAr

E40: Power Flow Results – 40% PV Penetration Level; PV Unit at the End of Circuit:

Actual Time	System Power, PCC		PV Total Generation		System Total Load		System Total Losses	
	Active Power, in KW	Reactive Power, in KVAR	Active Power, in KW	Reactive Power, in KVAR	Active Power, in KW	Reactive Power, in KVAR	Active Power, in KW	Reactive Power, in KVAR
Peak Load	771	421	0	0	744	374	27	47
8:00 AM	744	419	25	0	744	374	25	45
10:00 AM	716	416	52	0	744	374	24	43
12:00 PM	499	405	260	0	744	374	15	32
2:00 PM	517	406	243	0	744	374	15	32
4:00 PM	588	401	164	0	744	374	17	34
6:00 PM	735	418	34	0	744	374	25	44
8:00 PM	771	421	0	0	744	374	27	47

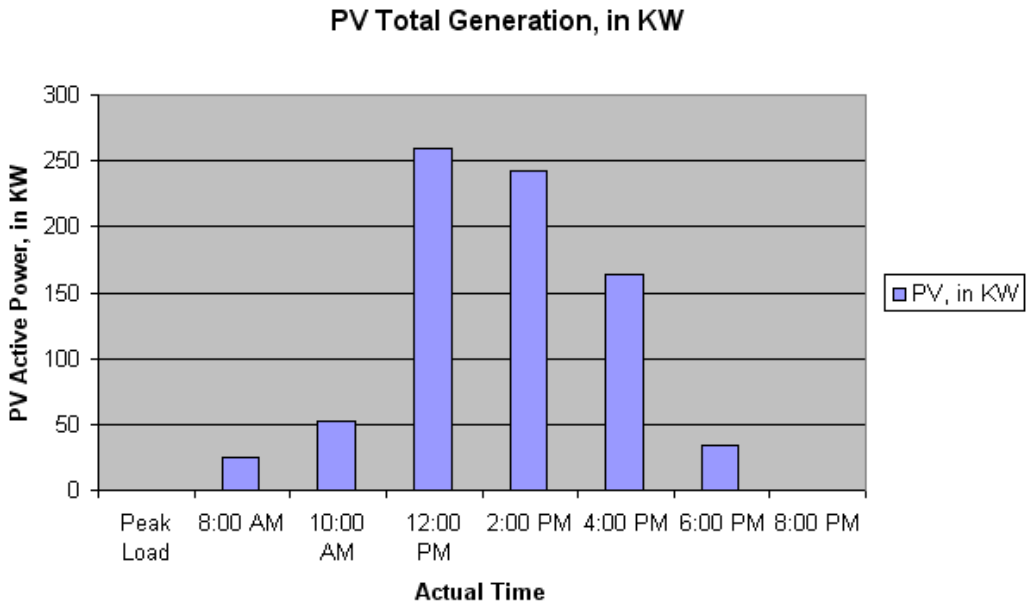
PV Total Generation, in KW
PV Active Power, in KW
300
250
200
150
100
50
0
Peak Load
8:00 AM
10:00 AM
12:00 PM
2:00 PM
4:00 PM
6:00 PM
8:00 PM
Actual Time
PV, in KW

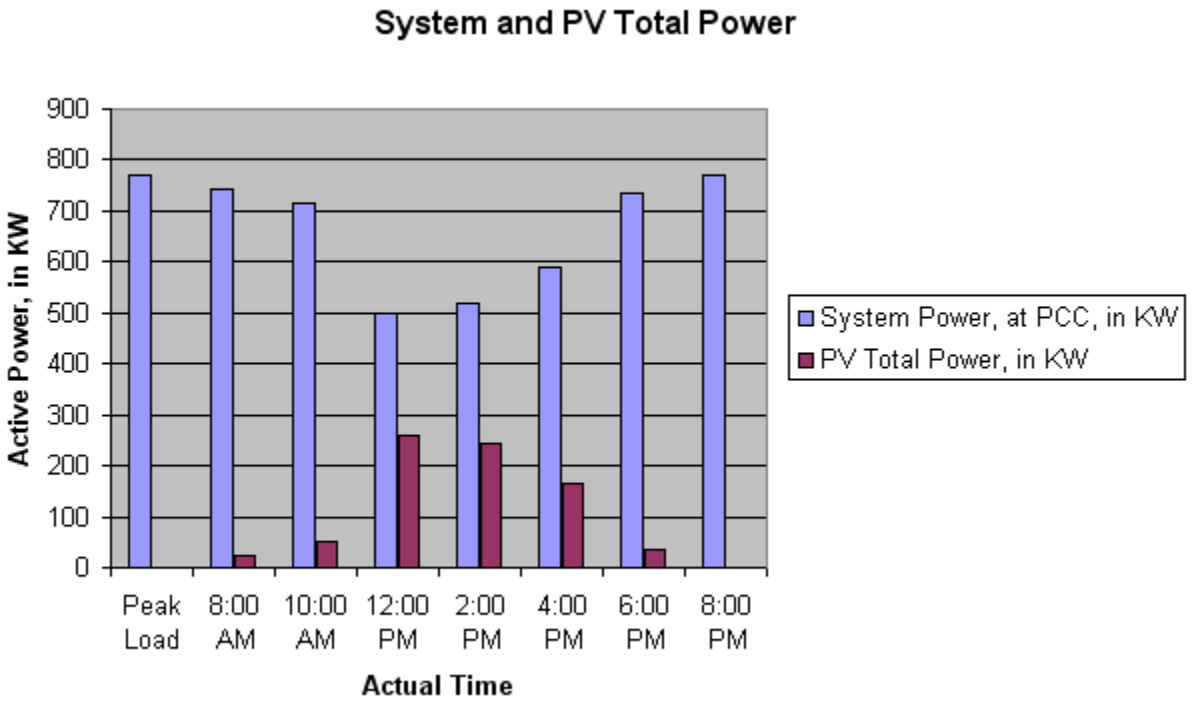
System and PV Total Power
Active Power, in KW
900
800
700
600
500
400
300
200
100
0
Peak Load
8:00 AM
10:00 AM
12:00 PM
2:00 PM
4:00 PM
6:00 PM
8:00 PM
Actual Time
System Power, at PCC, in KW
PV Total Power, in KW

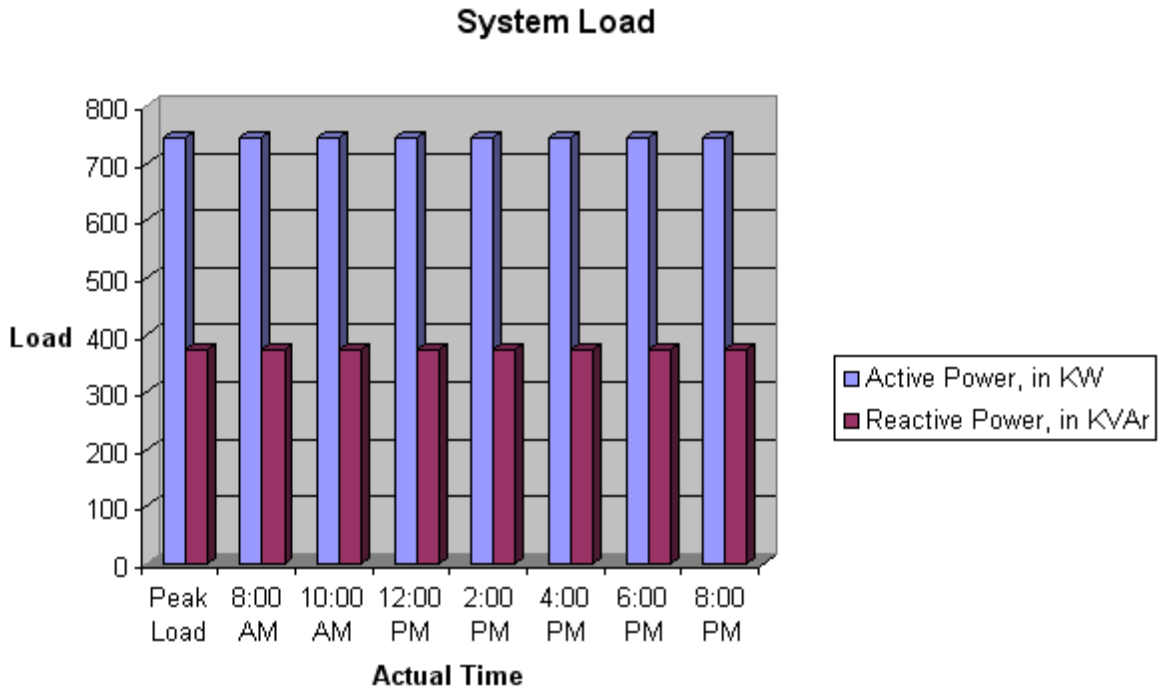
System Load
Load
800
700
600
500
400
300
200
100
0
Peak Load
8:00 AM
10:00 AM
12:00 PM
2:00 PM
4:00 PM
6:00 PM
8:00 PM
Actual Time
Active Power, in KW
Reactive Power, in KVAr

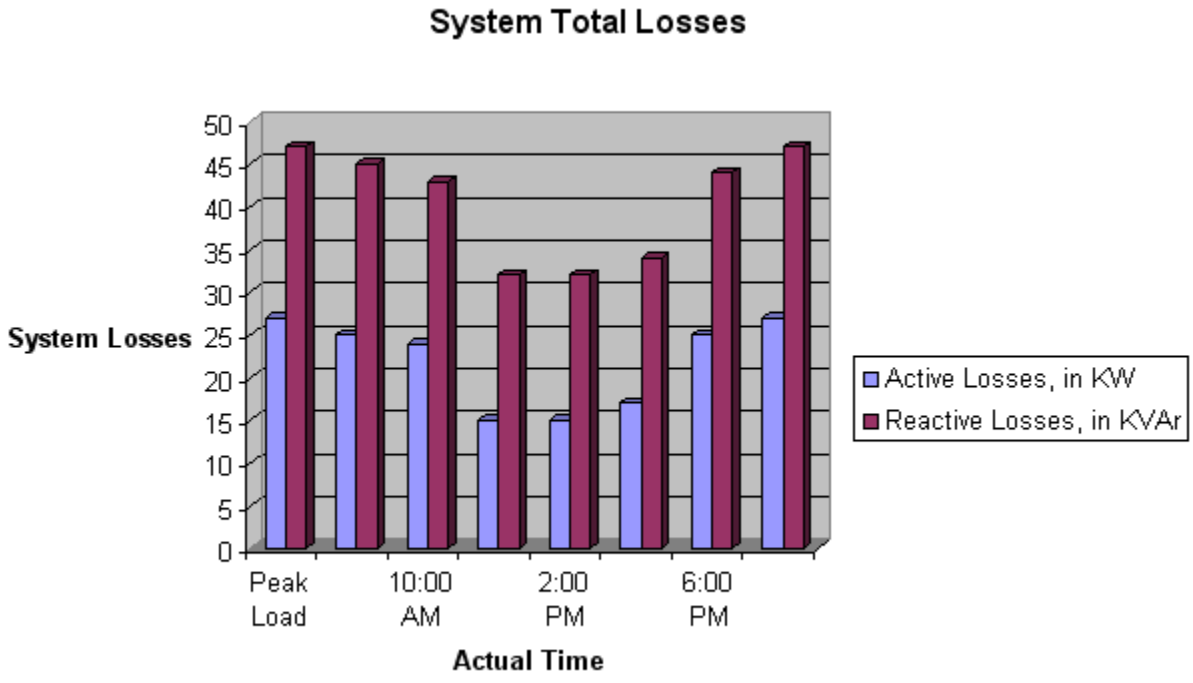
System Total Losses
System Losses
50
45
40
35
30
25
20
15
10
5
0
Peak Load
10:00 AM
2:00 PM
6:00 PM
Actual Time
Active Losses, in KW
Reactive Losses, in KVAr

E50: Power Flow Results – 50% PV Penetration Level; PV Unit at the End of Circuit:

Actual Time	System Power, PCC		PV Total Generation		System Total Load		System Total Losses	
	Active Power, in KW	Reactive Power, in KVAR	Active Power, in KW	Reactive Power, in KVAR	Active Power, in KW	Reactive Power, in KVAR	Active Power, in KW	Reactive Power, in KVAR
Peak Load	771	421	0	0	744	374	27	47
8:00 AM	738	418	31	0	744	374	25	44
10:00 AM	702	415	64	0	744	374	23	41
12:00 PM	432	404	325	0	744	374	13	30
2:00 PM	454	405	303	0	744	374	13	31
4:00 PM	545	399	206	0	744	374	16	32
6:00 PM	726	417	42	0	744	374	24	43
8:00 PM	771	421	0	0	744	374	27	47

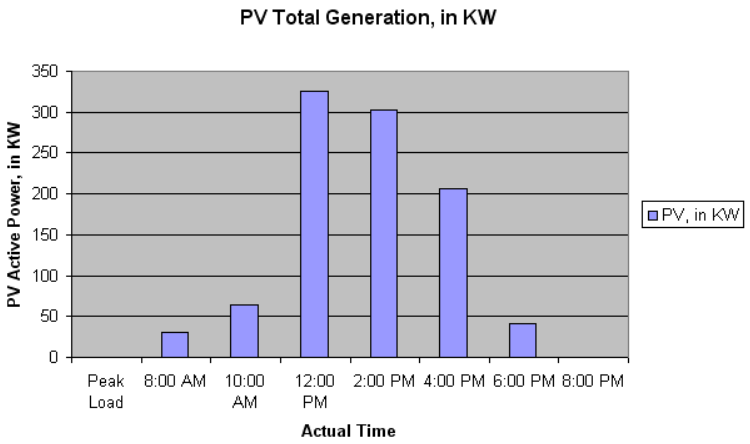
PV Total Generation, in KW
PV Active Power, in KW
350
300
250
200
150
100
50
0
Peak Load
8:00 AM
10:00 AM
12:00 PM
2:00 PM
4:00 PM
6:00 PM
8:00 PM
Actual Time
PV, in KW

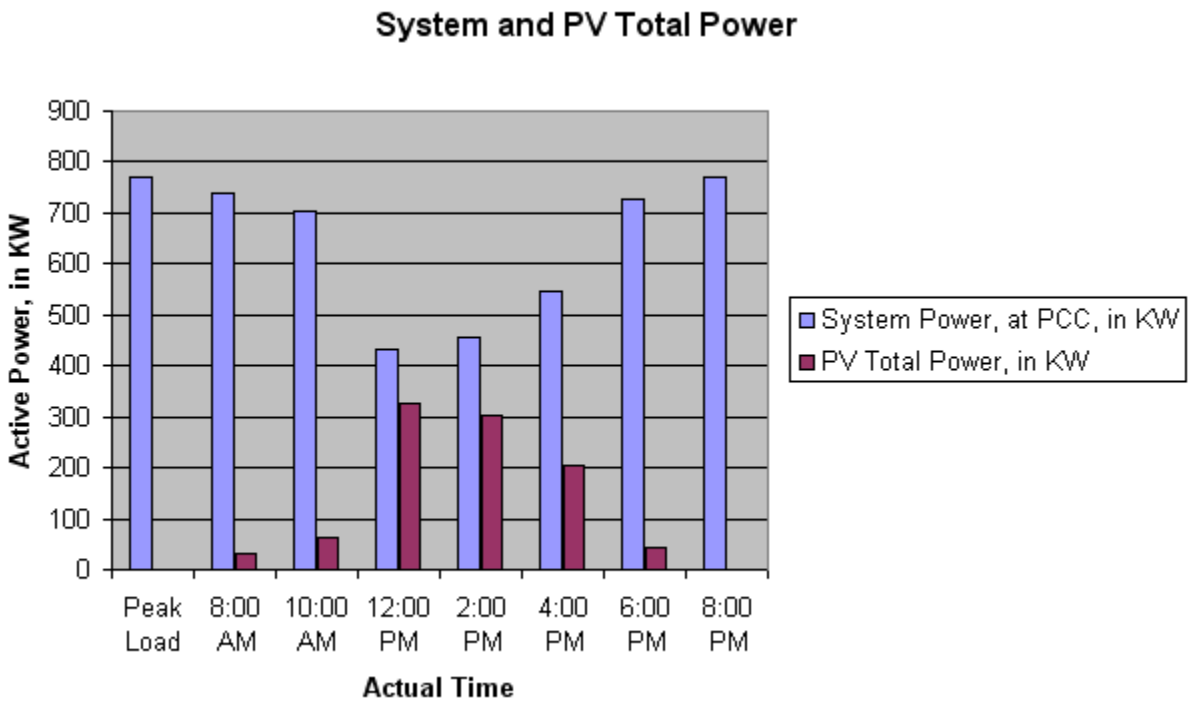
System and PV Total Power
Active Power, in KW
900
800
700
600
500
400
300
200
100
0
Peak Load
8:00 AM
10:00 AM
12:00 PM
2:00 PM
4:00 PM
6:00 PM
8:00 PM
Actual Time
System Power, at PCC, in KW
PV Total Power, in KW

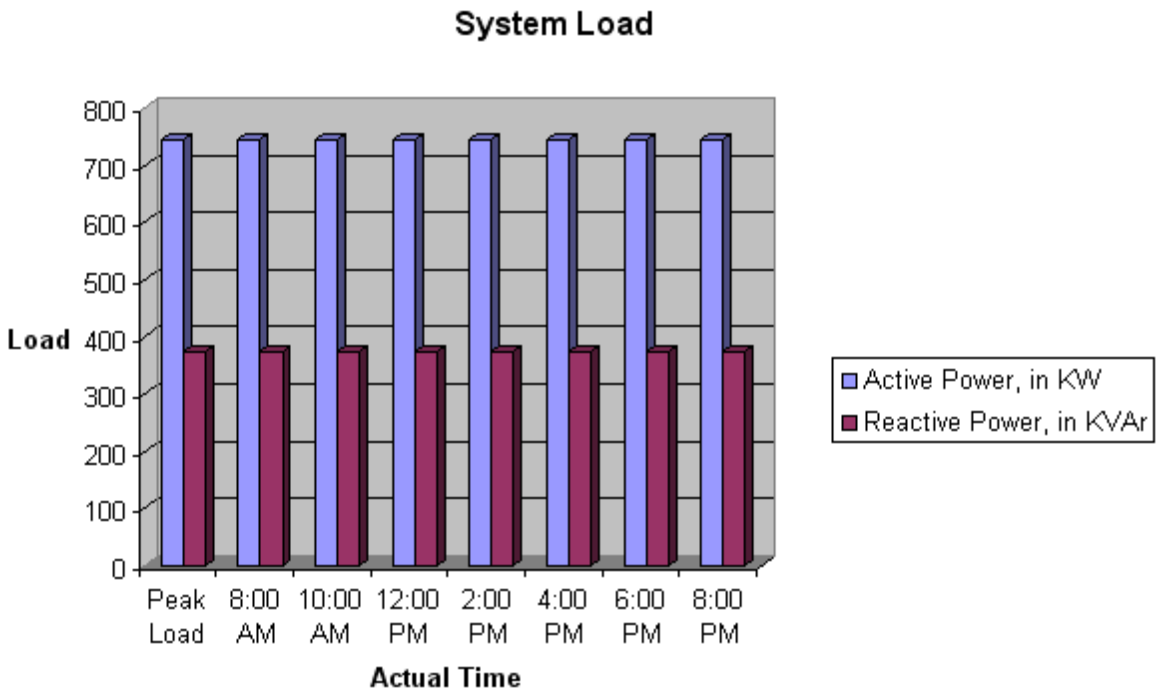
System Load
Load
800
700
600
500
400
300
200
100
0
Peak Load
8:00 AM
10:00 AM
12:00 PM
2:00 PM
4:00 PM
6:00 PM
8:00 PM
Actual Time
Active Power, in KW
Reactive Power, in KVAr

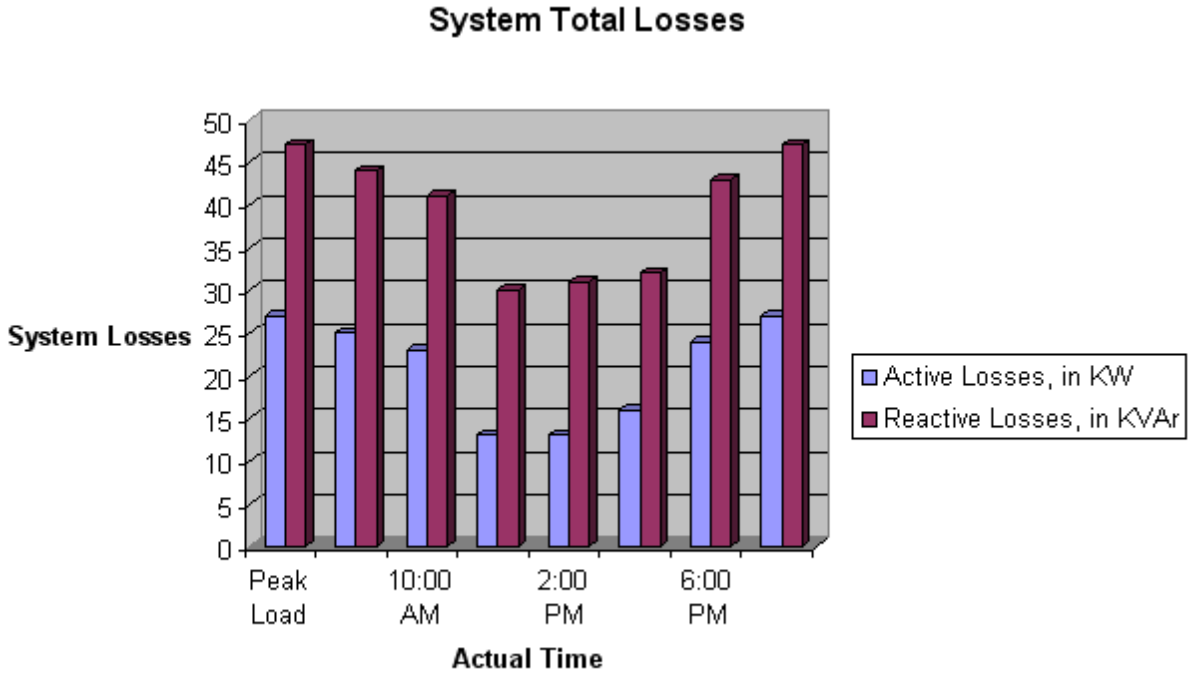
System Total Losses
System Losses
50
45
40
35
30
25
20
15
10
5
0
Peak Load
10:00 AM
2:00 PM
6:00 PM
Actual Time
Active Losses, in KW
Reactive Losses, in KVAr

Bus Voltages – 50% PV Penetration Level; PV Unit Near to Substation:

Bus Name	NoPV	8:00 AM	10:00 AM	12:00 PM	2:00 PM	4:00 PM	6:00 PM	8:00 PM
830-L	0.948	0.948	0.949	0.954	0.954	0.953	0.949	0.948
840-L	0.948	0.948	0.949	0.954	0.954	0.953	0.949	0.948
844-L	0.948	0.948	0.949	0.954	0.954	0.953	0.949	0.948
860-L	0.948	0.948	0.949	0.954	0.954	0.953	0.949	0.948
PV-BUS1	0.964	0.965	0.966	0.973	0.972	0.97	0.965	0.964
PV-BUS1-L	0.964	0.965	0.966	0.973	0.972	0.97	0.965	0.964
PV-BUS2	0.945	0.946	0.947	0.951	0.951	0.95	0.946	0.945
PV-BUS2-L	0.945	0.946	0.947	0.951	0.951	0.95	0.946	0.945
PV-G1	0	0.965	0.966	0.973	0.972	0.97	0.965	0

Bus Voltage:830-L

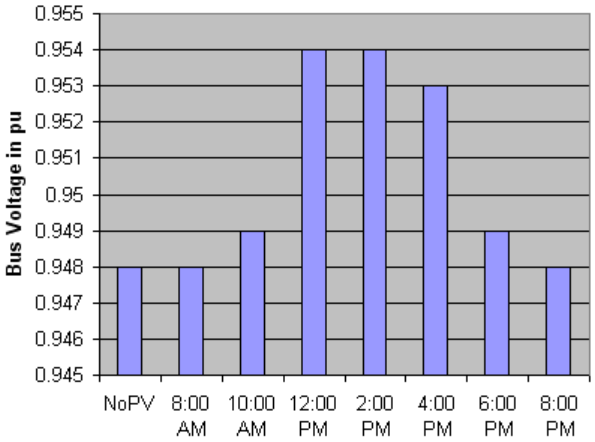

Bus Voltage: 840-L

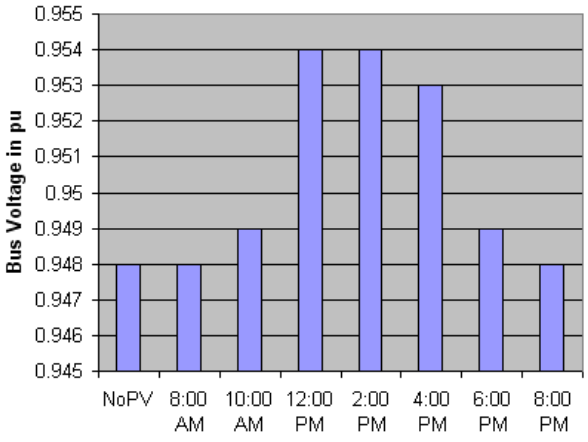

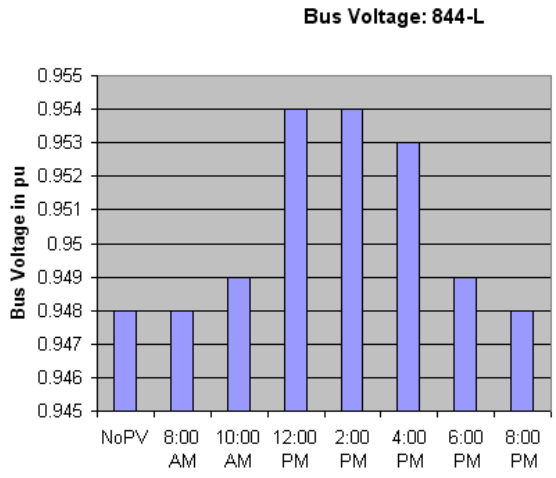
Bus Voltage: 844-L
Bus Voltage in pu
0.955
0.954
0.953
0.952
0.951
0.95
0.949
0.948
0.947
0.946
0.945
NoPV
8:00 AM
10:00 AM
12:00 PM
2:00 PM
4:00 PM
6:00 PM
8:00 PM

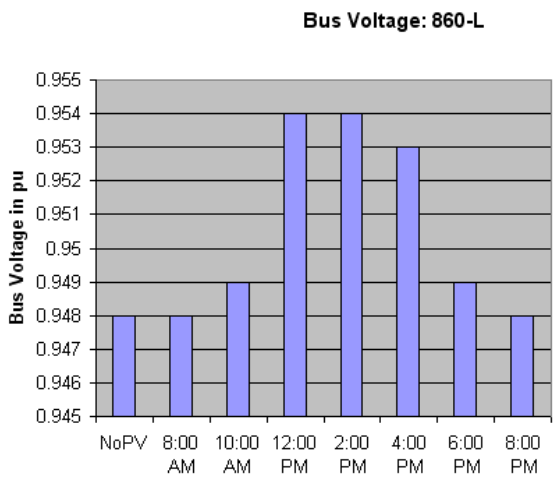
Bus Voltage: 860-L
Bus Voltage in pu
0.955
0.954
0.953
0.952
0.951
0.95
0.949
0.948
0.947
0.946
0.945
NoPV
8:00 AM
10:00 AM
12:00 PM
2:00 PM
4:00 PM
6:00 PM
8:00 PM

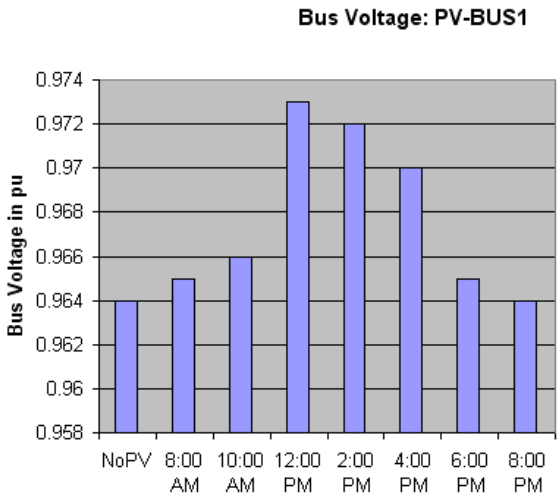
Bus Voltage: PV-BUS1
Bus Voltage in pu
0.974
0.972
0.97
0.968
0.966
0.964
0.962
0.96
0.958
NoPV
8:00 AM
10:00 AM
12:00 PM
2:00 PM
4:00 PM
6:00 PM
8:00 PM

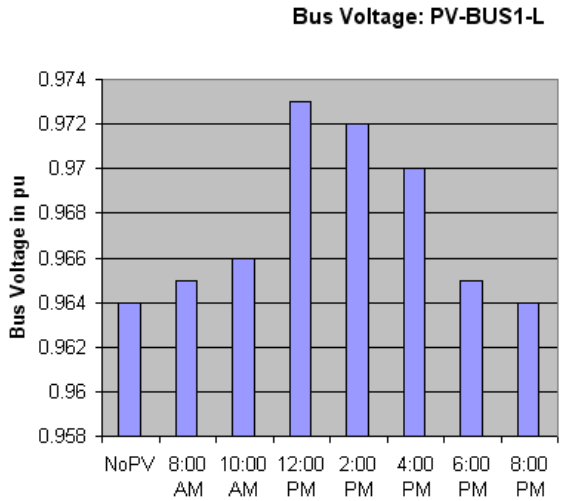
Bus Voltage: PV-BUS1-L
Bus Voltage in pu
0.974
0.972
0.97
0.968
0.966
0.964
0.962
0.96
0.958
NoPV
8:00 AM
10:00 AM
12:00 PM
2:00 PM
4:00 PM
6:00 PM
8:00 PM

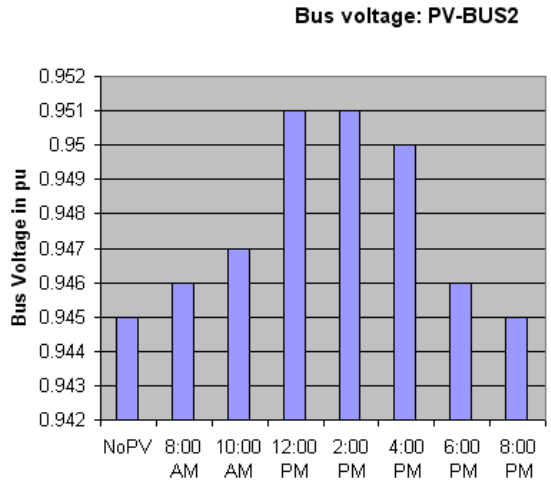
Bus voltage: PV-BUS2
Bus Voltage in pu
0.952
0.951
0.95
0.949
0.948
0.947
0.946
0.945
0.944
0.943
0.942
NoPV
8:00 AM
10:00 AM
12:00 PM
2:00 PM
4:00 PM
6:00 PM
8:00 PM

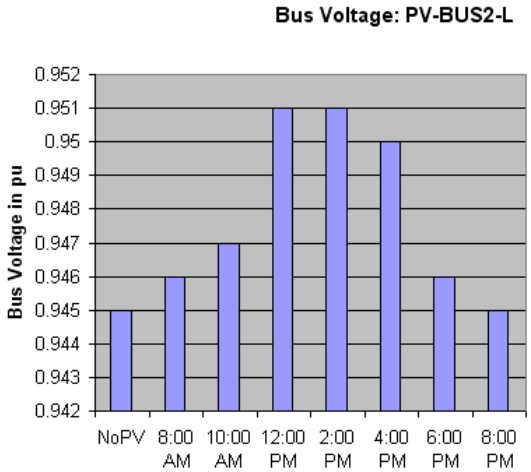
Bus Voltage: PV-BUS2-L
Bus Voltage in pu
0.952
0.951
0.95
0.949
0.948
0.947
0.946
0.945
0.944
0.943
0.942
NoPV
8:00 AM
10:00 AM
12:00 PM
2:00 PM
4:00 PM
6:00 PM
8:00 PM

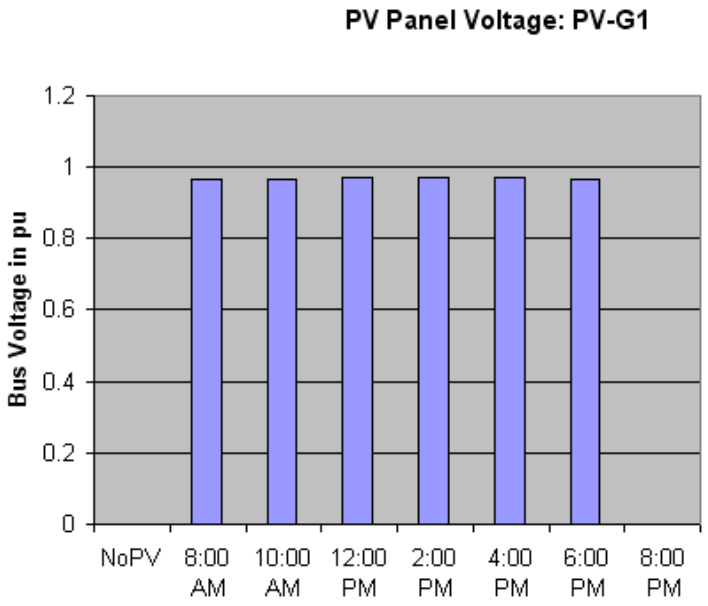

E50: Bus Voltages – 50% PV Penetration Level; PV Unit at the End of Circuit:

Bus Name	NoPV	8:00 AM	10:00 AM	12:00 PM	2:00 PM	4:00 PM	6:00 PM	8:00 PM
830-L	0.948	0.949	0.951	0.963	0.962	0.959	0.95	0.948
840-L	0.948	0.949	0.951	0.963	0.962	0.959	0.95	0.948
844-L	0.948	0.949	0.951	0.963	0.962	0.959	0.95	0.948
860-L	0.948	0.949	0.951	0.963	0.962	0.959	0.95	0.948
PV-BUS1	0.964	0.964	0.965	0.97	0.969	0.968	0.965	0.964
PV-BUS1-L	0.964	0.964	0.965	0.97	0.969	0.968	0.965	0.964
PV-BUS2	0.945	0.947	0.949	0.961	0.96	0.956	0.947	0.945
PV-BUS2-L	0.945	0.947	0.949	0.961	0.96	0.956	0.947	0.945
PV-G3	0	0.95	0.952	0.966	0.965	0.96	0.95	0

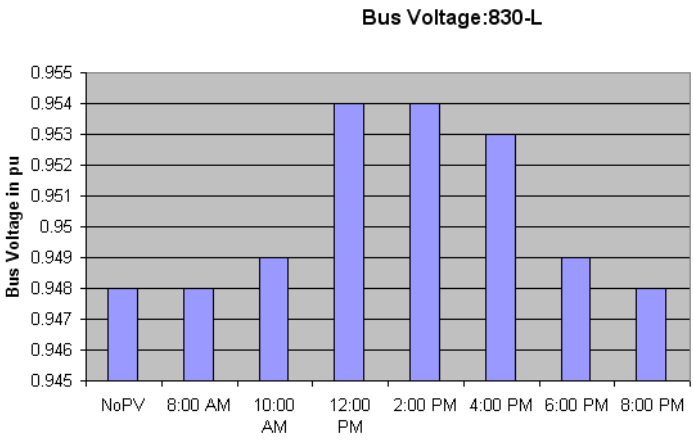
Bus Voltage:830-L
Bus Voltage in pu
0.955
0.954
0.953
0.952
0.951
0.95
0.949
0.948
0.947
0.946
0.945
NoPV
8:00 AM
10:00 AM
12:00 PM
2:00 PM
4:00 PM
6:00 PM
8:00 PM

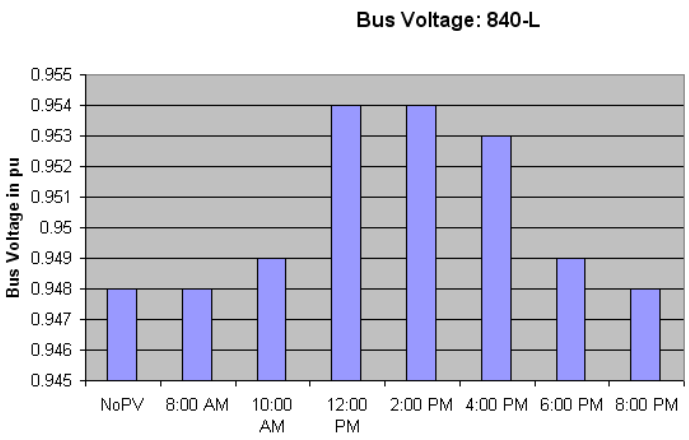
Bus Voltage: 840-L
Bus Voltage in pu
0.955
0.954
0.953
0.952
0.951
0.95
0.949
0.948
0.947
0.946
0.945
NoPV
8:00 AM
10:00 AM
12:00 PM
2:00 PM
4:00 PM
6:00 PM
8:00 PM

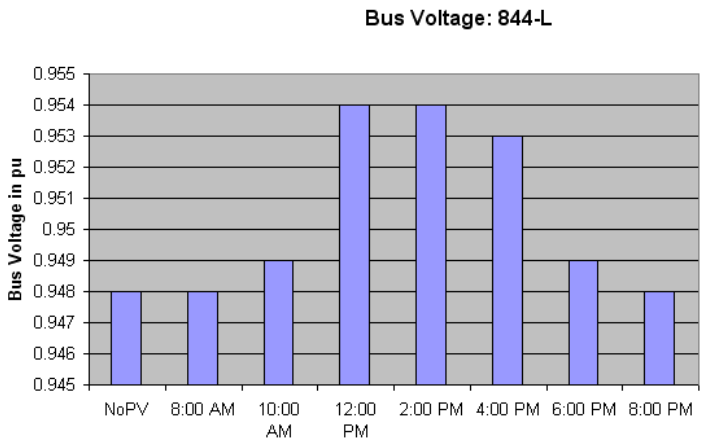
Bus Voltage: 844-L
Bus Voltage in pu
0.955
0.954
0.953
0.952
0.951
0.95
0.949
0.948
0.947
0.946
0.945
NoPV
8:00 AM
10:00 AM
12:00 PM
2:00 PM
4:00 PM
6:00 PM
8:00 PM

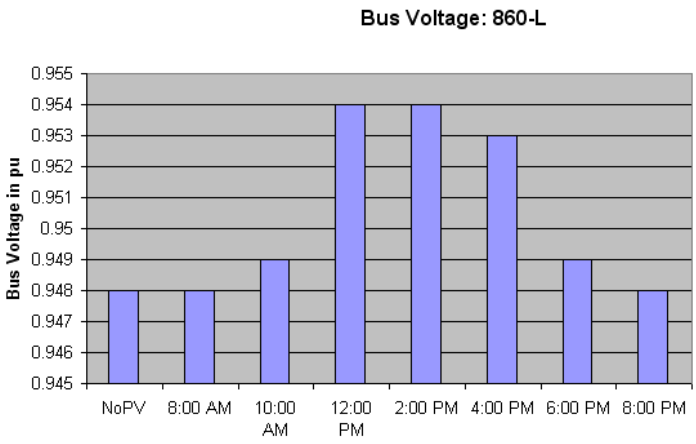
Bus Voltage: 860-L
Bus Voltage in pu
0.955
0.954
0.953
0.952
0.951
0.95
0.949
0.948
0.947
0.946
0.945
NoPV
8:00 AM
10:00 AM
12:00 PM
2:00 PM
4:00 PM
6:00 PM
8:00 PM

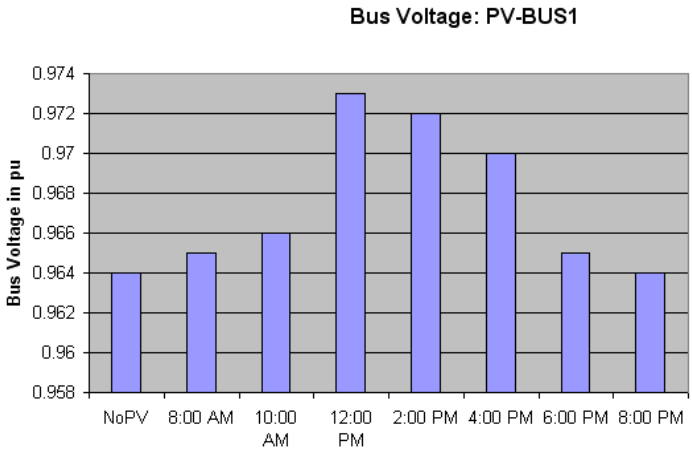
Bus Voltage: PV-BUS1
Bus Voltage in pu
0.974
0.972
0.97
0.968
0.966
0.964
0.962
0.96
0.958
NoPV
8:00 AM
10:00 AM
12:00 PM
2:00 PM
4:00 PM
6:00 PM
8:00 PM

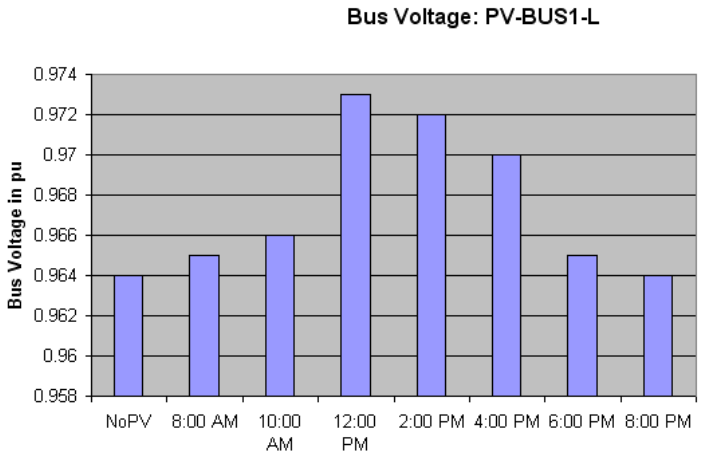
Bus Voltage: PV-BUS1-L
Bus Voltage in pu
0.974
0.972
0.97
0.968
0.966
0.964
0.962
0.96
0.958
NoPV
8:00 AM
10:00 AM
12:00 PM
2:00 PM
4:00 PM
6:00 PM
8:00 PM

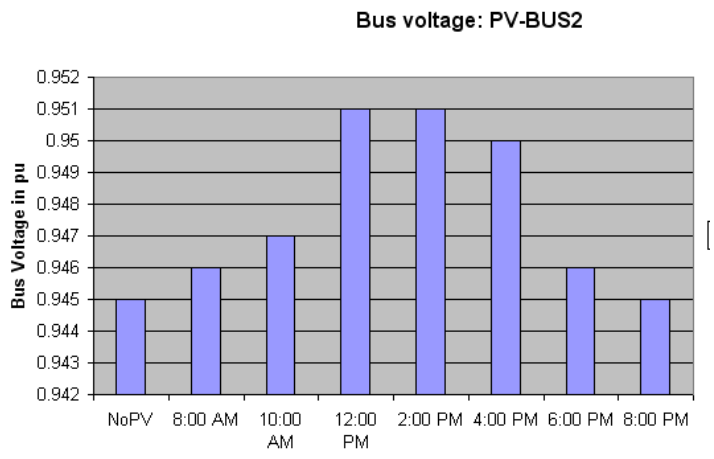
Bus voltage: PV-BUS2
Bus Voltage in pu
0.952
0.951
0.95
0.949
0.948
0.947
0.946
0.945
0.944
0.943
0.942
NoPV
8:00 AM
10:00 AM
12:00 PM
2:00 PM
4:00 PM
6:00 PM
8:00 PM

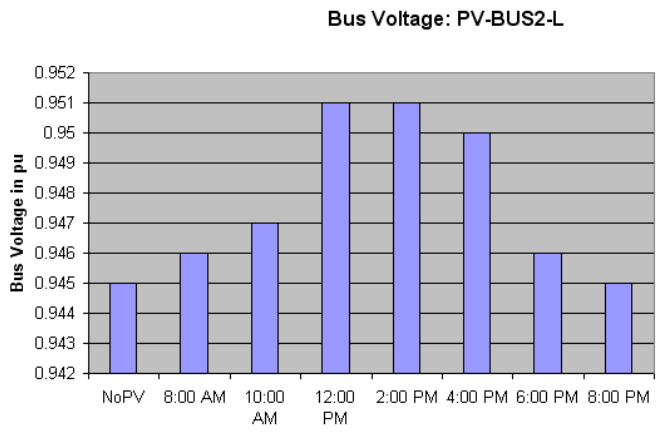
Bus Voltage: PV-BUS2-L
Bus Voltage in pu
0.952
0.951
0.95
0.949
0.948
0.947
0.946
0.945
0.944
0.943
0.942
NoPV
8:00 AM
10:00 AM
12:00 PM
2:00 PM
4:00 PM
6:00 PM
8:00 PM

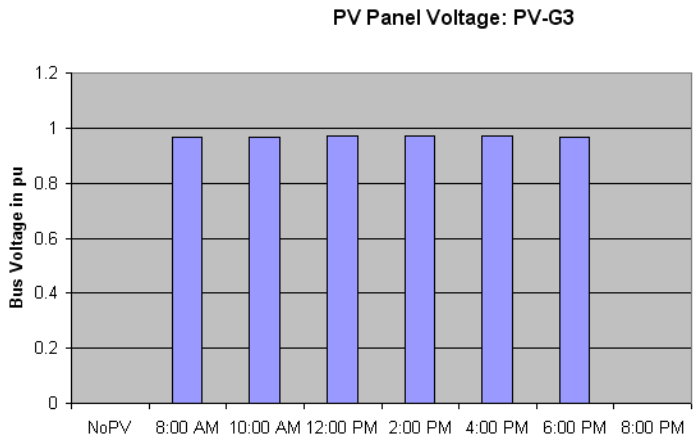
PV Panel Voltage: PV-G3
Bus Voltage in pu
1.2
1
0.8
0.6
0.4
0.2
0
NoPV
8:00 AM
10:00 AM
12:00 PM
2:00 PM
4:00 PM
6:00 PM
8:00 PM

A.2. Short Circuit Analysis: IEEE 34 Bus: 50% PV Penetration Level; PV Unit Close to Substation:

Item No.	Bus Name	Pre-Flt. Voltage, in V	X/R	3 Phase Bus Fault Current, 0.5 Cycle				L-G Fault Current, 0.5 Cycle			
				Isym, in A	IDC, in A	Iasym, in A	MF	Isym, in A	IDC, in A	Iasym, in A	MF
1	2	3	4	5	6	7	8	9	10	11	12
1	101	24900	1.7	280.75	62.32	287.58	1.02	220.11	48.86	225.46	1.02
2	3	69000	20	836.74	1011.32	1312.59	1.57	836.74	1011.32	1312.59	1.57
3	800	24900	9.33	549.09	554.57	780.41	1.42	596.06	602	847.17	1.42
4	802	24900	8.03	539.55	515.97	746.56	1.38	575.77	550.61	796.67	1.38
5	806	24900	7.36	533.26	492.08	725.6	1.36	562.82	519.36	765.84	1.36
6	808	24900	3.21	431.51	229.13	488.57	1.13	392.01	208.16	443.85	1.13
7	810	24900	3.11	419.18	215.87	471.5	1.12	372.85	192.01	419.39	1.12
8	812	24900	2.19	346.58	116.73	365.71	1.06	286.73	96.57	302.56	1.06
9	814	24900	1.84	297.79	76.52	307.46	1.03	235.77	60.58	243.43	1.03
10	816	24900	1.84	297.74	76.49	307.41	1.03	235.73	60.56	243.38	1.03
11	818	24900	1.8	294.1	72.32	302.86	1.03	232.62	57.2	239.55	1.03
12	820	24900	1.13	213.31	18.57	214.11	1.00	167.52	14.58	168.15	1.00
13	822	24900	1.04	196.74	13.47	197.2	1.00	154.7	10.59	155.06	1.00
14	824	24900	1.7	281.03	62.48	287.89	1.02	220.35	48.99	225.73	1.02
15	826	24900	1.63	275.14	56.87	280.96	1.02	215.52	44.55	220.07	1.02
16	828	24900	1.7	281	62.46	287.86	1.02	220.33	48.97	225.7	1.02
17	830	24900	1.7	280.97	62.45	287.83	1.02	220.3	48.96	225.68	1.02
18	830-L	24900	1.7	280.97	62.45	287.83	1.02	220.3	48.96	225.68	1.02
19	832	24900	1.7	280.89	62.4	287.74	1.02	220.23	48.92	225.6	1.02

20	834	24900	1.7	280.83	62.36	287.67	1.02	220.18	48.9	225.54	1.02
21	836	24900	1.7	280.78	62.33	287.61	1.02	220.13	48.87	225.49	1.02
22	838	24900	1.7	280.72	62.3	287.55	1.02	220.08	48.84	225.44	1.02
23	840-L	24900	1.7	280.75	62.32	287.58	1.02	220.11	48.86	225.46	1.02
24	842	24900	1.7	280.81	62.35	287.64	1.02	220.16	48.88	225.52	1.02
25	844	24900	1.7	280.78	62.33	287.61	1.02	220.13	48.87	225.49	1.02
26	844-L	24900	1.7	280.78	62.33	287.61	1.02	220.13	48.87	225.49	1.02
27	846	24900	1.7	280.75	62.32	287.58	1.02	220.11	48.86	225.46	1.02

Item No.	Bus Name	Pre-Flt. Voltage, in V	X/R	3 Phase Bus Fault Current, 0.5 Cycle				L-G Fault Current, 0.5 Cycle			
				Isym, in A	IDC, in A	Iasym, in A	MF	Isym, in A	IDC, in A	Iasym, in A	MF
1	2	3	4	5	6	7	8	9	10	11	12
29	846	24900	1.7	280.75	62.31	287.58	1.02	220.11	48.85	225.46	1.02
30	848	24900	1.7	280.72	62.3	287.55	1.02	220.08	48.84	225.44	1.02
31	848-L	24900	1.7	280.72	62.3	287.55	1.02	220.08	48.84	225.44	1.02
32	850	24900	1.84	297.77	76.51	307.45	1.03	235.76	60.58	243.41	1.03
33	852	24900	1.7	280.92	62.41	287.77	1.02	220.25	48.93	225.62	1.02
34	854	24900	1.7	280.95	62.43	287.8	1.02	220.28	48.95	225.65	1.02
35	856	24900	1.7	280.92	62.41	287.77	1.02	220.25	48.93	225.62	1.02
36	858	24900	1.7	280.86	62.38	287.71	1.02	220.2	48.91	225.57	1.02
37	860	24900	1.7	280.81	62.35	287.64	1.02	220.16	48.88	225.52	1.02
38	860-L	24900	1.7	280.81	62.35	287.64	1.02	220.16	48.88	225.52	1.02

39	862	24900	1.7	280.75	62.31	287.58	1.02	220.11	48.85	225.46	1.02
40	864	24900	1.7	280.83	62.36	287.68	1.02	220.18	48.89	225.54	1.02
41	888	4160	1.91	805.21	220.08	834.74	1.04	957.9	261.81	993.03	1.04
42	890	4160	1.91	803.87	219.06	833.18	1.04	955.12	260.28	989.95	1.04
43	890-L	4160	1.91	803.83	219.04	833.14	1.04	955.04	260.25	989.86	1.04
44	PV-BUS1	480	4.39	10705	7406.19	13017.2	1.22	12795	8852.21	15558.8	1.22
45	PV-BUS1-L	480	4.34	10694.5	7336.87	12969.3	1.21	12780.7	8768.12	15499.3	1.21
46	PV-BUS2	480	2.08	11551.4	3604.48	12100.7	1.05	15672.7	4890.49	16418	1.05
47	PV-BUS2-L	480	2.07	11532.5	3564.66	12070.8	1.05	15639.4	4834.1	16369.5	1.05
48	PV-G3	480	2.56	8751.58	3634.83	9476.4	1.08	10899.6	4526.99	11802.3	1.08

Short Circuit Analysis: IEEE 34 Bus: 50% PV Penetration Level; PV Unit at the End of Circuit:

Item No.	Bus Name	Pre-Flt. Voltage, in V	X/R	3 Phase Bus Fault Current, 0.5 Cycle				L-G Fault Current, 0.5 Cycle			
				Isym, in A	IDC, in A	Iasym, in A	MF	Isym, in A	IDC, in A	Iasym, in A	MF
1	2	3	4	5	6	7	8	9	10	11	12
2	101	24900	1.7	280.75	62.31	287.58	1.02	220.11	48.85	225.46	1.02
3	111	24900	1.7	280.75	62.31	287.58	1.02	220.11	48.85	225.46	1.02
4	3	69000	20	836.74	1011.32	1312.59	1.57	836.74	1011.32	1312.59	1.57
5	800	24900	9.33	549.09	554.56	780.41	1.42	596.06	602	847.16	1.42
6	802	24900	8.03	539.55	515.97	746.55	1.38	575.77	550.6	796.66	1.38
7	806	24900	7.36	533.25	492.07	725.6	1.36	562.82	519.36	765.83	1.36
8	808	24900	3.21	431.5	229.12	488.56	1.13	392.01	208.15	443.84	1.13
9	810	24900	3.11	419.18	215.86	471.5	1.12	372.85	192	419.38	1.12
10	812	24900	2.19	346.58	116.73	365.71	1.06	286.73	96.57	302.56	1.06
11	814	24900	1.84	297.79	76.52	307.46	1.03	235.77	60.58	243.43	1.03
12	816	24900	1.84	297.74	76.49	307.41	1.03	235.73	60.56	243.38	1.03
13	818	24900	1.8	294.1	72.32	302.86	1.03	232.62	57.2	239.55	1.03
14	820	24900	1.13	213.31	18.57	214.11	1.00	167.52	14.58	168.15	1.00
15	822	24900	1.04	196.74	13.47	197.2	1.00	154.7	10.59	155.06	1.00
16	824	24900	1.7	281.03	62.48	287.89	1.02	220.35	48.99	225.73	1.02
17	826	24900	1.63	275.14	56.87	280.96	1.02	215.52	44.55	220.08	1.02
18	828	24900	1.7	281	62.46	287.86	1.02	220.33	48.97	225.7	1.02
19	830	24900	1.7	280.97	62.44	287.83	1.02	220.3	48.96	225.68	1.02

20	830-L	24900	1.7	280.97	62.44	287.83	1.02	220.3	48.96	225.68	1.02
21	832	24900	1.7	280.89	62.4	287.74	1.02	220.23	48.92	225.6	1.02
22	834	24900	1.7	280.83	62.36	287.68	1.02	220.18	48.89	225.54	1.02
23	836	24900	1.7	280.78	62.33	287.61	1.02	220.13	48.87	225.49	1.02
24	838	24900	1.7	280.72	62.3	287.55	1.02	220.08	48.84	225.44	1.02
25	840-L	24900	1.7	280.75	62.31	287.58	1.02	220.11	48.85	225.46	1.02
26	842	24900	1.7	280.81	62.35	287.64	1.02	220.16	48.88	225.52	1.02
27	844	24900	1.7	280.78	62.33	287.61	1.02	220.13	48.87	225.49	1.02

Item No.	Bus Name	Pre-Flt. Voltage, in V	X/R	3 Phase Bus Fault Current, 0.5 Cycle				L-G Fault Current, 0.5 Cycle			
				Isym, in A	IDC, in A	Iasym, in A	MF	Isym, in A	IDC, in A	Iasym, in A	MF
1	2	3	4	5	6	7	8	9	10	11	12
29	846	24900	1.7	280.75	62.31	287.58	1.02	220.11	48.85	225.46	1.02
30	848	24900	1.7	280.72	62.3	287.55	1.02	220.08	48.84	225.44	1.02
31	848-L	24900	1.7	280.72	62.3	287.55	1.02	220.08	48.84	225.44	1.02
32	850	24900	1.84	297.77	76.51	307.45	1.03	235.76	60.58	243.41	1.03
33	852	24900	1.7	280.92	62.41	287.77	1.02	220.25	48.93	225.62	1.02
34	854	24900	1.7	280.95	62.43	287.8	1.02	220.28	48.95	225.65	1.02
35	856	24900	1.7	280.92	62.41	287.77	1.02	220.25	48.93	225.62	1.02
36	858	24900	1.7	280.86	62.38	287.71	1.02	220.2	48.91	225.57	1.02
37	860	24900	1.7	280.81	62.35	287.64	1.02	220.16	48.88	225.52	1.02
38	860-L	24900	1.7	280.81	62.35	287.64	1.02	220.16	48.88	225.52	1.02

39	862	24900	1.7	280.75	62.31	287.58	1.02	220.11	48.85	225.46	1.02
40	864	24900	1.7	280.83	62.36	287.68	1.02	220.18	48.89	225.54	1.02
41	888	4160	1.91	805.21	220.08	834.74	1.04	957.9	261.81	993.03	1.04
42	890	4160	1.91	803.87	219.06	833.18	1.04	955.12	260.28	989.95	1.04
43	890-L	4160	1.91	803.83	219.04	833.14	1.04	955.04	260.25	989.86	1.04
44	PV-BUS1	480	4.39	10705	7406.19	13017.2	1.22	12795	8852.21	15558.8	1.22
45	PV-BUS1-L	480	4.34	10694.5	7336.87	12969.3	1.21	12780.7	8768.12	15499.3	1.21
46	PV-BUS2	480	2.08	11551.4	3604.48	12100.7	1.05	15672.7	4890.49	16418	1.05
47	PV-BUS2-L	480	2.07	11532.5	3564.66	12070.8	1.05	15639.4	4834.1	16369.5	1.05
48	PV-G3	480	2.56	8751.58	3634.83	9476.4	1.08	10899.6	4526.99	11802.3	1.08

A.3. IEEE 34 Bus system – Reliability Analysis*:* PV Unit Close to Substation

```
Project No. :                                    Date & Time : 03/07/11 10:07:37 AM
Project Name:                                    Title       :
Drawing No. :                                    Company     :
Revision No.:                                    Engineer    :
Jobfile Name: IEEE_34_Node_Test_Feeder           Check by    :
Scenario    : 12H                                Date        :
```

System Information

==========

Base Power	=	100000.00	(kva)
Frequency	=	60	(Hz)
MaxIterations	=	1000	
Error Tolerance	=	10.000	(kva), 0.0100 (%)
# of Active Buses	=	50	
# of Swing Buses	=	1	
# of Generators	=	1	
# of Lines/Breakers	=	41	
# of Transformers	=	5	
# of Loads	=	8	
# of Shunts	=	0	

Generator outages considered	=	upto 3
Branch outages considered	=	upto 3
Combine generator & branch outages	=	Yes

Abbreviations

==========

2-W xfmr = 2-winding transformer	FeederM = Feeder in Magnetic Conduit
3-W xfmr = 3-winding transformer	occ/yr = Occurrences per year
Autoxfmr = Autotransformer	IEAR = Interrupted Energy Assessment Rate
curt = Curtailment or curtailed	PhS xfmr = Phase-Shift Transformer

f./y = Failures per year SeriesC = Series Capacitor

Generator Reliability Input Information

Generator Name	Pmax (MW)	Qmax (MVAR)	Qmin (MVAR)	Failure Rate (f./y)	Repair Time (hours)	Priority 1 to 99	Consider Reliability (Yes/No)
3	200.000	0.000	0.000	0.100000	20.0	1	Yes
PV-G1	0.250	0.000	-0.000	0.100000	10.0	1	Yes

Branch Reliability Input Information

==========

Branch Name	Type	Carrying Capacity (MVA)	Failure Rate (f./y)	Repair Time (hours)	Consider Reliability (Yes/No)
10	Feeder	10.247	0.500000	10.0	Yes
11	Feeder	9.678	0.330000	8.0	Yes
12	Feeder	6.831	0.330000	10.0	Yes
13	Feeder	5.313	0.230000	0.0	Yes
14	Feeder	12.904	0.330000	8.0	Yes
15	Feeder	9.678	0.330000	10.0	Yes
16	Feeder	9.678	0.330000	15.0	Yes
17	Feeder	9.678	0.200000	8.0	Yes
18	Feeder	1.617	0.300000	0.0	Yes
19	Feeder	9.678	0.330000	20.0	Yes
20	Feeder	9.678	0.330000	10.0	Yes
21	Feeder	9.678	0.330000	15.0	Yes
22	Feeder	5.313	0.150000	0.0	Yes
23	Feeder	5.313	0.330000	0.0	Yes
24	Feeder	9.678	0.340000	15.0	Yes
26	Feeder	5.313	0.500000	0.0	Yes
32	Feeder	9.678	0.450000	12.0	Yes
33	Feeder	9.678	0.300000	10.0	No
34	Feeder	9.678	0.000000	0.0	No
35	Feeder	9.678	0.000000	0.0	No
36	Feeder	9.678	0.000000	0.0	No
37	Feeder	9.678	0.000000	0.0	No
38	Feeder	9.678	0.000000	0.0	No
39	Feeder	9.678	0.300000	10.0	Yes
40	Feeder	9.678	0.350000	12.0	No
41	Feeder	9.678	0.330000	12.0	Yes
42	Feeder	9.678	0.220000	15.0	Yes
5	Feeder	8.712	0.100000	5.0	Yes
6	Feeder	8.712	0.100000	5.0	Yes
7	Feeder	8.729	0.330000	10.0	Yes
74	Feeder	9.678	0.100000	10.0	Yes

75	Feeder	1.617	0.100000	10.0	No
76	Feeder	9.678	0.000000	0.0	No
77	Feeder	9.678	0.330000	10.0	No
78	Feeder	9.678	0.220000	18.0	Yes
79	Feeder	9.678	0.330000	12.0	Yes
8	Feeder	8.626	0.450000	8.0	Yes
88	Breaker	0.499	0.000000	0.0	No
89	Breaker	0.499	0.000000	0.0	No
9	Feeder	8.729	0.350000	12.0	Yes
93	Breaker	0.499	0.100000	8.0	No
103	2-W xfmr	1.050	0.000000	0.0	No
PV-T1	2-W xfmr	1.050	0.230000	15.0	Yes
PV-T2	2-W xfmr	1.050	0.100000	15.0	Yes
SUBST A	2-W xfmr	1.050	0.006000	356.1	Yes
XFM-1	2-W xfmr	1.050	0.100000	15.0	Yes

Bus Availability Checking

==========

Bus Name	Type	Required Availability (%)	Calculated Availability (%)	Pass/Fail
830-L	P_Load	99.00000	100.00000	Pass
840-L	P_Load	100.00000	100.00000	Fail
844-L	P_Load	98.00000	99.60301	Pass
848-L	P_Load	98.00000	99.95516	Pass
860-L	P_Load	100.00000	99.98867	Fail
890-L	P_Load	98.00000	99.75684	Pass
PV-BUS1-L	P_Load	99.00000	99.99964	Pass
PV-BUS2-L	P_Load	99.00000	99.73858	Pass

System Summary - Expected Indices

==========

		Power supply disturbances			
		All Causes &Problems Load Level	Load Interruption Events	Voltage violations NO MVAR	Voltage Violations WITH MVAR
Probability		0.004714	0.004714	0.000000	0.000000
Frequency	(occ/yr)	3.488034	3.488034	0.000000	0.000000
Duration	(hrs/yr)	41.290508	41.290508	0.000000	0.000000

Power system interruption index = 1.525273 (Mw/Mw-yr)

Power system average MW interruption index = 0.327966 (Mw/curt.)

Power system energy interruption index = 16.990925 (Mwh/Mw-yr)

Modified power system energy interruption index = 0.001940

Severity index = 1019.455505 (Sys-Min)

System availability = 99.806038 (%)

Expected loss of load probability	=	0.004714	
Expected power not supplied	=	0.001455	(Mw/occ)
Expected energy not supplied	=	0.017390	(Mwh/occ)

Expected reactive power injection	=	0.00	(Mvar/yr)
Average reactive power injection	=	0.00	(Mvar/viol)

Expected outage cost	=	34.07	(K$/yr)
Average outage cost	=	9.77	(K$/curt.)

==========

Power supply disturbances

	All Causes &Problems Load Level	Load Interruption Events	Voltage violations NO MVAR	Voltage Violations WITH MVAR
Probability	0.004714	0.004714	0.000000	0.000000
Frequency (occ/yr)	3.488034	3.488034	0.000000	0.000000
Duration (hrs/yr)	41.290508	41.290508	0.000000	0.000000

Power system interruption index	=	1.525273	(Mw/Mw-yr)
Power system average MW interruption index	=	0.327966	(Mw/curt.)
Power system energy interruption index	=	16.990925	(Mwh/Mw-yr)
Modified power system energy interruption index	=	0.001940	
Severity index	=	1019.455505	(Sys-Min)
System availability	=	99.806038	(%)
Expected loss of load probability	=	0.004714	
Expected power not supplied	=	0.001455	(Mw/occ)
Expected energy not supplied	=	0.017390	(Mwh/occ)
Expected reactive power injection	=	0.00	(Mvar/yr)
Average reactive power injection	=	0.00	(Mvar/viol)
Expected outage cost	=	34.07	(K$/yr)
Average outage cost	=	9.77	(K$/curt.)

Bus Summary - Expected Indices

==========

Bus	Prob	Freq (occ/yr)	Load curt (MW/yr)	Energy curt (MWh/yr)	Duration (hrs/yr)	Availability (%)
844-L	.003970	2.852486	0.3992	4.868	34.776	99.603012
PV-BUS2-L	.002614	2.189125	0.4376	4.578	22.901	99.738579
890-L	.002432	1.986310	0.2978	3.194	21.300	99.756844
848-L	.000448	0.332935	0.0067	0.079	3.928	99.955162
860-L	.000113	0.100691	0.0020	0.020	0.992	99.988670
PV-BUS1-L	.000004	0.004843	0.0007	0.004	0.031	99.999641

Bus Summary - Maximum Load Curtailed

BUS	Load curt (Mw)	PROB	Freq (occ/yr)	Load level (%)
PV-BUS2-L	0.20	.000564	0.499623	100.0
PV-BUS1-L	0.20	.000000	0.000113	100.0
890-L	0.15	.000564	0.499623	100.0
844-L	0.14	.000564	0.499623	100.0
848-L	0.02	.000447	0.330556	100.0
860-L	0.02	.000113	0.099970	100.0

Bus Summary - Maximum Energy Curtailed

==========

Bus	Energy Curt (Mwh)	PROB	Freq (occ/yr)	Load level (%)
PV-BUS2-L	2.95	.000558	0.331668	100.0
844-L	2.74	.000745	0.333521	100.0
PV-BUS1-L	2.38	.000000	0.000086	100.0
890-L	2.21	.000558	0.331668	100.0
848-L	0.24	.000447	0.330556	100.0
860-L	0.20	.000113	0.099970	100.0

IEEE 34 Bus – Reliability Analysis: PV Unit at the End of Circuit:

```
Project No. :                                    Date & Time : 03/07/11 10:14:29 AM
Project Name:                                    Title       :
Drawing No. :                                    Company     :
Revision No.:                                    Engineer    :
Jobfile Name: IEEE_34_Node_Test_Feeder           Check by    :
Scenario    : 12H                                Date        :
```

System Information

==========

```
Base Power              =    100000.00 (kva)
Frequency               =           60 (Hz)
MaxIterations           =         1000
Error Tolerance         =       10.000 (kva), 0.0100 (%)
# of Active Buses       =           50
# of Swing Buses        =            1
# of Generators         =            1
# of Lines/Breakers     =           41
# of Transformers       =            5
# of Loads               =            8
# of Shunts              =            0

Generator outages considered          =      upto  3
Branch outages considered             =      upto  3
Combine generator & branch outages    =          Yes
```

Abbreviations

==========

```
2-W xfmr = 2-winding transformer        FeederM  = Feeder in Magnetic Conduit
3-W xfmr = 3-winding transformer        occ/yr   = Occurrences per year
Autoxfmr = Autotransformer              IEAR     = Interrupted Energy Assessment Rate
```

curt = Curtailment or curtailed PhS xfmr = Phase-Shift Transformer

f./y = Failures per year SeriesC = Series Capacitor

Generator Reliability Input Information

==========

Generator Name	Pmax (MW)	Qmax (MVAR)	Qmin (MVAR)	Failure Rate (f./y)	Repair Time (hours)	Priority 1 to 99	Consider Reliability (Yes/No)
3	200.000	0.000	0.000	0.100000	20.0	1	Yes
PV-G3	0.250	0.000	-0.000	0.100000	10.0	1	No

Branch Reliability Input Information

==========

Branch Name	Type	Carrying Capacity (MVA)	Failure Rate (f./y)	Repair Time (hours)	Consider Reliability (Yes/No)
10	Feeder	10.247	0.500000	10.0	Yes
104		14.341	0.000000	0.0	No
11	Feeder	9.678	0.330000	8.0	Yes
12	Feeder	6.831	0.330000	10.0	Yes
13	Feeder	5.313	0.230000	0.0	Yes
14	Feeder	12.904	0.330000	8.0	Yes
15	Feeder	9.678	0.330000	10.0	Yes
16	Feeder	9.678	0.330000	15.0	Yes
17	Feeder	9.678	0.200000	8.0	Yes
18	Feeder	1.617	0.300000	0.0	Yes
19	Feeder	9.678	0.330000	20.0	Yes
20	Feeder	9.678	0.330000	10.0	Yes
21	Feeder	9.678	0.330000	15.0	Yes
22	Feeder	5.313	0.150000	0.0	Yes
23	Feeder	5.313	0.330000	0.0	Yes
24	Feeder	9.678	0.340000	15.0	Yes
26	Feeder	5.313	0.500000	0.0	Yes
32	Feeder	9.678	0.450000	12.0	Yes
33	Feeder	9.678	0.300000	10.0	No
34	Feeder	9.678	0.000000	0.0	No
35	Feeder	9.678	0.000000	0.0	No
36	Feeder	9.678	0.000000	0.0	No
37	Feeder	9.678	0.000000	0.0	No
38	Feeder	9.678	0.000000	0.0	No
39	Feeder	9.678	0.300000	10.0	Yes
40	Feeder	9.678	0.350000	12.0	No
41	Feeder	9.678	0.330000	12.0	Yes
42	Feeder	9.678	0.220000	15.0	Yes
5	Feeder	8.712	0.100000	5.0	Yes
6	Feeder	8.712	0.100000	5.0	Yes
7	Feeder	8.729	0.330000	10.0	Yes

74	Feeder	9.678	0.100000	10.0	Yes
75	Feeder	1.617	0.100000	10.0	No
76	Feeder	9.678	0.000000	0.0	No
77	Feeder	9.678	0.330000	10.0	No
78	Feeder	9.678	0.220000	18.0	Yes
79	Feeder	9.678	0.330000	12.0	Yes
8	Feeder	8.626	0.450000	8.0	Yes
89	Breaker	0.499	0.000000	0.0	No
9	Feeder	8.729	0.350000	12.0	Yes
93	Breaker	0.499	0.100000	8.0	No
103	2-W xfmr	1.050	0.000000	0.0	No
PV-T1	2-W xfmr	1.050	0.230000	15.0	Yes
PV-T2	2-W xfmr	1.050	0.100000	15.0	Yes
SUBST A	2-W xfmr	1.050	0.006000	356.1	Yes
XFM-1	2-W xfmr	1.050	0.100000	15.0	Yes

Bus Availability Checking

==========

Bus Name	Type	Required Availability (%)	Calculated Availability (%)	Pass/Fail
830-L	P_Load	99.00000	100.00000	Pass
840-L	P_Load	100.00000	100.00000	Fail
844-L	P_Load	98.00000	99.60311	Pass
848-L	P_Load	98.00000	99.95515	Pass
860-L	P_Load	100.00000	99.98867	Fail
890-L	P_Load	98.00000	99.75682	Pass
PV-BUS1-L	P_Load	99.00000	99.99900	Pass
PV-BUS2-L	P_Load	99.00000	99.73868	Pass

System Summary - Expected Indices

==========

		Power supply disturbances			
		All Causes &Problems Load Level	Load Interruption Events	Voltage violations NO MVAR	Voltage Violations WITH MVAR
Probability		0.004714	0.004714	0.000000	0.000000
Frequency	(occ/yr)	3.488310	3.488310	0.000000	0.000000
Duration	(hrs/yr)	41.294239	41.294239	0.000000	0.000000

Power system interruption index = 1.528006 (Mw/Mw-yr)

Power system average MW interruption index = 0.328527 (Mw/curt.)

Power system energy interruption index = 17.009100 (Mwh/Mw-yr)

Modified power system energy interruption index = 0.001942

Severity index = 1020.546021 (Sys-Min)

System availability = 99.805832 (%)

```
Expected loss of load probability          =      0.004714
Expected power not supplied                =      0.001456 (Mw/occ)
Expected energy not supplied               =      0.017402 (Mwh/occ)


Expected reactive power injection          =          0.00 (Mvar/yr)
Average reactive power injection           =          0.00 (Mvar/viol)

Expected outage cost                       =         34.12 (K$/yr)
Average outage cost                        =          9.78 (K$/curt.)
```

Bus Summary - Expected Indices

==========

Bus	Prob	Freq (occ/yr)	Load curt (MW/yr)	Energy curt (MWh/yr)	Duration (hrs/yr)	Availability (%)
844-L	.003969	2.850754	0.3991	4.867	34.768	99.603111
PV-BUS2-L	.002613	2.187207	0.4374	4.578	22.892	99.738678
890-L	.002432	1.986049	0.2979	3.195	21.302	99.756821
848-L	.000448	0.333101	0.0067	0.079	3.928	99.955154
860-L	.000113	0.100736	0.0020	0.020	0.992	99.988670
PV-BUS1-L	.000010	0.014528	0.0029	0.018	0.088	99.999001

Bus Summary - Maximum Load Curtailed

==========

BUS	Load curt (Mw)	PROB	Freq (occ/yr)	Load level (%)
PV-BUS2-L	0.20	.000564	0.499623	100.0
PV-BUS1-L	0.20	.000000	0.000374	100.0
890-L	0.15	.000564	0.499623	100.0
844-L	0.14	.000564	0.499623	100.0
848-L	0.02	.000447	0.330556	100.0
860-L	0.02	.000113	0.099970	100.0

Bus Summary - Maximum Energy Curtailed

==========

Bus	Energy Curt (Mwh)	PROB	Freq (occ/yr)	Load level (%)
PV-BUS1-L	3.71	.000000	0.000086	100.0

PV-BUS2-L	3.71	.000000	0.000086	100.0
890-L	2.78	.000000	0.000086	100.0
844-L	2.74	.000745	0.333521	100.0
848-L	0.24	.000447	0.330556	100.0
860-L	0.20	.000113	0.099970	100.0

A.4. IEEE 34 Bus system – Security Analysis: PV Unit Close to Substation

Power Analytics Voltage Stability & Contingency Analysis Program V2.20.00

==========

Project No. :
Page : 1
Project Name:
Date : 03/07/2011
Title :
Time : 10:19:27
Drawing No. :
Company :
Revision No.:
Engineer :
Jobfile Name: IEEE_34_Node_Test_Feeder
Check by :
Scenario : 12H
Date :

Contingency Analysis Report

==========

Events for Contingency: Base Case

==========

Branch Overload Violation (100.% limit) for: Base Case

==========

From Bus Name	To Bus Name	Circuit #	Ampacity	Loading(%)

PV-BUS1	PV-G1	1	600.0	304.9

Transformer Overload Violation (100.% limit) for: Base Case

From Bus Name	To Bus Name	Circuit #	Capacity	Loading(%)
810	PV-BUS1	1	1000.0	131.5

Events for Contingency: Gen Outage: PV-G1

==========

Outage of generator at bus PV-G1

Bus Voltage Violation (normal limits) for: Gen Outage: PV-G1

==========

Bus Name	System kV	Vmin(%)	Vmax(%)	Voltage(%)
101	24.9000	95.0	105.0	94.8
824	24.9000	95.0	105.0	94.8
826	24.9000	95.0	105.0	94.8
828	24.9000	95.0	105.0	94.8
830	24.9000	95.0	105.0	94.8
830-L	24.9000	95.0	105.0	94.8
832	24.9000	95.0	105.0	94.8
834	24.9000	95.0	105.0	94.8
836	24.9000	95.0	105.0	94.8
838	24.9000	95.0	105.0	94.8
840-L	24.9000	95.0	105.0	94.8
842	24.9000	95.0	105.0	94.8
844	24.9000	95.0	105.0	94.8
844-L	24.9000	95.0	105.0	94.8
846	24.9000	95.0	105.0	94.8
848	24.9000	95.0	105.0	94.8
848-L	24.9000	95.0	105.0	94.8
852	24.9000	95.0	105.0	94.8
854	24.9000	95.0	105.0	94.8
856	24.9000	95.0	105.0	94.8
858	24.9000	95.0	105.0	94.8
860	24.9000	95.0	105.0	94.8
860-L	24.9000	95.0	105.0	94.8
862	24.9000	95.0	105.0	94.8
864	24.9000	95.0	105.0	94.8
888	4.1600	95.0	105.0	93.5
890	4.1600	95.0	105.0	93.5

890-L	4.1600	95.0	105.0	93.5
PV-BUS2	0.4800	95.0	105.0	94.5
PV-BUS2-L	0.4800	95.0	105.0	94.5

Ranking of the Contingencies

==========

Contingency Name	Severity %
Base Case	100.00
Gen Outage: PV-G1	0.16

IEEE 34 Bus system – Security Analysis: PV Unit at the End of Circuit

Power Analytics Voltage Stability & Contingency Analysis Program V2.20.00

==========

Project No. : Page : 1

Project Name: Date : 03/07/2011

Title :

Drawing No. :

Revision No.:

Jobfile Name: IEEE_34_Node_Test_Feeder

Scenario : 12H

Time : 12:08:56

Company :

Engineer :

Check by :

Date :

Contingency Analysis Report

==========

Events for Contingency: Base Case

==========

Transformer Overload Violation (100.% limit) for: Base Case

==========

From Bus Name	To Bus Name	Circuit #	Capacity	Loading(%)
111	PV-G3	1	1000.0	150.7

Events for Contingency: Gen Outage: PV-G3

Outage of generator at bus PV-G3

Bus Voltage Violation (normal limits) for: Gen Outage: PV-G3

Bus Name	System kV	Vmin(%)	Vmax(%)	Voltage(%)
PV-G3	0.4800	95.0	105.0	94.8
101	24.9000	95.0	105.0	94.8
111	24.9000	95.0	105.0	94.8
824	24.9000	95.0	105.0	94.8
826	24.9000	95.0	105.0	94.8
828	24.9000	95.0	105.0	94.8
830	24.9000	95.0	105.0	94.8
830-L	24.9000	95.0	105.0	94.8
832	24.9000	95.0	105.0	94.8
834	24.9000	95.0	105.0	94.8
836	24.9000	95.0	105.0	94.8
838	24.9000	95.0	105.0	94.8
840-L	24.9000	95.0	105.0	94.8
842	24.9000	95.0	105.0	94.8
844	24.9000	95.0	105.0	94.8
844-L	24.9000	95.0	105.0	94.8
846	24.9000	95.0	105.0	94.8
848	24.9000	95.0	105.0	94.8
848-L	24.9000	95.0	105.0	94.8
852	24.9000	95.0	105.0	94.8
854	24.9000	95.0	105.0	94.8
856	24.9000	95.0	105.0	94.8
858	24.9000	95.0	105.0	94.8
860	24.9000	95.0	105.0	94.8
860-L	24.9000	95.0	105.0	94.8
862	24.9000	95.0	105.0	94.8
864	24.9000	95.0	105.0	94.8
888	4.1600	95.0	105.0	93.5
890	4.1600	95.0	105.0	93.5

890-L	4.1600	95.0	105.0	93.5
PV-BUS2	0.4800	95.0	105.0	94.5
PV-BUS2-L	0.4800	95.0	105.0	94.5

Ranking of the Contingencies

==========

Contingency Name	Severity %
Base Case	100.00
Gen Outage: PV-G3	0.35

APPENDIX B:
Modeling of PV system in the Power Analytics' Power System Analysis Software

As noted in the introduction, part of the work was to conduct an in-depth powerflow analysis as a basis for developing a valid model of a PV system. UCSD worked with partner Power Analytics (PA) to develop a model and conduct power system analyses namely steady-state Powerflow and Short Circuit, and Transient Stability. The approach was to conduct a literature survey to review the available PV models applicable to simulation of the steady state and transient behavior. The models reviewed include features such as primary source (solar irradiance), DC/DC, DC/AC, protections and controls. The developed model was then bench marked against available field tests or published work.

Also in this effort, PA developed a dynamic model of a PV system, including its protection and control using the's Universal Control Logic Modeling and Simulation (UCLMS) feature available in the PA Advanced transient stability program. UCLMS supports a fully graphical environment to assemble power system component models and control similar to MATLAB Simulink with major exception that the models developed can be communicating directly with Power Analytics's Transient Stability Program through interface variables. The developed models don't require recompilation and re-linking of object modules, thereby greatly minimizing the development and testing effort.

B.1. Power Electronic Interface Models

A typical structure of a power source with a converter interface is shown in Figure B.1. The energy source may be a DC-power source by itself (e.g. BES, PV etc.) or an AC source, which is rectified into DC (a wind turbine, a micro-turbine etc.). In any case, the source itself may include other power electronics converters (AC/DC and DC/DC), in order to create and/or regulate the DC voltage or current.

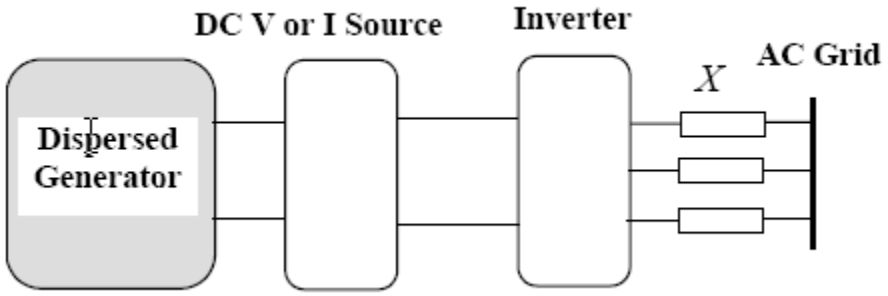

Figure B.1: Typical Power Electronic Interface to Grid

Although it is not possible to derive a general model, which would represent with sufficient accuracy the dynamics of all possible converter interfaces, some general principles and typical examples are presented. In the following section the modeling and control of the grid side converter is described.

In Figure B.2 the most commonly used scheme i.e., a *voltage source* DC/AC converter is illustrated. However, other types of converter interfaces (such as current source inverters or converter cascades used in the rotor

circuits of doubly fed induction generators) are also used in practice and require a different modeling approach, not covered in the following (PV is of primary concern).

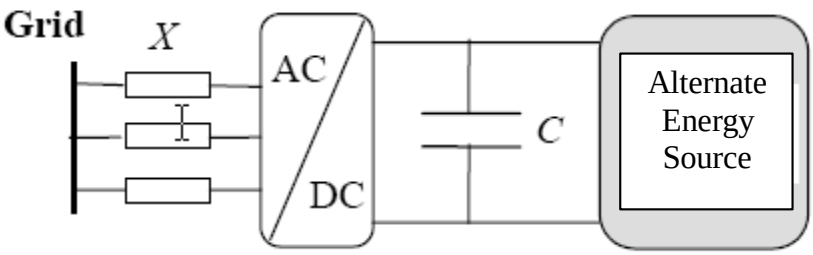

Figure B.2: Typical Converter Interface to Grid

First the operating and control principle of such a device is outlined and average value models are presented (i.e. non-fundamental frequency components are neglected), since they are simpler, more general and often be sufficient for examining the interaction between the dispersed generation and the power system.

In Fig. C.3, the fundamental frequency simplified diagrams are shown for the *voltage source* DC/AC converter. The following relations give the active and reactive power at the output:

$$P = \frac{V_i V_b}{X_f} \sin(\delta)$$

$$Q = \frac{V_i^2}{X_f} - \frac{V_i V_b}{X_f} \cos(\delta)$$

The active power is predominantly dependent on the power angle δ between the inverter and grid voltage phasors, while reactive power mainly determined by the inverter voltage magnitude V_i. The control of the active and reactive power flow to the grid is performed by the DC/AC converter. In the case of a *voltage source* inverter, the controlled variables are the frequency ω_i and the magnitude V_i of the fundamental component of its AC voltage, which is synthesized by properly switching on and off its valves (usually IGBTs). The fairly decoupled regulation of P and Q permits the implementation of the control principle schematically illustrated in Figure B.3. The active and reactive power regulation loops are independent, but not fully decoupled.

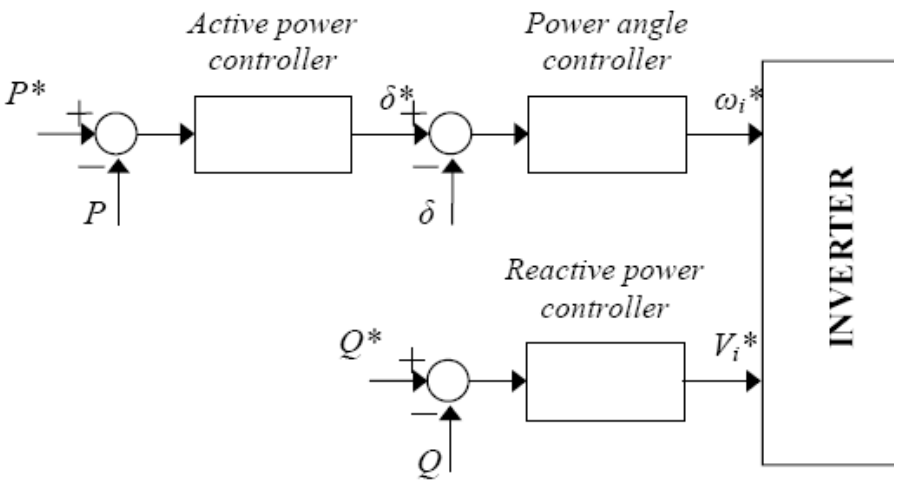

Figure B.3a: Active & Reactive Power Control for the Voltage Source Inverter

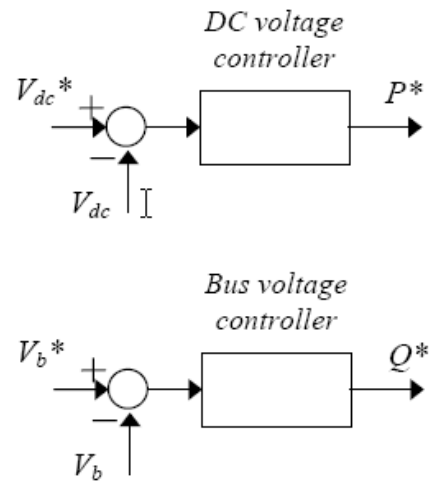

Figure C.3b: DC Voltage & AC Voltage Control

*P** and *Q** are the active and reactive powers order, whereas the actual *P* and *Q*, along with the power angle δ, are calculated from measurements of the phase voltages and currents. The determination of the *P** and *Q** reference values depends on the specific application and installation considered. It is common to practice to utilize *Q** in order to maintain constant power factor (normally unity i.e., *Q**=0). Alternatively, *Q** may be varied in order to control bus voltage at or near to the converter, provided that the current rating of the converter permits it.

Recently, with the advent of fast switching elements at high power levels, such as IGBTs, the current control principle is increasingly selected, among others due to its advantage in case of system disturbances, such as faults, voltage dips etc. If the DC/AC converter is current controlled, then the full decoupling of the active and reactive power can be easily achieved, employing the vector control principle, as shown in Figure B.4.

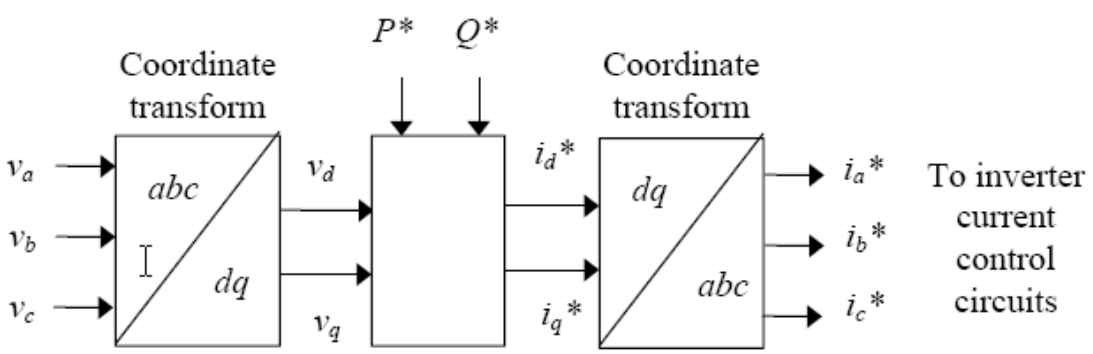

Figure B.4: Active and Reactive Power Regulation with a Current Controlled Converter

A more detailed implementation of this principle is illustrated in Figure B.5 and Figure B.6. In the block diagram of Figure B.5, the DC voltage error determines the active power order, *P*,* through a PI controller. From *P**, *Q**

and the measured terminal voltages, the desired phase currents are found, i_{a*}, i_{b*} and i_{c*}, which are the inputs to the hysteresis controllers. Outputs of the controllers are the gating signals to the inverter bridge switches. To overcome the limitations and drawbacks of the hysteresis scheme, such as the varying switching frequency, a triangle comparison PWM current controller may be adopted. This scheme is shown in Figure B.6, where the current reference determination portion of it has been omitted, being identical to that of Figure B.5.

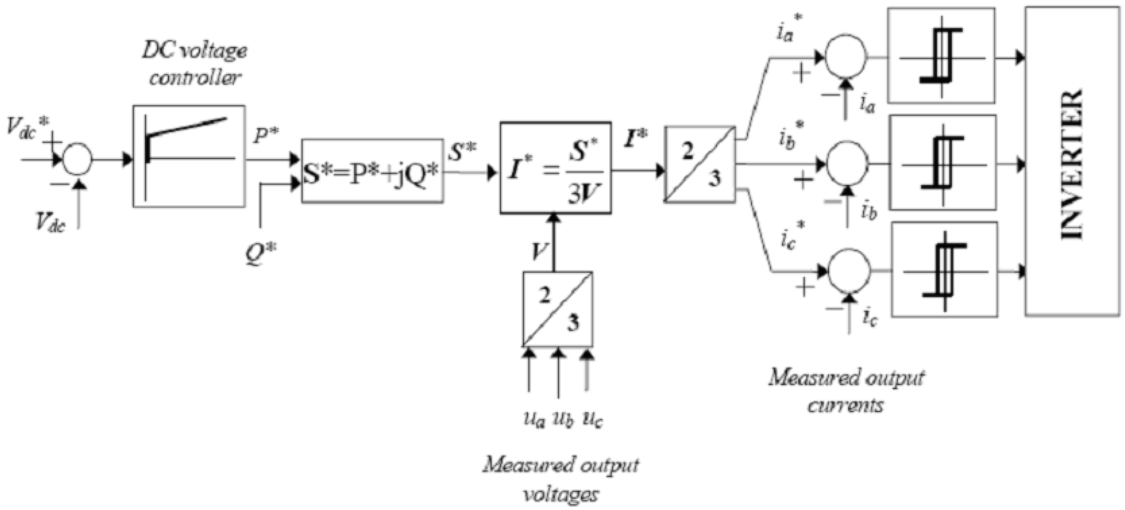

Figure B.5: Current Control Hysteresis PWM Schemes

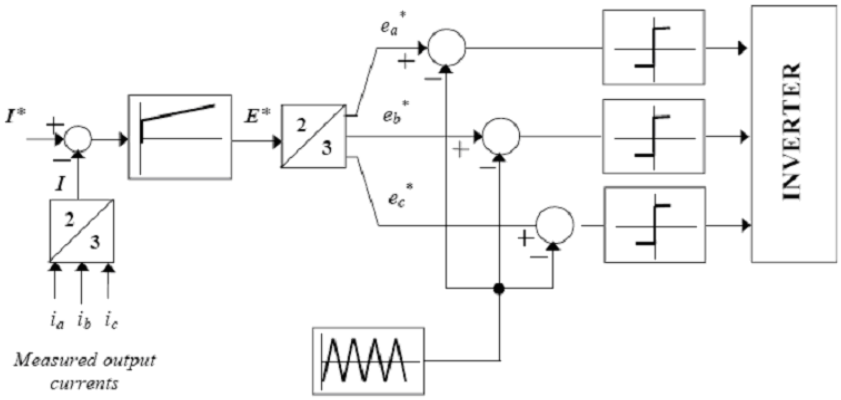

Figure B.6: Current Control Triangular Carrier PWM Schemes

When interfaced to the power system with a battery to supply the transient need of power, the details on the distributed source behaviour tend to lose importance when looking at the performance of the unit as seen from the point of connection to the system. In fact the inverter will be connected to the terminals of the battery, and will only see a relatively stiff DC voltage. The power source is no longer required to have a significantly speedy transient response, since its task will only be to keep the battery charged. The fact the system can be considered as an inverter connected to a battery is the simplification that makes the design and analysis of the power electronic interface less difficult. These details, along with the load sensitivities during island operation are only required to size the battery.

The most basic requirements for the inverter operations are the capability of delivering a preset amount of active power to the power system along with the ability to maintain the voltage at the point of connection with the AC system to a desired value.

B.2. Photovoltaic System Model

The typical structure of a system connected photovoltaic generator is shown in Figure B.7. Its main components are the PV array, the DC/DC, DC/AC converters and the associated (converter and overall system) controls. A storage device is absent in large grid-connected installations (except maybe for small critical loads).

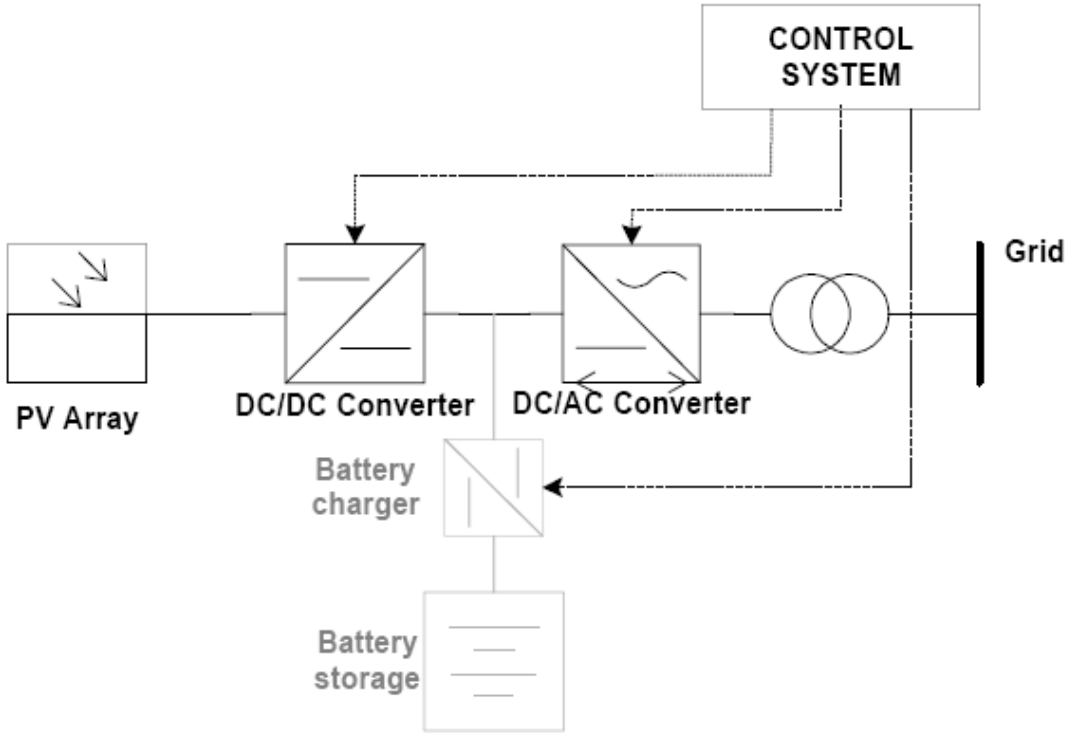

Figure B.7: Typical Structure of a Grid Connected PV Generator.

In Figure B. the electrical equivalent circuit of a PV cell is shown. Its main elements are the DC photocurrent I_L source and the shunt diode D. The series resistance R_s represents the internal losses due to the current flow, whereas the shunt resistance R_{sh} corresponds to the leakage current to the ground and it is normally ignored. In an ideal cell $R_s = R_{sh} = 0$, which is a common assumption. The equivalent circuit of a PV module, which consists of a combination of series and parallel-connected cells are the same.

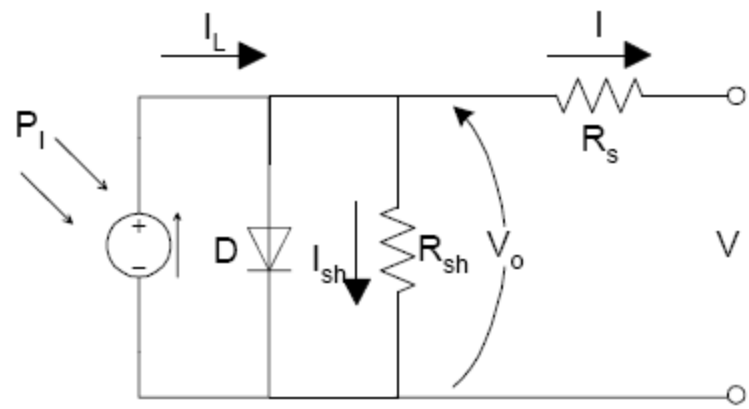

Figure B.8: PV Cell Equivalent Circuit.

The governing equations of the equivalent circuit of Figure B. are:

$$V = V_0 - R_s I$$

$$I = I_L - I_D(e^{\frac{qV_0}{AkT}} - 1) - I_{sh}$$

$$I_{sh} = \frac{V_0}{R_{sh}}$$

$$I_L = I_{sc1}(\frac{P_I}{1000})$$

Where V, I are the output voltage and current, q the electron charge ($1.6*10^{-19}$ Cb), k the Boltzmann constant ($1.38*10^{-23}$ J/K), T the temperature in K, A the quality factor (constant), I_D the reverse saturation current of the diode, I_L the photocurrent, dependent on P_I the insolation level in W/m^2, and I_{sc1} the short circuit current at 1000 W/m^2 solar radiation

Multiple PV modules are connected in series and in parallel to form the PV array. Similar equations hold for the whole array, provided that all modules are identical and subject to the same insolation. In Figure B. the V-I characteristics of a 250 kW array are shown at three solar radiation (P_I) levels. On the same diagram three constant power curves (red lines) have been drawn. It is clear that, for a given insolation, the array produces maximum power only when operating near the knee point of the corresponding V-I curve (maximum power point). The task of tracking the maximum power point (MPPT) is usually performed by a DC/DC converter at the output of the array, which regulates the voltage to the desired value. Since no moving parts are employed in this process, the response of the MPPT can be considered instantaneous for system studies.

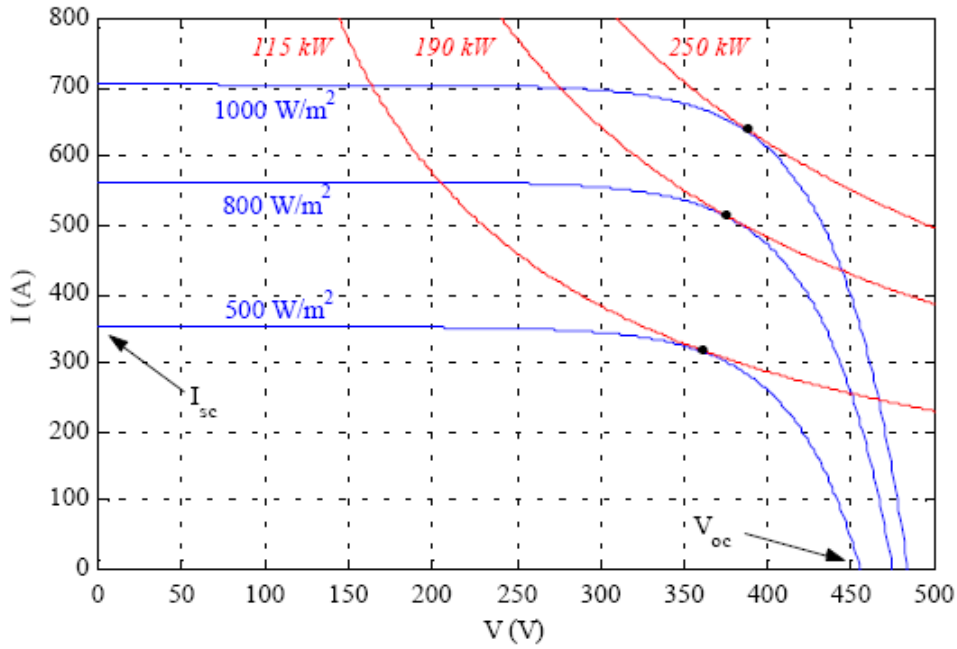

Figure B.9: Typical PV array V-I characteristics.

A device that may affect the response of the PV generator output in case of solar radiation changes is the sun-tracking system of the panels, which adjusts the orientation of the panels with respect to the sun, a task performed by the use of properly controlled servomotors. However, these are relatively slow acting devices and may be ignored in transient stability studies.

As discussed, the remaining of the system components (dc bus, inverter and grid-connection devices) are of similar nature and characteristics as for other dispersed generators (e.g. variable speed wind turbines). Consequently, the remaining system components do not require new modeling techniques.

B.3. Modeling of Xantrex GT250/500PV Inverters

In this section modeling of two of the Xantrex PV inverters, namely, GT250 and GT500 will be discussed. The objective is to develop models that are most appropriate for power system simulation including power flow and time domain simulation mainly transient stability (the time frame of interest normally ranges from a few cycles to several seconds). These models have been implemented in the Power Analytics's Advanced Powerflow, Short Circuit, and Transient Stability analysis software package (DesignBase). Xantrex inverters are in general imbedded with an array of photovoltaic, transformer, and other components necessary to convert solar irradiance suitable for delivery to transmission or distribution system voltages. The modular characteristics of PV generation allow a common inverter model to be used which can be scaled to a desirable capacity rating for power system integration studies.

Xantrex GT250 and GT500 PV modules are series connected to create DC operating voltages in the range of 300 to 600 volts. The currents from these series connected circuits are then paralleled to create DC sources with power capacities of several hundred kilowatts. The Xantrex GT250/500 are IGBT type inverters that convert the DC to AC power at three phase 480 volts AC voltages. In a PV power plant that is connected to a distribution system, AC voltage normally converted to higher voltages through step-up transformer which provides voltage transformation for integration of the inverter and its associated PV with the medium voltage 15 kV-35 kV. For transmission interconnected PV plants, another transformation to even higher voltage would occur at a collection substation similar to a wind farm power plant.

The PV units that serve as input sources to the inverter consist of solid-state semiconductor cells that produce direct current, in an almost instantaneous manner, as a function of the solar radiation and their operating voltage to which they are applied. Therefore, the inverter characteristics and controls dominate the behaviour of the PV plant and its interaction with power system. The Xantrex's GT series inverters are a high frequency, PMW (Pulse Width Modulated), current-regulated inverters. They operate to regulate their respective AC output currents in response to a current command through high carrier frequency ~10 kHz PWM. This provides a fairly pure sinusoidal output current waveform that is both synchronized to the grid voltage waveform (i.e., it follows the grid frequency) and phase locked to the grid voltage (i.e., unity power factor operation). The Xantrex GT250 and GT500 PV models for implementation in the Powerflow, Short Circuit, and Transient Stability Analysis are described below.

3.1. Power Flow and Short Circuit Modeling of Xantrex GT250/500 PV Inverters

PV power generation using Xantrex inverters can be modeled (similar to a classical synchronous generator) as a generator connected to power system for powerflow modeling purposes. The voltage rating of the generator for the Xantrex GT250 and GT500 PV is 480 volts. The PV plant power rating (MVA) is equal to an integral multiple of the individual inverter MVA rating. However, the active power output for the powerflow simulation (Pgen) can be anywhere in the range of zero to rated MVA depending on the available solar irradiance for the time of interest. As the inverters are configured for fixed unity power factor operation in the Xantrex GT250 and GT500 PV, the reactive power output and corresponding reactive power capability limits should all be set to zero.

For the Xantrex GT250 and GT500 PV there is no contribution from PV power plant (inverters) to short circuit. For this modeling work, the generators were represented by sub-transient (X"d) and transient (X'd) reactances of very high magnitude (e.g. 100 per unit = 100 p.u.). Since the generator may represent an aggregate PV, the reactance used would be the same value if all the generators have the same characteristics on a plant base (sum of the MVAs of the individual inverters).

3.2. Transient Stability Dynamic Modeling of Xantrex GT250/500 PV Inverters

The Xantrex GT250/500 PV inverter dynamic model has been implemented as a user-defined model in the Power Analytics Advanced Transient Stability Program (ATSP). The ATSP model consists of a reduced order representation of the inverter controls. An overview of the control block diagram of the model is shown below:

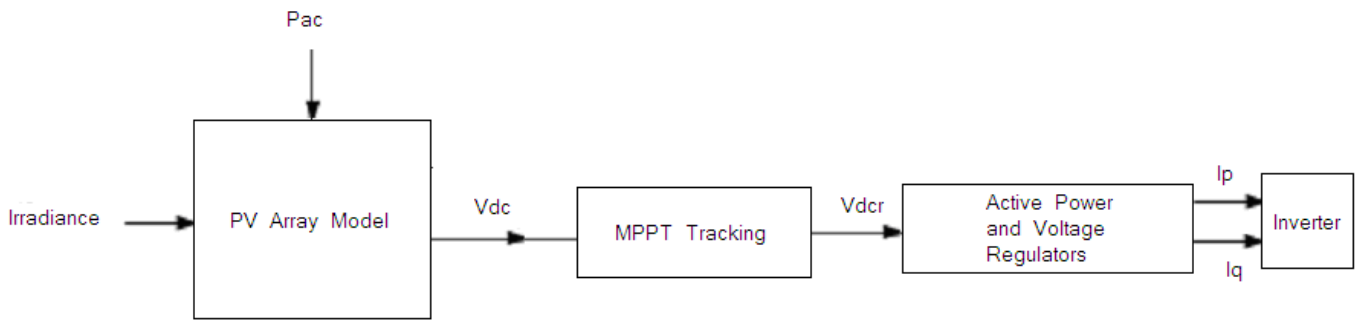

Figure B.2: Overview of the Control Block Diagram of the Xantrex GT250/500 PV Inverters

The above control system consists of PV array model, Maximum Power Point Tracking system, voltage and active power controllers, and inverter. The over/under voltage and frequency protections are normally imbedded in the inverter model and will be discussed later.

The irradiance model for the implementation in the transient stability type program is shown in Figure C.3. The inputs to this model are solar irradiance and active power output. The DC voltage is the only output. In this figure the DC capacitor is also included. The DC voltage output of the PV array is then fed into the MPPT model to calculate the optimum DC voltage reference (Vdcr).

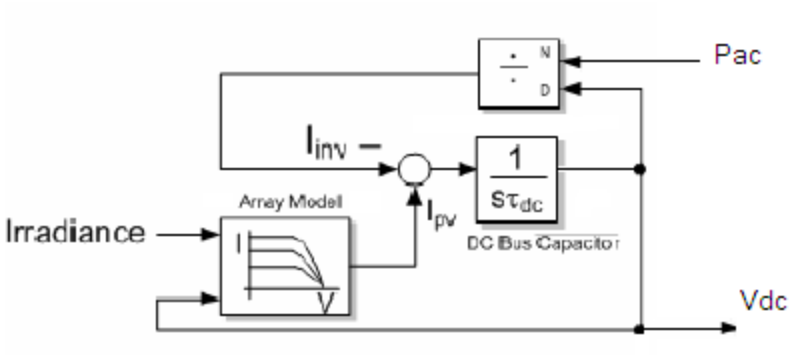

Figure C.3: PV Array Model for the Xantrex GT250/500 PV Inverters

The voltage and active power regulators for the Xantrex GT250/500 PV Inverters are shown below.

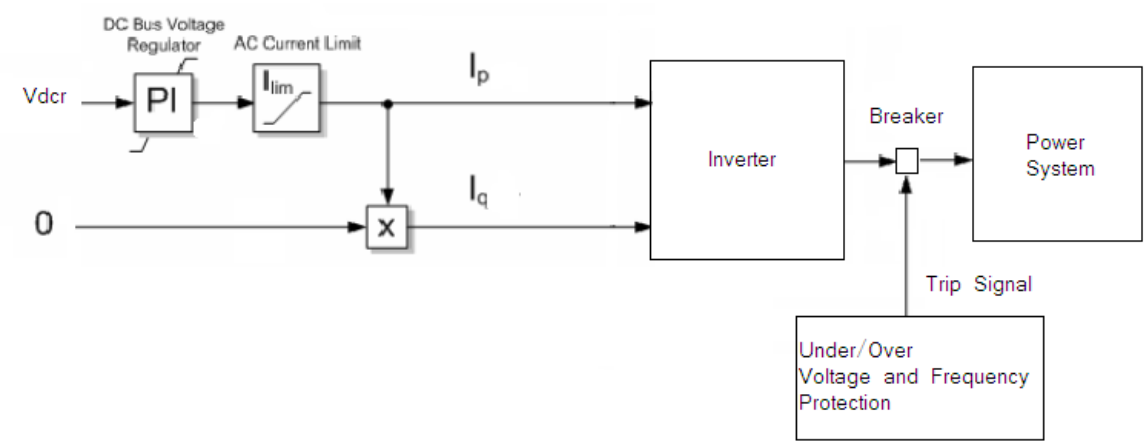

Figure C.4: Active Power Regulators for the Xantrex GT250/500 PV Inverters

The regulator model has only one output that is current injected into the power system shown in rectangular coordinates in the PV terminal bus reference frame as I_p and I_q. For most transient stability studies, the response of the PV plant to power system disturbances such as faults are of most importance. For these studies, in the model, initial solar radiation is calculated according to the initial PV active power output in the power flow solution. The initial solar radiation is then held constant through the time domain simulation. However, the ability to simulate the response of the PV plant to irradiance transients can also be provided which is discussed later. The Xantrex GT250/500 PV inverters do not have the capability to perform voltage regulation which is reflected in Figure C.4. Therefore, in the powerflow model the reactive power limits (maximum and minimum are both set to zero.

The solar radiation and DC voltage which is controlled (maintained) by the inverter result in a DC current from the PV array that is a predictable function of the PV cell physics. There is almost no dynamics associated with the PV characteristics. Characterization of the particular PV module type applied in the PV power plant is through the *fill factor*, defined by input parameters V_r (V_o/V_{pk})[3] and I_r $(I_{sc}/I_{pk})^2$. The control algorithm of the

[3] Ratio of PV array open circuit to peak power voltage

maximum power point tracker (or MPPT) which is a high efficiency DC to DC converter produces a reference DC voltage. The DC voltage error is then processed through a PI (proportional-integral) regulator whose output is the inverter direct axis current that results in active power output.

The model also supports under/over voltage protection in addition to under/over frequency protection. Two levels of over/under voltage tripping and one level of over/under frequency tripping are included in the model. Each of these trip functions has an independent associated time delay.

3.3. Implementation of the Xantrex PV Inverter in Power Analytics' Transient Stability Model Builder

Power Analytics' Transient Stability Program supports a large number of built in dynamic models for exciters, governors, Power System Stabilizers (PSS) offered by a variety of manufactures. To cope with the recent advances in the power electronic digital controllers, and new alternative source of power generation such as PV, wind farms, Power Analytics has developed a user defined modeling feature whereby the user can build their own models. The principle of operation of user-defined models is shown in Figure C.13. The transient stability program and the user-defined models interact with each other through the so-called "Interface Variables". For example, to build a user defined excitation model, the controls normally require that generator terminal voltage to be measured and compared with a reference quantity (voltage set point). Based on the specific control logic of the excitation and AVR, the model should then compute the generator field voltage and returns its value back to the transient stability program. Power Analytics' Transient Stability Program offers an extremely powerful tool for defining a variety of control systems. The user-defined modeling supports a large number of pre-defined control blocks (functions) that are used to assemble the required control systems. In the following section the process of building a user-defined Xantrex PV Inverter model will be described.

---

[2] Ratio of PV array short circuit to peak power current

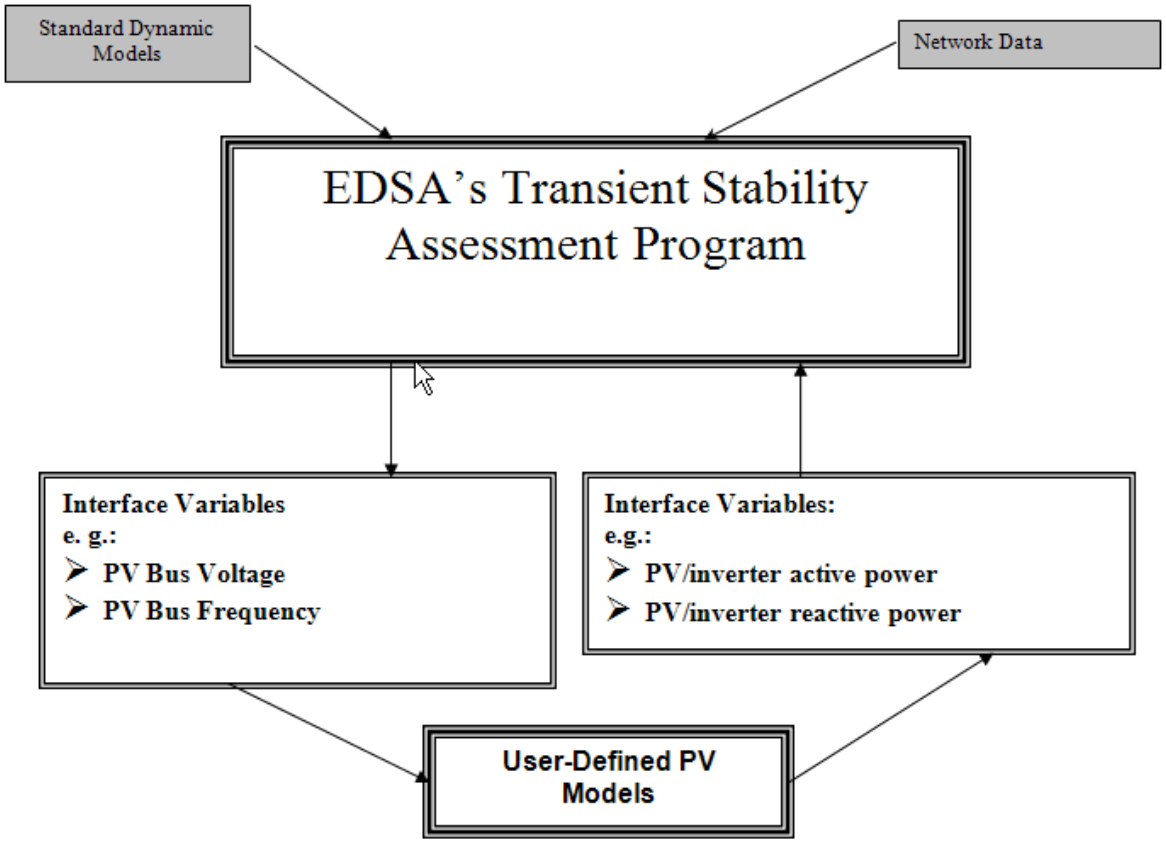

Figure C.13: Interaction between Power Analytics' Transient Stability and User-defined PV/Inverter Model

3.4 Building User Defined Model for Xantrex PV Inverter

In order to build a user-defined model, in general the steps should be followed:

1. Obtain the control block diagram of the control system (normally provided by the manufacturer) to be constructed with Power Analytics' user-defined module (e.g. see Figure C.4)
2. Examine the list of control functions supported in the Power Analytics Transient Stability Program and decide which control functions are needed to build the required control system model
3. Identify the required "Interface Variables"
4. Identify which block output requires initialization. Normally, the reference voltage, governor load reference (initial loading) of the turbine, and initial value of "Integrator" blocks require initialization
5. Build the control system model using the Power Analytics' graphical interface.
6. Add the new model into either AVR, Governor, or PV library
7. Now the models should be ready to test in a power system

Initializing the variables of a control system is an important part of building a user-defined model. To initialize the variables of the control system, note the followings:

- Identify the boundary conditions; these are normally generator terminal and field voltages, generator mechanical (electrical) power, etc.
- In the control blocks set the Laplace Symbol to zero (if applicable). For example, the LEAD-LAG block reduces to a block with gain of one (i.e., initial output= initial input).
- Work your way from the known boundary conditions inward to initialize other variables
- When reaching an “Integrator” block set the input to zero (this is due to the fact that in steady-state the input to an integrator has to be zero in order that the output be in steady-state condition) and try to find the output of the block from the known boundary conditions. Also, the output of a “Differentiator” Block should be zero in steady-state.

To start building the model, start Power Analytics’ Designbase program and select “New” icon from the main dialog of the Power Analytics program as shown in Figure C.14:

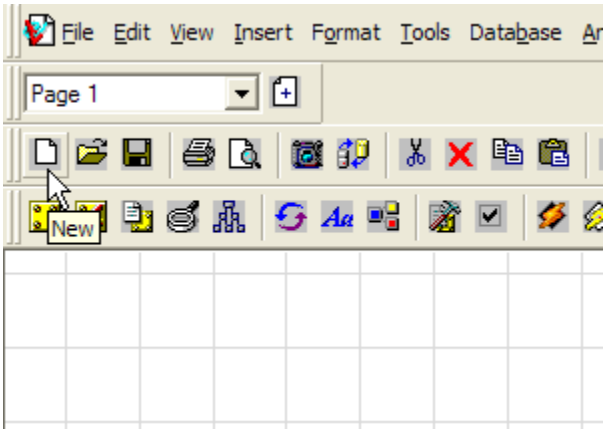

Figure C.14: Creating a New Model or Job file

Select, from Power Analytics tab, the “Power Analytics PV Model Builder.axt”. Next, enter a name for the model (job file) to be created. Next the user is prompted to general (jobfile) parameters and description. The program will open a draw area where this user-defined model can be defined.

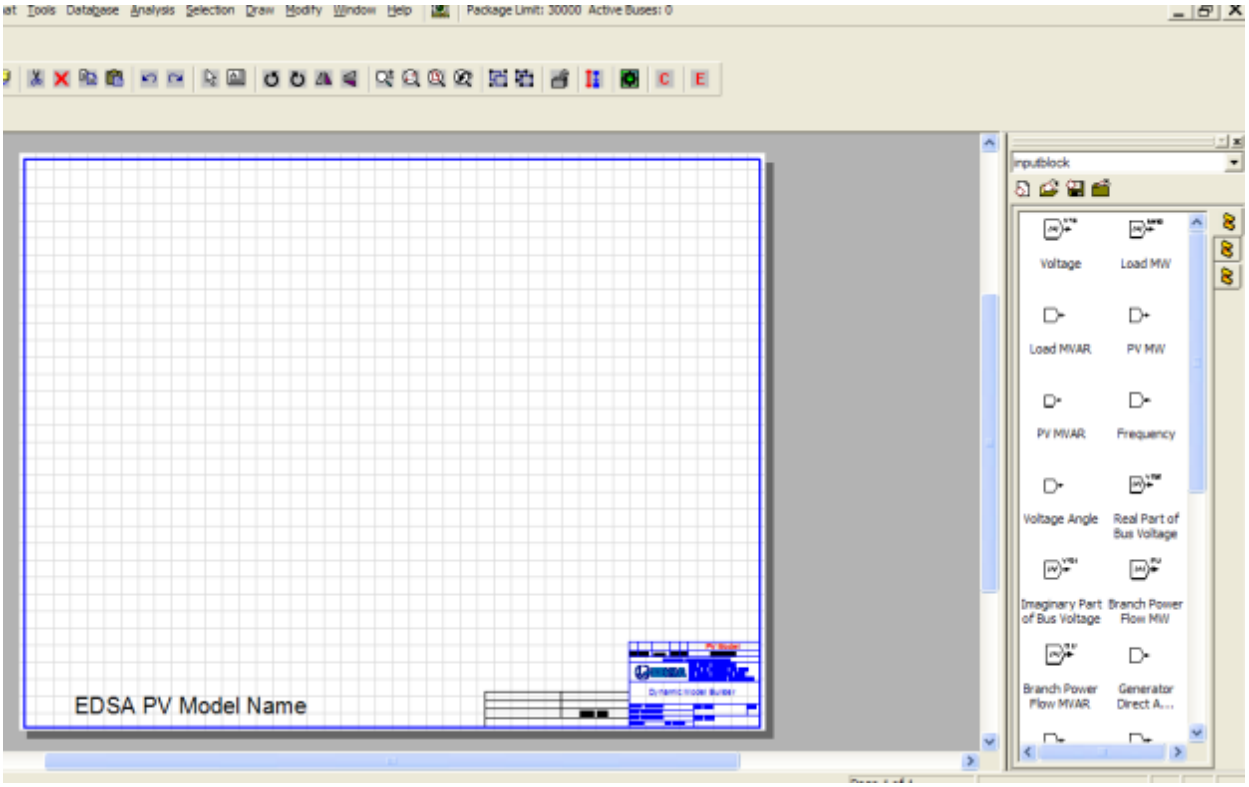

Figure C.15: Draw Area for a User-defined (jobfile) Model

On the right hand side of Figure C.15 there are several icons that can be used to assemble the user-defined model. These icons are of three different types, namely, “Input Blocks”, “General Functions”, and “Output Blocks”. Now the PV control system can be assembled. The model from PV array shown in Figure C.3 will be built. The first block (function) to select is “Input” block. This is the PV active power injected into network (note that PV active power output is also calculated in the PV inverter model) as shown in the highlight section in Fig. C.24.

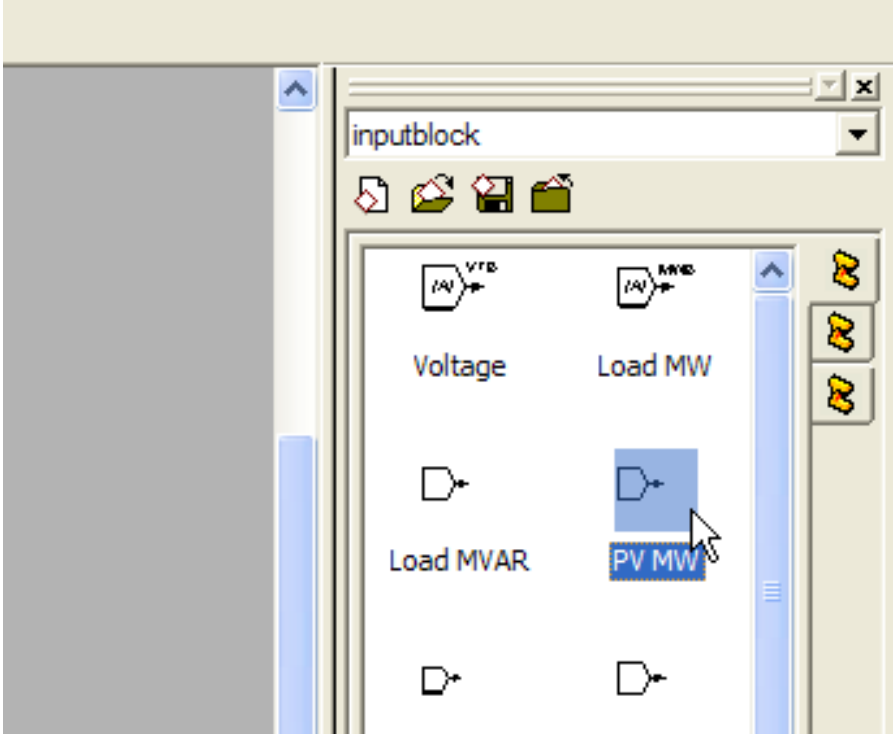

Figure C.16: Selecting the “Active Power” for a PV system from Input Blocks

The selected icon should be drag into the draw area to a desired location. To define the necessary parameters and give a name to the output of the “Active Power” input block, double click right mouse button on its icon. The definition dialog will appear as shown in Figure C.5.

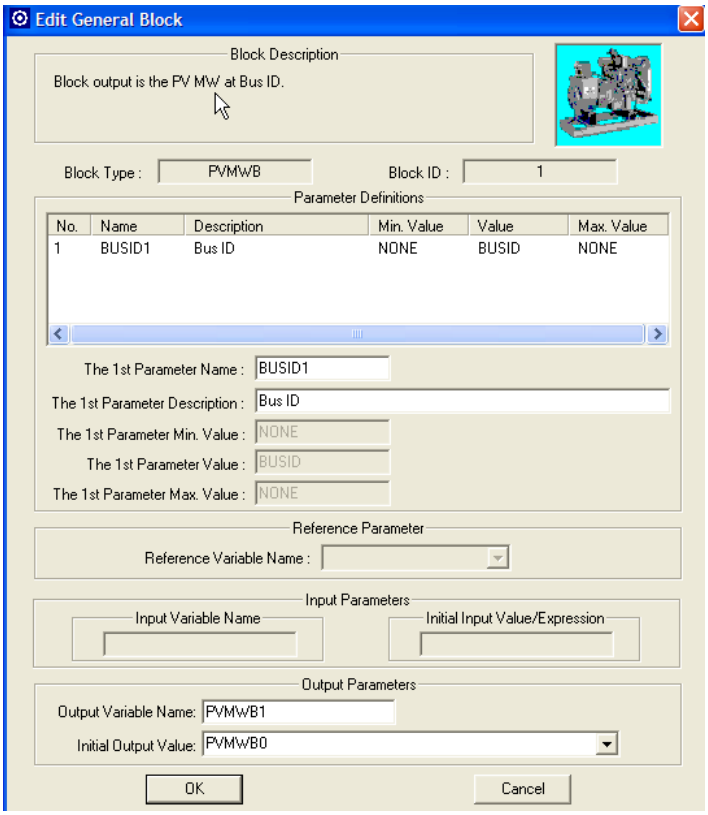

Figure C.5: Parameters Dialog for PV Active Power

Note that the active power output of a PV in this input block will be in the unit of MW. Since there may be several PV plants in a given power system, then, the user should specify where (at which system bus) this PV is located. However, this bus ID information can be provided in “Symbolic” form at this stage of model building. It can be seen that this input block has only one parameter, Bus Identification of the PV, which has been named symbolically as “IB”. The output of this block, “Output Variable Name”, is named PACC.

Since the the unit of Active Power block is defined in MW, this value should be converted into per unit based on the PV plant MVA rating. In order to achieve this, the following steps should be performed.

First there is a need for a constant block which can be obtained from “General Blocks”. To define the necessary parameters and name the output of this block by double clicking the right mouse button on its icon. The definition dialog will appear as shown below:

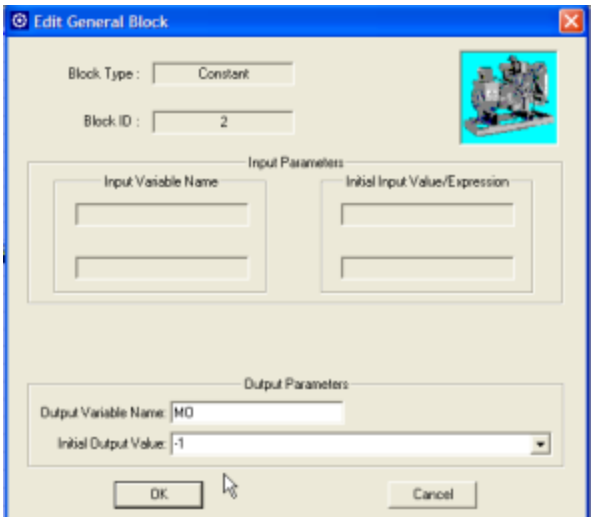

Figure C.6: Defining Parameter and Output Variable Name for a Constant Block

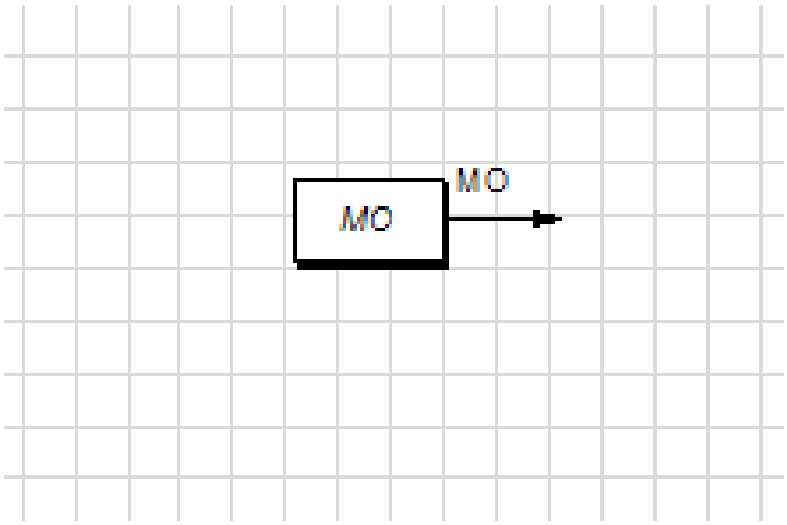

Figure C.7: The Fully Defined Icon of a Constant Block Shown in the Draw Area

The “Output Variable Name” is assigned to be “MO” and “Initial Output Value” is given a value of -1

The fully defined constant block is now shown in Figure C.7.

Next a Gain function is selected from the General Function Blocks and dropped at a desired location.

To edit and enter the parameters associated with the Gain block double click the right mouse button on its icon and the parameter Dialog will appear as seen in the following figure.

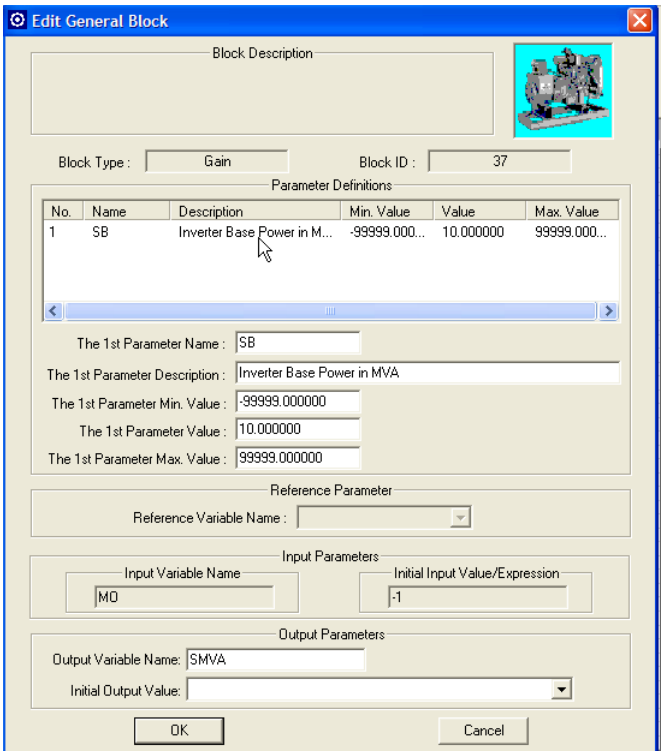

Figure C.8: Defining the Parameters of a Gain Block

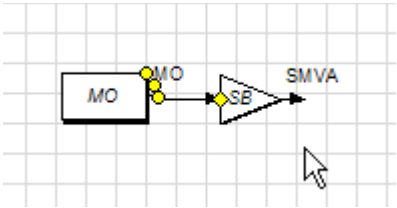

Figure C.9: Connecting Constant Block to Gain Block

In Fig. C.20 the “Output Variable Name” was renamed to be “SMVA”, the 1st parameter is symbolically named “SB” with description of “Inverter Base Power in MVA”. Note that this value is sum of power of all individual PV plant inverters. The exact numerical value of the Gain will be defined when the completed PV model is used in a power system (will be shown in the next section). The default value of the 1st parameter has been given a value of 10. Note that the user can also define a range (minimum and maximum) for this gain. Now that the Gain block is completely defined, connect the Constant block to the input of the Gain block as shown below.

Now the active power can be converted into p.u. Select “Division” block and drag the icon in the model area. Then connect the nominator and denominator of the division block

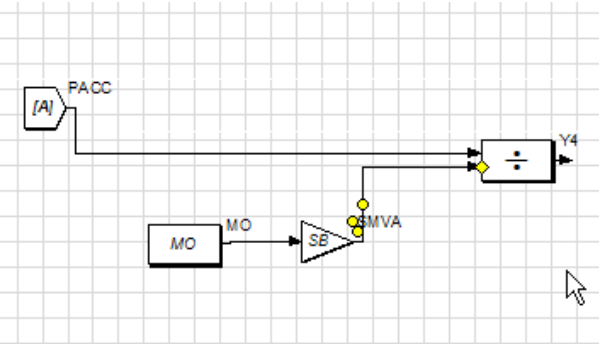

Figure C.10: Connecting the Denominator of the Division Block

Double click the right mouse button to assign a name to the division block as show:

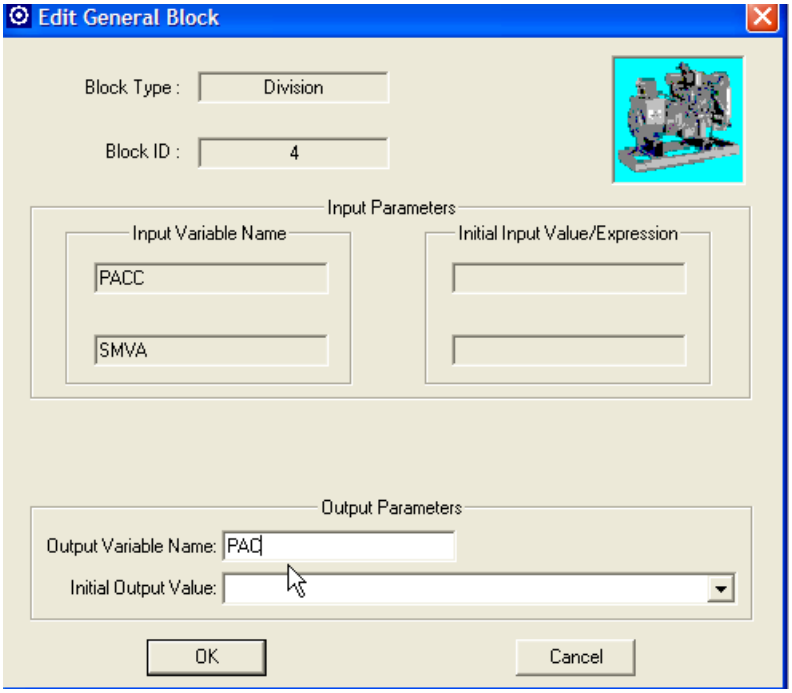

Figure C.11: Naming the Output of a Division Block

3.5. Complete Xantrex PV and Inverter Model

Since the principal of adding functional blocks and input block is covered in details above, the important blocks of the completed PV array model shown in Figure C.12 will be discussed below.

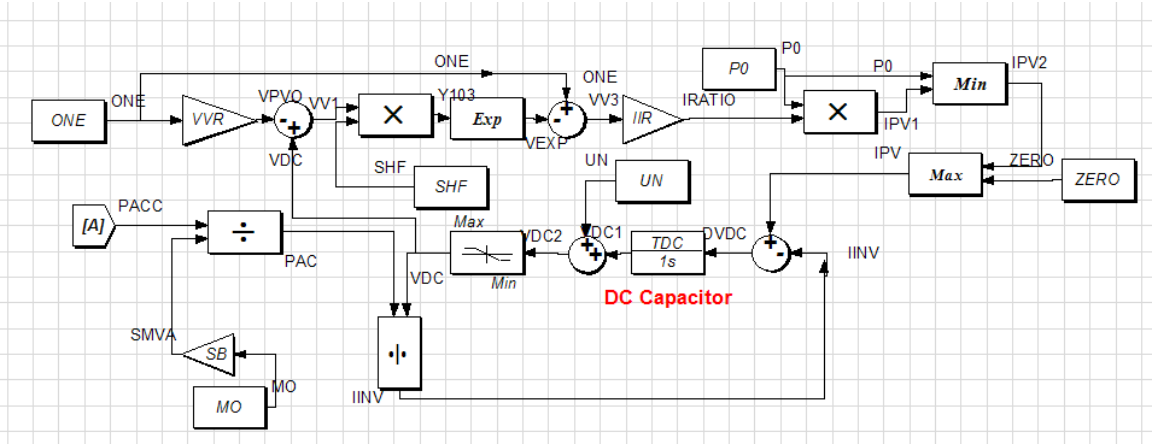

Figure C.12: Completed PV Array Model in the Power Analytics User-defined Model Builder

- "Ratio of Open Circuit to Peak Output Voltage" is defined via a gain block shown at top left corner of Figure C.12, with Parameter Name (1st) of VVR", the block parameter is shown below:

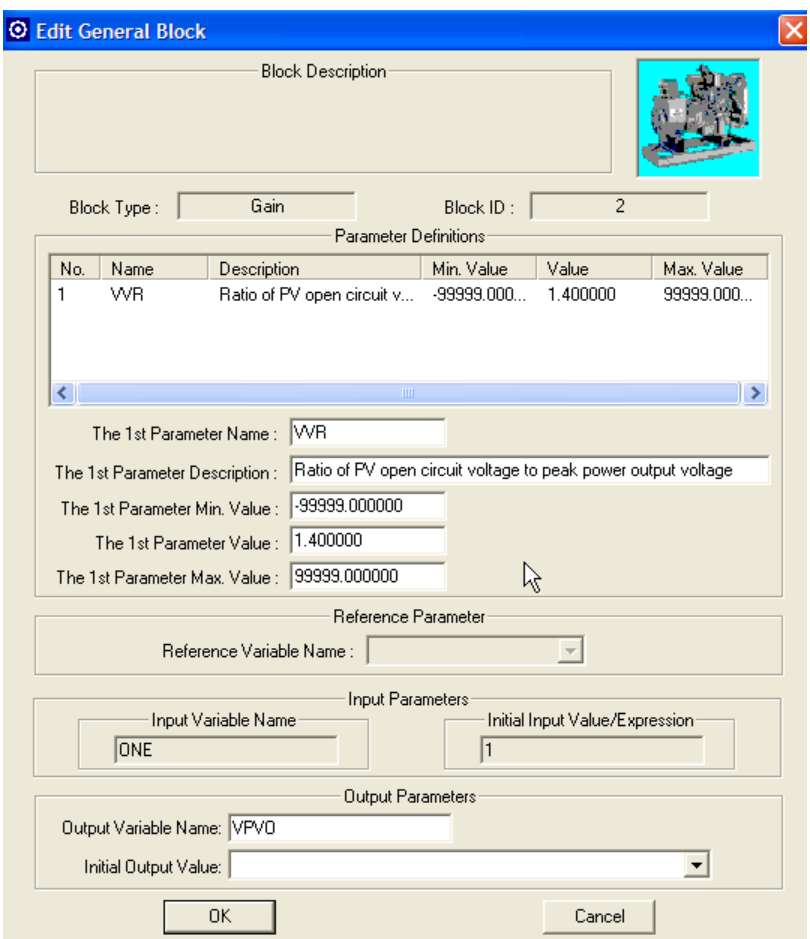

Figure C.13: Defining Ratio of Open Circuit to Peak Output Voltage of PV Array

- The shape factor of the PV is defined in a constant block named “SHF” shown in Figure C.14. The value of the constant can be inspected by double clicking left mouse button:

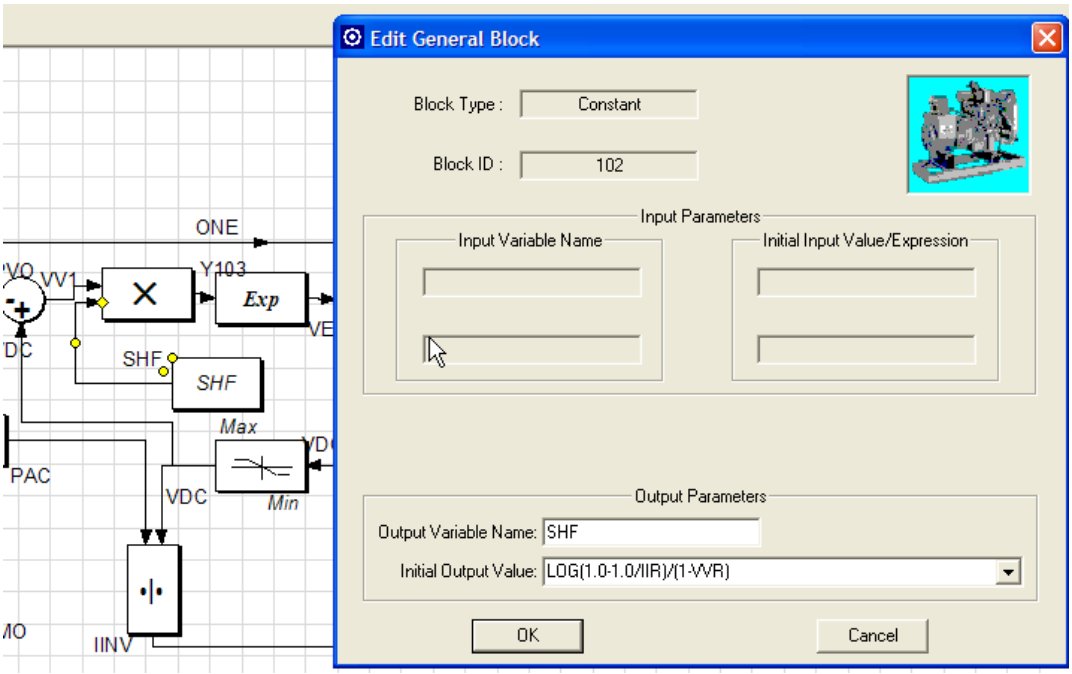

Figure C.14: Defining Shape Factor of PV Array

- “Ratio of Short Circuit to Peak Output Current” is defined via another gain block with Parameter Name of “IIR”, the block parameter is shown below:

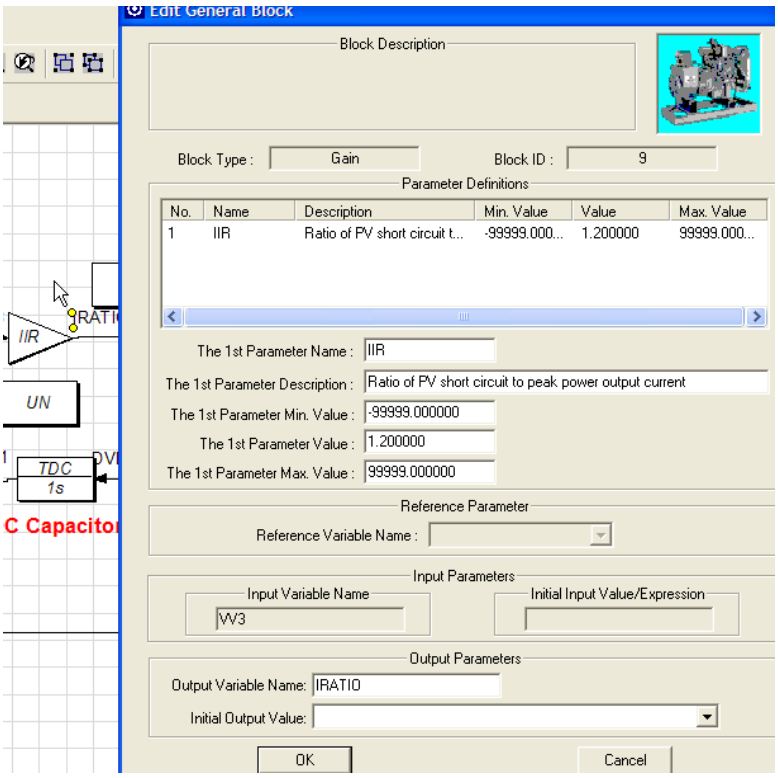

Figure C.15: Defining Ratio of Short Circuit to Peak Output Power Current of PV Array

- As mentioned earlier, the integrator block requires initialization. The input of an integrator block should always be zero in the steady-state (otherwise integrator will not be in steady-state). The easiest way to initialize an integrator it is through a summer block at its output and add constant equal to the initial value to it. This is seen in Figure C.12 and summer at the output of the integrator " DC Capacitor". This is result of the following relationship:

$$C\frac{dV_{DC}}{dt} = i$$

$$V_{DC} = \frac{1}{C}\int idt$$

- The "Min" and "Max" blocks are important to control the limits of current as a result of solar radiation. Special attention should be paid to the "Max" block. First, one of the input of this block has been assigned a value of 0 (zero). The second input is the result of array characteristics and initial solar radiation. This block (as is which is shown in Figure C.12), assures that during time domain simulation the PV does not generate more power than initially (i.e., assumes solar radiation does not change during a normal time frame of transient stability assessment which is in the range of a few cycles to 10-20 second period). However, if the variation of the solar radiation is to be simulated, then, the input 0 (zero) should be replaced by a lookup table representing solar radiation variation as a function of time. An example will be shown later

Next part of the PV model to discuss is the active power/voltage regulators. The completed control block diagram for voltage control is shown below:

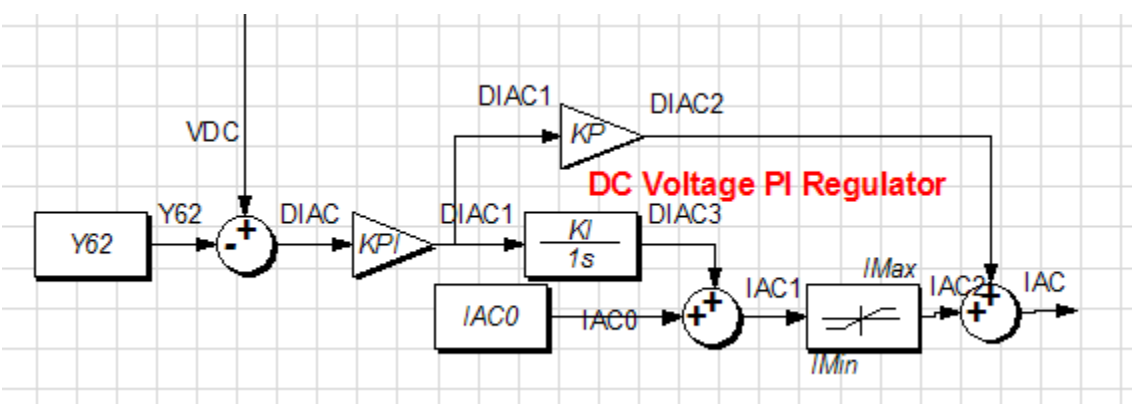

Figure C.16: Power/Voltage Regulator in Xantrax Inverter

In the above it is important to note:

1) The constant block Y62 is representing the output of an MPPT controller. Inspection of this constant block shows that the value of constant in this block is 1 (one). A summer adds the MPPT

output to the actual DC voltage and the PI controller will act until it achieves equality between actual DC voltage and the optimum value found by MPPT.

2) A PI controller with a gain of KP (proportional), and an integrator with a gain of KI.

3) Again, the initial value of the integrator in the above controller is taken into account by using a summer at the output of the integrator summed with a signal that its value is equal to the initial condition of the integrator.

4) The limiter assures that the output stays with the practical limits.

3.6. Under/Over Voltage and Frequency Protection

The projection of PV inverter against abnormal voltage and frequency operation is extremely important not only from device protection point of view also from the power utility operation the planning/operation engineer would like to know under disturbances how long and to what level PV can ride through disturbances. The under/over voltage protection and under/over frequency protection scheme used in the Xantrex PV model is shown in the following figure.

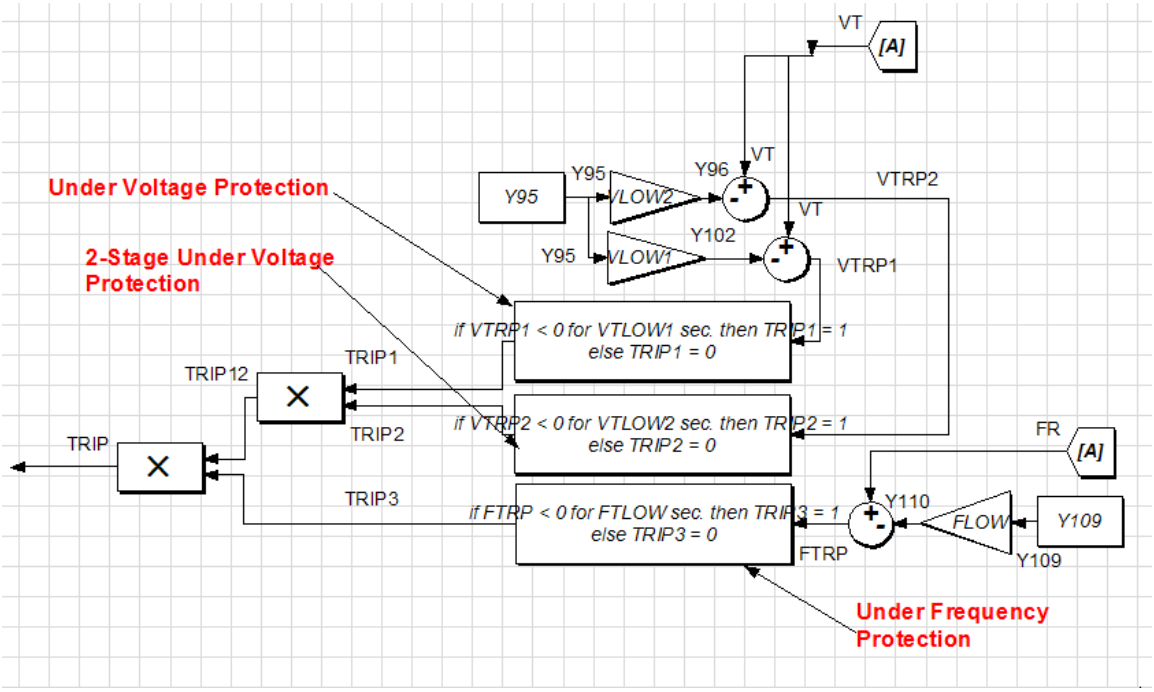

Figure C.17: Under/Over Frequency and Voltage Protection Model in Xantrex Inverter

At the top right hand side and lower right hand side of the above figure the bus voltage and frequency are used (these are “Input Block”). The inverter has two level of under voltage with different trip times and one under-frequency trip. A logical function from the “General Block” is then used to send trip signal. This logical block is shown below.

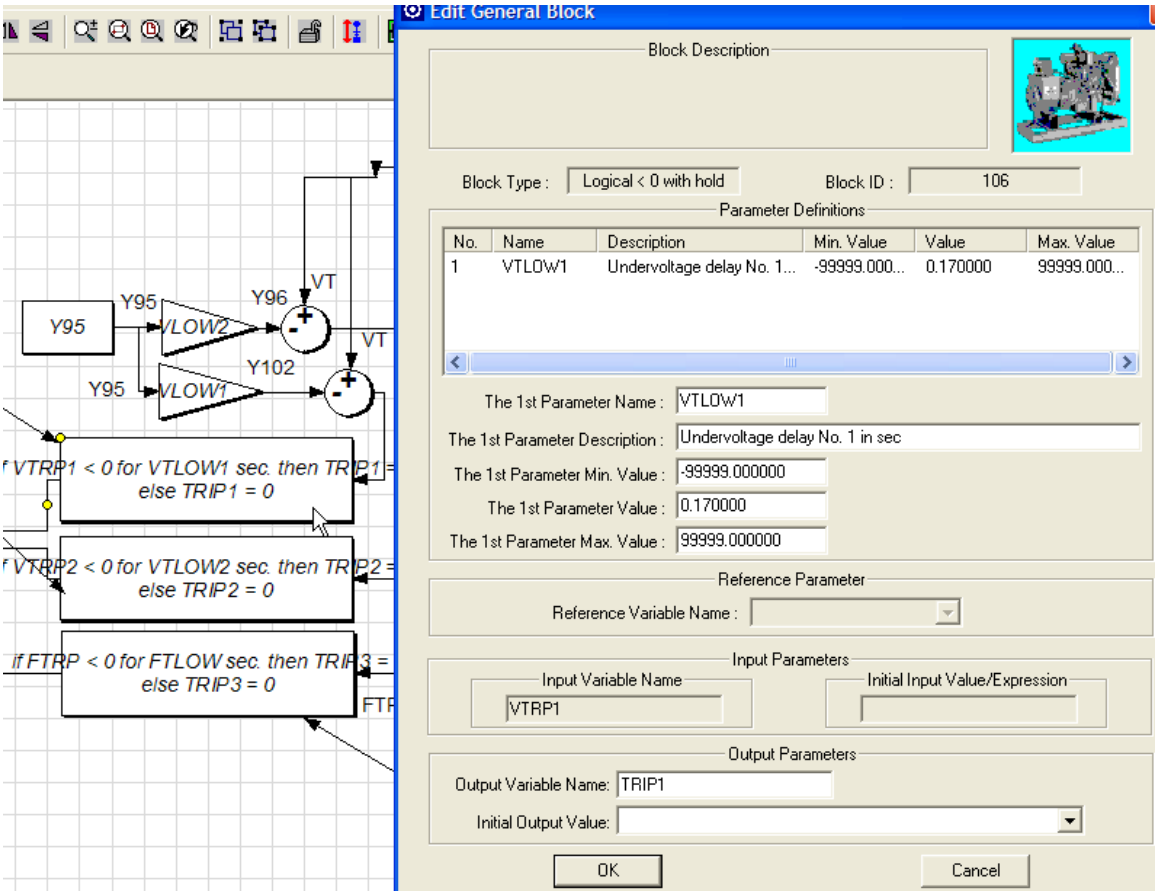

Figure C.18: Logical Block for Building Relay Trip Signal

The trip signal is generated when the input of the block becomes less than zero for specified time (relay time). It should be noted that the input of this block is:

VT-VLOW1

where VT is the terminal voltage of PV inverter bus and VLOW1 is defined as seen in Figure C.19 to be 0.57 for this inverter (Xantrex). I.e. if the voltage drops to less than 0.57 p.u. for longer than VTLOW1 seconds, then, the trip signal (TRIP1) is generated.

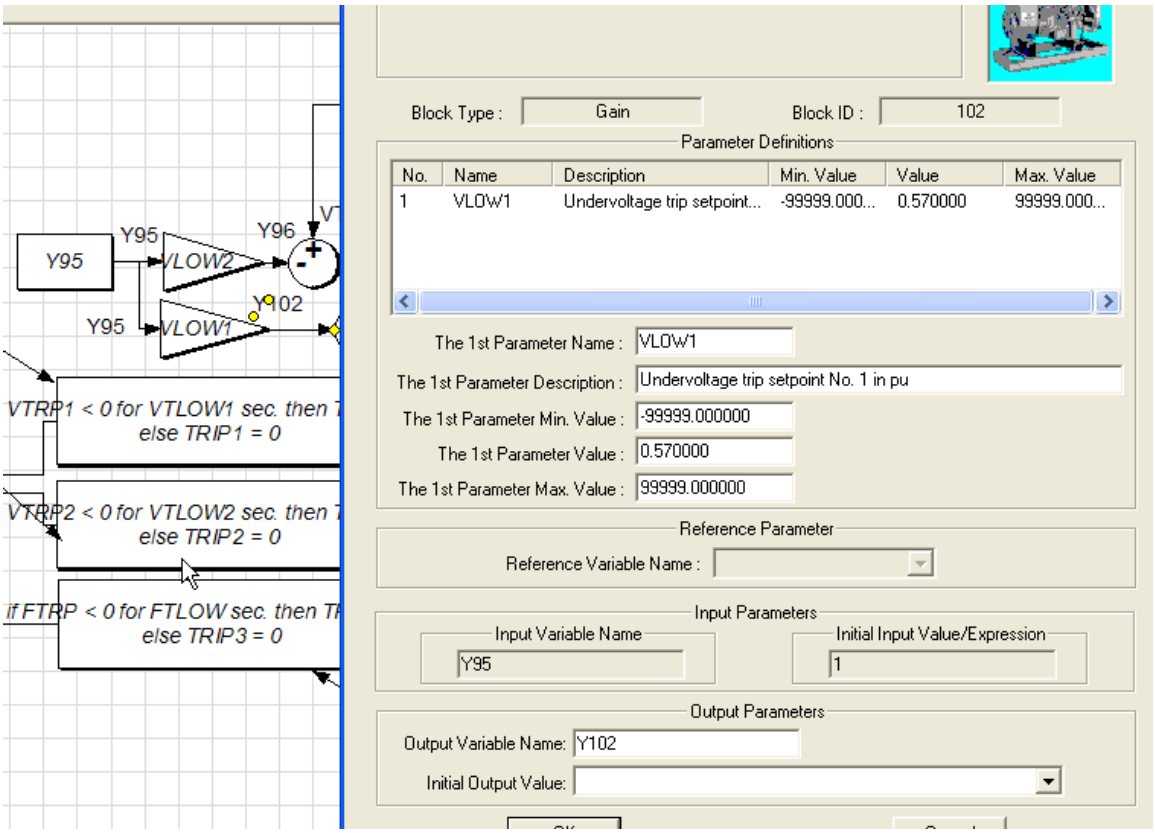

Figure C.19: Defining the 1st under voltage Trip Setting

Similarly multiple levels of under/over voltage and frequency relays can be defined. It should be noted that when more than one relay is used then the trip signal generated from each one should be used in “OR” function. It can be seen that the output of each pair of relay is used in a “Multiplication Function”

3.7. Testing of Xantrex Inverter in Sample Power System

The model of Xantrex 250/500 KW unit was developed in the Power Analytics Advanced Transient Stability Program and details provided in the previous sections. In this part of the report, the model will be used in a sample power system to assess its performance under disturbances (fault simulation is of the most common and interest for power system engineers).

The standard modeled WECC 9 bus power system shown in Figure C.20 is used to test the PV model. Even though this is a relative small network it has most of the ingredients of a real power system. The system is comprised of three synchronous generators. Details of loads/generation and initial voltages without the PV are outlined in Table C.2.

Table C.2: Characteristics of the WECC 9-bus system.

Bus Name	Bus Type	Voltage (p.u.)	Voltage Angle	Gen/Load MW	Gen/Load MVAR
1	Gen	1	0	72	10
2	Gen	1.025	-2.5	163	18
3	Gen	1.025	-2.5	85	0
4	Load	0.995	0.5		
5	Load	0.9719	2.81	-125	-50
6	Load	0.9895	1.05	-90	-30
7	Load	1.0191	-1.91		
8	Load	1.0093	-0.93	-100	-35
9	Load	1.0262	-2.62		
11	Load	1.0191	-1.91		
PV	PV	1.0191	-1.91		

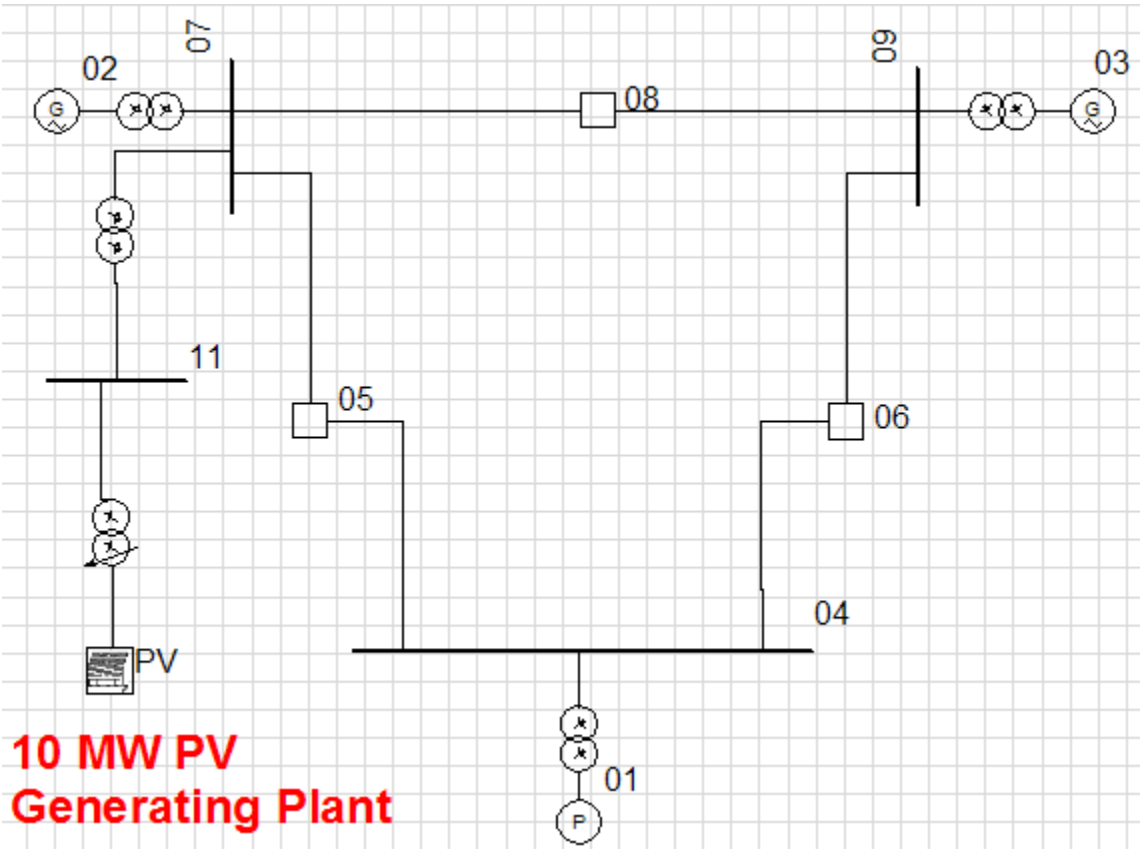

Figure C.20: Sample Power System for Testing a Xantrex PV plant

The result of powerflow for assuming a 10 MW PV plant is shown below. It can be seen that the PV inverter is not capable of voltage regulation or reactive power compensation.

Table C.3: Powerflow results for 10 MW PV Plant on WECC 9 bus system.

Bus Name	Bus Type	Voltage (p.u.)	Voltage Angle	Gen/Load MW	Gen/Load MVAR
1	Gen	1.000	0	64	11
2	Gen	1.025	-2.5	163	19
3	Gen	1.025	-2.5	85	0
4	Load	0.994	0.57	64	15
5	Load	0.971	2.94	-125	-50
6	Load	0.989	1.13	-90	-30
7	Load	1.019	-1.86	171	4
8	Load	1.009	-0.88	-100	-35
9	Load	1.026	-2.59	85	8
11	Load	1.020	-2	8	0
PV	PV	1.025	-2.52	8	0

The power system shown in Figure C.20 is assembled similar to other network with the exception of PV. To add a PV plant to a power system select the PV icon from the list as shown below and drag it into system model area. To edit the parameters of the PV inverter, double click the right mouse button on PV icon. The parameters dialog a PV is shown in Figure C.22. It should be noted that since Xantrex 250/500 PV inverters do not provide reactive power supply capability (are not generally of voltage source type), the reactive power capability (both QG max and min) set to zero (see Figure C.22).

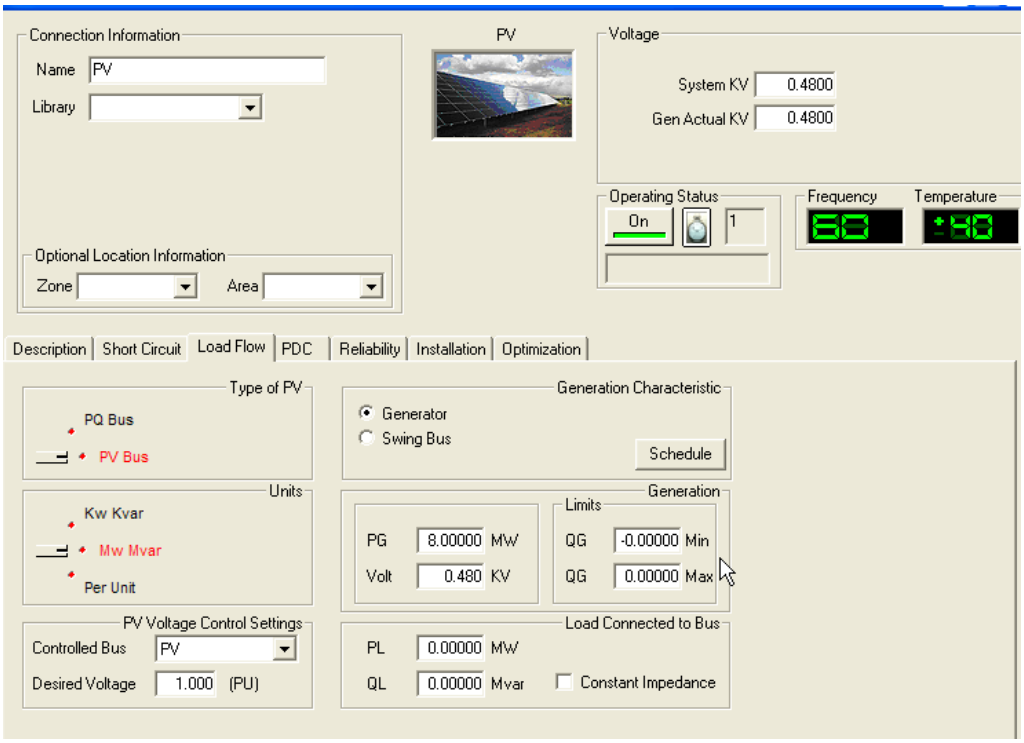

Figure C.22: Powerflow Parameter Dialog of PV Plant

Also note that even though majority of PV inverters cannot contribute to the fault current, Power Analytics decided to leave this option to the user. If a PV unit is capable of feeding faults for a short period of time, then, equivalent resistance and reactance can be specified.

To prepare a transient stability simulation case for this system, the dynamic data for the Xantrex inverter needs to be specified. This can be done by first selecting transient stability icon and "Data and Event Manager" for Defining PV Inverter Data

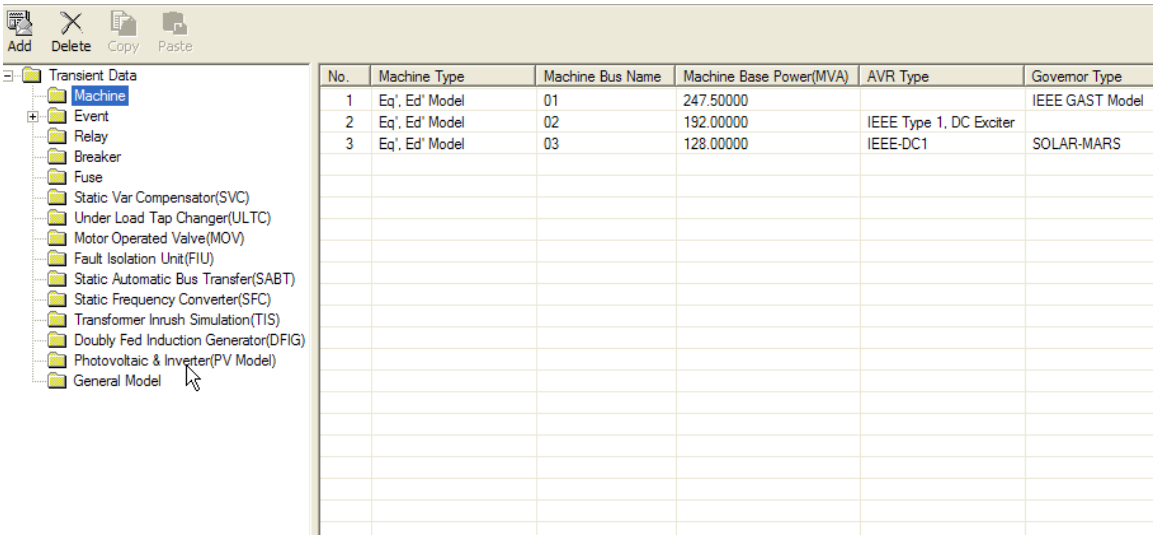

Figure C.21: Adding/Deleting PV Models

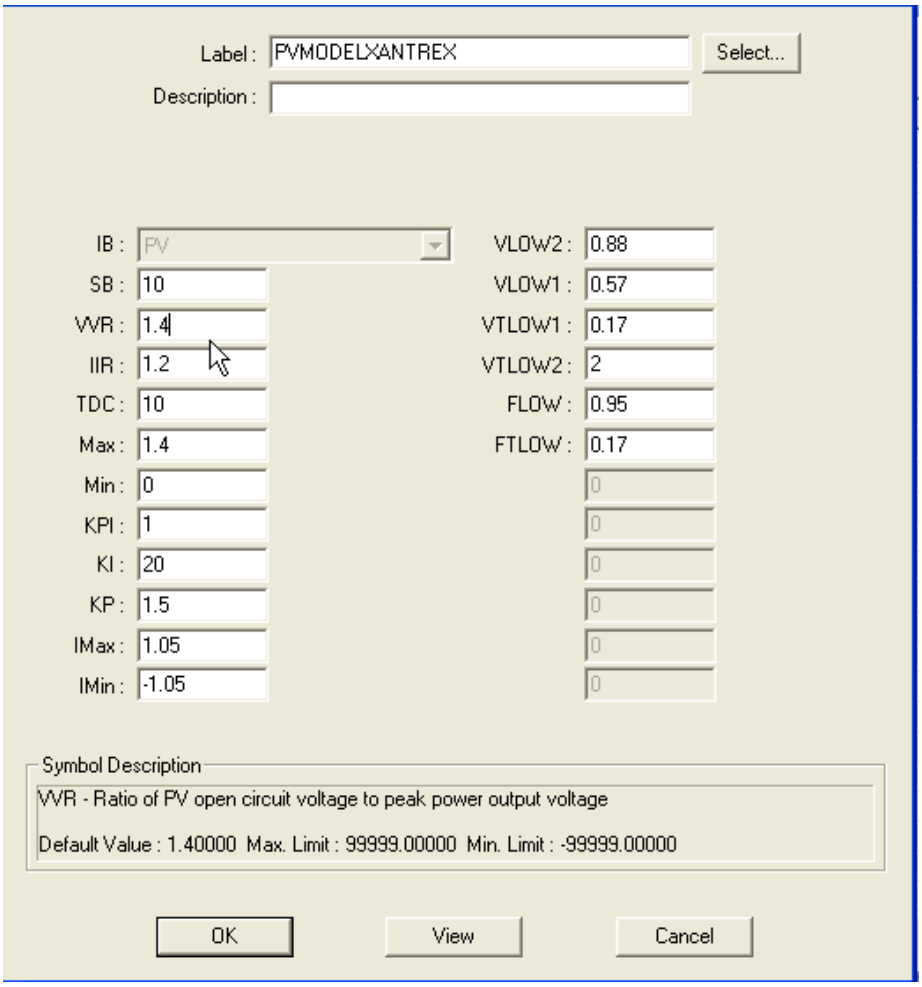

Figure C.22: Dynamic Data for Xantrex PV Inverter Plant

If the user wishes to examine available PV models, the “select” button shown at the top right hand side of above figure should be pressed. The available PV models namely, “Sun Power”, “Xantrex”, “OptiSolar”, and “General Power Analytics” Model are shown below:

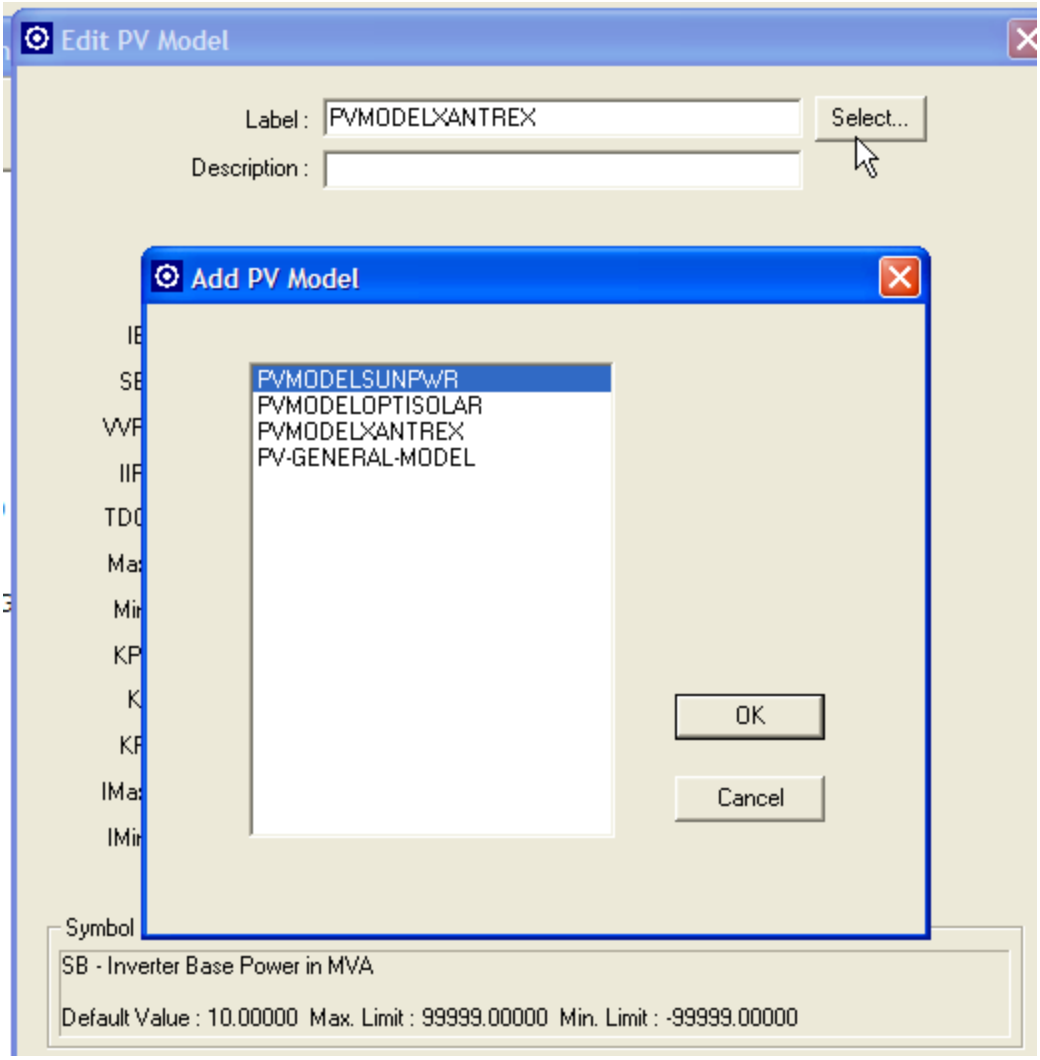

Figure C.23: Available PV Inverter Models in Power Analytics' Transient Stability Software

The disturbance that will be examined for this test with PV plant is application of a fault at bus 5 for a period of 6 cycles (0.1 second). To specify this fault select "Event" and add one fault application event.

Now this fault can be simulated by selecting "Analyze". Next the simulation dialog will appear. Press the "Start Simulation" to perform the simulation. Upon completion of the simulation the result can be view by selecting "View Graphic Result" depicted in Figure C.24.

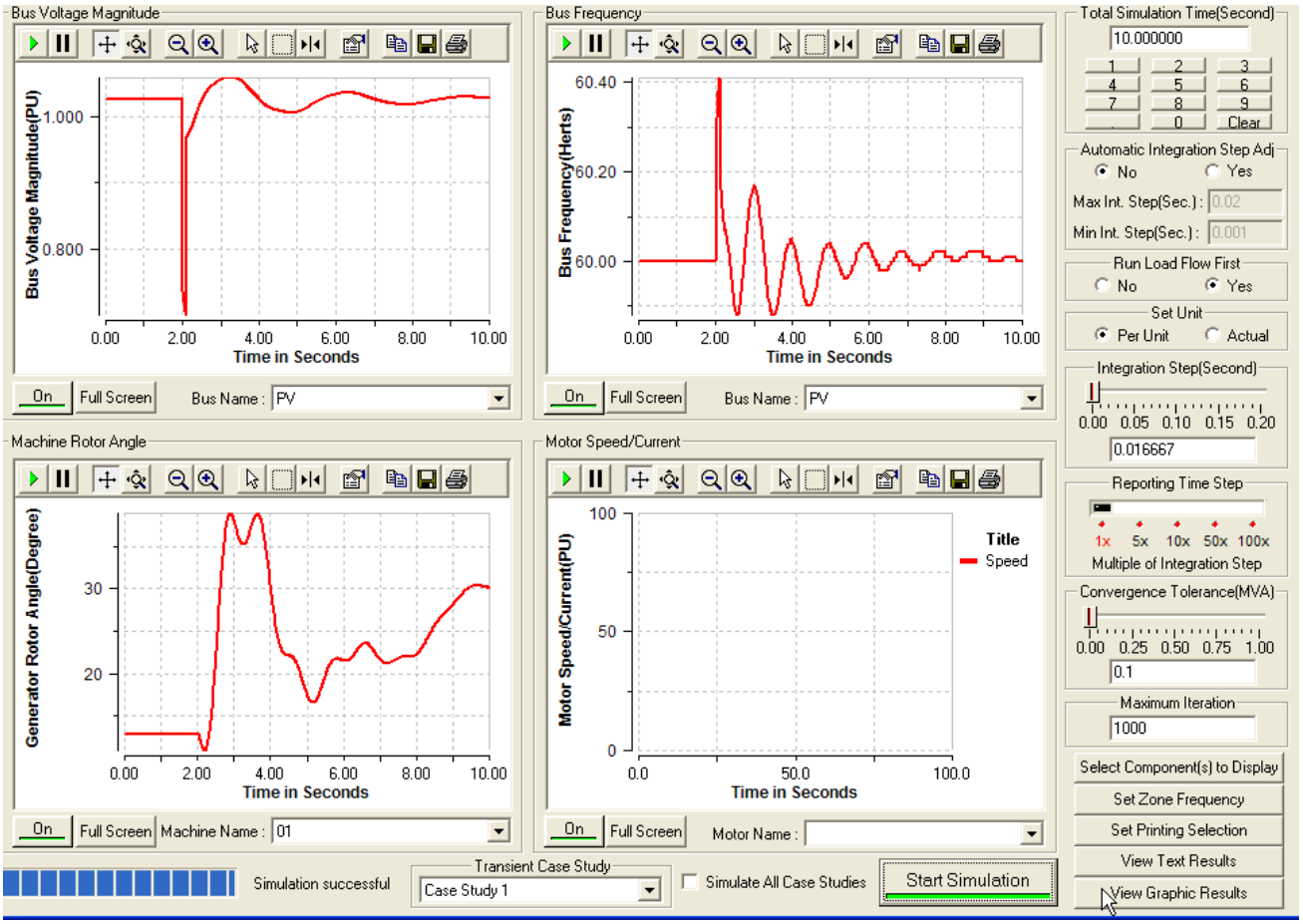

Figure C.24: Viewing Graphic Result of a Transient Stability Simulation

All of the monitored variables related to generators, buses, branches, PV, etc. can be examined. Figure below shows several tabs. For example, the generator rotor angles, frequency, mechanical power, terminal voltage and field voltage are shown in Figure C.25.

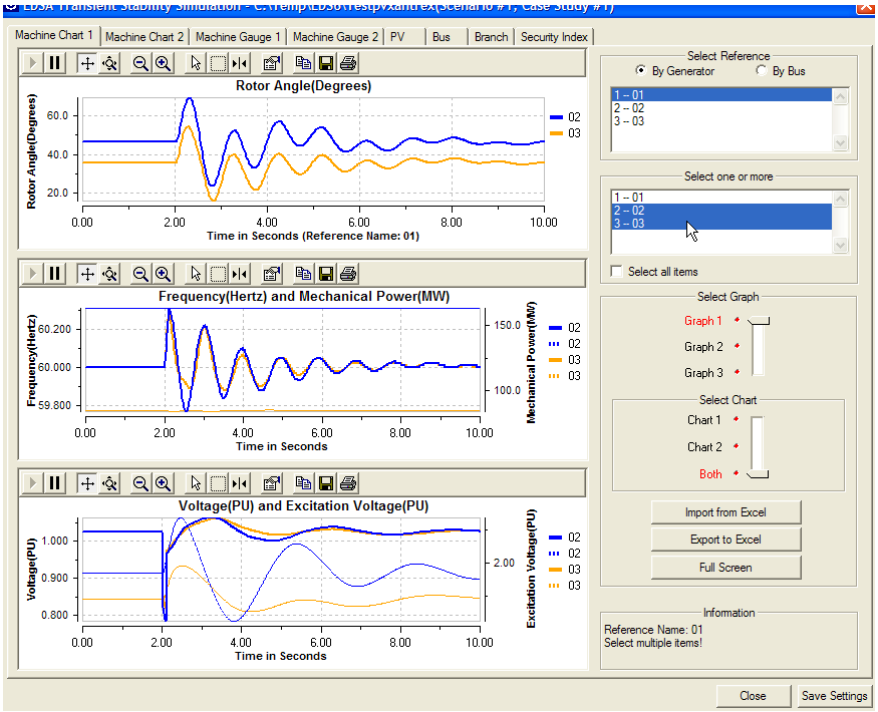

Figure C.25: Graphs of Monitored Generator Variables

To examine the monitored variables for the PV model select “PV” tab shown above. The variables to be monitored are defined at the time PV model is added to the PV library. Power Analytics transient stability program gives the user the option to monitor any of the internal variables (signals) within the model. This unique feature helps the user to assess the performance of the control system of the PV inverter and optimize its performance (e.g. by examining the effect changing gain, time constant, etc. on the performance of any controller internal to the inverter).

The time response of the DC voltage of the PV array in the Xantrex inverter due to a fault is shown in Figure C.26. This figure shows that upon fault occurrence, the array will respond by increasing the voltage to maintain the active power output. The DC voltage will quickly recover following removal of the fault. Other variable of the PV model can be examined by selecting them from the list shown in the bottom middle part of the Figure C.26.

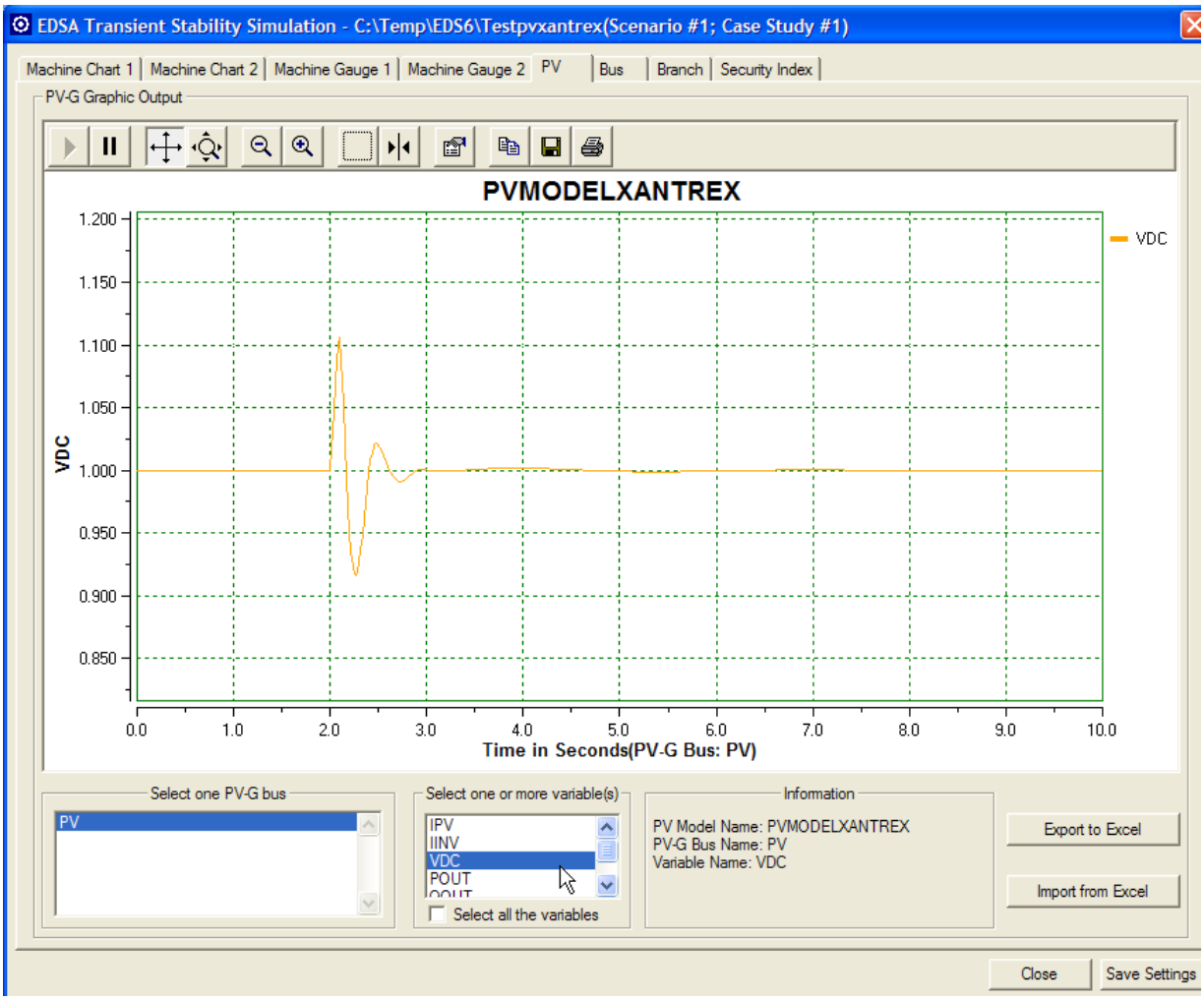

Figure C.26: Time Response of DC Voltage of the PV Array of the Xantrex PV/Inverter to a Fault

B.4. Modeling of SunPower PV Inverters

Similar to the Xantrex Model development, the objective is to build up models that are most appropriate for power system simulation including power flow and time domain to be used by power system planners to perform PV power plant integration studies. These models have been implemented in the Power Analytics Advanced Powerflow, Short Circuit, and Transient Stability analysis software package.

A SunPower power plant comprises of PV modules, step-up transformers and other power system components necessary to convert solar radiation to AC power for delivery at transmission/distribution voltages. The modular structure of PV plant allows for grid integration studies to be performed with a common plant model that is scalable to the power rating of the particular project under study.

SunPower PV modules are series connected to create DC voltages in the range of 300 to 900 volts. The currents are then paralleled to create DC sources with power capacities in the range of 100 kW - 2 MW. The SunPower inverters are IGBT type inverters that convert the DC power to AC power three-phase 400 volts or 480 volts AC. For utility scale PV power plant, low AC voltage should be connected to a step-up transformer which provides voltage for integration of the inverter and its associated PV source circuits with the medium voltages in the range of 15-35 kV. For transmission interconnected plants, another transformation to high voltage as required for the transmission network interconnection at the collection substation. The PV modules that serve as input sources to the inverter consist of solid-state semiconductor cells that produce direct current as a function of the solar radiation and terminal voltage on an ***almost instantaneous basis***. Therefore, it is the inverter and controls that govern the transient behavior of the plant and its interaction with the grid. The inverters utilized by SunPower are classified as high frequency, pulse-width-modulated, current-regulated inverters. They operate to regulate their respective AC output currents in response to a current command through high carrier frequency (~10 kHz) PWM of the connected DC source. This provides extremely pure sinusoidal output current waveform which is synchronized to the grid voltage waveform (i.e., it follows the grid frequency).

4.1. Power Flow and Short Circuit Modeling of SunPower PV Inverters

PV power generation using SunPower inverters can be modeled (similar to a classical synchronous generator) as a generator connected to power system for powerflow modeling purposes. The voltage rating of the generator (representing the SunPower inverter) has a nominal value of 0.40 kV or 0.48 kV. The PV plant power rating (MVA) is equal to an integer multiple of the individual inverter MVA rating. However, the active power output for the powerflow simulation can be anywhere in the range of zero to rated MVA depending on the available solar radiation for the time of interest. The maximum reactive power delivery to the system and maximum reactive power absorbed from the system (Qmax and Qmin) should both be set such that to limit the generator power factor to 0.95 leading to 0.95 lagging.

SunPower PV inverter has no or very little contribution to short circuit. It is therefore, recommended that the generators be represented by reactance of very high magnitude (e.g. 100 p.u.). Since the generator may represent an aggregate PV, the reactance used would be the same value if all the generators have the same characteristics on a plant base (sum of the MVAs of the individual inverters).

4.2 Transient Stability Dynamic Modeling of SunPower PV Inverters

The SunPower PV inverter dynamic model has been implemented as a user-defined model in the Power Analytics Advanced Transient Stability Program. This model consists of a reduced order representation of the inverter controls. An overview of the control block diagram of the model is shown below:

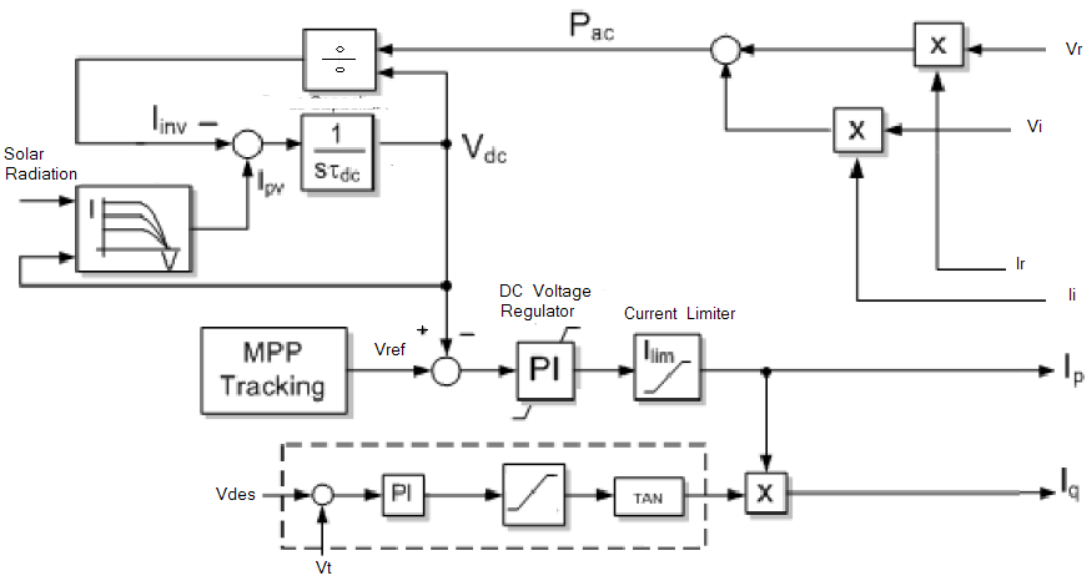

Figure C.27: Overview of the Control Block Diagram of the SunPower PV Inverters

The above control system consists of PV array model, Maximum Power Point Tracking system, voltage and active power controllers, and inverter. The over/under voltage and over/under frequency protections are normally imbedded in the inverter model and will be discussed later.

The solar radiation and DC voltage that is controlled (maintained) by the inverter result in a DC current from the PV array that is a predictable function of the PV cell characteristics. There is almost no dynamics associated with the PV characteristics. Characterization of the particular PV module type applied in the PV power plant is through the *fill factor*, defined by parameters V_o/V_{pk}[4] and I_{sc}/I_{pk}[2]. The control algorithm of the maximum power point tracking (or MPPT) which is a high efficiency DC to DC converter produces a reference DC voltage. The DC voltage error is then processed through a PI (proportional-integral) controller whose output is the inverter direct axis current that results in active power output.

[4] Ratio of PV array open circuit to peak power voltage

[2] Ratio of PV array short circuit to peak power current

The model also supports under/over voltage protection in addition to under/over frequency protection. Two levels of over/under voltage tripping and one level of over/under frequency tripping are included in the model. Each of these trip functions has an independent associated operating time (relay + intentional delay + other).

The quadrature axis current (Iq) is calculated to either maintain a fixed power factor or to regulate the voltage at the AC bus of the inverter. The Power Analytics transient stability software internally provides the phase rotation function to transform these currents from the terminal axes to the network axes (**Ir**, **Ii**) for use in the network solution.

For simulations involving solar radiation variations, the user may create text files containing time series of the solar radiation. Sample of such a file will be shown in later sections. Data in the first column is time, expressed in seconds from the start of the simulation and data in the second column is solar radiation values expressed in p.u. on the plant PV (total inverters) base. The program uses linear interpolation to calculate intermediate data points.

4.3 Implementation of the SunPower PV Inverter in the Power Analytics Transient Stability Model Builder

Similar to Xantrex PV model described in the previous chapter, the SunPower PV model can be built using the user-defined feature of the Power Analytics' transient stability software. Since the principal of adding functional blocks and input block was demonstrated in previous chapter in details for assembling Xantrex model, only the important blocks of the completed SunPower PV model shown in Figure C.28 will be discussed below.

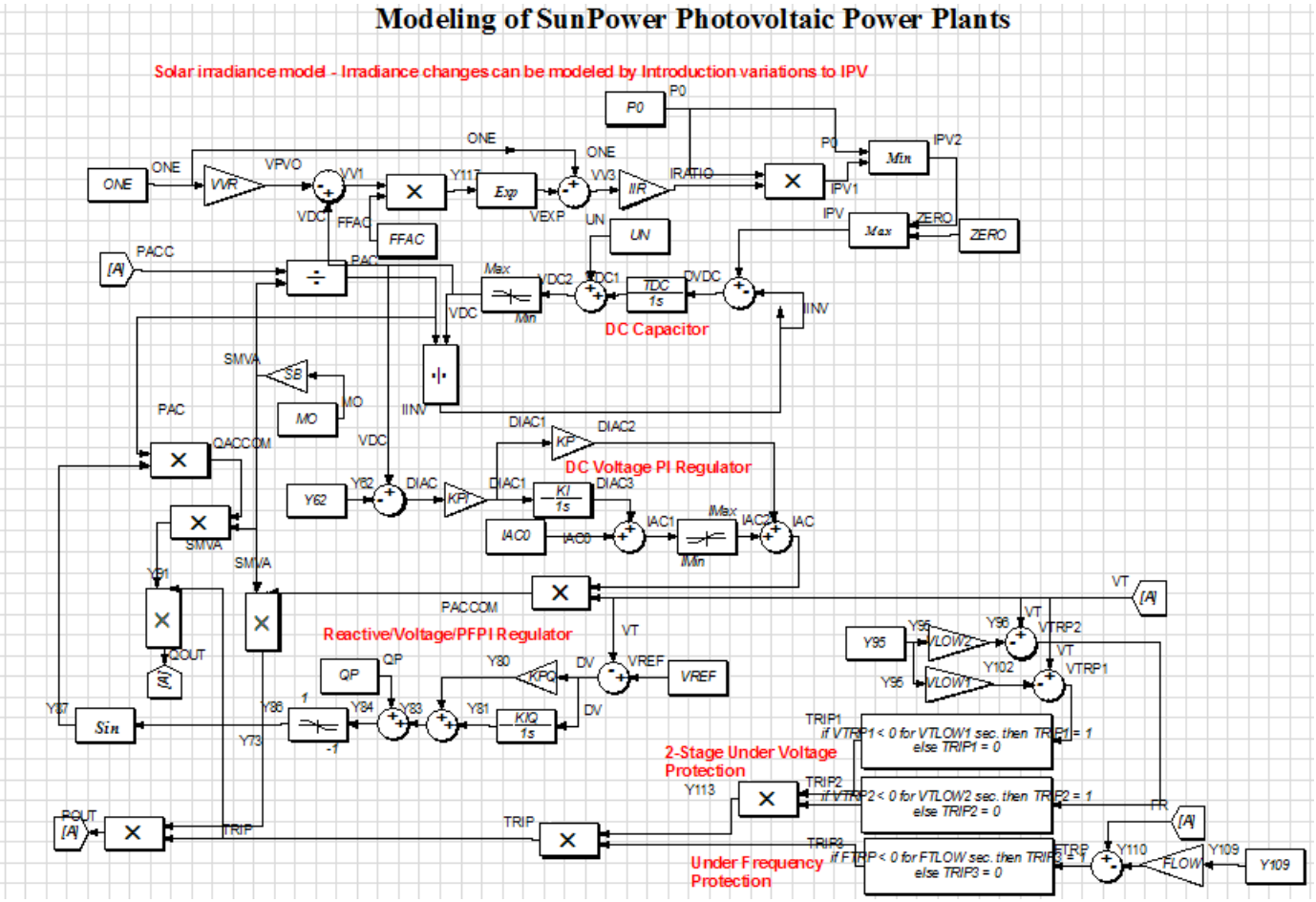

Figure C.28: Control Block Diagram of the SunPower PV Inverters Implemented in Power Analytics Transient Stability

4.4 Reactive/Voltage/PF Controller in the SunPower PV Inverters

The SunPower inverters can regulate the AC bus voltage or maintain constant power factor. An example of the control block diagram of the controller which is implemented in the Power Analytics Advanced Transient Stability is software shown in the below figure. The controlled bus voltage (VT) is compared to a reference voltage (VREF) and then a PI (proportional-integral) controller is used to the process the error signal. The initial

value of the integrator is realized through a summer block (function) by adding a constant. The final output is then passed through a limiter to assure the output stays within practical values.

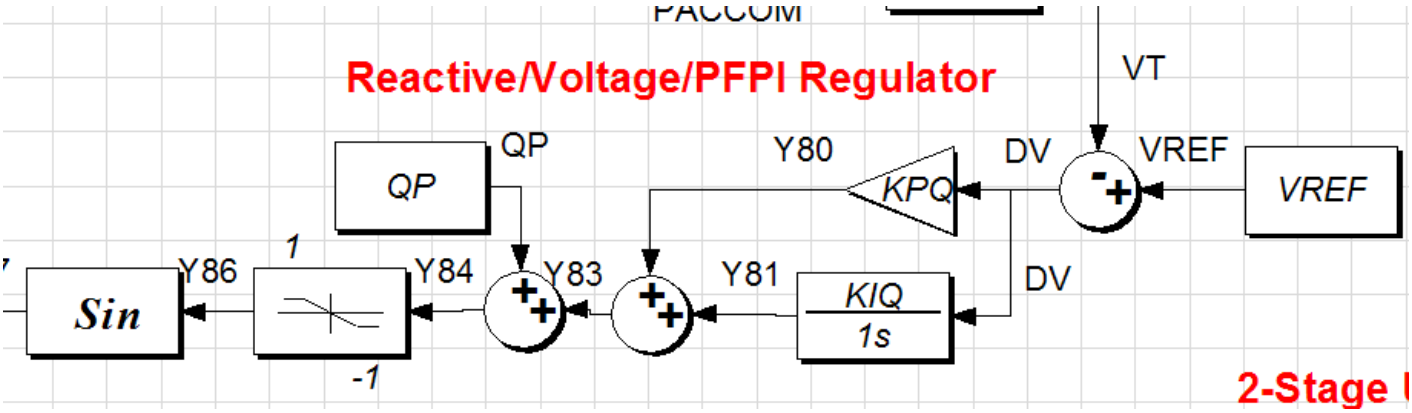

Figure C.29: Block Diagram of the Reactive/Voltage/PF Controller in the SunPower PV Inverters

The initial value of the integrator that is realized by a constant block named “QP” is shown below. The constant value can be verified by inspection of the control block and having the knowledge of initial power output of the PV (initial condition is provided in powerflow) in steady-state. It should be noted that the keywords “PVQ0(IB)”, “PVP0(IB)” are active and reactive power output of a PV at a bus with identification of “IB”. “ASIN” is the inverse of sinuous function.

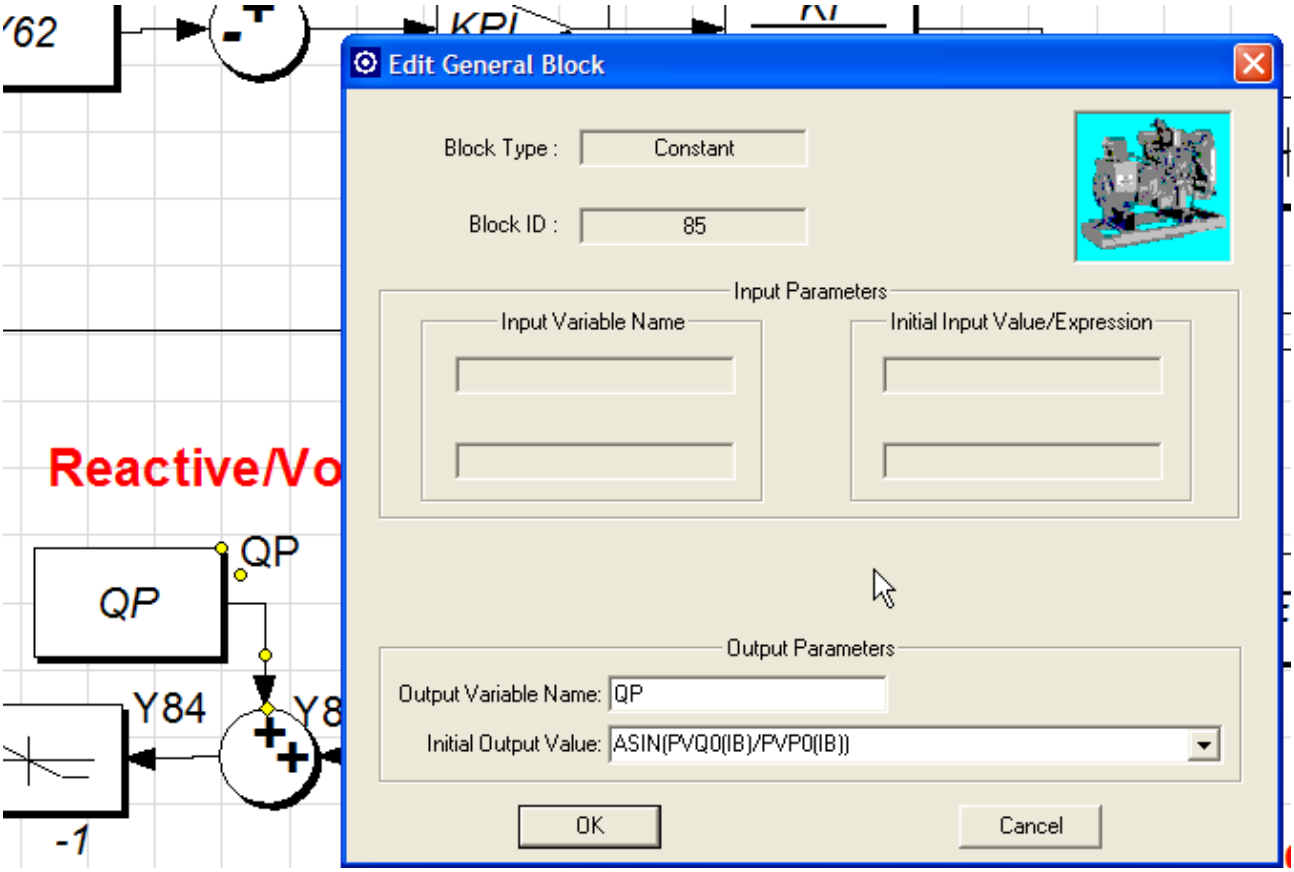

Figure C.32: Initial Condition for the Reactive/Voltage/PF Controller in the SunPower PV Inverters

4.5 Under/Over Voltage and Frequency Protection

The protection of PV inverter against abnormal voltage and frequency operation is extremely important not only from device protection point of view also from the power utility operation. The planning/operation engineers would like to know under disturbances and how long and to what extent PV can ride through disturbances. The under/over voltage protection and under/over frequency protection scheme used in the SunPower PV inverters.

Two levels of under/over voltage and one level of over/under frequency tripping are included in the SunPower PV model. Each of these trip functions has an independent time delay. It should be noted that when more than one relay is used then the trip signal generated from each one should be used in “OR” function. It can be seen that the output of each pair of relay is used in a “Multiplication Function”. Typical settings for protection under/over voltage and frequency relays used in the SunPower Inverters are summarized in table below.

Table C.4: Typical Protection Relay Setting for SunPower PV Inverters

Relay Type	**Setting Type**	**Setting Value**
Over-voltage	**Setting No. 1, pu**	**1.2**
Over-voltage	**Time delay No. 1, sec**	**0.1**
Over-voltage	**Setting No. 2, pu**	**1.1**
Over-voltage	**Time delay No. 2, sec**	**1**
Under-voltage	**Setting No. 1, pu**	**0.1**
Under-voltage	**Time delay No. 1, sec**	**0.2**
Under-voltage	**Setting No. 2, pu**	**0.9**
Under-voltage	**Time delay No. 2, sec**	**2**
Over-frequency	**Setting, Hz**	**61**
Over-frequency	**Time delay, sec**	**0.5**
Under-frequency	**Setting, Hz**	**59**
Under-frequency	**Time delay, sec**	**0.5**

4.6. Testing of SunPower Inverter in Sample Power System

The model of SunPower PV Inverter unit was developed in the Power Analytics Advanced Transient Stability Program and details of its control scheme were provided in the previous section. In this part of the report, the

model will be used in a sample power system to assess its performance under disturbances (fault simulation is of the most common and interest for power system engineers).

The power system shown in Figure C.20 is used to test the PV model. Even though this is a relative small network it has most of the ingredients of a real power system. This power system is known as “WECC 9-bus system”. The system is comprised of three synchronous generators. Details of loads/generation and initial voltages were provided in previous chapters.

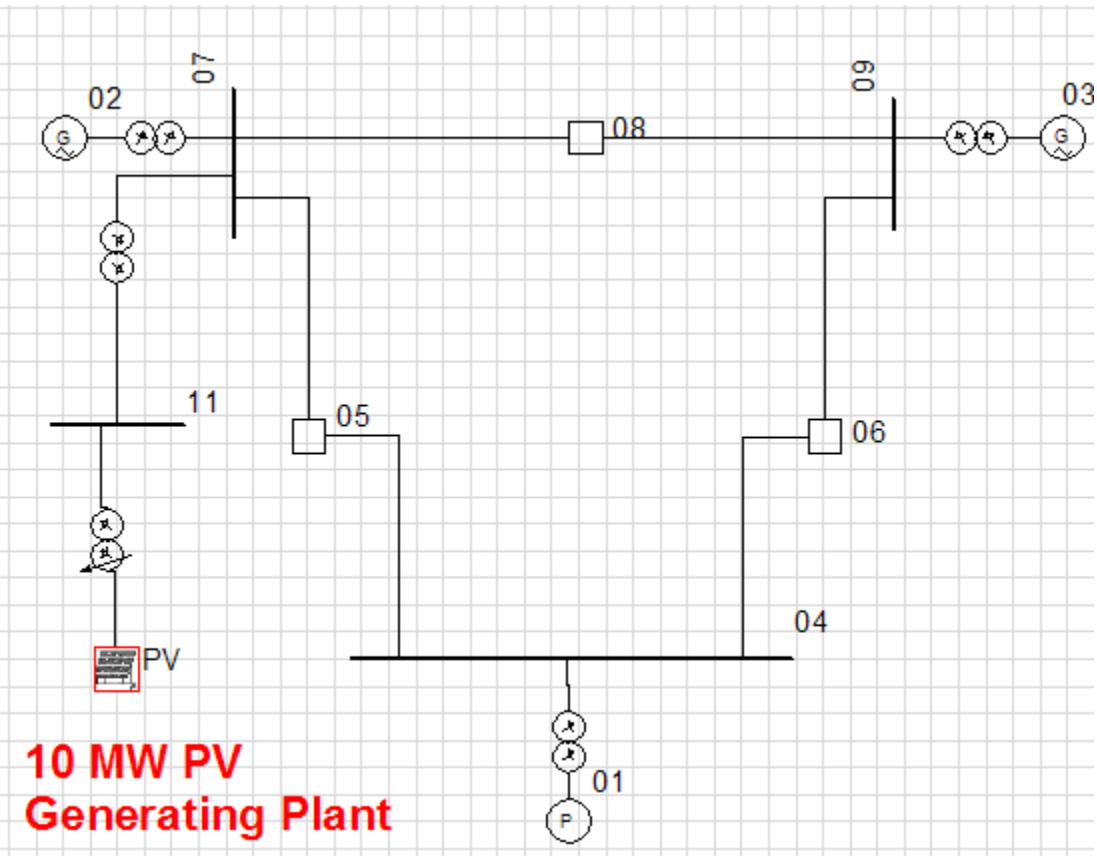

Figure C.33: Sample Power System for Testing a SunPower PV plant

The SunPower PV Inverter data used in this sample power system is shown in Figure C.304. It can be seen that the PV inverter has the capability to control voltage on the PV low voltage AC bus. The result of bus voltage and angle for the solved power is shown below:

Bus Name	Type	V (KVOLTS)	DROP (%)	ANG (DEG)	P (MW)	Q (MVAR)	PF (%)

01	Swing		16.500	0.00	0.0	64.23	10.82	98.61
02	Gen	*	18.450	-2.50	10.0	163.00	17.34	99.44
03	Gen	*	14.145	-2.50	5.0	85.00	0.03	100.00
PV	Gen	*	0.504	-5.00	-19.0	8.00	1.59	98.09
04	Busbar		228.725	0.55	-2.1	64.27	14.94	97.40
05	P_Load		223.332	2.90	-3.8	-125.00	-50.00	92.85
06	P_Load		227.439	1.11	-3.6	-90.00	-30.00	94.87
07	Busbar		234.435	-1.93	4.4	170.86	2.79	99.99
08	P_Load		232.132	-0.93	1.2	-100.00	-35.00	94.39
09	Busbar		236.011	-2.61	2.3	85.03	7.85	99.58
11	Busbar		34.193	-3.62	-21.4	7.95	1.24	98.80

The above result shows that PV inverter delivers 8 MW and 1.6 MVAR to the system and is able to maintain 1.05 pu voltage at the AC bus as specified.

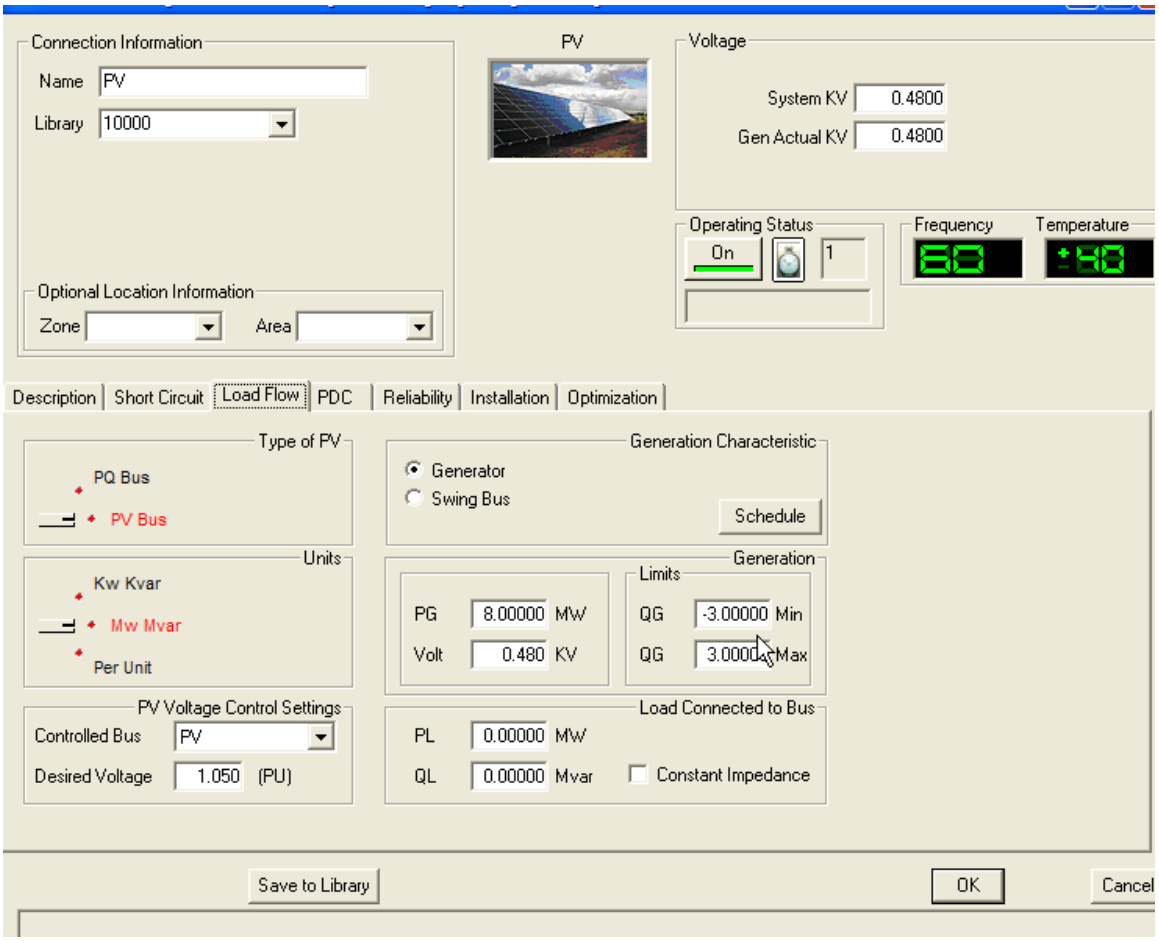

Figure C.304: Powerflow Data for the SunPower PV plant used in the Sample Power System

To prepare a transient stability simulation case for this system, the dynamic data for the SunPower inverter needs to be specified. This can be done by first selecting transient stability icon. Then select the “Event and Data Manager”. Add the SunPower PV model and the data dialog of the model as shown in Figure C.316 will appear.

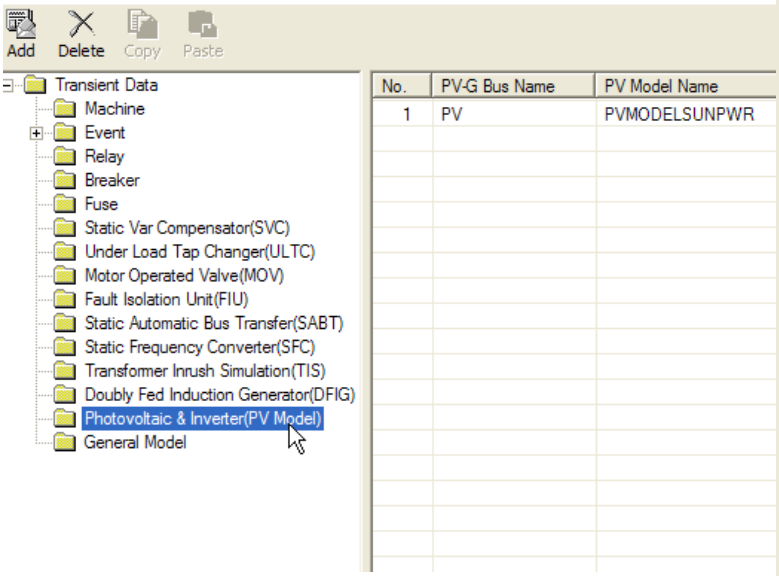

Figure C.35: Adding/Deleting PV Models

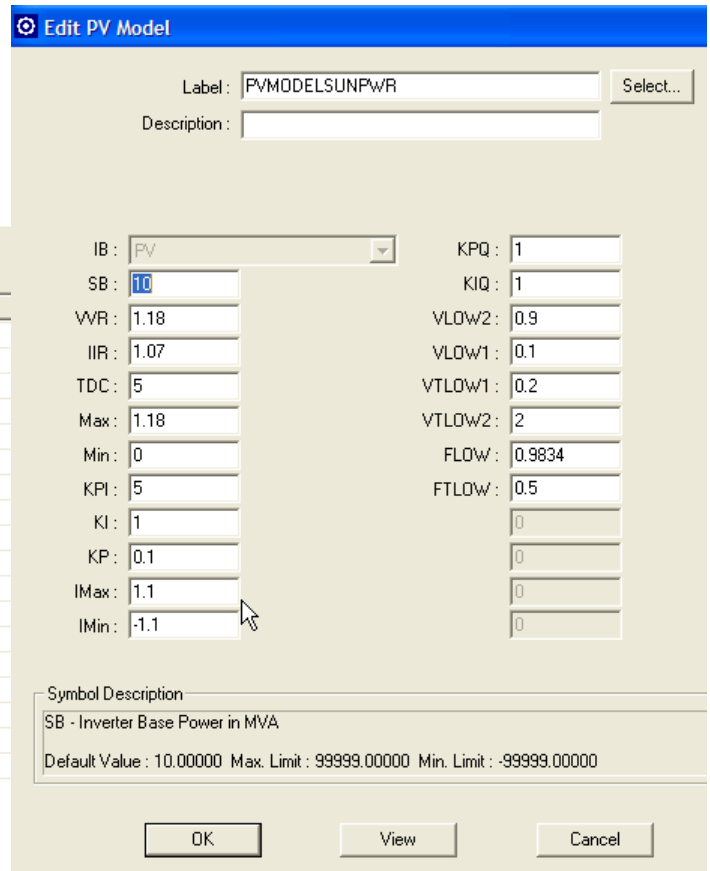

Figure C.316: Dynamic Data for SunPower PV Inverter Plant

Similar to the sample system used for Xantrex PV plant, the disturbance will be examined for this sample power system is application of a fault at bus 5 for a period of 6 cycles (0.1 second). To simulate this fault select “Analyze” and press the “Start Simulation” to perform the simulation. Upon completion of the simulation the result can be view by selecting “View Graphic Result”. All of the monitored variables related to generators, buses, branches, PV, etc. can be examined. Figure below shows several tabs. For example, the generator rotor angles, frequency, mechanical power, terminal voltage and field voltage are shown in Figure C.25. In this figure the branch flow (1st PV transformer) MW, MVAR, and Current is shown.

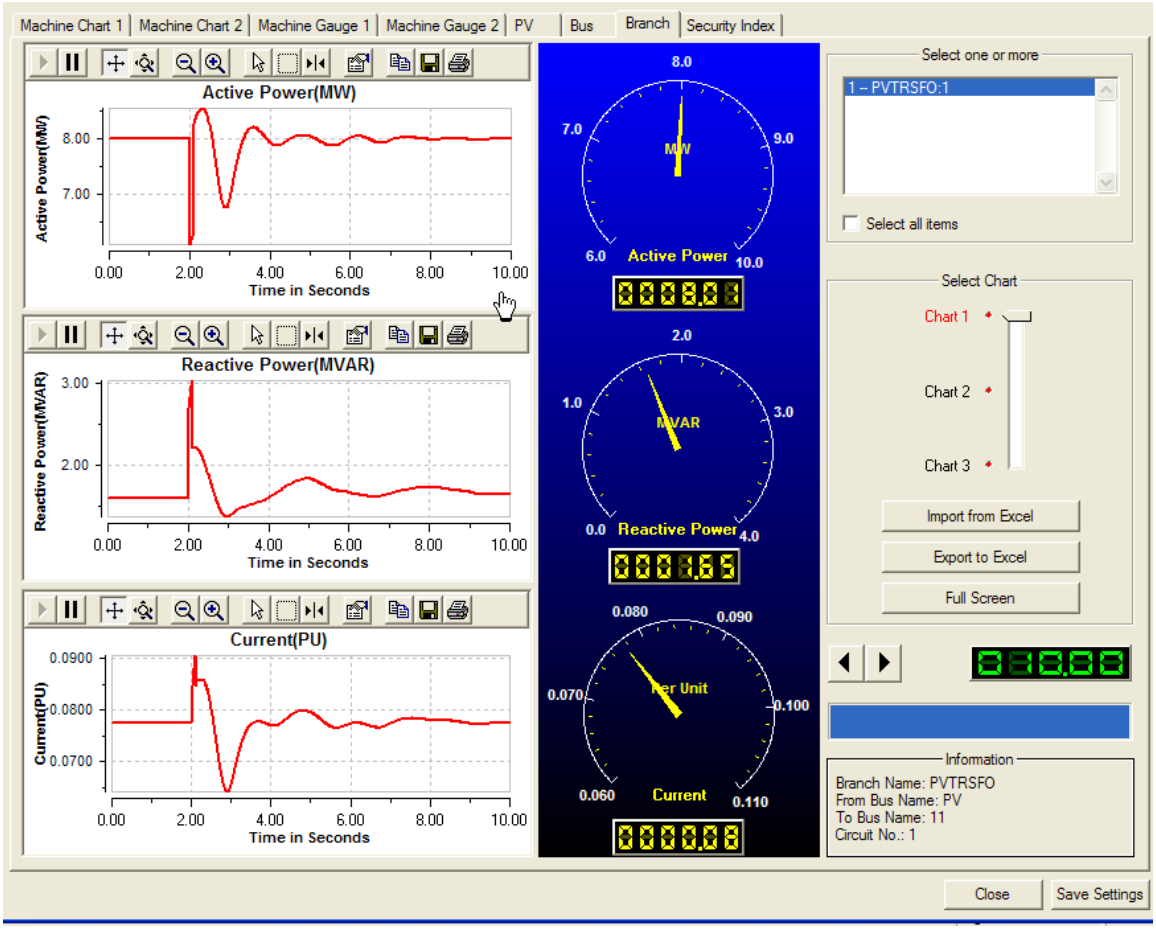

Figure C.327: Graphs of Monitored Branch Variables

To examine the monitored variables for the PV model select “PV” tab shown above. The variables to be monitored are defined at the time PV model is added to the PV library. Power Analytics’ transient stability program gives the user the option to monitor any of the internal variables (signals) within the model. This unique feature helps the user to assess the performance of the control system of the PV inverter and optimize its performance (e.g. by examining the effect changing gain, time constant, etc. on the performance of any controller internal to the inverter).

The time response of the DC voltage and current of the PV array in the SunPower inverter due to a fault is shown in Figure C.26. This figure shows that upon fault occurrence, the array will respond by increasing the voltage to maintain the active power output. The DC voltage will quickly recover following removal of the fault. Other variable of the PV model can be examined by selecting them from the list shown in the bottom middle part of the Figure C.26.

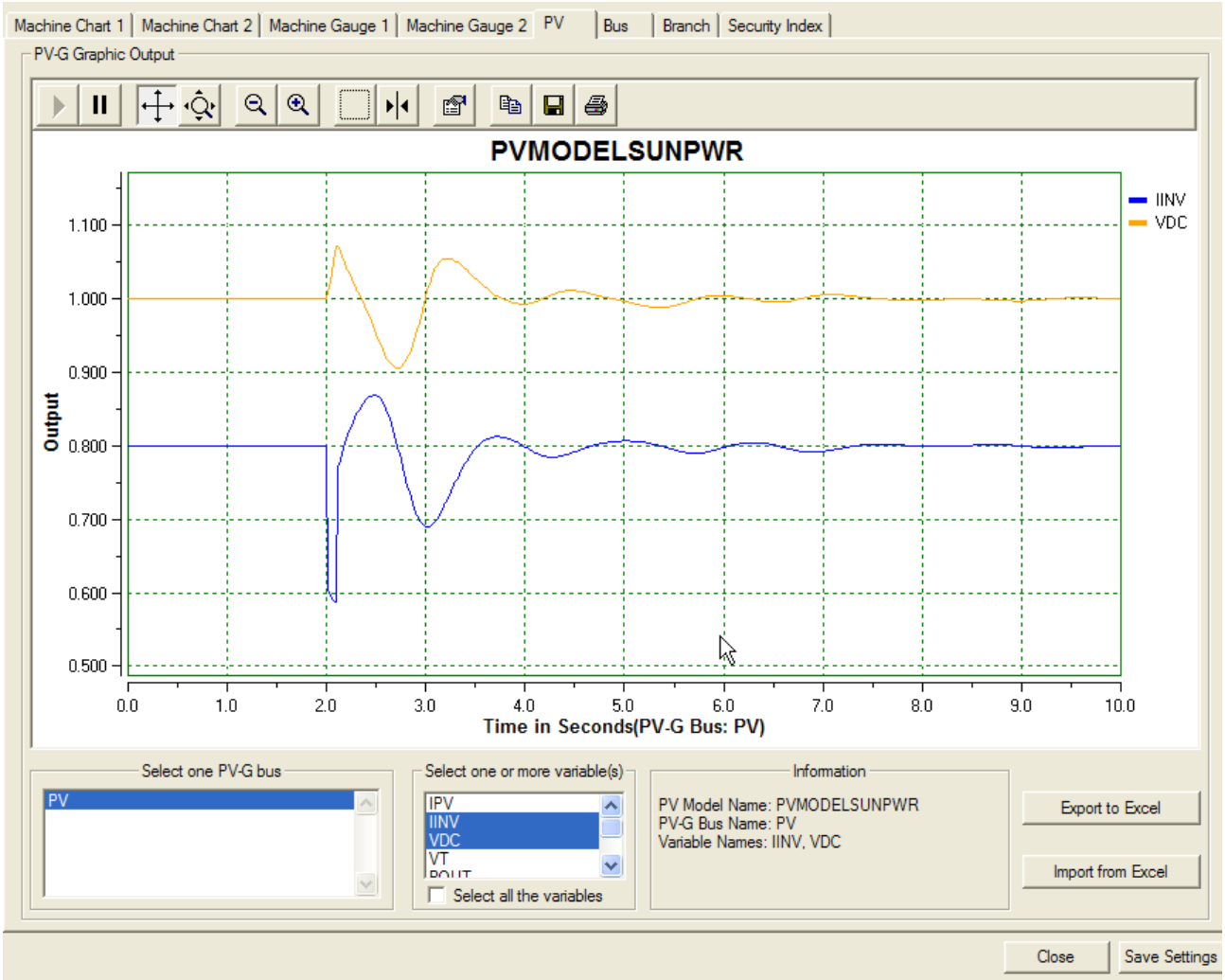

Figure B.338: Time Response of DC Voltage and Current of the PV Array for the SunPower PV/Inverter to a Fault

B.5. Modeling of OptiSolar Inverters

In this section modeling of the Optisolar PV inverters will be covered. The objective is to develop models that are most appropriate for power system simulation including power flow, fault analysis, and time domain simulations. These models have been implemented in the Power Analytics Advanced Powerflow, Short Circuit, and Transient Stability analysis software package. OptiSolar inverters are in general imbedded with an array of PV, transformer, and other components necessary to convert solar radiation suitable for delivery to transmission or distribution system voltages. The modular characteristics of PV generation allow a common inverter model to be used which can be scaled up to a desirable capacity rating for power system integration studies.

An OptiSolar solar power plant is an array of ground mounted PV modules, DC-to-AC power inverters and other system components that are necessary to convert solar radiation to network grade AC power. The specific design details of an individual plant vary from project to project, however, the modular structure of the plant let power system interconnection studies be performed with common models that are scalable.

OptiSolar PV modules are series connected to create source with DC operating voltages in the range of 400 - 600 volts. The currents from these sources are then put in parallel configuration to create DC sources in the power range of several hundred kilowatts.

IGBT type inverters rated at 500 kVA each convert the DC power to AC power at a three-phase output voltage of 208 volt AC. This low AC voltage should then be connected to a transformer for integration of the inverter to the medium voltages, i.e., 25 kV-35 kV. Each transformer may serve one or more inverters. Another voltage change to higher voltages may be required for a particular transmission network interconnection.

The PV modules consist of solid-state semiconductor cells that produce direct current as a function of the solar radiation and voltage to which they are subjected on an almost instantaneous basis. Therefore, inverter characteristics and controls dominate the behavior of the PV plant and its interaction with the power system. OptiSolar inverters are classified as high-frequency, PWM, current-regulated inverters. Inverters operate to control AC output currents in response to a current command through high carrier frequency in the range of 5 to 10 kHz PWM of the DC source. For a given level of solar radiation, only one value of DC voltage, on the PV array, maximizes active power output. The inverter controls include the necessary logic to regulate DC voltage to its optimal value by adjusting AC output current. This is known as maximum power point tracking (MPPT).

In unity power factor operation, the entire inverter current rating is available for active power maximization. OptiSolar inverters offer voltage control capability with an optional reactive power capability. With this option, the inverters respond to power factor commands in the range of 0.95 leading to 0.95 lagging. Thus, only 95% of the inverter’s current rating remains available for active power optimization, with the remaining capacity dedicated to reactive power production or consumption.

5.1. Power Flow and Short Circuit Modeling of OptiSolar PV Inverters

PV power generation using OptiSolar inverters can be modeled (similar to a classical synchronous generator) as a generator connected to power system for powerflow modeling purposes. The voltage rating of this equivalent generator for the OptiSolar PV inverter is 208 volts. The PV plant power rating (MVA) is equal to an integer multiple of the individual inverter MVA rating. However, the active power output for the powerflow simulation can be anywhere in the range of zero to rated MVA depending on the available solar radiation for the time of interest. As the inverters are configured for fixed unity power factor operation in the OptiSolar inverter the reactive power output and corresponding reactive power capability limits should all be set to zero. If the desired operational mode is a fixed non-unity power factor, then, maximum and minimum reactive power capability should both be set to a value close to one-third of the active power dispatch.

OptiSolar PV power plants (inverters) do not contribute to short circuit. It is therefore, recommended that the generators be represented by a reactance of very high magnitude (e.g. 100 p.u.). Since the generator may represented as an aggregate PV, the reactance used would be the same value if all the generators have the same characteristics on a plant base (sum of the MVAs of the individual inverters).

5.2. Transient Stability Dynamic Modeling of OptiSolar PV Inverters

The OptiSolar PV inverter dynamic model has been implemented as a user-defined model in the Power Analytics' Advanced Transient Stability Program. This model consists of a reduced order representation of the inverter controls. An overview of the control block diagram of the model is shown below:

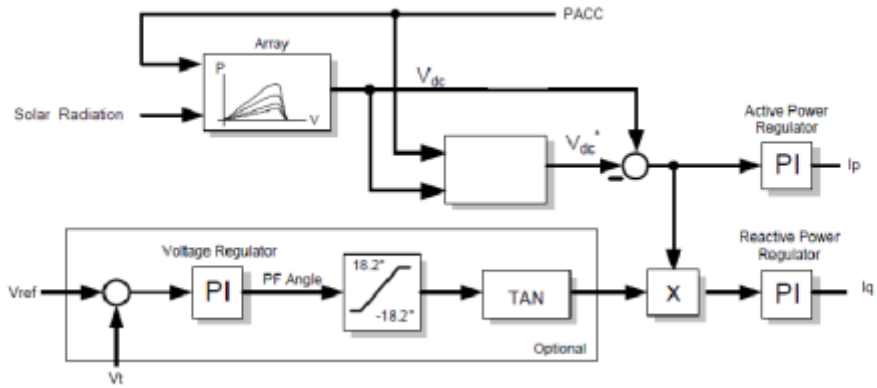

Figure C.34: Overview of the Control Block Diagram of the OptiSolar PV Inverters

For most transient stability studies, the response of the plant to grid disturbances (short circuits) is of most interest. For these studies, the model should calculate the initial solar radiation based on the plant's active power output in the power flow solution. This radiation should be kept constant throughout the transient

simulation time. The output power of the inverter and radiation result in a DC voltage that is a predictable function of the PV characteristics with virtually no dynamics. The DC voltage error is processed through a proportional-integral regulator whose output is the inverter direct axis current Ip that results in active power production.

The algorithm used to maximum power generated from the PV (MPPT) determines a reference DC voltage. At steady state operating point the MPPT reference voltage remains almost constant since the MPPT voltage is not a strong function of radiation. For applications that require the optional reactive power control capability, an additional source of excitation is the power factor angle command that produces a quadrature axis current Iq that results in reactive power absorption or delivery.

The model also supports under/over voltage protection in addition to under/over frequency protection. Two levels of overvoltage tripping, three levels of under-voltage tripping and one level of over and under- frequency tripping are included in the OptiSolar Inverter model. Each of these trip functions has an independent associated time delay.

5.3. Implementation of the OptiSolar PV Inverter in the Power Analytics Transient Stability Model Builder

Similar to Xantrex and SunPower PV models described in the previous chapters, the OptiSolar PV model can be built using the user-defined feature of the Power Analytics transient stability software. The principal of adding functional blocks, input blocks, and output blocks were demonstrated in previous chapters in details for assembling Xantrex model. Here only the completed OptiSolar PV model will be presented. The control block diagram for OptiSolar is shown in Figure C.28.

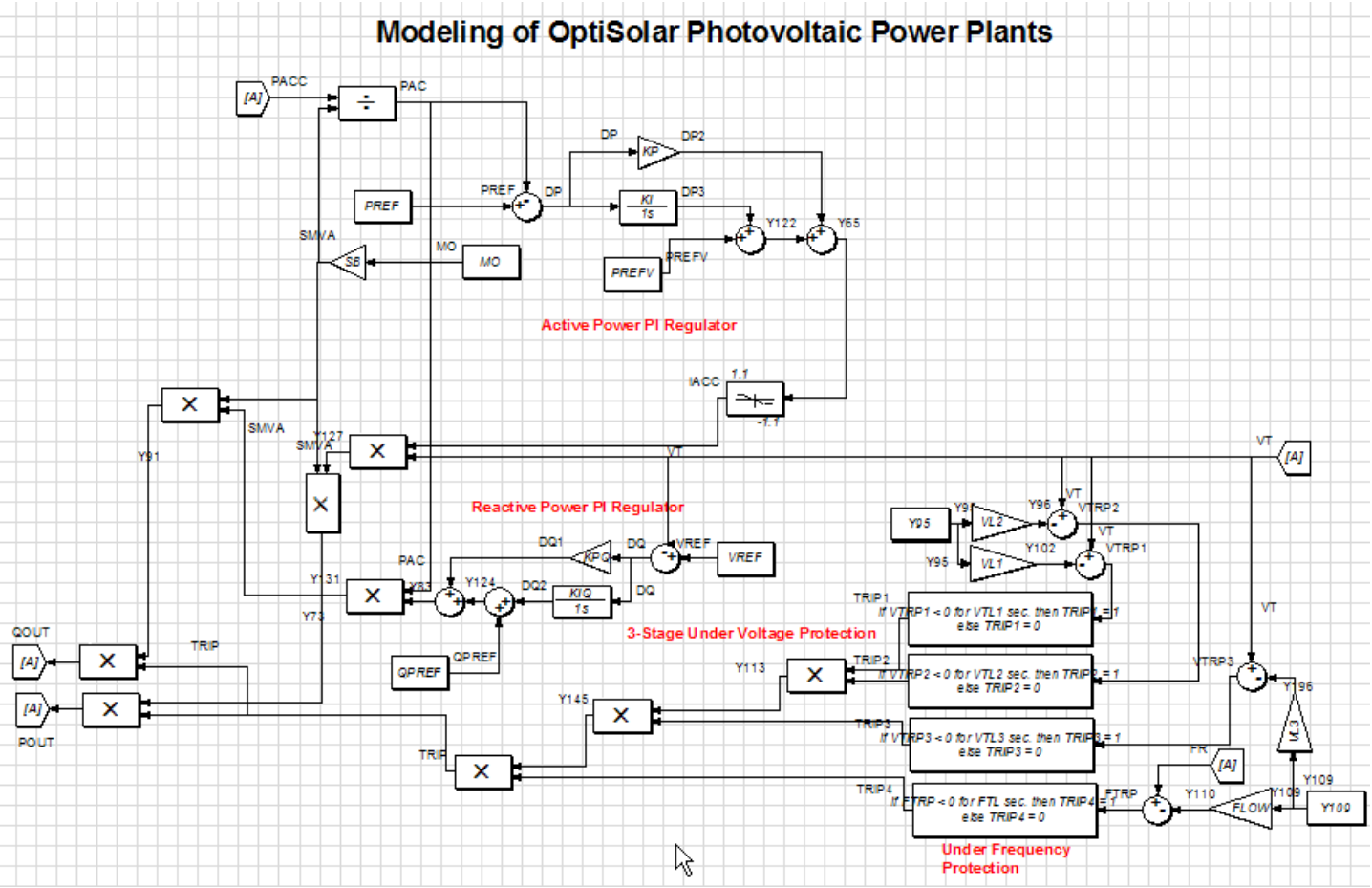

Figure B.40: Control Block Diagram of the OptiSolar PV Inverters Implemented in Power Analytics' Transient Stability

The OptiSolar control system shown in the above figure consists of three major functions. These are two PI controllers for active and reactive power control and a protection scheme. Multiple levels of under/over voltage and frequency relays can be defined. It should be noted that when more than one relay is used then the trip signal generated from each one should be used in "OR" function. It can be seen that the output of each pair of relay is used in a "Multiplication Function".

5.4. Testing of OptiSolar Inverter in Sample Power System

The model of OptiSolar PV inverter unit was developed in the Power Analytics Advanced Transient Stability Program and details provided in the previous sections. The model will be used in a sample power system to assess its performance under disturbances (fault simulation is of the most common and interest for power system engineers).

The power system shown in Figure C. is used to test the PV model. Even though this is a relative small network it has most of the ingredients of a real power system. This power system is known as "WECC 9-bus

system". The system is comprised of three synchronous generators. This power system is assembled similar to other network with the exception of PV. To add a PV plant to a power system select the PV icon and drag it into system model area. To edit the parameters of the PV inverter, double click the right mouse button on PV icon.

To prepare a transient stability simulation case for this system, the dynamic data for the OptiSolar inverter needs to be specified. This can be done by first selecting transient stability icon. Then select the "Event and Data Manager". Add the SunPower PV model and the data dialog of the model as shown in Figure C.3142 will appear. The dynamic data for the OptiSolar PV inverter is shown in Figure B.42.

The disturbance that will be examined for this test power system with PV plant is application of a fault at bus 5 for a period of 6 cycles (0.1 second). To specify this fault select "Event and Data Manager" and add one fault application event.

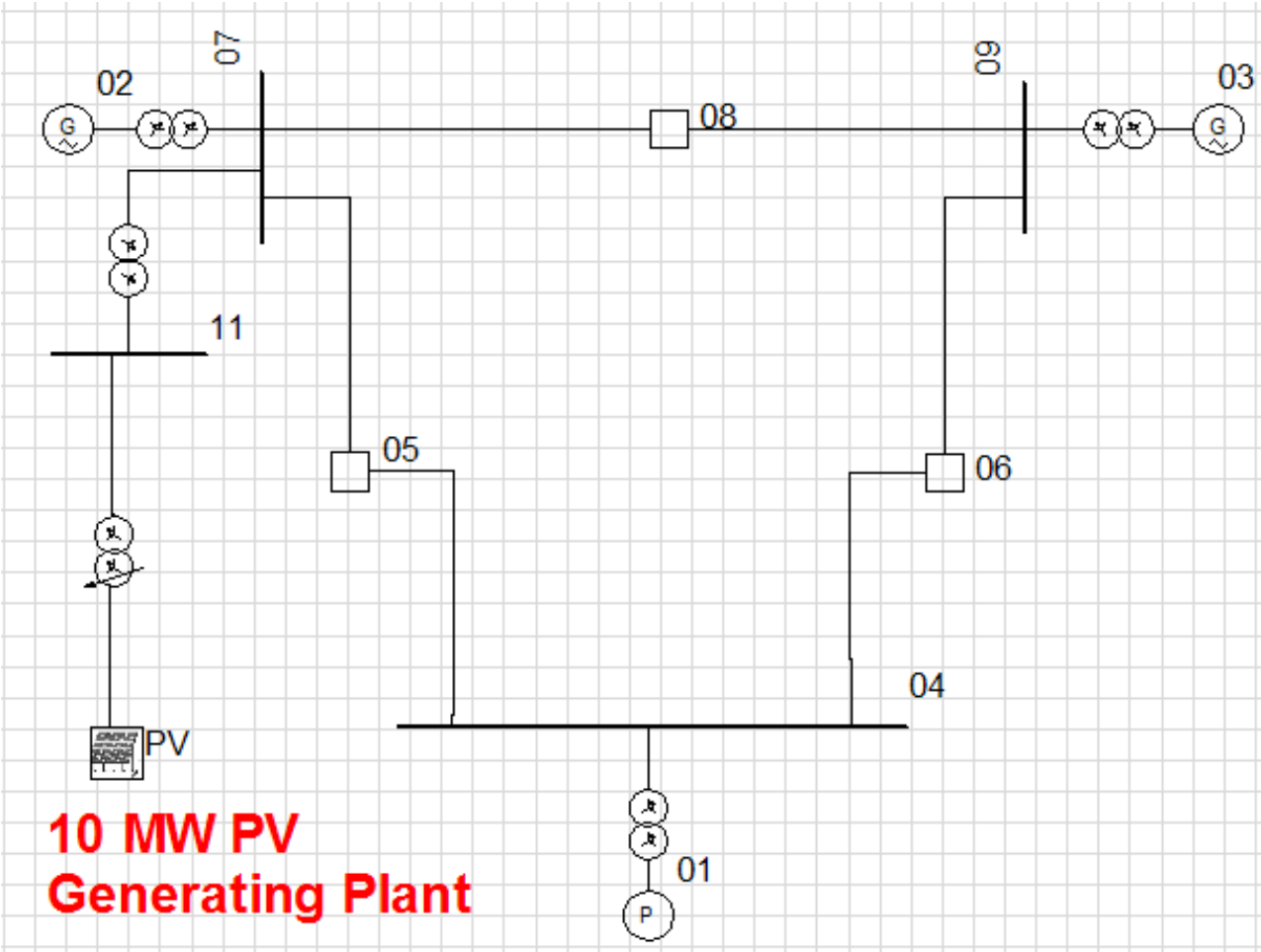

Figure C.41: Sample Power System for Testing a OptiSolar PV plant

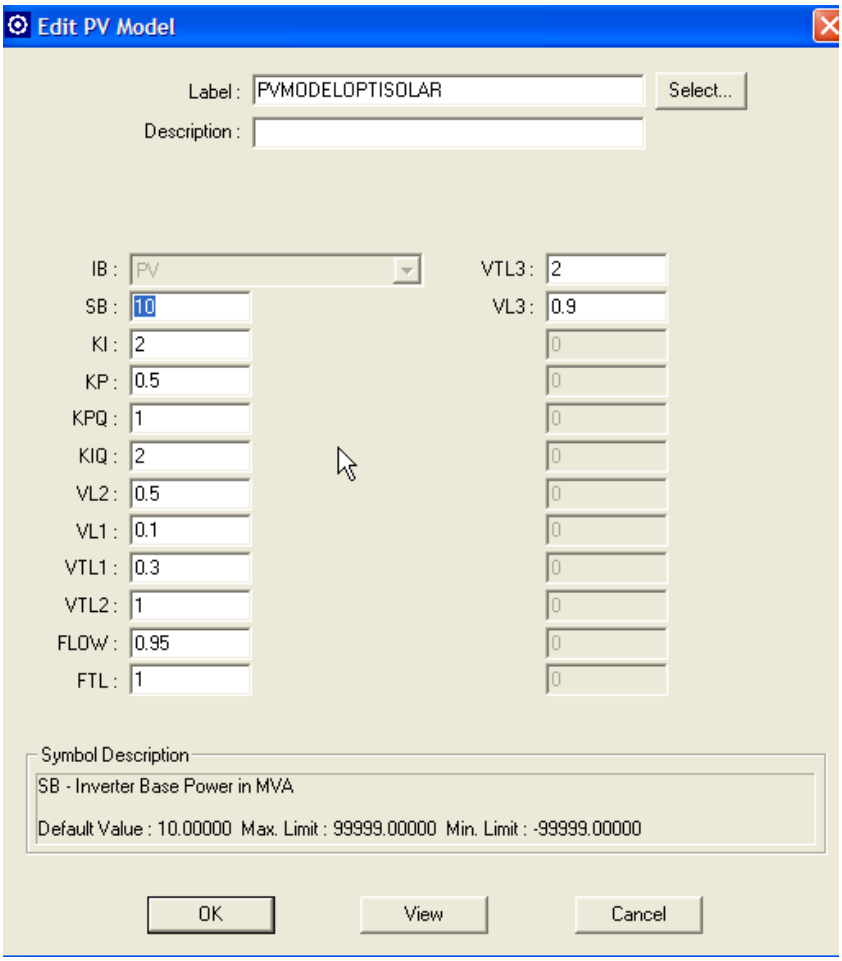

Figure B.42: Dynamic Data for OptiSolar PV Inverter Plant

To start the time domain simulation, select “Analyze” and in the simulation dialog press “Start Simulation” to perform the simulation. Upon completion of the simulation the result can be viewed by selecting “View Graphic Result”.

All of the monitored variables related to generators, buses, branches, PV, etc. can be examined. Figure below shows several tabs. For example, the generator rotor angles, frequency, mechanical power, terminal voltage and field voltage can all be examined.

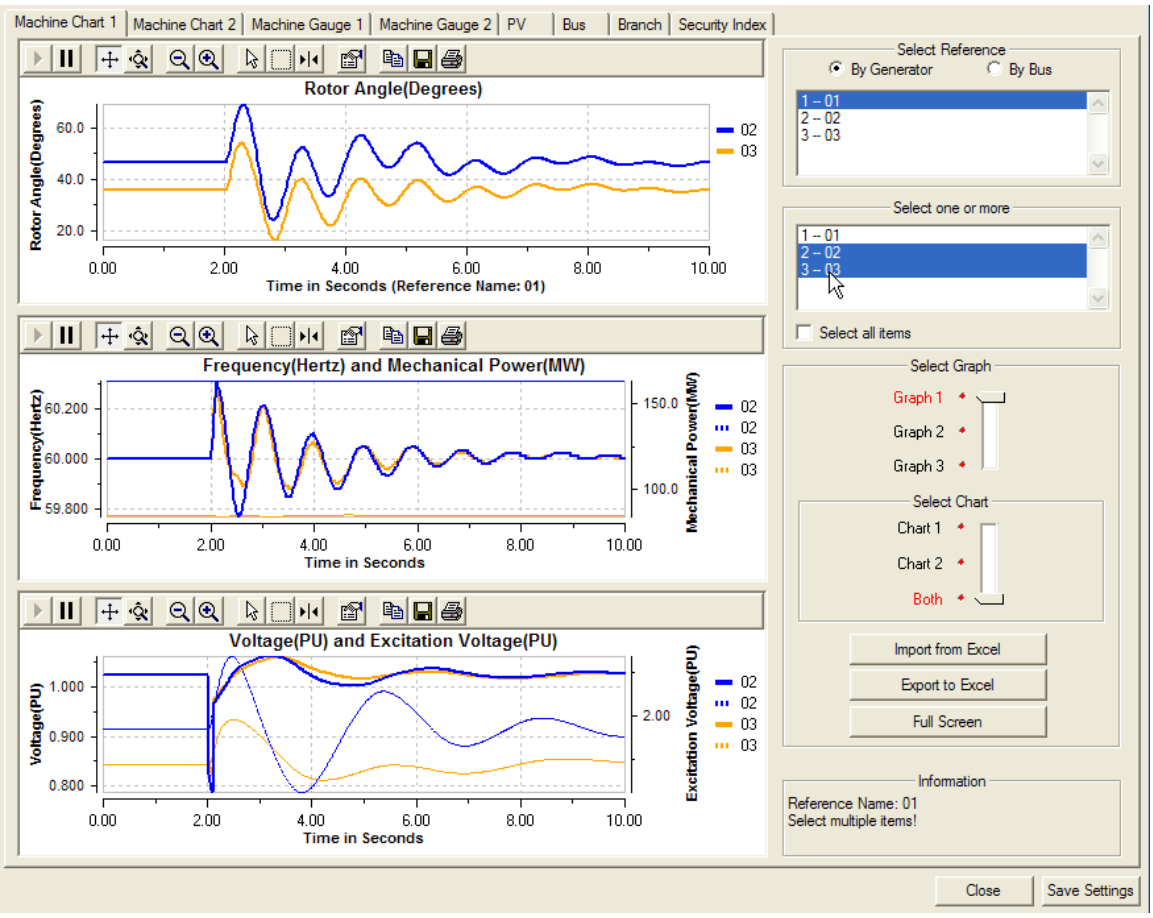

Figure B.35: Graphs of Monitored Generator Variables

To examine the monitored variables for the PV model select “PV” tab shown above. The variables to be monitored are defined at the time PV model is added to the PV library. Power Analytics transient stability program gives the user the option to monitor any of the internal variables (signals) within the model. This unique feature helps the user to assess the performance of the control system of the PV inverter and optimize its performance (e.g. by examining the effect changing gain, time constant, etc. on the performance of any controller internal to the inverter).

The time response of the active and reactive power in the OptiSolar inverter due to a fault is shown in Figure C.264. This figure shows that upon fault occurrence, the array will respond by increasing the reactive power to maintain the voltage constant (note that if active and reactive power a PV model are negative the power is delivered into power system). Also, due to the fault, the active power output of the PV drops and after fault removal recovers quickly to its pre-fault condition. Other variable of the PV model can be examined by selecting them from the list shown at the bottom middle part of the Figure C.26.

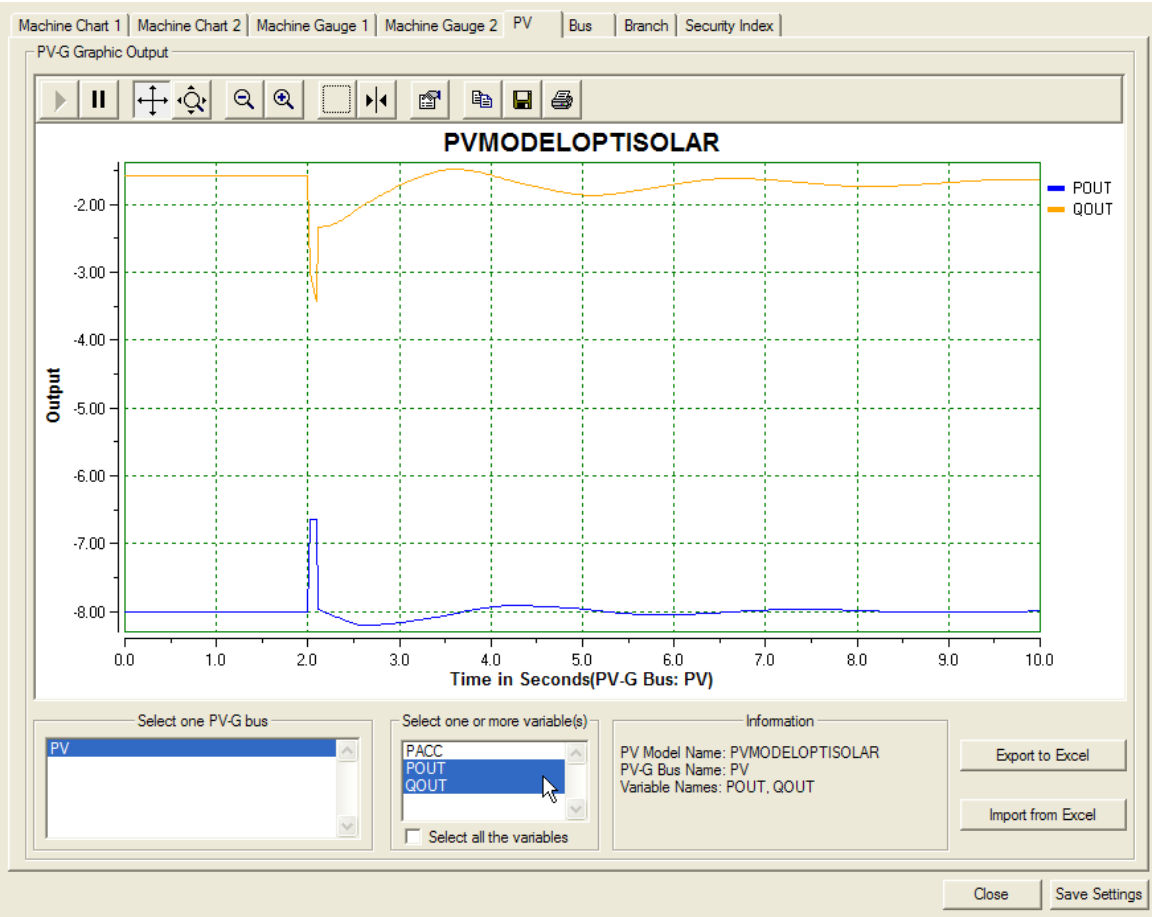

Figure B.364: Time Response of Active and Reactive Power of OptiSolar PV/Inverter to a Fault